Spring 5-15-2017

B7H6: A Cancer Biomarker for the Development of Novel Immunotherapy Approaches

Mariana Phillips
mariana.phillips@student.shu.edu

B7H6: A Cancer Biomarker for the Development of Novel Immunotherapy Approaches

A thesis submitted to Seton Hall University in partial fulfillment of the requirements for the degree of Doctor of Philosophy

By:

Mariana Phillips

May 2017

Department of Chemistry and Biochmistry
Seton Hall University
South Orange, NJ, 07079

DISSERTATION COMMITTEE APPROVALS

We certify that we read this thesis and in our opinion, it is sufficient in scientific scope and quality as a dissertation for the degree of Doctor in Philosophy.

APPROVED BY:

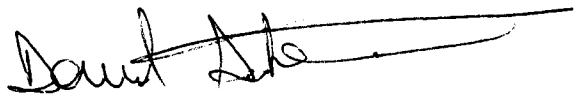

David Sabatino, Ph.D.

Research Mentor, Seton Hall University

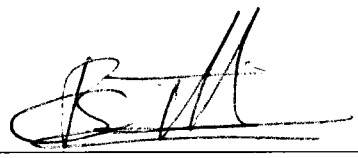

Constantine Bitsaktsis, Ph.D.

Reader, Member of Dissertation Committee,

Seton Hall University

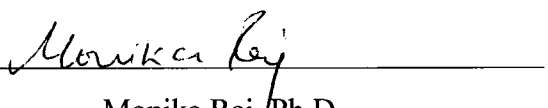

Monika Raj, Ph.D.

Reader, Member of Dissertation Committee,

Seton Hall University

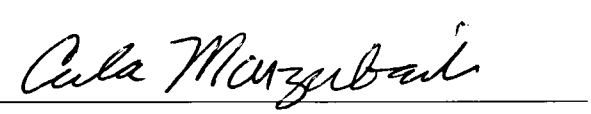

Cecilia Marzabadi, Ph.D.

Chair, Department of Chemistry and Biochemistry,

Seton Hall University

Dedicated to Javier and Marianne, my forever inspiration to become a better version of myself.
Dad, wherever you are, I will always miss you, and know I will always do my best to make you proud.

ABSTRACT

Cancer-based immunotherapy has led the evolution of biologics that can stimulate immune responses towards tumor eradication. For example, the monoclonal antibodies (mAb) and their related analogs have shown promise in the clinic for the treatment of a wide range of cancer types. In spite of their utility, novel therapeutics that may overcome their production, administration, and pharmacological limitations are still in widespread demand. Therefore, the synthesis of small to intermediate size molecules with the targeting and effector functions of mAb may represent a novel class of immunotherapeutics that may overcome the limitations of their biological counterparts.

Towards this research objective, B7H6 has been identified as a protein ligand localized on the cell surface of transformed tumor cells. It functions as a tumor associated antigen (TAA) which binds specifically to the activating receptor NKp30, constitutively expressed on all resting and active NK cells. Upon ligand:receptor binding, B7H6 triggers NK cell activation and release of chemokines and pro-inflammatory cytokines such as TNF-α and IFN-γ, leading to tumor cell lysis and death. Interestingly, B7H6 was found to be expressed on the surface of tumors but not on healthy cells making it an interesting bio-marker for NK cell mediated cytotoxicity. Moreover, it was recently discovered that tumor cells escape immunosurveillance by the downregulation or shedding of B7H6. In an effort to overcome this resistance mechanism, the development of new B7H6 derived ligands that may effectively target NKp30 and activate NK cells towards B7H6 deficient tumors may result in a more effective NK-cell-based cancer therapy approach.

In this thesis, the rational design of a novel class of immunostimulatory peptides (IPs) derived from the binding interface of B7H6:NKp30 was developed. The IPs were composed of the B7H6 active site sequence for NKp30 binding and immunostimulatory activity. The addition of

an aminohexanoic acid linker was used for FITC-labeling by Fmoc-solid phase peptide synthesis. The secondary structures of the peptides were evaluated by CD spectroscopy in H_2O, PBS and a H_2O:TFE mixture which demonstrated flexible peptide structures which adapted to the solvent conditions and were found to transition from random coil (H_2O) to α-helical (PBS) and turn-type (H_2O:TFE) conformations. The evaluation of their biological properties showed an occupancy of the synthetic peptides to a human NK cell line comparable to the natural NKp30 ligand, B7H6, and the human anti-NKp30 monoclonal antibody (mAb), in a concentration dependent manner. A competitive binding assay in between the human anti-NKp30 mAb or B7H6, and the synthetic peptides, demonstrated partial displacement of the ligands upon anti-NKp30 mAb treatment, suggesting specific NKp30 receptor binding by the synthetic peptides. Moreover, the immunostimulatory activity of B7H6 was demonstrated by the secretion of the pro-inflammatory cytokines, tumor necrosis factor-alfa (TNF-α) and interferon gamma (IFN-γ) by the human NK cell line. The immunostimulatory effects of the IPs on the NK cells was assessed by the production of TNF-α alone as IFN-γ was undetectable in our ELISA. In a cell death assay, the IPs were found to be non-toxic, without any observable evidence of early or late stage apoptosis within the NK92-MI cells. Taken altogether, this novel class of synthetic peptides may prove to be a promising lead in the development of a new peptide-based immunotherapy approach, especially against B7H6 expressing tumors.

Alternatively, Pep42, a cyclic peptide selected from phage display bio-panning experiments, CTVALPGGYVRVC, has been shown to bind specifically to the heat shock family member Glucose-Regulated Protein 78 (GRP78) receptor, while internalizing poorly within tumor cells by receptor mediated endocytosis. GRP78 has been found to be exclusively overexpressed and cell surface localized on a variety tumor cells, where it promotes cancer initiation, proliferation

and metastatic spread, but not on healthy tissue, making it a great biomarker for the development of targeted forms of cancer immunotherapy techniques. Moreover, Pep42, as a GRP78 ligand, has been conjugated to Taxol and pro-apoptotic peptide sequences, and used as a drug delivery vehicle triggering cell death selectively in *in vitro* and *in vivo* models.

In an effort to identify novel therapeutic leads this thesis also describes the application of Pep42, its FITC-labeled derivatives, and a series of poly(ethylene glycol)-linked Pep42 sequences in tumor immunotherapy applications. The peptide sequences were accomplished by solid phase synthesis and some were modified with reactive *N*-succinimidyl carbamate linkages. Pep42 and its FITC-labeled derivatives have been tested for their capabilities to bind to the HepG2 human hepatocellular carcinoma cells. Flow cytometry revealed comparable binding of the synthetic peptides relative to the anti-GRP78 primary antibody at equal concentrations (100 nM). A blocking binding assay in between the human anti-NKp30 mAb or Pep42, and the specific N-20 GRP78 peptide blocker showed similar blocking capabilities of either the primary antibody or Pep42, suggesting high specificity to GRP78. In a cell death assay, Pep42 was found to be non-toxic. Moreover, the reactive *N*-succinimidyl carbamate derived peptides were envisioned to behave as reactive probes for their incorporation within bioactive proteins such as B7H6. Therefore, Pep42 may prove to be a promising cancer targeting peptide for the development of immunostimulatory peptide-protein conjugates. Towards this ultimate goal, this thesis describes progress towards the design, development and application of novel semi-synthetic antibody mimics for NK-dependent treatment of tumors that overexpress GRP78 at the cell surface.

ACKNOWLEDGMENTS

To my family, for their patience, understanding and unconditional support in days of frustration, and for sharing with me the joy in days of happiness. To Javier, who even from a distance has been supportive of my professional and personal development. To my parents, my role models, who set an example of perseverance, honesty, and humility.

A special thank you to my mentor, Professor David Sabatino, for the incredible opportunity to develop a research project I felt passionate about. It has been a delight working daily with a man that helped build my professional and personal perspectives. It was an honor working with someone of integrity and excellence, and I will always be grateful for his trust and for the lessons learned during my time at Seton Hall University.

I would like to also thank Professor Constantine Bitsaktsis for his unconditional support and for guiding me through the field of biology. He was truly an inspiration and ignited in me a deep interest in the field of immunology.

Thank you to Dr. Allan Blake for opening the doors of his research laboratory to me. He help me gather a better understanding of all the biological techniques needed to develop my research project successfully. A special thank you to Dr. Robert Korngold, from Hackensack University Medical Center, for welcoming me in his research laboratory and allowing me to further develop my research project.

A special thank you to all my research collaborators, past and present, all of the "Sabatino" research group members, for their unconditional support and their contribution to my professional and personal growth. It was my pleasure working side by side with an extraordinary group of people, and for that, I will always be grateful.

TABLE OF CONTENTS

ABBREVIATIONS AND SYMBOLS

7-ADD	7- aminoactinomycin D
ADAM-10	A Disintegrin and metalloproteinase domain-containing protein 10
ADAM-17	A Disintegrin and metalloproteinase domain-containing protein 17
Ahx	Aminohexanoic acid
APC	Antigen presenting cell
Asn	Asparagine
ATF6	Activating transcription factor 6
Boc	tert-Butyloxycarbonyl
CARs	Chimeric antigen receptor
CD	Circular dichroism
CO_2	Carbon dioxide
CTIPPC	Cancer-targeting immunostimulatory protein-peptide conjugates
DCM	Dichloromethane
DMF	Dimethylformamide
DNA	Deoxyribonucleic acid
DNAM-1	DNAX accessory molecule-1
DPPC	1,2-dipalmitoyl-sn-glycero-3-phosphocholine
DSC	Disuccinimidyl carbonate
EC_{50}	Half maximal effective concentration
ECD	Extracellular domain
ELISA	Enzyme-linked immunosorbent assay
ER	Endoplasmic reticulum

ERK	Extracellular regulated kinase
ESI-MS	Electrospray ionization mass spectrometry
FA	Formic acid
FACS	Fluorescence-activated cell sorting
FBS	Fetal bovine serum
FITC	Fluorescein isothiocyanate
Fmoc-SPPS	Fmoc-based solid phase peptide synthesis
FRP2	N-formyl peptide receptor 2
Glu	Glutamic acid
Gly	Glycine
GRP78	Glucose regulated protein 78
HA	Hemagglutinin
HATU	1-[Bis(dimethylamino)methylene]-1*H*-1,2,3-triazolo[4,5-*b*]pyridinium 3-oxid hexafluorophosphate
HCTU	2-(6-chloro-1H-benzotriazole-1-yl)-1,1,3,3-tetramethylaminium hexafluorophosphate
HDACi	Class I-specific histone deacetylases inhibitors
HSP70	Heat shock protein 70
IFN-γ	Interferon gamma
IgV-like	Immunoglobulin V- like
IL-10	Interleukin 10
IL-2	Interleukin 2
IPs	Immunostimulatory peptides

ITAM	Immunoreceptor tyrosine based activation motif
K_D	Dissociation constant
kDa	Kilo dalton
K_i	Inhibitor constant
KIRs	Killer immunoglobulin-like receptors
LCMS	Liquid chromatography–mass spectrometry
Lys	Lysine
mAbs	Monoclonal antibodies
MAPK	Mitogen-activated protein kinase
MAPs	Multiple antigen presenting peptides
MeCN	Acetonitrile
MeOH	Methyl alcohol
MHC Class 1	Major histocompatibility complex MHC class I molecules
mRNA	Messenger RNA
NCRs	Natural cytotoxicity receptor family
NIR	Near-infrared
NK	Natural Killer
NKG2D	Natural-killer group 2 member D
NMM	N-Methylmorpholine
NSC	N-succinimidyl carbamate
NSCLC	Non-small cell lung cancer
Pbf	2,2,4,6,7-pentamethyldihydrobenzofurane
PBS	Phosphate buffered saline

PRK	Protein kinase RNA-like ER kinase
Pro	Proline
ProT*a*	Prothymosin alpha
PS	Phosphatidylserine
QRT-PCR	Quantitative reverse transcription polymerase chain reaction
R.T.	Room temperature
RP HPLC	Reverse phase high performance liquid chromatography
scFv	Single chain fragment variable
SDS-PAGE	Sodium dodecyl sulfate polyacrylamide gel electrophoresis
siRNAs	Short Interfering RNAs
SPPS	Solid phase peptide synthesis
SPR	Surface plasmon resonance
TAAs	Tumor associated antigens
TAA-SP	Tumor-associated antigen derived small peptides
tBu	tert-butyl
TES	Triethylsilane
TFA	Trifluoroacetic acid
TFE	Trifluoroethanol
TFs	Transcription factors
T_H1	T helper cells
Thr	Threonine
TLR2	Toll-like Receptor2
TNF-α	Tumor necrosis factor alfa

Trt	trityl
UPR	Unfolded protein response
Val	Valine
VLP	Virus-like particles

LIST OF FIGURES

CHAPTER 1

LIST OF SCHEMES

CHAPTER 2

CHAPTER 3

CHAPTER 4

LIST OF TABLES

CHAPTER 2

CHAPTER 3

CHAPTER 4

CHAPTER 1: INTRODUCTION

Biological molecules that can trigger immune responses towards invading pathogens, allergens and cancer have led the advancement of immunotherapy.[1] Tumor immunotherapy involves the activation of white blood cells, either by stimulating lymphocytes *ex vivo,* followed by re-infusion of the activated cells into the patient. Alternatively, circulating tumor associated ligands *in vivo* can stimulate inflammatory responses towards the destruction of the invasive tumor or blockage of pro-survival signals.[2-5] In an effort to promote *in vivo* stimulation of lymphocytes towards the eradication of tumors, treatment methods implicating cancer vaccines, tumor-associated antigen derived small peptides (TAA-SP) or recombinant virus-like particles (VLP), cytokine therapy, and monoclonal antibodies (mAbs) have been developed and successfully administered in tumor immunotherapy applications.[1-7] (**Figure 1.1**)

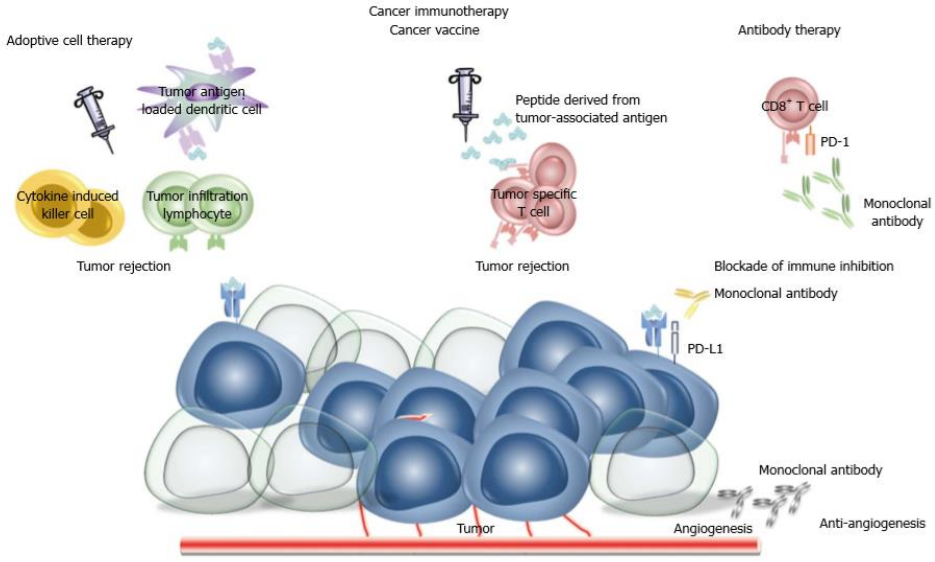

Figure 1.1. Immunological approaches to cancer therapy. Figure adapted from *World J. Gastroenterol*., **2014**, *20*, 1657-1666.[3]

1.3 IMMUNOSTIMULATORY PEPTIDES AND THEIR IMPACT ON IMMUNOTHERAPY

Among the promising immunotherapy treatment regimes, the peptide-based TAA-SPs potentially encompass an underexplored yet promising class of immunostimulatory ligands that may have significant utility in clinical oncology. A brief survey of the current literature unveils a small set of short immunostimulatory peptides (IPs), commonly derived from the binding site interfaces in between the tumor associated ligand and its lymphocytic receptor, peptide epitopes which display multiple antigenic activity and isolated native sequences which exhibit immunomodulatory effects *in vitro* and *in vivo*.[8-18,35-39]

For example, a new class of lipopeptides have been recently explored as agonists for the Toll-like Receptor2 (TLR2) found on the cell surface of pancreatic tumors.[8] These peptides were based on the crystal structure analysis of the TLR2:ligand complexes in which the hydrophobic Cys(*S*-[2,3-bispalmitoly)oxy-(*R*)-propyl] formed the minimal ligand binding site residue required for activity.[9,10] Variations were made to the remaining flexible peptide components by solid phase peptide synthesis (SPPS) to improve metabolic stability and immunostimulatory activity. From a series of thirteen modified lipopeptides, the Gly-D-Ser-PEGO-NH_2 derived sequence demonstrated the most potent bioactivity (EC_{50}: 20 nM) and the highest binding affinity (K_i: 25 nM) within TLR2 overexpressing pancreatic tumor cells. The labeled sequence containing a near-infrared (NIR) dye was used to track *in vivo* activity, which was maintained within TLR2 overexpressing pancreatic mice xenografts. These studies elegantly demonstrated the ability of the IPs to bind selectively to the TLR2 and stimulate immunostimulatory activity of the antigen specific CD8+ T cells, which were capable of recognizing and killing the targeted tumor cells.

In a related example, a 20-amino acid MUC1 glycopeptide with a Gal-*N*-Ac-*O*-Thr residue was incorporated within a lead TLR ligand by a combination of solid phase glycopeptide synthesis and the azide-alkyne Huisgen cycloaddition reaction.[11] The latter facilitated conjugation of the palmitate-derived cysteine, Pam_3Cys, residue to the glycopeptide sequence. A nanoparticle formulation was then prepared by combining L-rhamnose-cholesterol conjugates tethered to a tetra(ethylene)glycol linker with 1,2-dipalmitoyl-*sn*-glycero-3-phosphocholine (DPPC) and the lead palmitate glycopeptide sequence. This nanoparticle formulation showed a >8-fold increase in antibody titers in comparison to the control mice groups that did not receive treatment. This nanoparticle formulation displayed active antigenic epitope components that may potentially serve as a cancer vaccine formulation.

The multiple antigen presenting peptides (MAPs) have gained some of the most widespread uses in cancer vaccine applications.[12] Pioneered by Tam in the late 1980s to off-set the poor immunogenicity of single peptide vaccine units, the MAPs traditionally incorporated a Lys residue that was used for the introduction of multiple antigenic peptide epitopes which enhanced inflammatory responses.[13] In a recent study, two B-cell and a T-cell epitope peptides were ligated by a maleimide-thioether conjugation strategy to afford the branched MAP system.[14] (**Figure 1.2**) The branched MAP displayed greater proteolytic stability, enhanced antibody titers and T cell stimulation over the linear peptide counterparts. The superior biological activity of the branched *vs.* linear peptides was attributed to the multiple antigen presentation which synergized inflammatory responses and enhanced resistance towards degradation which extended its duration of action. Most recently, Pachymodulin, a new hexapeptide sequence (SSLSKL) was isolated from the Mexican frog *Pachymedusa dacnicolor* and shown to favor leukocyte migration through the binding and activation of the *N*-formyl peptide receptor 2 (FRP2).[15] Migration of human

neutrophils, monocytes and T cells resulted from binding Pachymodulin (10 μM) to FRP2, which stimulated a $G_{i\alpha}$ protein coupled receptor (GPCR) signaling cascade that increased calcium flux, activated the mitogen-activated protein kinase (MAPK) and the extracellular regulated kinase (ERK) pathways. Inflammatory responses were also observed *in vivo*, upon peptide injections (40 mg, three-times daily) in saline (150 mM) solution. Following 24 h post-treatment, the number of monocytes, macrophages and neutrophils were elevated in the peritoneal cavity and in the blood according to flow cytometry analyses relative to the saline treated control group. This new lead peptide may also exhibit promising immunotherapy responses within a tumor microenvironment.

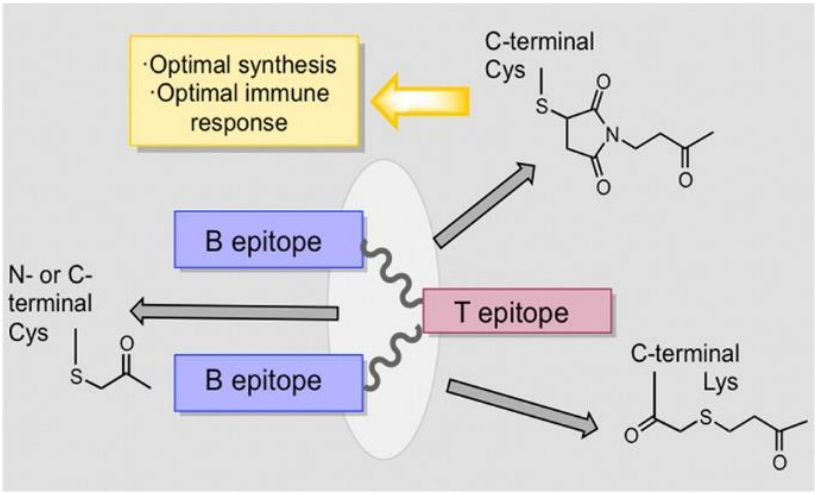

Figure 1.2. Multimeric presentation of peptidic epitopes targeting B and T cells, resulting in a peptide vaccine. Figure adapted from *Bioconjug. Chem*. **2013**, *24*, 578-585.[14]

The discovery of the immunomodulator, prothymosin alpha (ProTα) has been found to trigger potent anti-cancer responses by activating CD8+ T-cell lymphocytes.[16] Its immunostimulatory activity was found to be associated with the *C*-terminal decapeptide sequence, proTα(100-109) which activated the TLR on antigen presenting tumor cells.[17] This peptide sequence (25 ng/mL) triggered cytotoxic K562 tumor cell line activity *in vitro* and a reduction in tumor volume in mice

xenografts due to immune responses which favored the stimulation and expansion of anti-cancer effector cells. Thus, IPs have been proven to be viable candidates in a variety of tumor immunotherapy approaches. This is based on their desirable pharmacological properties which includes, aqueous solubility, serum stability, potent immunogenicity and effective tissue penetration for *in vivo* activity.[18]

It has been established that NK cells play a pivotal role in tumor detection and immunotherapy.[27-34] Representatively, the TAA-SP derived from the heat shock chaperone protein of 70 kilodalton (Hsp70) has been found to activate and expand NK cells towards potent tumor-targeted immunotherapy responses.[35,39] Peptide scanning revealed an *N*-terminal 14 amino acid sequence (TKDNNLLGRFELSG) capable of stimulating NK cell cytolytic activity at 10 mg/mL.[35] Antibody and peptide blocking analyses identified CD94 as the activating NK cell receptor responsible for Hsp70 mediated cytolytic activity by granzyme B-mediated apoptosis.[36,37] Further *in vivo* studies demonstrated that after *ex vivo* stimulation of NK cells with the Hsp70 peptide and IL-2, reinfusion of the activated NK cells into $Hsp70^{+}$ colon carcinoma bearing mice resulted in significant tumor weight reduction.[38] Moreover, a phase I clinical trial validated that reinfusion of *ex vivo* stimulated human NK cells with a combination of Hsp70 peptide and IL-2 into patients with colorectal and non-small cell lung cancer (NSCLC) was safe and well tolerated setting the stage for phase II clinical trials.[39] Thus, activated and expanded NK cells by the TAA-SP have proven to be a safe, well tolerated and clinically effective treatment regimen in cancer immunotherapy.

1.4 B7H6: A PROMISING LIGAND FOR ACTIVATING NK CELLS FOR CANCER IMMUNOTHERAPY

1.4.1 NKp30: A MEMBER OF THE NCR FAMILY AND ITS ROLE IN IMMUNOSURVAILANCE AND NK CELL ACTIVATION

Natural Killer (NK) cells are a class of cytotoxic lymphocytes that own the ability to rapidly eliminate transformed or infected cells upon activation and without prior sensitization.[19,20] It has been established that deficiencies in NK cell population, impaired expression or blocking of their activating receptors, gives rise to the spontaneous development of tumors and hematological malignancies.[21-23] Alternatively, infiltration of NK cells into tumors has been associated with potent cancer cell death effects and immunosurveillance which mitigates tumor recurrence and metastasis.[24-26] NK cells play a pivotal role in cancer immunosurveillance through recognition of major histocompatibility complex MHC class I molecules on target cells by inhibitory receptors of the KIR family, thus preventing NK cell activation.[40] NK cell activation requires the formation of a synapse between the NK cell and the target cells. This recognition site occurs when an inhibitory signal is absent, also known as recognition of 'missing self', in addition to the engagement of its cell surface expressed activating receptors.[41] (**Figure 1.3**) Activation of NK cell triggers the secretion of cytokines such as TNF-α and IFN-γ, and results in effective cytolytic activity against virus infected cells and transformed cells. NK cells also play a key role in maturing dendritic and pancreatic β-cells.[42] For example, NK cells express a wide variety of activating receptors; including the natural-killer group 2 member D (NKG2D), the activating killer immunoglobulin-like receptors (KIRs), DNAM-1, and the non-homologous Ig-like superfamily known as the natural cytotoxicity receptor family (NCRs), which includes NKp46 (NCR1, CD335), NKp44 (NCR2, CD336), and NKp30 (NCR3, CD337).[43] Unlike other receptors, NCRs are expressed only on NK cells and contain multiple interaction sites within their ectodomains. These binding sites facilitate recognition of a variety of structurally different ligands, such as

HSPG, BAT3, MLL5.[44] Moreover, even when most of the NCR ligands are pathogen derived, reduced expression or blockage of the NCRs results in significantly reduced efficiency of malignant cell killing and increased resistance of cancerous cells. These combined effects suggests NCRs play a critical role in cancer immunosurveillance and antitumor activity.[45] All activating NCR signaling pathways require the association to an immunoreceptor tyrosine based activating motif (ITAM) bearing molecule.[46] (**Figure 1.4**) Upon association of the NCR to the adaptor protein in the corresponding transmembrane segments, SCR-family kinase-mediated phosphorylation of the tyrosine motifs within the ITAM molecule initiates a phosphorylation signaling cascade. This signaling pathway results in cytoskeletal reorganization, degranulation, secretion of cytokines and chemokines via Ca^{2+} flux, including IL-2, TNF-α, INF-γ, granzyme B and perforin which ultimately lead to NK -dependent malignant cell death [47,48,49]

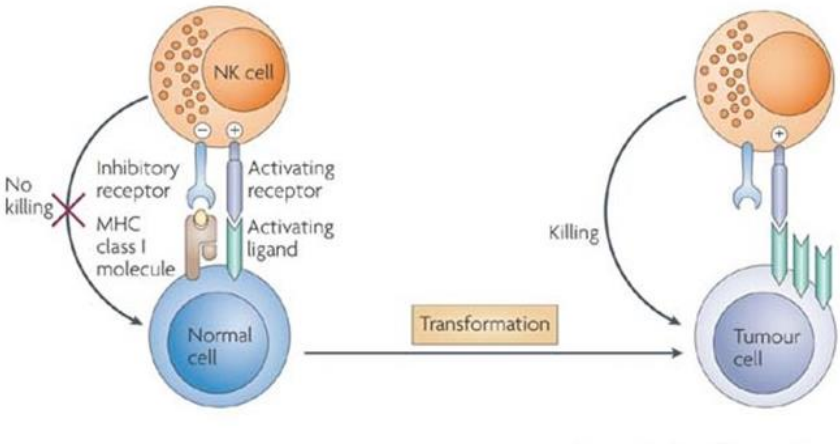

Figure 1.3. NK cell activation by recognition of "missing self". Figure adapted from *Nat. Rev. Immunol*. **2007**, *7*, 329-339.[25]

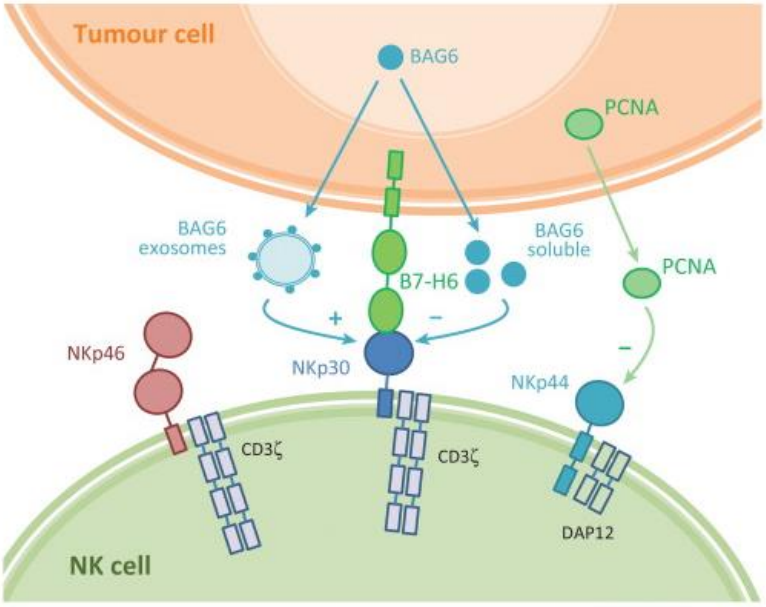

Figure 1.4. Schematic representation of the NCR family members and their associated ligands. Figure adapted from *Trends Immunol.* **2013**, *34*, 182-191.[47]

Importantly, NKp30 has been determined to be a dominant activating receptor involved in the lysis of various primary tumor cell lines by both, resting and activated NK cells.[(41)] The 30-kDa activating receptor is a type I transmembrane protein, with an extracellular IgV-like ligand-binding domain that contains a short α-helical stalk region, a transmembrane domain, and a short intracellular domain that lacks functionality.[(42)] Upon binding to its activating receptors, an arginine residue located in the transmembrane region of NKp30 associates with an aspartic acid in the ITAM adaptor protein domain,.[(50)] (**Figure 1.5**) When engaged with an inhibitory ligand, like the protein pp65 of HCMV and vaccinia virus haemagglutinin (HA), the transmembrane region of NKp30 dissociates form the CD3ζ chain, resulting in NK cell inhibition and pathogen immune escape.[(51)] NK cells also engage in immunosurveillance through recognition of activating cellular derived ligands. NKp30 recognizes cell membrane localized antigens, like the BCL-2 associated

athanogene 6 (BAG6, also known as HLA-B- associated transcript 3 or BAT3) present on immature dendritic cells and stressed cells, heparin sulfate, and the recently discovered plasma membrane protein B7H6, expressed on malignantly transformed tumor cells and activated monocytes and neutrophils.[48-51] Thus, B7H6 has been found to play a pivotal role in tumor immunosurveillance and triggering the inflammatory response during infectious and/or malignant conditions.[48,52-54] The stalk domain and the glycosylation status of NKp30 modulates its ligand-binding properties and regulates NK cells' cytotoxicity.[55] Notably, a recent study revealed that the human NKp30 gene encodes six different variants, three of which produce V-type Ig extracellular domains (*a, b, c*). In this case study, isoform *a* and *b* transmit immunostimulatory T_H1 cytokine production, and isoform *c* promotes immunosuppressive secretion of IL-10.[56]

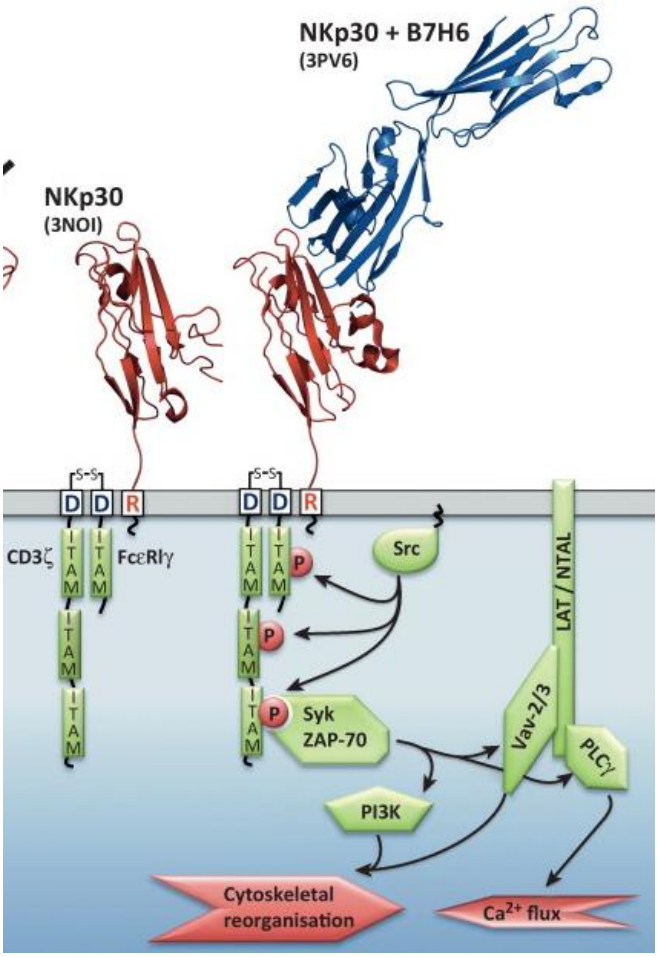

Figure 1.5. Schematic representation of NKp30 and the phosphorylation signaling pathway when bound to it cellular ligand B7H6. Figure adapted from *Trends Immunol.* **2013**, *34*, 182-191.[47]

1.4.2 B7H6: A TUMOR LIGAND OF NKP30

B7H6, a 51 kDa protein and member of the B7 family, was recently identified as a ligand of NKp30. Its sequence was revealed by chemical cross-linking studies, followed by tryptic digestion, tandem mass spectrometry and proteomic analyses of the leukemia cell line K562 with the soluble NKp30-Fc fusion protein.(57) The transmembrane proteins of the B7 family, B7H6 included, have two extracellular Ig domains encoded by exons with adjacent phase 1 introns. These sequences contribute to the regulation of the immune responses through co-stimulatory and co-

inhibitory signals.[58] B7H6, is considered a tumor specific antigen because it was found to be constitutively expressed on the surface of malignantly transformed tumor cells but not on healthy cells. This observation has been confirmed experimentally by quantitative reverse transcription polymerase chain reaction QRT-PCR of B7H6 mRNA, gene microarray analysis, and protein expression of normal tissues and transformed tumor cells. [48] The absence of B7H6 mRNA on normal tissues and its abundance on the surface of several tumor types, including T- and B-cell lymphomas, melanomas and carcinomas, suggests the expression is mediated by tumor transformation. [48] Moreover, it was recently reported that B7H6 evolved as a damage-associated molecular marker to initiate innate immunity against malignantly transformed or stressed cells.[59]

Interestingly, the intracytoplasmic region of B7H6 contains various signaling domains, suggesting a role in response induction on NK cell targets. [49] The extracellular region of B7H6 comprises two immunoglobulin-like domains with several potential N-glycosylation sites.[48] According to surface plasmon resonance (SPR) experiments between a recombinant Fc fusion form of B7H6 and NKp30, B7H6-Fc demonstrated binding to NKp30-Fc (K_D = 1.0 ± 0.2 x10^{-6} M). No binding was detected with CTLA-4 or any other members of the CD28 family that share homology to NKp30, nor with any other NK cell-activating receptors. Additionally, no binding of NKp30-Fc with any other members of the B7 family could be detected, especially the closest B7H6 homologs B7-H1 and B7-H3, suggesting selective binding between B7H6 and NKp30.[48,57] Moreover, the binding interactions in between the soluble B7H6-Fc with the NKp30-Fc fusion protein were abolished in the presence of the anti-NKp30 mAbs (1849 and AZ20), known to block NKp30-dependent cell activation.[48] Furthermore, murine T cells expressing a chimeric receptor of NKp30 fused with CD3ζ were capable of secreting IL-2 upon exposure to B7H6 expressing cells, but not when exposed to B7H1 expressing cells. The levels of IL-2 were significantly

reduced when in the presence of blocking anti-NKp30 mAb F(ab')$_2$ or B7H6 antiserum. Additionally, these B7H6 expressing cells were susceptible to cytolysis by primary NK cells and the human derived NK-92 cell line, and this effect was abolished in the presence of soluble NKp30-Fc.[48] Additionally, downregulation or shedding of B7H6 on tumor cells was shown to reduce NKp30 dependent effector functions of the NK cells.[60,63] Interestingly, neither B7H6 nor NKp30 orthologues exist in mice.[59]

1.4.3 B7H6 BINDING INTERACTION WITH NKp30

As a member of the B7 family, B7H6 is composed of distal *N*-terminal V-like domains and a proximal C-like domain, where the *N*-terminal is sufficient for NKp30 recognition.[61] The V-like domain of B7H6 contains two antiparallel β-sheets, two potential *N*-glycosylation sites, and the NKp30 receptor binding site. The active site is located at the front β-sheet where amino acid residues located in the GFCC' strand and loops BC, C'C" and FG engage in receptor binding. The crystal structure analyses of the B7H6:NKp30 binding interface also revealed a 1:1 ligand:receptor stoichiometry in an antibody-type structure. [57] This stable complex is based on twelve NKp30 amino acid residues bound to eleven B7H6 residues through predominantly stable hydrophobic interactions. These non-covalent bonding interactions are complimented by 16 van der Waals contacts (Thr127 and Pro128 in B7H6), 2 hydrogen bonding interactions (B7H6 Thr127 Oγ-N NKp30 Gly51 and B7H6 Pro128 O-N NKp30 Val53) and one salt bridge (B7H6 Lys130 Nζ-Oε NKp30 Glu113), with no bound water at the binding interface.[57] (**Figure 1.6**) Shape correlation statistic calculations demonstrated that the binding interface is characterized by high-shape complementarity (S_c value of 0.77), characterized also by the exclusion of bulk solvent. [57] Furthermore, superposition of the V-like domain of the bound and un-bound form of B7H6 to

NKp30 demonstrated structural adjustment of the C'C", BC and FG loops of B7H6 to avoid steric hindrance, as well as a shift in B7H6 Gly83 towards NKp30 active site for binding contact. Ultimately, these interactions contributed to selective B7H6:NKp30 binding and activation of NK cells. In spite of its immunostimulatory activity, B7H6 retains moderate NKp30 binding affinity, limited stability and bioavailability which hinders its therapeutic efficacy. [57]

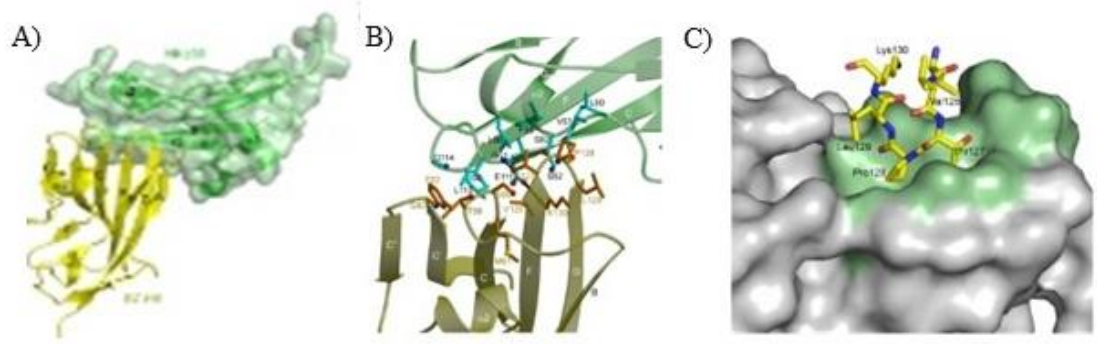

Figure 1.6. The NKp30-B7H6 binding interface. A) Docking mode of NKp30 (green) bound to B7H6 (yellow), B) Stereo view of NKp30 (green) bound to B7H6 (orange) with interacting residues in ball and stick representation, C) NKp30 molecular surface (grey) bound to residues 125-130 of the FG loop of B7H6 in stick format. Figure adapted from *J. Exp. Med.* **2011**, *208*, 703-714.[57]

1.4.7 APPLICATIONS IN CANCER IMMUNOTHERAPY

As a cancer cell biomarker, B7H6 could be an interesting target for selective NK-cell mediated immunotherapy approaches with a comprehensive understanding of the biological mechanisms underlining its modulation. Recently, it was discovered that the class I-specific histone deacetylases inhibitors (HDACi), regulate gene expression by inhibiting enzymes that remove acetyl groups in the promoter regions of histone and non-histone proteins, causing downregulation of B7H6 expression on hematological and solid tumors.[60] Additionally, qRT-

PCR and protein expression studies, along with pharmacological inhibition of transcription factors (TFs) associated with tumorigenesis, revealed that regulation of B7H6 expression in tumor cells is related to the proto-oncogene Myc. Myc proteins in complex with Myc-associated factor X (Max), bind to defined DNA sequences (enhancer boxes, E-boxes) and activate transcription of certain target genes.[62] Silencing of c-Myc or N-Myc led to downregulation of B7-H6 on many primary tumors, including hepatocellular carcinomas, lymphomas and neuroblastomas. Therefore, targeting B7H6 could be a promising target for NK cell mediated immunotherapy on Myc-driven tumors.

Furthermore, a study for posttranscriptional modifications regulating B7H6 expression on tumor cells revealed that some tumors express comparably high levels of B7H6 mRNA but low protein levels on the cell membrane (**Figure 1.7**).[63] According to Western blot and ELISA analyses of concentrated supernatants of different types of harvested tumor cell cultures; the glycosylated ectodomain of B7H6, containing an *N*-terminal myc-tag, was found to be released from the cell surface of tumor cells.[63] Moreover, reduced levels of soluble B7H6 in concentrated supernatants of tumor cell cultures incubated with batimastat or G1254023X, two metalloprotease inhibitors. Alternatively, elevated surface levels of B7H6 was detected in cells transfected with different metalloprotease siRNAs, suggested proteolytic shedding driven by the metalloproteases "a disintegrin and metalloproteases" ADAM-10 and ADAM-17.[63] Finally, soluble B7H6 is not responsible for modulating the expression of the corresponding receptor on NK cells. This was demonstrated by surface expression of NKp30 in NK92-CI cells incubated in concentrated supernatant of tumor cells. Upregulation of membrane B7H6 expression improved recognition and degranulation of NK92-CI cells.[63]

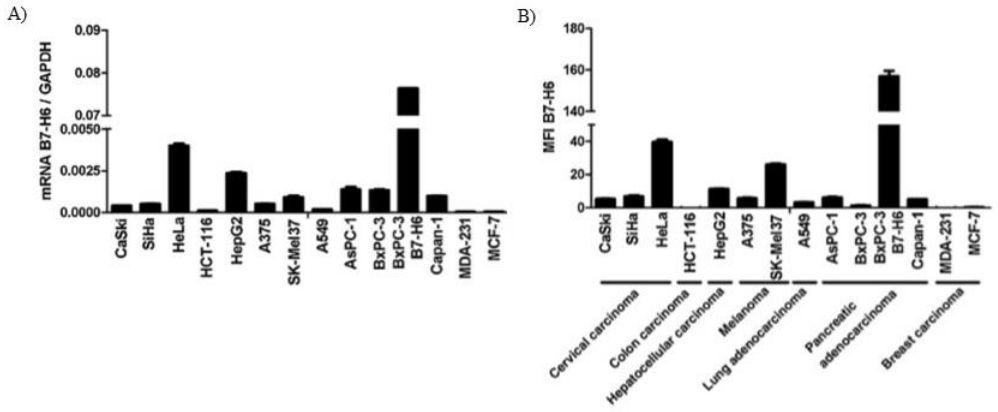

Figure 1.7. Analysis of a) B7H6 mRNA and b) B7H6 cell surface expression on different tumor cell lines. Figure adapted from: *Cancer Res*., **2014**, *74*, 3429-3440.[63]

In an effort to develop new B7H6 derived immunotherapy methodologies, a novel immunoligand composed of a recombinant fusion protein of a CD20-specific single chain fragment variable (scFv) and the extracellular domain (ECD) of B7H6, namely B7H6:7D8, was successfully expressed in eukaryotic cells, deglycosylated and purified by affinity chromatography (**Figure 1.8**).[(64)] The immunoligand B7H6:7D8 demonstrated the ability to crosslink $CD20^+$ cancer cells with NK cells. This binding interaction resulted in activation and degranulation of NK cells as measured by the expression of the early inducible activation marker CD69, surface exposure of the degranulation marker CD107a (LAMP-1), and production of the inflammatory cytokines TNF-α and IFN-γ.[(64)] The binding activity of the immunoligand was confirmed by flow cytometry which demonstrated exclusive binding to CD20 presenting tumor cells, and to the soluble NKp30-Fc receptor.[(64)] Alternatively, genetically modified primary T-cells with a tumor targeting chimeric antigen receptor (CARs) composed of the extracellular domain of NKp30 (chNKp30), fused to the transmembrane and signaling domains of CD3ζ, have been developed.[(65)]

The chimeric NKp30 transduced human T cells responded to $B7H6^+$ tumor cells, resulting in measurable responses of INF-γ secretion which ultimately resulted in tumor cell death. [65]

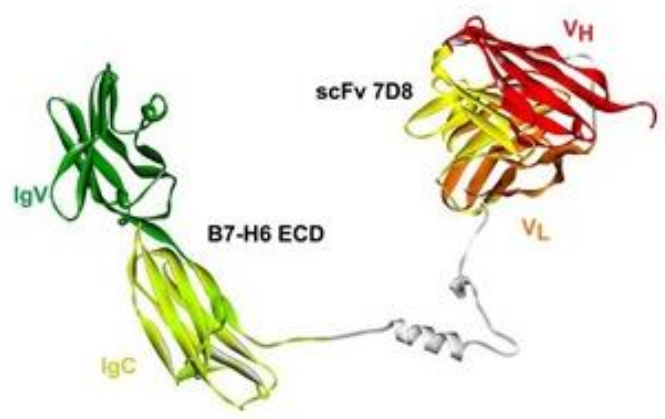

Figure 1.8. Ribbon structure of the recombinant B7H6:7D8. Figure adapted from: *J. Immunol*., **2012**, *189*, 5037-5046.[64]

1.5 Pep42: A GRP78 SELECTIVE PEPTIDIC LIGAND

The discovery of peptide ligands, and their cyclic analogs, that can selectively target cancer cells have led to more efficient delivery of drug payloads while reducing the harmful side effects in cancer patients.[66,67] In an effort to identify novel peptidic ligands, a series of cyclic peptides generated by the phage-display bio-panning methodology was proven successful for the isolation of peptidic ligands which targeted and penetrated human melanoma Me6652/4 tumor cells.[68] DNA sequencing of the bound phages revealed that a 13-mer cyclic peptide, composed of CTVALPGGYVRVC-$CONH_2$ and designated Pep42, bound selectively to Me6652/4 tumor cells (**Figure 1.9**).[69] Interestingly, confocal laser scanning microscopy and flow cytometry analyses of the fluorescently labeled Pep42 sequence revealed that the cyclic Pep42, but not its linear structure, bound and internalized selectively in cancer cells through receptor-mediated endocytosis.[69]

Additional photoaffinity cross-linking and antibody uptake inhibition studies identified the glucose regulated protein of 78 kilodaltons (GRP78), as the cancer cell surface membrane expressed receptor responsible for selective binding and internalization of Pep42.[69] Interestingly, Pep42 binds to recombinant GRP78 but not to recombinant HSP70, another member of the HSP family that shares a high degree of sequence homology.[70] Furthermore, flow cytometry and photoaffinity labeling studies on HepG2 and HDFa cells revealed that Pep42 binds selectively to cell surface localized GRP78 on primary tumor cells. The binding was significantly diminished in the presence of the blocking anti-GRP78 polyclonal antibodies or when cells were treated with GRP78-specific siRNA for gene knockdown. This studies confirmed GRP78 as the cancer-cell molecular target for the peptidic ligand Pep42.[68,69] The capability of Pep42 to induce cancer-cell targeted cytotoxicity was evaluated *in vitro* using a Pep42 derivative conjugated to an apoptosis-inducing peptide, D-(KLAKLAK)$_2$. Pep42-D-(KLAKLAK)$_2$-mediated cytotoxicity was dependent on the cell surface expression of GRP78 and was significantly reduced when GRP78 expression was downregulated with GRP78 siRNA.[69] More importantly, Pep42 has significant tumor homing capabilities *in vivo*, as revealed in studies with xenograph mice, highlighting the promising capabilities of Pep42 as a cancer targeted drug-delivery vector.[69]

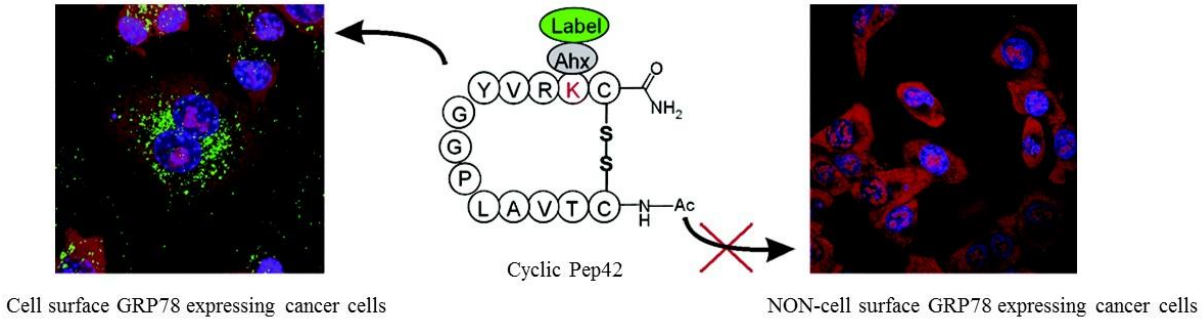

Figure 1.9. Sequence of Pep42 and GRP78 specificity within Me6652/4 tumor cells.

Figure adapted from: *Biochemistry*, **2006**, *45*, 9434-9444.[68]

In normal cells, the 78 kDa member of the heat shock family HSP70 namely GRP78, is localized in the endoplasmic reticulum (ER). It plays a key role as an intracellular chaperone protein regulating protein folding events as part of the unfolded protein response (UPR), thus mediating protective cellular responses during stress conditions.[70] Interestingly, under malignant transformation, GRP78 is overexpressed and cell membrane localized in cancer cells, where it exhibits a pivotal role in tumor initiation, progression, metastatic events, and drug resistance.[71-73,] More importantly, GRP78 has been found to be expressed in plasma membrane of cancer cells but not in normal cell, thus making it a good target for selective cancer therapy approaches.[74,75]

1.6 THESIS RESEARCH OBJECTIVES

1.6.4 B7H6 DERIVED PEPTIDES

B7H6 was recently discovered as a cell surface protein uniquely expressed in tumor cells. B7H6 is also a ligand for NKp30, a receptor expressed constitutively on all resting and activated NK cells. Upon B7H6-NKp30 binding, B7H6 triggers NKp30 dependent NK cell activation, resulting in the release of cytokines and chemokines that ultimately leads to tumor cell lysis and death. In an effort to develop novel and effective immunotherapy approaches, the rational design, synthesis, characterization and biological evaluation of a novel class of immunostimulatory peptides (IPs) is described in Chapter 2.

Towards this goal, the rational design of a small library of synthetic peptides derived from the crystal structure analysis of the B7H6-NKp30 binding interface is described. The methodology for the Fmoc-based solid phase peptide synthesis, the introduction of fluorescent tags (FITC), and the characterization methodologies of the library of peptides by LCMS, RP HPLC, and CD spectroscopy, are also outlined.

With pure peptides in hand, analyses of the binding interactions of the synthetic FITC labeled peptides for the NKp30 receptor expressed on the surface of NK92-MI cells were accomplished by flow cytometry. The capabilities of the non-labeled peptides to induce NK92-MI cells' immunostimulatory responses was also assessed via the release of the inflammatory cytokines, TNFα and INFγ by an enzyme-linked immunosorbent assay (ELISA). Moreover, the cytotoxicity of the synthetic peptides was also evaluated by flow cytometry, to determine the therapeutic applicability of the IPs.

1.6.5 Pep42 DERIVED PEPTIDES

Chapter 3 of this thesis describes the relevance of Pep42 and its biological activity on the GRP78 overexpressing HepG2 liver cancer cells. These experiments have served to validate the HepG2 cells as a good model cell line to test the biological activities of the Pep42 derived peptides. The optimized Fmoc-solid phase synthetic methodology of Pep42 and the characterization methodologies using LC/MS and RP-HPLC are outlined and described in this chapter. Also described are orthogonal synthetic methods for Pep42 activation for bio-conjugation onto bio-active proteins such as B7H6. Moreover, the relevance of the Pep42 secondary structures, determined by CD spectroscopy, on their biological activity is also highlighted in this chapter.

1.6.6 B7H6-Pep42 DERIVED BIOCONJUGATES

Tumor associated antigens (TAAs) are a class of protein biologics that are rapidly emerging in cancer immunotherapy strategies. Characteristically, B7H6 has been identified as a TAA uniquely localized on the cell surface of transformed cells. B7H6 binds selectively to the NKp30 receptor, a family member of the NCRs located on resting and activated NK cells. It was also

recently discovered that tumor cells escape immunosurveillance by shedding B7H6, therefore impeding NK-mediated recognition and activation. To overcome this resistance mechanism, the development of new B7H6 derived ligands that may effectively target NKp30 and activate NK cells towards B7H6 deficient tumors is proposed in Chapter 4 of this thesis. In this new immunotherapy approach, a novel class of B7H6-Pep42 derived cancer-targeting immunostimulatory protein-peptide conjugates (CTIPPC) that may potentially mimic the targeting and effector functions of antibodies is described.

1.7 REFERENCES

1. Harris, T.J.; Drake, C.G. *J. Immunother. Cancer* **2013**, *1*, 1-9.

2. Kantoff, P.W.; Higano, C.S.; Shore, N.D.; Berger, E.R.; Small, E.J.; Penson, D.F.; Redfern, C.H.; Ferrari, A.C.; Dreicer, R.; Sims, R.B.; Xu,Y.; Frohlich, M. W.; Schelhammer, P.F. *N. Engl. J. Med.* **2010**, *363*, 411-422.

3. Matsueda, S.; Graham, D.Y. *World J. Gastroenterol*., **2014**, *20*, 1657-1666.

4. Nishimura, Y.; Tomita, Y.; Yuno, A.; Yoshitake, Y.; Shinohara, M. *Cancer Sci*. **2015**, *106*, 505-511.

5. Verma, S.; Miles, D.; Gianni, L.; Krop, I.E.; Welslau, M.; Baselga, J.; Pegram, M.; Oh, D.Y.; Diera, V.; Guardino, E.; Fang, L.; Lu, M.W.; Olsen, S.; Blackwell, K. *N. Engl. J. Med*. **2012**, *367*, 1783-1791.

6. Rosenberg, S.A.; Yang, J.C.; Restifo, N.P. *Nat. Med*. **2004**, *10*, 909-915.

7. Kim, J.W.; Gulley J.L. *Expert Opin. Biol. Ther.* **2012**, *12*, 463-478.

8. Huynh, A.S.; Chung, W.J.; Cho, H.; Moberg, V.E.; Celis, E.; Morse, D.L.; Vagner J. *J. Med. Chem.* **2012**, *55*, 9751-9762.

9. Jin, M.S.; Kim, S.E.; Heo, J.Y.; Lee, M.E.; Kim, H.M.; Paik, S.G.; Lee, H.; Lee, J.O. *Cell* **2007**, *130*, 1071-1082.

10. Mühlradt, P.F.; Kiess, M.; Meyer, H.; Süssmuth, R.; Jung, G. *J. Exp. Med*. **1997**, *185*, 1951-1958.

11. Sarkar, S.; Salyer, A.C.; Wall, K.A.; Sucheck, S.J. *Bioconjug. Chem.* **2013**, *24*, 363-375.

12. Fujita, Y.; Taguchi, H. *Chem. Cent. J.* **2011**, *5*, 1-8.

13. Tam, J.P. *Proc. Natl. Acad. Sci.* **1988**, *85*, 5409-5413.

14. Monsó, M.; de la Torre, B.G.; Blanco, E.; Moreno, N.; Andreu, D. *Bioconjug. Chem*. **2013**, *24*, 578-585.

15. Lacombe, C.; Piesse, C.; Sagan, S.; Combadière, C.; Rosenstein, Y.; Auvynet, C. *J. Med. Chem.* **2015**, *58*, 1089-1099.

16. Ioannou, K.; Samara, P.; Livaniou, E.; Derhovanessian, E.; Tsitsilonis, O.E. *Cancer Immunol. Immunoter*. **2012**, *61*, 599-614.

17. Voutsas, I.F.; Pistamaltzian, N.; Tsiatas, M.L.; Skopeliti, M.; Katsila, T.; Mavrothalassiti, I.; Spyrou, S.; Dimopoulos, M.A.; Tsitsilonis, O.E.; Bamias, A. *Eur. J. Cancer*, **2013**, *49*, 1706-1714.

18. Bhutia, S.K.; Maiti, T.K. *Trends Biotechnol.* **2008**, *26*, 210-217.

19. Vivier, E.; Tomaselo, E.; Baratin, M.; Walzer, T.; Ugolini, S. *Nat. Immunol*. **2008**, *9*, 503-510.

20. Waldhauer, I.; Steinle, A. *Oncogene* **2008**, *27*, 5932-5943.

21. Kaplan, D.H.; Shankaran. V.; Dighe. A.S.; Stockert. E.; Aguet. M.; Old. L.J. *Proc. Natl. Acad. Sci.* **1998**, *95*, 7556-7561.

22. Shankaran. V.; Ikeda. H.; Bruce. A.T.; White. J.M.; Swanson. P.E.; Old. L.J. *Nature* **2001**, *410*, 1107-1111.

23. Kim, S.; Iizuka, K.; Aguila, H.L.; Weissman,I.L.; Yokoyama, W.M. *Proc. Natl. Acad. Sci.* **2000**, *97*, 2731-2736.

24. Villegas. F.R.; Coca, S.; Villarrubia, V.G.; Jimenez, R.; Chillon, M.J.; Jareno, J.; Zuil, M.; Callol, L. *Lung Cancer* **2002**, *35*, 23-28.

25. Ljunggren, H.G.; Malmberg, K.J. *Nat. Rev. Immunol*. **2007**, *7*, 329-339.

26. Langers, I.; Renoux, V.M.; Thiry, M.; Delvenne, P.; Jacobs, N. *Biologics*. **2012**, *6*, 73-82.

27. Cheng, M.; Chen, Y.; Xiao, W.; Sun, R.; Tian, Z. *Cell Mol. Immunol*. **2013**, *10*, 230-252.

28. Swann. J.B.; Smyth. M.J. *J. Clin. Invest*. **2007**, *117*, 1137-1146.

29. Dunn, G.P.; Ikeda, H.; Bruce, A.T.; Koebel, C.; Uppaluri, R.; Bui, J.; Chan, R.; Diamond, M.; White, J.M.; Sheehan, K.C.; Schreiber, R.D. *Immunol. Res*. **2005**, *32*, 231-45.

30. Cheng, M.; Zhang, J.; Tian, Z. *Front Med*. **2012**, *6*, 56-66.

31. Klingemann, H.; Boissel, L. *Horm. Metab. Res*. **2008**, *40*, 122-125.

32. Eguizabal, C.; Zenarruzabeitia, O.; Monge, J.; Santos, S.; Vesga, M.A.; Maruri, N.; Arrieta, A.; Riñón, M.; Tamayo-Orbegozo, E.; Amo, L.; Larrucea, S.; Borrego, F. *Front Immunol*. **2014**, *5*, 1-10.

33. Farag, S.S.; Fehniger, T.A.; Becknell, B.; Blaser, B.W.; Caligiuri, M.A. *Expert Opin. Biol. Ther*. **2003**, *3*, 237-250.

34. Srivastava, S.; Lundqvist, A.; Childs, R.W. *Cytotherapy*. **2008**, *10*, 775-783.

35. Multhhoff, G.; Pfister, K.; Gehrmann, M.; Hantschel, M.; Gross, C.; Hafner, M. *Cell Stress Chaperones.* **2001**, *6*, 337-344.

36. Gross, C.; Hansch, D.; Gastpar, R.; Multhhoff, G. *Biol. Chem*. **2003**, *384*, 267-279.

37. Gross, C.; Koelch, W.; DeMaio, A.; Arispe, N.; Multhhoff, G. J. *Biol. Chem*. **2003**, *278*, 41173-41181.

38. Moser, C.; Schmidbauer, C.; Gurtler, U.; Gross, C.; Gehrmann, M.; Thonigs, G. *Cell Stress Chaperones*. **2002**, *7*, 365-373.

39. Specht, H.M.; Ahrens, N.; Blankenstein, C.; Duell, T.; Fietkau, R.; Gaipl, U.S.; Günther C.; Gunther, S.; Habl, G.; Hautmann, H.; Hautman, M.; Huber, R.M.; Molls, M.; Offner, R.; Rödel, C.; Rödel, F.; Schütz, M.; Combs, S.E.; Multhoff, G. *Frontiers Immunol.* **2015**, *6*, 1-9.

40. Vivier, E.; Raulet, D. H.;Moretta,A.; Caligiuri, A.; Zitvogel, L.; Lanier, L.L.; Yokoyama, W.M.; Ugolini, S. *Science* **2011**, *331*, 44-49.

41. Rak, G.D.; Mace, E.M.; Banerjee, P.P.; Svitkina, T.; Orange, J.S. *PloS Biol.* **2011**, *9*, e1001151.

42. Lanier, L.L. *Annu. Rev. Immunol*. **2005**, *23*, 225-274.

43. Pende, D.; Parolini, S.; Pessino, A.; Sivori, S.; Augugliaro, R.; Morelli, L.; Marcenaro, E.; Accame, L.; Malaspina, A.; Biassoni, R.; Bottino, C.; Moretta, L.; Moretta, A. *J. Exp. Med.* **1999**, *190*, 1505-1516.

44. Seidel, E.; Glasner, A.; Mandelboim, O., *Cell Mol. Life Sci.*, **2012**, *69*, 3911-3920.

45. Fauriat, C.; Just-Landi, S.; Mallet, F.; Arnoulet, C.; Sainty, D.; Olive, D.; Costello, R.T. *Blood* **2007**, *109*, 323-330.

46. Watzl, C.; Long E.O. *Curr. Protoc. Immunol*. **2010**, 1-19.

47. Koch, J.; Steinle, A.; Watzl, C.; Mandelboim, O. *Trends Immunol.* **2013**, *34*, 182-191.

48. Brandt, C.S.; Baratin, M.; Yi, E.C.; Kennedy, J.; Gao, Z.; Fox, B.; Haldeman, B.; Ostrander, C.D.; Kaifu, T.; Chabannon, C.; Moretta, A.; West, R.; Xu, W.; Vivier, E.; Levin, S.D. *J. Exp. Med.*, **2009**, *206*, 1495-1503.

49. Kaifu, T.; Escaliere, B.; Gastinel, L.N.; Vivier, E.; Baratin, M. *Cell Mol. Life Sci*., **2011**, *68*, 3531-3539.

50. Moretta, L. and Moretta A. *EMBO J.* **2004**, *23*, 255-259.

51. Arnon, T.I.; Achdout, H.; Levi, O.; Markel, G.; Saleh, N.; Katz, G.; Gazit, R.; Gonen-Gross, T.; Hanna, J.; Nahari, E.; Porgador, A.; Honigman, A.; Plachter, B.; Mevorach, D.; Wolf, D.G.; Mandelboim, O. *Nat. Immunol*., **2005**, *6*, 515-523.

52. Matta, J.; Baratin, M.; Chiche, L.; Forel, J.M.; Cognet, C.; Thomas, G.; Farnarier, C.; Piperoglou, C.; Papazian, L.; Chaussabel, D.; Ugolini, S.; Vély, F.; Vivier, E. *Blood*, **2013**, *122*, 394-404.

53. Pogge von Strandmann E.; Simhadri, V.R.; von Tresckow, B.; Sasse, S.; Reiners, K.S.; Hansen, H.P.; Rothe, A.; Böll, B.; Simhadri, V.L.; Borchmann, P.; McKinnon, P.J.; Hallek, M.; Engert, A. *Immunity* **2007**, *27*, 965-974.

54. Soriani, A.; Zingioni, A.; Cerboni, C.; Iannitto, M.L.; Ricciardi, M.R.; Di Gialleonardo, V.; Cippitelli, M.; Fionda, C.; Petrucci, M.T.; Guarini, A.; Foà, R.; Santoni, A. *Blood*, **2009**, *113*, 3503-3511.

55. Hartmann, J.; Tran, T.V.; Kaudeer, J.; Oberle, K.; Herrmann, J.; Quagliano, I.; Abel, T.; Cohnen, A.; Gatterdam, V.; Jacobs, A.; Wollscheid, B.; Tampé, R.; Watzl, C.; Diefenbach, A.; Koch J. *J. Biol. Chem.*, **2012**, *287*, 31527-31539.

56. Delahaye, N.F.; Rusakiewicz, S.; Martins, I.; Ménard, C.; Roux, S.; Lyonnet, L.; Paul, P.; Sarabi, M.; Chaput, N.; Semeraro, M.; Minard-Colin, V.; Poirier-Colame, V.; Chaba, K.; Flament, C.; Baud, V.; Authier, H.; Kerdine-Römer, S.; Pallardy, M.; Cremer, I.; Peaudecerf, L.; Rocha, B.; Valteau-Couanet, D.; Gutierrez, J.C.; Nunès, J.A.; Commo, F.; Bonvalot, S.; Ibrahim, N.; Terrier, P.; Opolon, P.; Bottino, C.; Moretta, A.; Tavernier, J.; Rihet, P.; Coindre, J.M.; Blay, J.Y.; Isambert, N.; Emile, J.F.; Vivier, E.; Lecesne, A.; Kroemer, G.; Zitvogel, L. *Nat. Med*., **2011**, *17*, 700-707.

57. Li, Y.; Wang, Q.; Mariuzza, A. *J. Exp. Med.* **2011**, *208*, 703-714.

58. Zou, W.; Chen, L. *Nat. Rev. Immunol*., **2008**, 8, 467-477.

59. Baratin, M. Vivier, E. *Med. Sci*., **2010**, *26*, 119-120.

60. Fiegler, N.; Textor, S.; Arnold, A.; Rölle, A.; Oehme, I.; Breuhahn, K.; Moldenhauer, G.; Witzens-Harig, M.; Cerwenka, A. *Blood*, **2013**, *122*, 684-693.

61. Joyce M.G.; Tran, P.; Zhuravleva, M.A.; Jaw, J.; Colonna, M.; Sun, P.D. *Proc. Natl. Acad. Sci. U S A.* **2011**, *108*, 6223-6228.

62. Textor, S.; Bossler, F.; Henrich, K.O.; Gartlgruber, M.; Pollmann, J.; Fiegler, N.; Arnold, A.; Westermann, F.; Waldburger, N.; Breuhahn, K.; Golfier, S.; Witzens-Harig, M.; Cerwenka, A. *Oncoimmunology*, **2016**, *5*, e1116674.

63. Schlecker, E.; Fiegler, N.; Arnold, A.; Altevogt, P.; Rose-John, S.; Moldenhauer, G.; Sucker, A.; Paschen, A.; von Strandmann, E.P.; Textor, S.; Cerwenka, A. *Cancer Res*., **2014**, *74*, 3429-3440.

64. Kellner, C.; Maurer, T.; Hallack, D.; Repp, R.; van de Winkel, J.G.; Parren, P.W.; Valerius, T.; Humpe, A.; Gramatzki, M.; Peipp, M. *J. Immunol*., **2012**, *189*, 5037-5046.

65. Zhang, T.; Wu, MR.; Sentman, C.L. *J. Immunol.* **2012**, *189*, 2290-2299.

66. Aina, O.H.; Liu, R.; Sutcliffe, J.L.; Marik, J.; Pan, C.X.; Lam, K.S. *Mol. Pharm*. **2007**, *4*, 631-651.

67. Janssen, M.L.; Oyen, W.J.; Dijkgraaf, I.; Massuger, L.F.; Freilink, C.; Edwards, D.S.; Rajopadhye, M.; Boonstra, H.; Corstens, F.H.; Boeman, O.C. *Cancer Res*. **2002**, *62*, 6146-6151.

68. Kim, Y.; Lillo, A.M.; Steiniger, S.C.J.; Liu, Y.; Ballatore, C.; Anichini, A.; Mortarini, R.; Kaufmann, G.F.; Zhou, B.; Felding-Habermann, B.; Janda, K.D. *Biochemistry*, **2006**, *45*, 9434-9444.

69. Liu, Y.; Steiniger, S.C.J.; Kim, Y.S.; Kaufmann, G.F.; Felding-Habermann, B.; Janda, K.D. *Mol. Pharma*., **2007**, *4*, 435-447.

70. Pfaffenbach, K.T.; Lee, A.S. *Curr. Opin. Cell Biol*., **2011**, *23*, 150-156.

71. Su, R.; Li, Z.; Li, H.; Song, H.; Bao, C.; Wei, J.; Cheng, L. *BMC Cancer*, **2010**, *10*, 20.

72. Reddy, R.K.; Mao, C.; Baumeister, P.; Austin, R.C.; Kaufman, R.J.; Lee, A.S. J. Biol. Chem., **2003**, *278*, 20915-20924.

73. Chatterjee, S.; Cheng, M.F.; Berger, R.B.; Berger, S.J.; Berger, N.A. *Cancer Res*., **1995**, *55*, 868-873.

74. Arap, M.A.; Lahdenranta, J.; Mintz, P.J.; Hajitou, A.; Sarkis, A.S.; Arap, W.; Pasqualini, R. *Cancer Cell* **2004**, *6*, 275-284.

75. Joseph, S.C.; Blackman, B.A.; Kelly, M.L.; Phillips, M.; Beaury, M.W.; Martinez, I.; Parronchi, C.J.; Bitsaktsis, C.; Blake, A.D.; Sabatino D. *J. Pept. Sci.* **2014**, *20*, 736-745.

CHAPTER 2: THE DISCOVERY OF B7H6-DERIVED IMMUNOSTIMULATORY PEPTIDES OF LYMPHOCYTIC NK92-MI CELLS

2.1. ABSTRACT

The rise of biologics that can stimulate immune responses towards the destruction of tumors has led to the advancement of cancer-based immunotherapy. B7H6 has been recently identified as an immunostimulatory protein ligand on tumor cells that binds specifically to the NKp30 receptor. Upon binding, NKp30 activation triggers NK cell-derived cytokine release, which ultimately leads to tumor cell lysis and death. In an effort to develop effective immunotherapy approaches, the rational design of a novel class of immunostimulatory peptides (IPs) derived from the binding interface of B7H6:NKp30 is described in this chapter. The IPs are composed of the B7H6 active site sequence for NKp30 binding and immunostimulatory activity. An aminohexanoic acid linker was also introduced at the *N*-terminus of the peptides for FITC-labeling by Fmoc-solid phase peptide synthesis. The peptides were characterized by LCMS to confirm identities and purities >95%. The secondary structures of the peptides were evaluated by CD spectroscopy in H_2O, PBS and a H_2O:TFE mixture which demonstrated flexible peptide structures which adapted to the solvent conditions and were found to transition from random coil (H_2O) to α-helical (PBS) and turn-type (H_2O:TFE) conformations. Their biological properties were then evaluated by flow cytometry, enzyme-linked immunosorbent assays (ELISAs) and cell death assays. The occupancy of the synthetic peptides to a human NK cell line resulted in comparable binding relative to the natural NKp30 ligand, B7H6, and the human anti-NKp30 monoclonal antibody (mAb), in a concentration dependent manner. A competitive binding assay in between the human anti-NKp30 mAb or B7H6, and the synthetic peptides, demonstrated partial displacement of the ligands upon anti-NKp30 mAb treatment, suggesting specific NKp30 receptor

binding by the synthetic peptides. Moreover, the immunostimulatory activity of B7H6 was demonstrated by the secretion of the pro-inflammatory cytokines, tumor necrosis factor-alfa (TNF-α) and interferon gamma (IFN-γ) by the human NK cell line. The immunostimulatory effects of the IPs on the NK cells was assessed by the production of TNF-α alone as IFN-γ was undetectable in our ELISA. In a cell death assay, the IPs were found to be non-toxic, without any observable evidence of early or late stage apoptosis within the NK92-MI cells. Taken altogether, this novel class of synthetic peptides may prove to be a promising lead in the development of a new peptide-based immunotherapy approach, especially against B7H6 expressing tumors.

2.2. INTRODUCTION

Natural Killer (NK) cells are a class of cytotoxic lymphocytes that own the ability to rapidly seek and destroy transformed or infected cells upon activation or without prior sensitization.[1,2] It has been established that deficiencies in NK cell population, impaired expression or blocking of their activating receptors, gives rise to the development of tumors and blood disorders.[3-5] Alternatively, infiltration of NK cells into tumors has been associated with potent cancer cell death effects and immunosurveillance which minimizes tumor recurrence and metastasis, even in the absence of a functional adaptive immune system.[6-8] Therefore, it has been established that NK cells play an important role in tumor detection and immunotherapy.[9-16] Their biological and therapeutic functions are based on a series of activating NK cell receptors. These include the natural-killer group 2 member D (NKG2D), activating KIRs, NKp80, CD94/NKG2C, DNAX accessory molecule (DNAM)-1, 2B4, and the transmembrane immunoglobulin-like natural cytotoxicity receptors (NCRs) NKp30, NKp44, and NKp46.[17,18] Representatively, the NKp30 receptor is a key mediator of NK cell immunostimulatory activity, and is expressed constitutively

on resting and activated NK cells. Activation of the NKp30 receptor stimulates the secretion of pro-inflammatory cytokines and chemokines, and the release of cytotoxic agents such as membrane disrupting proteases that trigger tumor cell lysis and death.[19] Thus, activated NK cells have effectively formed a first line of defense against a wide range of human tumor malignancies leading towards their successful clinical applications in cancer immunotherapy.

In the search for activating NKp30 ligands, chemical cross-linking studies followed by tryptic digestion, tandem mass spectrometry and proteomic analyses of the leukemia cell line K562 with the soluble NKp30-Fc fusion protein revealed B7H6 as a cellular membrane expressed protein ligand of the NKp30 receptor.[20] B7H6 is a 454 amino acid (51 kDa) type I transmembrane protein with an extracellular domain implicated in NKp30 binding and a cytosolic region that is homologous to the GAG polyprotein and involved in signaling activity.[21] Interestingly, B7H6 was found to be expressed on the surface of tumors but not on healthy cells and functions as a bio-marker for NK cell mediated cytotoxicity.[21] In a direct binding assay, B7H6 was found to bind specifically to the NKp30 receptor according to surface plasmon resonance (SPR) ($K_D = 1.0 \pm 0.2$ $x10^{-6}$ M).[20,21] Moreover, the binding interactions in between the soluble B7H6-Fc with the NKp30-Fc fusion protein were inhibited in the presence of the anti-NKp30 mAbs (1849 and AZ20), known to block NKp30-dependent cell activation.[21] Furthermore, downregulation of B7H6 on tumor cells was shown to reduce NKp30 dependent effector functions of the NK cells.[22] It has been previously described that upon binding to its activating ligand, a transmembrane arginine charged residue of NKp30 associates to a negatively charged transmembrane residue of an immunoreceptor tyrosine based activation motif (ITAM)-containing adaptor protein. This includes the disulfide linked homodimers of CD3ζ, which initiates the signaling cascade.[18,21,23] The latter results in the reorganization of the NK cells' cytoskeleton and initiation of Ca^{2+} flux,

that leads to the secretion of inflammatory cytokines such as IL-2, TNF-α, INF-γ, as well as the release of granzyme B and perforin, which trigger tumor cell lysis and death.[19,24,25] The crystal structure analyses of the B7H6:NKp30 binding interface also revealed a 1:1 ligand:receptor stoichiometry. This stable complex was based on twelve NKp30 amino acid residues bound to eleven B7H6 residues through predominantly stable hydrophobic interactions, complemented by van der Waals contacts, hydrogen bonding and salt bridges.[20] These interactions contributed to selective B7H6:NKp30 binding and activation of NK cells. In spite of its immunostimulatory activity, B7H6 exhibits moderate NKp30 binding affinity, limited stability and bioavailability which hinders its therapeutic efficacy.

However, the discovery of the B7H6:NKp30 binding interaction offers a new opportunity in the development of novel NK cell-dependent immunostimulatory ligands. In this study, the design, synthesis and biological evaluation of short peptidic ligands derived from the B7H6:NKp30 binding domain are reported. This new class of IPs may have a potential impact in tumor immunotherapy applications, while overcoming some of the limitations of the high molecular weight biologicals, such as B7H6 or the monoclonal antibodies.

2.3. PROJECT OBJECTIVES

The main effort of this research project is related to the rational design, synthesis, structure characterization, and biological activity of a new class of immunostimulatory peptides (IPs). This research project will be completed by the following objectives.

2.3.1. RATIONAL DESIGN

The crystal structure analysis of the B7H6:NKp30 binding interface revealed 11 amino acids on B7H6 responsible for the binding and activation of the NKp30 receptor.[20] The design of a small library of immunostimulatory peptides was derived from the B7H6 primary sequence and secondary structure amino acid residues that bound to the active site of NKp30. Molecular docking studies will provide further insight into the binding capabilities of this new class of synthetic peptides.

2.3.2. SYNTHESIS AND CHARACTERIZATION

The Fmoc solid phase peptide synthesis (Fmoc-SPPS) method will be employed for the rapid production of the immunostimulatory peptide sequences. Furthermore, this conventional synthetic method may also facilitate the introduction of fluorescein isothiocyanate (FITC) for biological studies. Following peptide synthesis, LCMS will be used to analyze and confirm the identities of the peptides by molecular weight analyses. Peptide purification will be completed by semi-preparative RP HPLC. Circular dichroism spectroscopy will be employed to determine the secondary structures, if any, adopted by the synthetic peptides in a variety of solvent systems.

2.3.3. IN-VITRO BIOLOGICAL ACTIVITY

The binding affinity and specificity of the library of FITC labeled immunostimulatory peptides to NKp30 expressed on NK92-MI cells will be assessed via flow cytometry. Upon binding determination, the capability of the non-labeled peptides to induce an immune response of NK92-MI cells will be assed via the release of TNFα and INFγ. The release of the inflammatory cytokines will be evaluated by an enzyme-linked immunosorbent assay (ELISA). The toxicity of these

synthetic peptides to NK92-MI cells will be assessed by determination of apoptotic events using a Guava Nexin® Reagent.

2.4. RESULTS

2.4.1. DESIGN OF B7H6-DERIVED PEPTIDES.

The rational design of the synthetic peptides was based on the crystal structure of the binding interface of the B7H6:NKp30 ligand:receptor.[20] Residues 125-130 of the FG loop region of B7H6 (VTPLK, **3**) facilitated binding to its receptor by means of sixteen Van der Waals contacts with NKp30 residues. Additionally, two hydrogen bonds (B7H6; Thr127 and Pro128 with NKp30; Gly51 and Val53, respectively) and a salt bridge interaction (B7H6; Lys130 with NKp30 Glu111) contributed to the B7H6:NKp30 binding interaction.[20] Residues 59-62 (TSMG, **2**) found within the BC loop region and 82-83 (FG, **1**) located in the C'C" region of B7H6 complement NKp30 binding predominantly through Van der Waals contacts.[20] The peptide (FGTSMGVTPLK, **4**) was selected based on the primary sequence of B7H6 which bound to the active site of NKp30. Whereas peptide (TSMGFGVTPLK, **5**) was based on the residues bound in the secondary structure of B7H6, which adopted a turn-type geometry at the active site of the NKp30 receptor.[20] Finally, a modified sequence was rationally designed to enhance the binding interactions with NKp30. The peptide (TVPLN, **6**) was derived from the binding site FG loop region of B7H6, but with exchange of the *N*-terminal Thr and Val, and replacement of the *C*-terminal Lys for Asn. These modifications were rationalized to enhance hydrogen bonding and to stabilize the putative turn conformation which contributed to binding in between the B7H6 ligand and the NKp30 receptor.[20] In a molecular docking study in between peptide **6** and the NKp30 binding pocket the turn conformation and H-bonding interactions with the NKp30 Gly51 and Val52 were found to be

conserved (**Figure 2.1**). The designed peptide sequences also contained an aminohexanoic acid (Ahx) linker at the *N*-terminus to facilitate the incorporation of a fluorescein isothiocyanate (FITC) for biological studies (**Table 2.1**, sequences **7**-**12**).

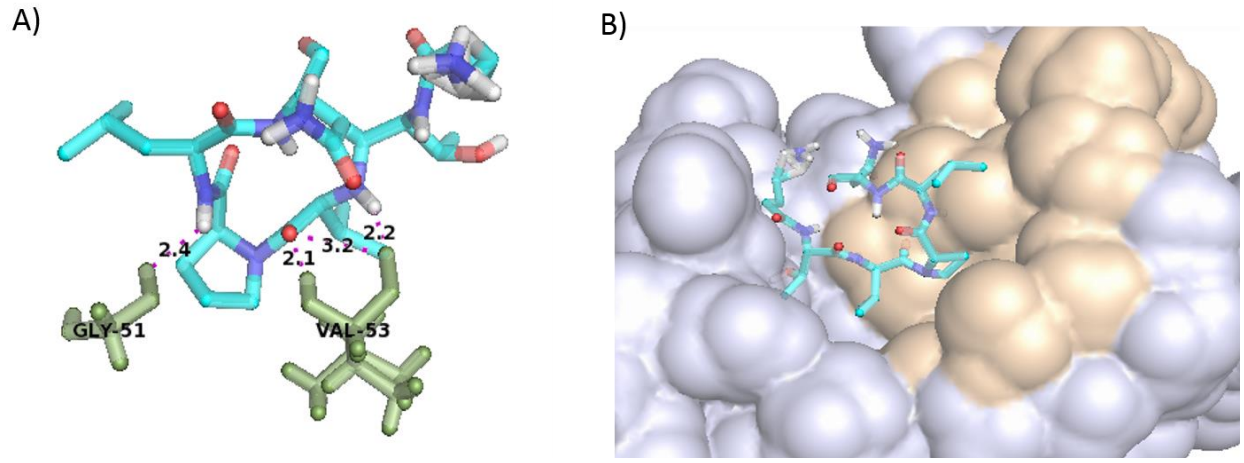

Figure 2.1. Molecular docking studies of peptide **6** bound to the NKp30 binding pocket. (A) Hydrogen bonding interactions between peptide **6** and NKp30 residues Gly51 and Val53 shown as dotted lines. The interacting residues are shown in ball and stick representation. NKp30 interacting residues are labeled and shown in green. Peptide **6** carbon atoms shown in cyan, nitrogen atoms in blue and oxygen atoms in red. (B) NKp30 molecular surface is shown in grey with the region containing the binding site for B7H6 colored in wheat. Peptide **6** shown in ball and stick representation.

2.4.2. SOLID PHASE PEPTIDE SYNTHESIS

The synthesis of the peptides was accomplished by conventional Fmoc-based solid phase peptide synthesis on a Rink amide linker hydrophilic poly(ethylene glycol) resin (NovaPEG, 0.52mmol/g).[26,27] Peptides **1**-**6** were further labeled with FITC to obtain peptides **7**-**12** for their use in biological studies (**Figure 2.2**). Peptides were recovered in crude yields (19-88%) and

purities (13-95%) according to RP HPLC. Synthetic peptides, **1-12**, were further purified by semi-preparative RP HPLC and isolated in purities ≥93%, and yields (10-44%) for structure-activity relationship studies. The identities of the synthetic peptides **1-12** were confirmed by mass spectrometry which validated sequence composition based on mass/charge ratios (**Table 2.1**).

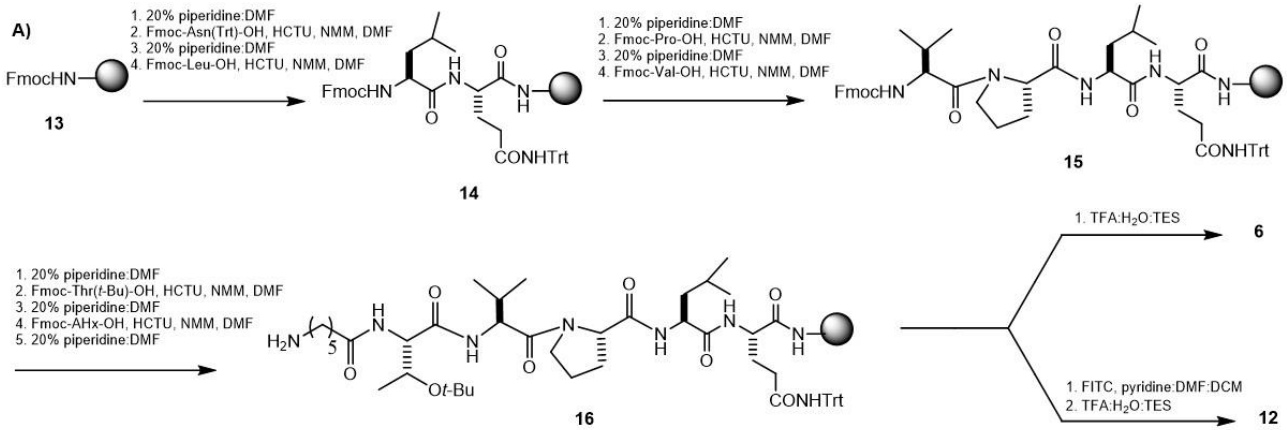

B)

Peptide **6**: NH_2-$(CH_2)_5$-TVPLN-$CONH_2$

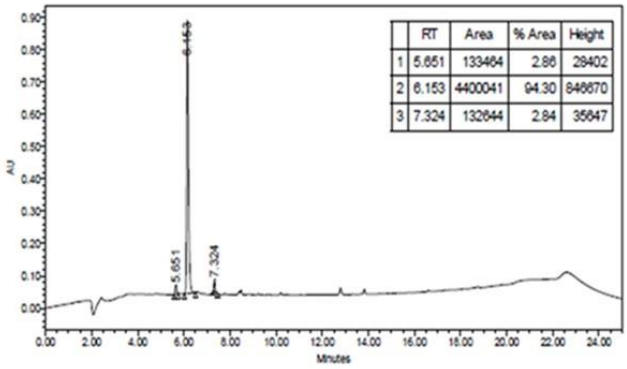

C)

Peptide **12**: FITC-NH_2-$(CH_2)_5$-TVPLN-$CONH_2$

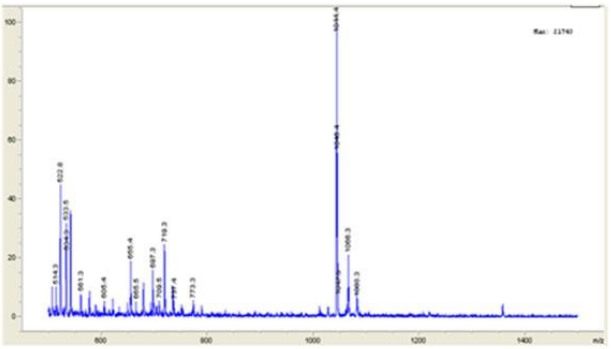

Table 2.1. Characterization of the synthetic peptides derived from the B7H6:NKp30 binding interactions.

Peptide	Residues	Sequence	Crude Purity (%)[b,c,d]	Purified Purity (%)[b,c,d]	Pure Yield (%)[e]	MW (g/mol)[f]	Z[g]	RT (min)[h]	RT (min)[i,j,k]
1	82-83	NH_2-$(CH_2)_5$-FG-$CONH_2$	13[b]	96[b]	10	335.2 (334.4)	1	4.37	7.40[i]
2	59-62	NH_2-$(CH_2)_5$-TSMG-$CONH_2$	71[b]	98[b]	13	507.2 (506.6)	1	3.59	5.67[i]
3	125-130	NH_2-$(CH_2)_5$-VTPLK-$CONH_2$	88[c]	>99[c]	44	669.5 (668.9)	1	7.70	5.97[j]
						335.3 (334.4)	2		
4	PS[a]	NH_2-$(CH_2)_5$-FGTSMGVTPLK-$CONH_2$	43[c]	97[c]	12	1249.6 (1249.6)	1	8.85	7.61[j]
						625.4 (624.8)	2		
5	SS[a]	NH_2-$(CH_2)_5$-TSMGFGVTPLK-$CONH_2$	59[c]	96[c]	21	1249.6 (1249.6)	1	8.95	7.66[j]
						625.4 (624.8)	2		
6	MS[a]	NH_2-$(CH_2)_5$-TVPLN-$CONH_2$	95[c]	95[c]	22	655.4 (655.4)	1	6.69	6.15[j]
7		FITC- NH-$(CH_2)_5$-FG-$CONH_2$	60[d]	93[d]	20	723.4 (722.9)	1	7.41[l]	15.2[k]
								9.71[l]	
8		FITC- NH-$(CH_2)_5$-TSMG-$CONH_2$	83[d]	93[d]	35	896.2 (895.0)	1	13.9	9.52[k]
9		FITC- NH-$(CH_2)_5$-VTPLK-$CONH_2$	18[d]	>99[d]	18	1059.4 (1060.3)	1	13.2	8.24[k]
						529.8 (530.1)	2		
10		FITC- NH-$(CH_2)_5$-FGTSMGVTPLK-$CONH_2$	52[d]	98[d]	11	819.1 (819.4)	2	13.9	8.87[k]
						546.4 (546.3)	3		
11		FITC- NH-$(CH_2)_5$-TMSGFGVTPLK-$CONH_2$	39[d]	95[d]	16	819.1 (819.4)	2	13.8	8.69[k]
						546.4 (546.3)	3		
12		FITC- NH-$(CH_2)_5$-TVPLN-$CONH_2$	83[d]	94[d]	39	1044.4 (1043.8)	1	15.1	10.1[k]
						522.8 (521.9)	2		

[a]**PS** Based on the primary structure of B7H6. **SS** Based on the secondary structure adopted by B7H6 on the binding interface. **MS** Modified sequence.
[b]Crude and purified purities by RP-HPLC at 220 nm using 2-60% MeCN/H_2O with 0.1% TFA over 20 min.
[c]Crude and purified purities by RP-HPLC at 220 nm using 2-82% MeCN/H_2O with 0.1% TFA over 18 min.
[d]Crude and purified purities by RP-HPLC at 220 nm using 2-80% MeCN/H_2O with 0.1% FA over 18 min.
[e]Pure yields based on the resin loading.
[f]Observed mass (expected mass) as $[M + H]^+/Z$ detected by LCMS in positive mode.
[g]Charged state of the peptides as detected by LCMS in positive mode.
[h]Retention times using 2-80% MeOH/H2O (0.1% FA) over 18 min.
[i]Retention times using 2-60% MeCN/H2O (0.1% TFA) over 20 min.
[j]Retention times using 2-82% MeCN/H2O (0.1% TFA) over 18 min.
[k]Retention times using 2-82% MeCN/H2O (0.1% FA) over 18 min.
[l]Retention time variation dependent on FITC isomers.

2.4.3. CIRCULAR DICHROISM SPECTROSCOPY

A circular dichroism study in the far-UV region (190-280 nm) was conducted to determine the secondary structures (if any) adopted by the peptides (**3-6**).[28,29] The selected peptides were dissolved in water, phosphate buffered saline (PBS), or a mixture of 2,2,2-trifluoroethanol:water (TFE:H_2O, 50:50 v/v) at constant samples concentrations (40 μM) to analyze the influence of the solvent on peptide structure. All peptides showed different conformations that were dependent on the solvent system (**Figure 2.3**). The peptides (**3-6**) showed a CD signature characteristic of a random coil when dissolved in water, with the distinctive minimum band near 200 nm (**Figure**

2.3.A). In PBS, the peptides **3-6** were found to transition from random coils into helical type structures, with representative minimum bands near 210 and 220 nm and a maximum near 190 nm (**Figure 2.3.B**). Moreover, the peptides **3-6** adopt turn type conformations when dissolved in the TFE:H_2O mixture, as seen by the typical negative bands near 200 and 230 nm and maxima near 210 and 260 nm, (**Figure 2.3.C**). Interestingly, peptide **5**, was found to display a unique reverse turn geometry which opposed that of the remaining peptides (**3, 4** and **6**) with a broad minimum band observed in between 240-260 nm, another near 190 and 210 nm, and maximum peaks observed near 200 and 220 nm.

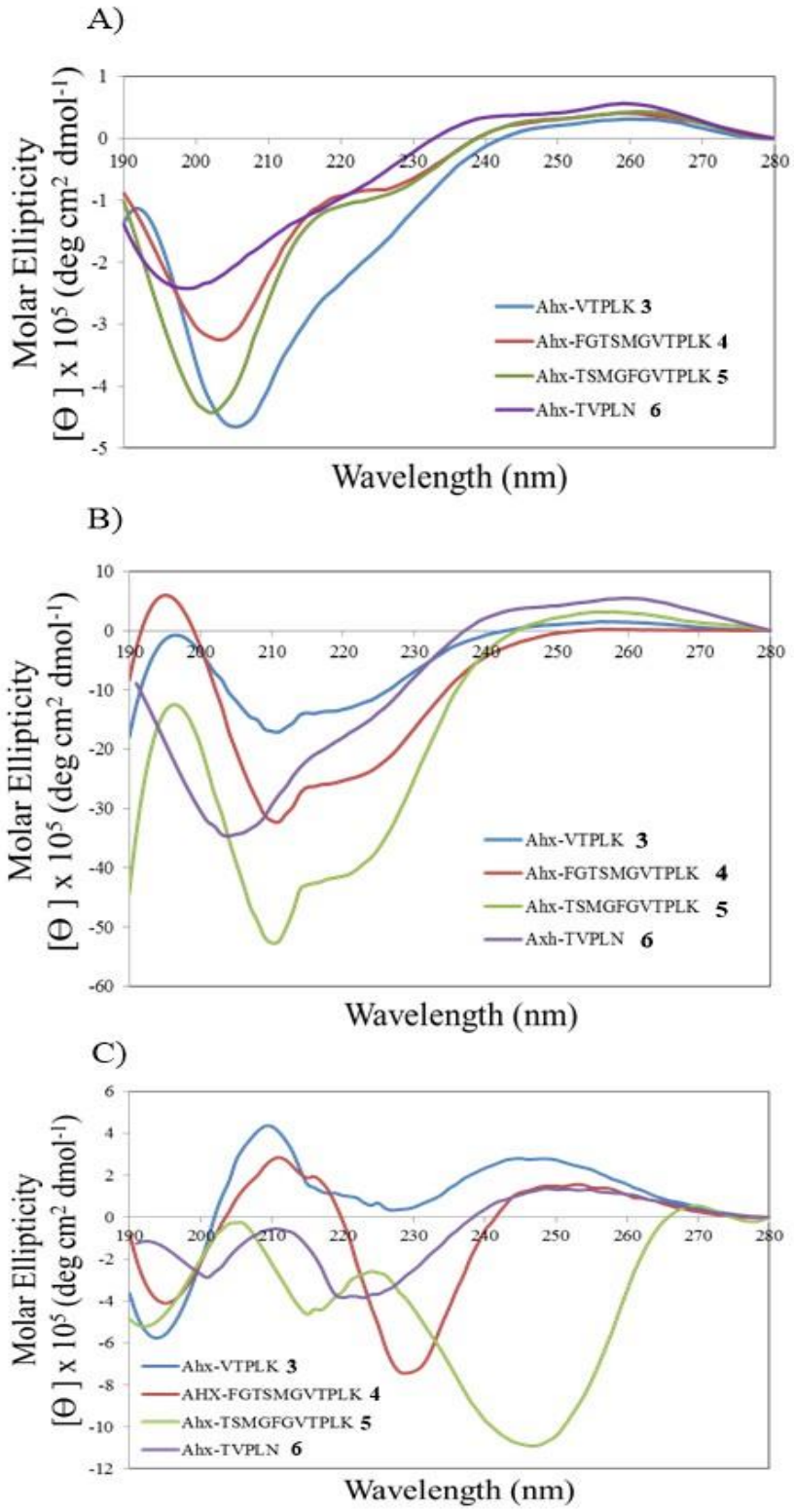

Figure 2.3. Circular dichroism spectra of peptides **3-6** (40 mM) in: A) water, B) PBS, and C) TFE: H_2O (50:50, v/v). Data representative of three independently conducted experiments.

2.4.4. DIRECT BINDING STUDIES ON THE NK92-MI CELLS.

In order to evaluate the ability of the FITC-labeled synthetic peptides, **7-12**, to bind to the cell surface of NK cells, the human NK cell line, NK92-MI, was incubated for 30 minutes with the peptides, **7-12**, at various concentrations (0.1, 1, 10 μM) in PBS. Their binding capabilities was compared to that of the natural ligand, soluble B7H6-Fc (1 μM), and the anti-NKp30 APC labeled mAb (2 μg/ml) (**Figure 2.4.A**). Flow cytometry revealed comparable NK cell occupancy (80-97%) between the anti-NKp30 mAb, B7H6, and all the FITC-labeled peptides, **7-12**, at a peptide concentration of 10 μM (**Figure 2.4.B**). Moreover, the peptides, were found to display dose-dependent binding on the NK cells, with optimal binding values (80-97%) observed at 10 μM, moderate binding (24-50%) at 1 μM and minimal binding at 0.1 μM (3-4%).

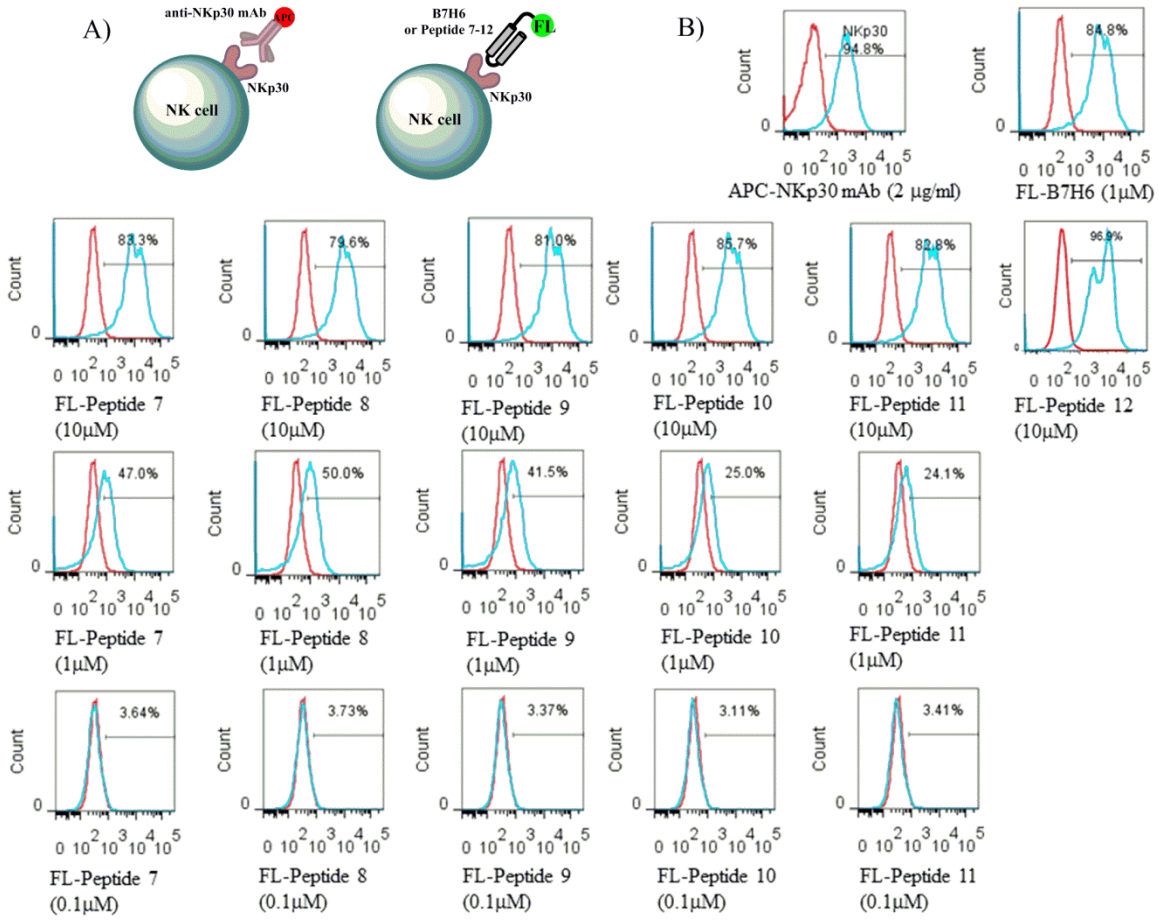

Figure 2.4. Direct binding studies with the NK92-MI cells. (A) Figurative representation of the NK cells' binding in between the anti-NKp30 mAb, B7H6 and the FITC-labeled peptides, **7-12**. (B) Flow cytometry analyses of the NK92-MI cells' binding with anti-NKp30 mAb (2 µg/mL, 2 µL), B7H6 (1 µM, 50 µL) and the FITC-labeled peptides, **7-12**, (0.1-1 µM, 50 µL) in PBS. Data representative of three independently conducted experiments.

2.4.5. CONCENTRATION DEPENDENT BINDING OF B7H6.

In an effort to confirm that the observed fluorescent signal of soluble FL-B7H6-Fc (1 µM, 50 µl) was due to the binding capabilities of B7H6-Fc with NKp30-Fc and not a result of a saturated signal, the human NK cell line, NK92-MI, was incubated for 30 minutes with soluble

FL-B7H6-Fc (1 μM, 20 μl and 50 μl) and the anti-NKp30 APC labeled mAb (2 μg/ml) (**Figure 2.5**). Flow cytometry assays revealed equal binding capabilities of B7H6-Fc on NK cells despite the varying amounts of sample, (50 μmol and 20 μmol, 74.6-80.6%) and comparable to anti-NKp30 mAb (94.8%).

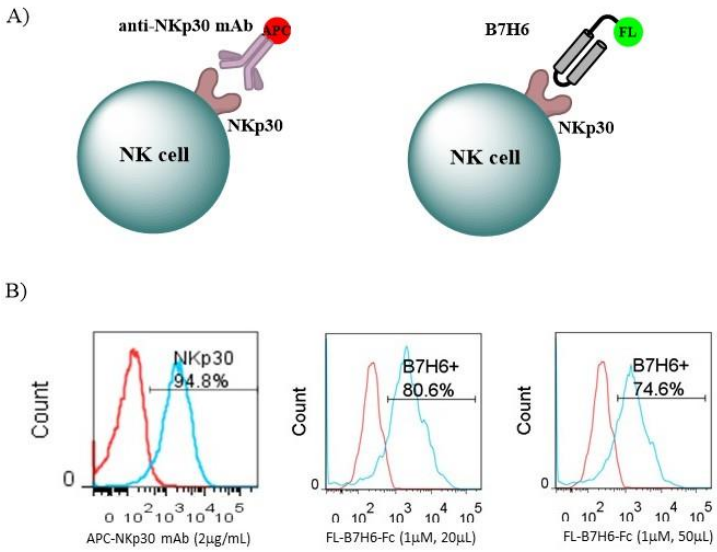

Figure 2.5. Direct binding studies with the NK92-MI cells. (A) Figurative representation of the NK cells' binding in between the anti-NKp30 mAb and B7H6. (B) Flow cytometry analyses of the NK92-MI cells' binding with anti-NKp30 mAb (2 μg/mL, 2 μL) and B7H6 (1 μM, 20 and 50 μL), in PBS.

2.4.6. COMPETITIVE BINDING STUDIES ON THE NK92-MI CELLS.

A competitive binding assay was conducted in between the FITC-labeled peptides, **7-12**, and the NKp30 ligands, Alexa Fluor 488-labeled B7H6 and the APC-labeled anti-NKp30 mAb (clone 210845, R&D systems) in order to evaluate NKp30 binding specificities (**Figure 2.6.A**). In this assay, the NK92-MI cells were initially incubated for 30 minutes with either the Alexa Fluor 488-labeled B7H6 ligand (1 μM) or the FITC-labeled peptides, **7-12** (10 μM), followed by a 30

minute treatment with the APC-labeled anti-NKp30 mAb (2 μg/ml). Flow cytometry revealed partial displacement of the Alexa Fluor 488-labeled B7H6 ligand (69%) and the peptides, (6-35%) upon APC-labeled anti-NKp30 mAb treatment (**Figure 2.6.B**).

In a complementary competitive binding assay, the NK92-MI cells were incubated first with the APC-labeled anti-NKp30 mAb (2 μg/ml), followed by treatment with either the Alexa Fluor 488-labeled B7H6 ligand (1 μM) or the FITC-labeled peptides, **7-12**, (10 μM) (**Figure 2.7.A**). No displacement of the mAb or blocking of the ligands, B7H6 and peptides, for the NK cells was observed. In this case, the NKp30 ligand B7H6 and the synthetic peptides maintained stable binding (80-84%) to the NK cells with and without prior treatment of the anti-NKp30 mAb (**Figure 2.7.B**).

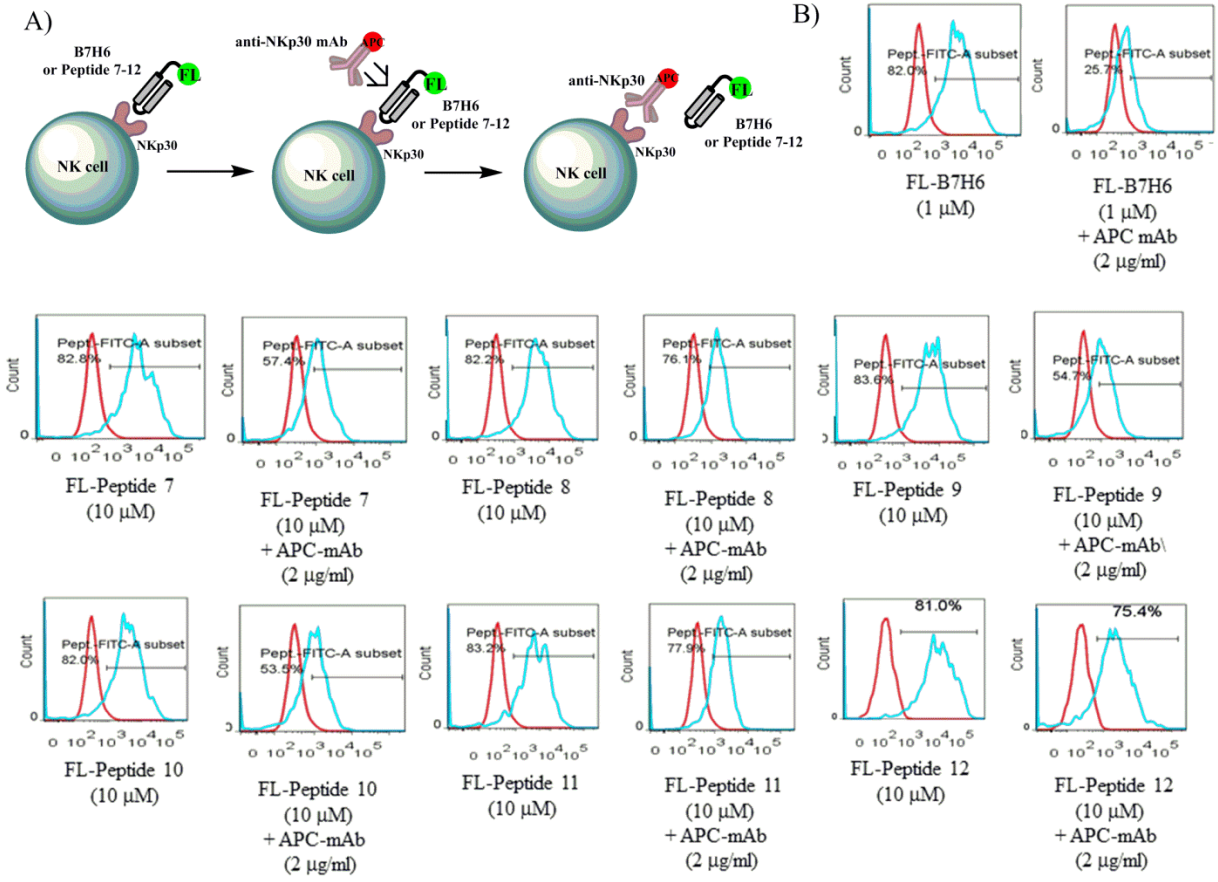

Figure 2.6. Competitive binding studies with the NK cells. (A) Figurative representation of the competitive binding studies in between fluorochrome-labeled B7H6, peptides, **7-12**, and the anti-NKp30 mAb. (B) Flow cytometry of the direct *vs.* competitive binding of Alexa Fluor 488-labeled B7H6 (1 μM, 20 μL PBS) and the FITC-labeled peptides, **7-12**, (10 μM, 50 μL PBS) without and with successive treatment of the APC-labeled anti-NKp30 mAb (2 μg/mL, 2 μL) on the NK92-MI cells. Data representative of three independently conducted experiments.

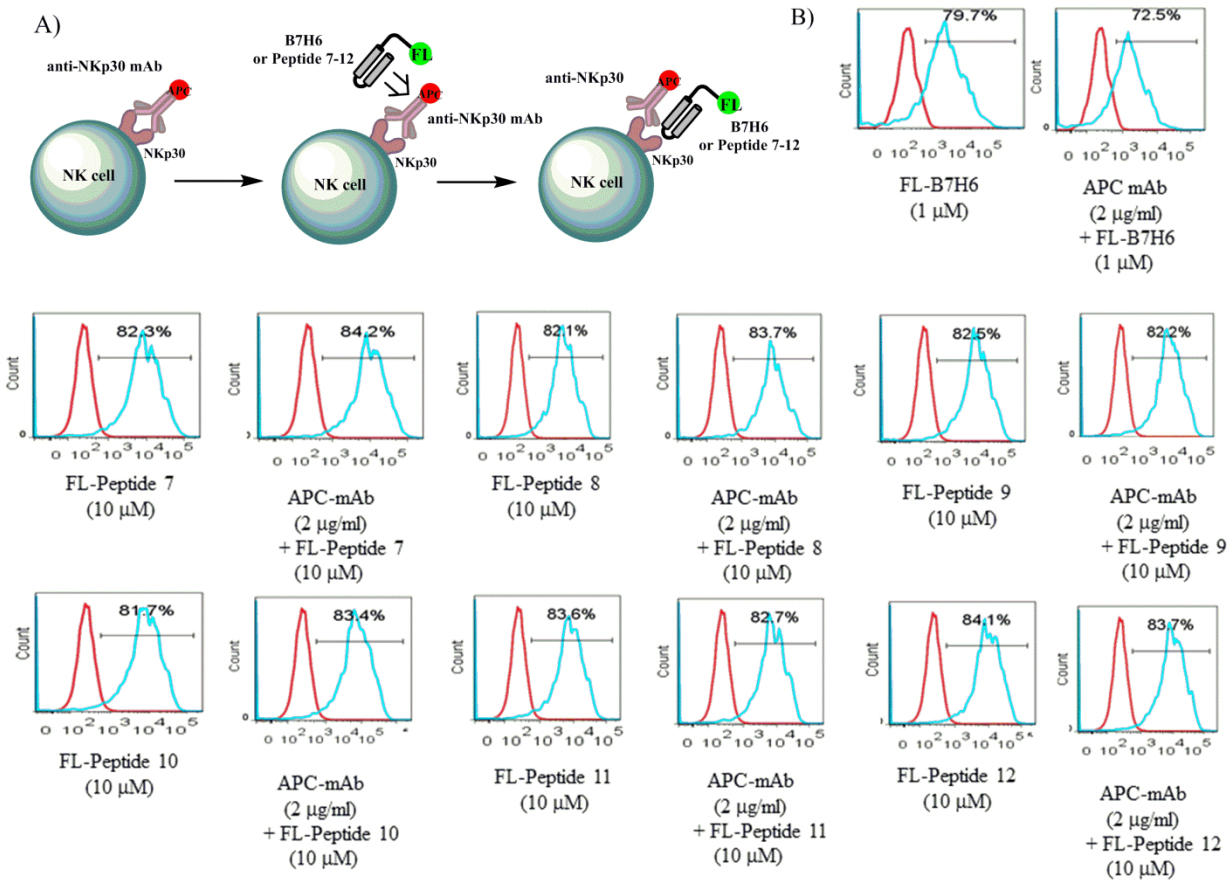

Figure 2.7. Complementary competitive binding studies with the NK cells. (A) Figurative representation of the fluorochrome-labeled anti-NKp30 mAb binding of the NK cells followed by

treatment with B7H6 and the peptides, **7-12**. (B) Flow cytometry analyses of the direct *vs.* competitive binding of Alexa Fluor 488-labeled B7H6 (1 μM, 20 μL PBS) and the FITC-labeled peptides, **7-12**, (10 μM, 50 μL PBS) without and with prior treatment of the APC-labeled anti-NKp30 mAb (2 μg/mL, 2 μL) on the NK92-MI cells. Data representative of three independently conducted experiments.

2.4.7. COMPETITIVE BINDING STUDY BETWEEN B7H6-FC AND THE B7H6-DERIVED PEPTIDES.

A competitive binding assay was conducted in between the FITC-labeled peptides, **7-12**, and the NKp30 ligand, soluble B7H6-Fc to evaluate NKp30 binding specificities of the FITC-labeled peptides (**Figure 2.8**). In this assay, the NK92-MI cells were initially incubated for 30 minutes with the B7H6 ligand (1 μM) followed by a 30 minute treatment with the FITC-labeled peptides, **7-12** (10 μM). Flow cytometry revealed efficient binding occupancy of the peptide ligands (>99%) with B7H6-Fc pre-treatment (**Figure 2.8**).

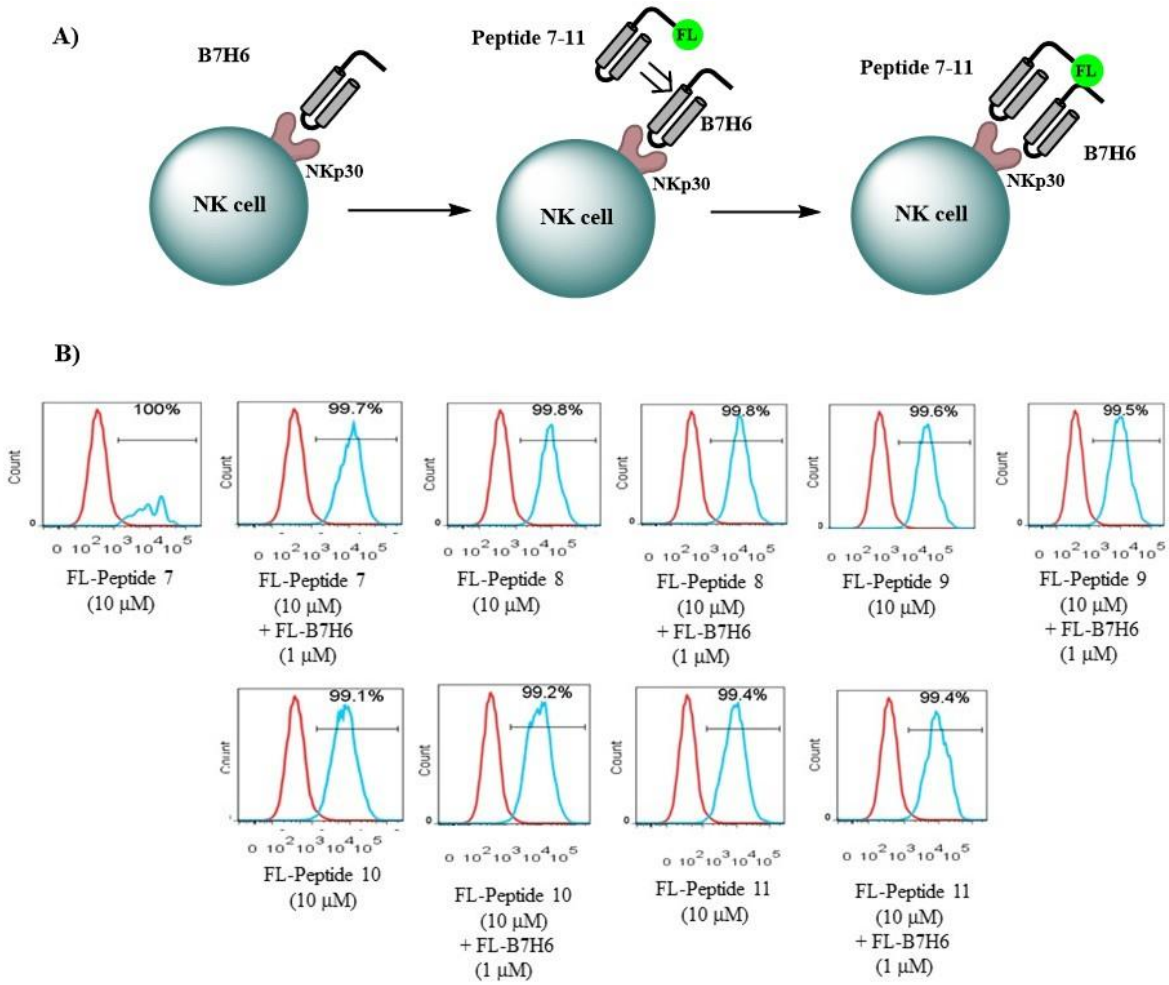

Figure 2.8. Competitive binding studies with the NK cells. (A) Figurative representation of the competitive binding studies in between soluble B7H6-Fc and B7H6 derived peptides, **7**-**12**. (B) Flow cytometry of the blocking experiment the FITC-labeled peptides, **7**-**12**, (10 µM, 50 µL PBS) with pre-treatment with soluble B7H6 (1 µM, 20 µL PBS) on the NK92-MI cells. Data representative of three independently conducted experiments.

2.4.8. SYNTHESIS OF NEGATIVE CONTROL PEPTIDES

To further assess the specific activities of the B7H6 derived peptides (**1**-**6**), a series of non-specific control peptides (**13**-**16**) were also synthesized by Fmoc-SPPS and isolated by LCMS.

Peptide **13** is the reversed version of peptide **6**; peptide **14** is a scrambled sequence that contains the same amino acid residues as peptide **6** but in a scrambled order; peptide **15** is a random sequence that lacks proline; and peptide **16** is a random sequence with proline at the *i*+2 position. (**Table 2.2**)

Table 2.2. Non-specific control sequences, where sequence **13** and **14** are modifications of peptide **6**, while **15** and **16** are random sequences.

Peptide		Sequence
13	Reversed	NH_2-$(CH_2)_5$-NLPVT-$CONH_2$
14	Scrambled	NH_2-$(CH_2)_5$-VLNTP-$CONH_2$
15	Negative	NH_2-$(CH_2)_5$-GAMGT-$CONH_2$
16	Negative	NH_2-$(CH_2)_5$-FAPGI-$CONH_2$

2.4.9. IMMUNOSTIMULATORY ACTIVITY OF THE NK92-MI CELLS.

The ability of the synthetic peptides to activate immune responses from the NK92-MI cells was evaluated by the detection of the soluble secreted cytokines, IFN-γ and TNF-α into the culture media by a standard ELISA (**Figure 2.9.A**).[30] In this assay, the NK92-MI cells were incubated with either B7H6 (0.5 μM) or the peptides **1-6** (10 μM) for 24 h. The cells were then harvested from culture and the media was examined by ELISA for the secretion of the inflammatory cytokines, TNF-α (**Figure 2.9.B**) and IFN-γ (**Figure 2.9.C**). Treatment with soluble B7H6 stimulated secretion of IFN-γ (260 pg/mL) and TNF-α (500 pg/mL) at 0.5 μM. Interestingly, peptides **1-6** (10 μM) activated the secretion of TNF-α at noticeable levels (50-180 pg/mL) relative to the untreated NK91-MI cells, albeit with about a 3-fold decrease in intensity *vs.* the native B7H6

ligand. Of the most promising candidates in the peptide series, peptide **5**, activated secretion of TNF-α at a concentration of 140 pg/mL and peptide **6** showed the highest levels of TNF-α production at 180 pg/mL. In this assay, none of the peptides stimulated any observable secretion of the inflammatory cytokine, IFN–γ. The ability of peptide **6** to stimulate TNF-α secretion on NK92-MI cells was further compared with four control peptides, **13**-**16** (**Figure 2.9.D**). The assay revealed that none of the control sequences (10 μM) stimulated TNF-α secretion after 24 hour treatment, even though peptides **13** and **14** are directly related to peptide **6**. Furthermore, peptide **6** maintained notable TNF-α stimulating capabilities of the NK cells which was observed at a 2.5-fold increase relative to the non-specific control peptides (**Figure 2.9.D**).

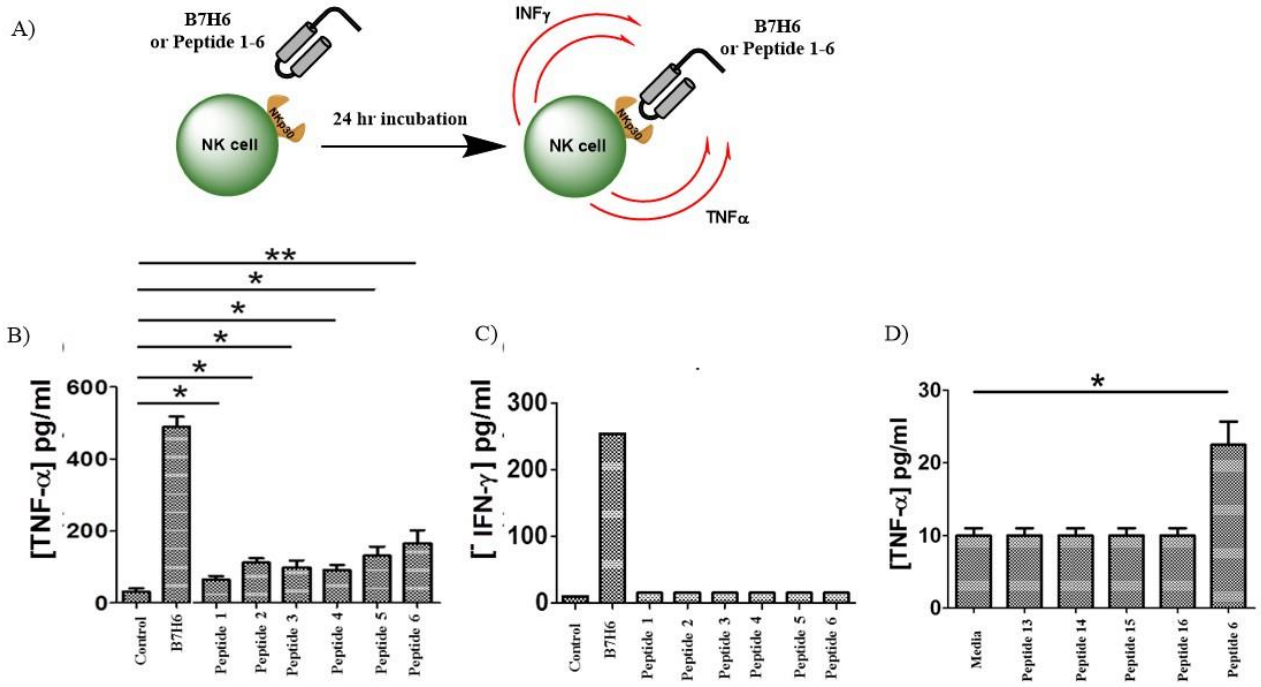

Figure 2.9. Immunostimulatory activities of B7H6 and the peptides, **1**-**6**, on the NK92-MI cells. (A) Figurative representation of the release of the inflammatory cytokines, TNF-α and IFN-γ, from the NK cells upon treatment with B7H6 and peptides, **1**-**6**. ELISA for (B) TNF-α and (C) IFN-γ detection following treatment of B7H6 (0.5 μM) and peptides, **1**-**6**, (10 μM) on the NK92-MI cells.

Production of TNF-α by NK cells cultured with the peptides was significantly higher than the recorded levels of the control, untreated cells (*****p< 0.05; ******p< 0.01). There was no significant difference for IFN-γ production. This data is the average of three independent experiments. (D) Immunostimulatory activities of the non-specific control peptides **13**-**16**, and the lead peptide **6** on the NK92-MI cells (*****p< 0.1). This data is the average of three independent experiments.

2.4.10. NK CELLS' VIABILITY.

In order to test whether the synthetic peptides, **1**-**6**, were non-toxic to the NK cells, or whether the stimulation of TNF-α resulted in NK cell-dependent cytoxicity, a Guava Nexin® Reagent (EMD Millipore) was used to assess early and late-stage apoptosis by flow cytometry.[31] In this assay, the NK92-MI cells were incubated for 24 hours with either B7H6 (0.5 μM) or the peptides, **1**-**6**, (10 μM). After incubation, the cells were centrifuged, washed and stained with the Guava Nexin® Reagent for NK cells' viability analyses using flow cytometry. The results revealed no early or late stage apoptotic events for the NK cells treated with soluble B7H6-Fc or the synthetic peptides, (**Figure 2.10**). In all cases, ≥95% non-apoptotic NK cells were detected following treatment.

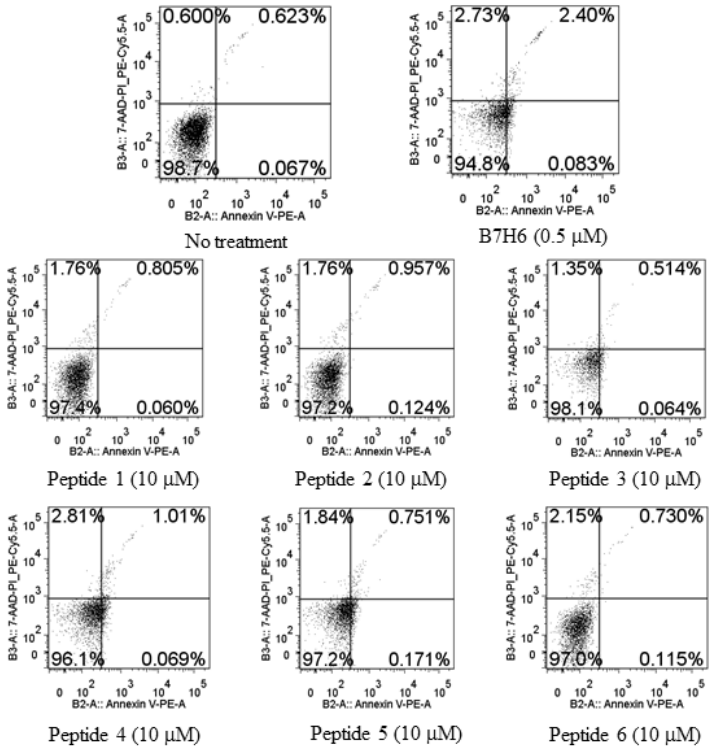

Figure 2.10. NK cells' viability assessed by the Guava Nexin Reagent (EMD Millipore) using flow cytometry. The NK92-MI cells were incubated with B7H6 (0.25 μM) or the synthetic peptides, **1**-**6**, (10 μM) for 24 h. The cells were washed with fluorescence-activated cell sorting (FACS) buffer and stained with the Guava Nexin Reagent. Flow cytometry analyses of the early (lower right), late (upper right), early and late (upper left) stages of apoptosis and the non-apoptotic (lower left) cells. Data representative of three independently conducted experiments.

2.5. DISCUSSION

Biological molecules that can trigger immune responses towards invading pathogens, allergens, and cancer have led to the advancement of immunotherapy.[32] Tumor immunotherapy involves the activation of white blood cells; either by stimulating lymphocytes *ex vivo*, followed

by re-infusion of the activated cells into the patient. Circulating tumor associated ligands can also stimulate inflammatory responses towards the destruction of the invasive tumor or blockage of pro-survival signals.[33-36] In an effort to promote *in vivo* stimulation of lymphocytes, treatment methods implicating cancer vaccines, tumor-associated antigen derived small peptides (TAA-SP) or recombinant virus-like particles (VLP), cytokine therapy, and monoclonal antibodies (mAbs) have been developed and successfully administered in tumor immunotherapy applications.[32,37,38] Among these promising treatment regimes, the peptide-based TAA-SPs potentially encompass an underexplored yet promising class of immunostimulatory ligands that may have significant utility in clinical oncology. Representatively, the TAA-SP derived from the heat shock chaperone protein of 70 kilodalton (Hsp70) has been found to activate and expand NK cells towards potent tumor-targeted immunotherapy responses.[39,40] In this study, the TAA-SPs derived from B7H6 are explored as a potential new class of ligands for eliciting NK cells' immunostimulatory activities.

The rational design of the synthetic peptides was based on the co-crystal structure of B7H6 bound to its receptor NKp30.[20] The peptide sequences were based on the amino acid residues selected from segments 82-83 (FG), 59-62 (TSMG) and 125-130 of the FG loop region (VTPLK) which constituted peptides **1-3**, respectively (**Table 2.1**). These selected peptides were based on the primary sequence of the binding site residues of B7H6 at the active site of the NKp30 receptor.[20] The binding site residues within the FG loop of B7H6, VTPLK, were found to play a key role in B7H6 binding and activation of the NKp30 receptor. Structure analyses revealed that a turn-type geometry contributed to binding affinity, which was stabilized by the Pro-Leu residues at the *i+2* and *i+3* positions and the Van der Waals contacts that were made predominantly within the hydrophobic NKp30 binding pocket.[20] Thus, the modified sequence **6**, TVPLN, was rationally designed to study the effect of hydrogen bonding and turn conformation on peptide binding and

activity. In this case, the rationale for the exchange of the *N*-terminal Thr and Val, and replacement of the *C*-terminal Lys for Asn was based on the short peptide sequences which promoted turn conformations due to stable hydrogen-bonding interactions with terminal Thr and Asn residues.[41,42] Moreover, molecular docking studies revealed four H-bonding interactions in between peptide **6** and the NKp30 binding site residues, Gly51 and Val53 (**Figure 2.1**). The Gly51 and Val53 residues of NKp30 also contributed in H-bonding of the FG loop residues 125-130 (VTPLK) of B7-H6, found at the B7H6:NKp30 binding interface.[20] The lengthier peptides (**Table 2.1**, sequences **4**, **5**) were based on the residues (59-62, 82-83, 125-130) of the full length B7H6 primary sequence that contributed to NKp30 binding, (FGTSMGVTPLK peptide **4**), and on the residues (82-83, 59-62, 125-130) that contributed to the B7H6 secondary structure which bound to the NKp30 receptor (TSMGFGVTPLK, peptide **5**). These full-length sequences (**Table 2.1**, sequences **4** and **5**) were selected to contain the binding site residues and structural elements that effected B7H6 binding and activation of the NKp30 receptor.[20]

For peptide synthesis, the hydrophilic poly(ethylene glycol) resin (NovaPEG, 0.52 mmol/g) was chosen because of its known advantages over the hydrophobic polystyrene (PS)-based resins.[26,29] The hydrophilicity and higher swelling capabilities of the NovaPEG resin in H_2O, DMF, DCM and TFA, led to improved coupling efficiencies, isolated peptide purities and yields of lengthy non-polar sequences that tend to aggregate during the course of SPPS.[26,29] For peptide coupling, HCTU was selected as activator, with NMM as base, due to its high coupling efficiencies at short coupling times and at lower costs when compared with HATU.[27] The Fmoc-based SPPS of the peptide sequences (**Table 2.1**, peptides **1**-**12**) was developed according to standard procedures.[26,27,29] Following peptide synthesis, the peptides were coupled with an Ahx linker at the *N*-terminus and selected peptides (**Table 2.1**, peptides **7**-**12**) were functionalized with

FITC for biological studies. Peptides were then cleaved and deprotected with trifluoroacetic acid (TFA), using water and triethylsilane (TES) as scavengers for any reactive components. The efficiency of the peptide synthesis was determined by RP HPLC and related to the crude purity analyses (13-95%) which resulted in sufficient isolated yields (10-44%) for structure-activity relationship studies. Furthermore, the integrity of the peptides was confirmed by preparative RP HPLC which resulted in peptides of purity>93%. Sequence identities were also validated by ESI MS, which confirmed the molecular weights of the peptides as selected mass:charge ratios (**Table 2.1**).

With pure peptides in hand, circular dichroism (CD) spectroscopy was used to evaluate their structures in solution.[28,29] Peptides (**Table 2.1**, sequence **3-6**) were dissolved in deionized H_2O, PBS and a mixture of TFE:H_2O (50:50, v/v) in order to assess the influence of solvent on peptide structure. In this study, the solvent was found to play a pivotal role on the structures adopted by the peptide sequences, as seen by the transitions in conformations from random coil (H_2O), to alpha-helix (PBS) and turn-type structures (TFE:H_2O) (**Figure 2.3**). All peptides adopted similar conformations within the same solvent system, possibly because of their similarities in sequences, which included the putative turn-inducing motif, VTPLK, in peptides **3-5**, which was expected to be stabilized in the modified TVPLN sequence, **6**. These peptides were found to adopt turn conformations in the TFE:H_2O mixture that is known to mimic amphiphilic biological environments (*i.e.* membrane receptors) and stabilize the structure for the most favored peptide conformation by promoting intramolecular hydrogen bonding.[43] This was shown to be based on the ability for TFE to aggregate around the peptide, while displacing water, and favoring the formation of the intra-peptide hydrogen bonds responsible for the peptide secondary structures. In this model TFE:H_2O serve to mimic the amphiphilic lipid bilayer microenvironments or those

found in membrane spanning proteins.[44,45] Interestingly, the bioactive FG loop region of B7H6 containing the VTPLK sequence was also found to favor a turn-type conformation when bound to the active site of the NKp30 receptor.[20] Thus, this peptide secondary structure motif may be contributive towards binding and activity of the B7H6-derived peptides synthesized in this study.

The NKp30 receptor has been found to be constitutively expressed on all activated and resting NK cells.[19] Flow cytometry was used to ascertain the cell surface expression of NKp30 on resting NK92-MI cells. High cell surface expression levels (95%) of NKp30 on the NK92-MI cells was confirmed by incubating the cells with the APC-labeled anti-NKp30 mAb. Comparatively, the soluble form of the Alexa Fluor 488-labeled natural NKp30 ligand, B7H6-Fc, also demonstrated high binding affinity (86%, 1 μM) for the NK92-MI cells regardless of the amount of sample used (20 μl vs. 50 μl) (**Figure 2.5**). This is in agreement with the SPR experiments, which revealed an equilibrium dissociation constant value in between B7H6 and NKp30 of $1.0 \pm 0.2 \times 10^{-6}$ M.[21] The binding occupancy of the peptides on the NK92-MI cells were then determined in a concentration dependent manner (0.1 - 10 μM). All FITC-labeled peptides, **7-12**, were able to bind to the NK92-MI cells with comparable occupancy (80-97%) at 10 μM relative to the anti-NKp30 mAb (95%) and B7H6 (86%), albeit at a 10-fold higher concentration relative to the native B7H6 ligand. Moreover, binding of the peptides to the NK92-MI cells was found to be dose-dependent, with strong (80-97%, 10 μM), moderate (24-50%, 1 μM) and weak (3-4%, 0.1 μM) binding detected by flow cytometry (**Figure 2.4**). Thus, all peptides were able to bind to the NK92-MI cells with strong occupancy (80-97%) at 10 μM.

Competitive binding experiments were next conducted in order to determine whether the peptides bound to the NKp30 receptor on the surface of the NK cells. The NK92-MI cells were initially incubated with either Alexa Fluor 488-labeled B7H6 (1 μM) or the FITC-labeled peptides,

7-12 (10 μM) for 30 minutes, followed by treatment with the APC-labeled anti-NKp30 mAb. In this assay, the anti-NKp30 mAb was found to partially displace B7H6 (69%) and the peptides (6-35%) suggesting NKp30 binding specificities for these ligands (**Figure 2.6**). The partial displacement of the peptides and B7H6 may be attributed to the proximal NKp30 binding site differences in between the anti-NKp30 mAb (NKp30 residues 91-107 for anti-NKp30 mAb clone 210845) and B7H6 or the peptide ligands (NKp30 residues 82-83, 59-62, 125-130 for B7H6 and peptides).[20,46] Taken altogether, these observations suggests adjacent (allosteric) binding of the anti-NKp30 mAb and the NKp30 ligands, B7H6 and the peptides, **7-12**, accommodating proximal binding site interactions with the NKp30 receptor. In order to evaluate this hypothesis, a complementary competitive binding assay was developed, in which the NK92-MI cells were initially incubated with the APC-labeled anti-NKp30 mAb, followed by treatment with either the Alexa Fluor 488-labeled B7H6 (1 μM) or the FITC-labeled peptides, **7-12** (10 μM). In this study, no blocking or displacement of the anti-NKp30 mAb was observed after treatment with the ligands B7H6 or the peptides (**Figure 2.7**).These results lend further evidence of the putative allosteric binding of the anti-NKp30 mAb and the ligands (B7H6, peptides **7-12**) with the target NKp30 receptor on the surface of the NK92-MI cells. To further asses the binding specificities of the B7H6 derived peptides, a competitive binding study in which NK92-MI cells were incubated first with unlabeled B7H6 (1 μM) for 30 min, following incubation with FITC-labeled peptides (**7-12**), (**Figure 2.8**). Flow cytometry results revealed consistent binding of the peptidic ligands, even after B7H6 treatment, suggesting strong binding occupancy of the peptidic ligands on the NK92-MI cells.

Following the binding studies, the immunostimulatory activities of B7H6 and the peptides, **1-6**, on the NK92-MI cells were next evaluated by the release of the inflammatory cytokines, TNF-

α and IFN-γ. In this assay, the NK92-MI cells were incubated with either B7H6 (0.5 μM) or the peptides **1**-**6** (10 μM) for 24 hours followed by the recovery of the supernatant which was analyzed for the release of TNF-α and IFN-γ by ELISA. The soluble B7H6 was capable of activating the secretion of TNF-α (>500 pg/mL), whereas, peptides **1**-**4** scarcely activated secretion (<100 pg/mL), and peptides **5** and **6** showed notable production of this cytokine (140 pg/mL and 180 pg/mL, respectively) from the NK cells (**Figure 2.9.B**). Interestingly, peptide **6**, which was designed to stabilize the putative turn geometry responsible for NK cells' binding and activation showed the highest TNF-α secretion. This bio-active turn conformation was confirmed by the CD studies in TFE:H_2O (**Figure 2.3.C**) and suggests a potential link in between peptide turn geometry and the NK cells' immunostimualtory activity observed for this lead peptide sequence. Moreover, B7H6 was found to activate secretion of IFN-γ (>260 pg/mL) whereas the peptides had little (<100 pg/mL) effect on the stimulation of this inflammatory cytokine (**Figure 2.9.C**). Further mechanistic studies will be conducted in order to elucidate the observed selectivity of the secreted cytokines from the NK cells. Four control, non-specific peptides, **13**-**16**, based on reverse, scrambled and random sequences were evaluated for their ability to stimulate TNF-α secretion from the NK92-MI cells. None of the control peptides **13**-**16** were capable of activating cytokine release despite peptides **13** and **14** being directly related to peptide **6** (**Figure 2.9.D**) Comparatively, peptide **6** triggered a notable 2.5-fold increase in TNF-α secretion from the NK cells when directly compared to the control, non-specific peptides.

In a final experiment, the toxicity of the peptides, **1**-**6**, was analyzed by probing for the characteristic markers of early (externalization of phosphatidylserine, PS) and late-stage (loss of membrane integrity) apoptosis.[47] Apoptosis was evaluated by flow cytometry using the Guava Nexin Reagent ®.[31] This reagent utilizes Annexin V as a marker of early apoptotic events due to

its high affinity for PS, and 7- aminoactinomycin D (7-AAD), a cell permeable dye in the event of compromised cell membranes which occur during late-stage apoptosis. In this assay, the NK92-MI cells were incubated (24 h) with B7H6 (0.5 μM) or peptides **1**-**6** (10 μM) and then analyzed by flow cytometry using the Guava Nexin Reagent®. In all treatment cases, flow cytometry revealed viable NK cells, with little (<5%) observable cells in early, late or both stages of apoptosis (**Figure 2.10**). Thus, B7H6 (0.5 μM) and the peptides **1**-**6**, (10 μM) were found to be well tolerated within the NK92-MI cells at concentration levels which were used for the binding and immunostimulatory studies.

2.6. CONCLUSIONS

In this study, the design, synthesis, and characterization of a novel class of NK cell-dependent immunostimulatory peptides (IPs), derived from the binding interface of B7H6 and NKp30 have been discovered. A structure–activity relationship study revealed that the synthetic peptides, **3**-**6**, exhibited secondary structures that varied on the solvent system. They also displayed the putative turn conformation in a TFE:H_2O mixture that was expected to contribute to NKp30 receptor binding and the NK cells' immunostimulatory activities. Flow cytometry analyses confirmed binding of the FITC-labeled peptides, **7**-**12**, to the NK cells at 10 μM concentrations, and partial displacement upon treatment with the anti-NKp30 mAb suggests NKp30 binding specificities. Moreover, ELISA demonstrated that peptides **5** and **6** notably stimulated the secretion of TNF-α but not IFN-γ, while exhibiting no observable cytotoxicity (apoptosis) to the NK92-MI cells. Taken altogether, these studies have effectively paved the way for the analyses of this new class of B7H6-derived TAA-SP in tumor immunotherapy applications. The latter is a current focus of our on-going research program in anti-cancer drug design and development.

2.7. MATERIALS AND METHODS

2.7.1 MATERIALS

Aminoacids for the synthesis of all peptides, Fmoc-Lys(Boc), Fmoc-Leu, Fmoc-Pro, Fmoc-Thr(tBu), Fmoc-Val, Fmoc-Gly, Fmoc-Phe, Fmoc-Met, Fmoc-Ser(tBu), Fmoc-Thr(tBu), and Fmoc-εAhx, were purchased from Novabiochem (San Diego, CA, USA). Peptide syntheses were conducted on a Rink Amide ChemMatrix (0.52 mmol/g) (Biotage Inc., Charlotte NC, USA). 2-(6-chloro-1H-benzotriazole-1-yl)-1,1,3,3-tetramethylaminium hexafluorophosphate, HCTU, was purchased from Advanced ChemTech (Louisville, KY, USA). Fluorescein isothiocyanate, FITC, was purchased from ThermoScientific (Rockford, IL, USA) as a mixture of isomers and used in the dark to fluorescently label all peptides. Trifluoroacetic acid, TFA, (Biograde) was purchased from VWR (Radnor, PA, USA); *N*-*N*-dimethylformamide, DMF, acetonitrile, MeCN, methyl alcohol, MeOH, and dichloromethane, DCM, were all purchased from MACRON in ACS grade (Center Valley, PA, USA). Piperidine was purchased from EMD Millipore (Billerica, MA, USA); formic acid (97%), FA, triethylsilane (98+%), TES and pyridine (ACS, 99%) were purchased form Alfa Aesar (Ward Hill, MA, USA). *N*-methylmorpholine (99%), NMM, was purchased from Acros Organics (Pittsburg, PA, USA). Diethyl ether (99%, ACS), Et_2O, used to precipitate peptides was purchased from Sigma Aldrich (St. Louis, MO, USA). All chemicals were used directly as received.

2.7.2. PEPTIDE SYNTHESIS

All peptides were synthesized by stepwise manual solid phase peptide synthesis using Fmoc-chemistry. Fmoc-amino acids (300 mol%, 0.45 mmol) were coupled on a Rink amide linker poly(ethylene glycol) solid support (0.52 mmol/g, 0.15 mmols) for 1 h using [HCTU (300 mol%,

0.45 mmol), NMM (600 mol%, 0.9 mmol) in DMF (4 mL). A 20% piperidine in DMF solution (4 mL) was used for Fmoc deprotection (30 min). Amino acid couplings and Fmoc deprotections were repeated until the desired sequences were completed. Following peptide synthesis, solid support bound peptide was separated (100 mg, 0.052 mmol) for FITC-labeling. The resin was swollen in DMF for 1 h. A slurry of FITC (1.1 equiv., 0.057 mmol) in pyridine/DMF/DCM (12:7:5 v/v) was prepared and added to the reaction vessel for overnight reaction on an overhead shaker. After FITC-labeling was completed, the resin was washed with DMF (3 x 3 mL), MeOH (3 x 3 mL), and DCM (3 x 3 mL). Peptide cleavage and deprotection from the solid support was accomplished using a mixture of TFA:TES:H_2O, (95:2.5:2.5 v/v/v) for 3 h. Peptide samples were concentrated under nitrogen to a viscous oil, precipitated with cold Et_2O, and centrifuged to a white pellet. The supernatant was decanted and the peptide pellets were dissolved in MeOH/H_2O for LCMS analyses. Sample analyses were performed on an Agilent 1100 series ESI-LCMS with single quadrupole mass analyzer and LC conditions which used a linear binary gradient (2-80% MeOH/H_2O, 0.1% TFA, over 18 min) in positive mode. Analytical RP-HPLC was performed using a Waters 2695 Symmetry® C18 column (3.9 x 150 mm, 5 μm particle size) using a linear binary gradient, 2-60% or 2-82% MeCN/H_2O, 0.1% TFA, over 18 min at 25°C, with a 1 mL/min flow rate and detection at 220 nm. Samples collected after purification were lyophilized to a white solid and re-dissolved in 50:50 v/v H_2O:MeOH to confirm purity and identity by LCMS analyses.

2.7.3. UV-VIS SPECTROSCOPY

The concentrations of the peptide solutions were determined by UV/Vis spectrophotometry at 214 nm (ε value of peptides was calculated as described by Kuipers *et. al*. $\varepsilon_{214} = (\varepsilon_{peptidebond})(n_{peptidebonds}) + \Sigma\,(\varepsilon_{aminoacid(i)})(n_{aminoacid(i)})$.[48] The analyses were conducted on an 8452A

Diode Array Spectrophotometer from Hewlett Packard, and concentrations were standardized at accordingly for each peptide.

2.7.4. CIRCULAR DICHROISM SPECTROSCOPY

The secondary structures of the synthetic peptides were determined by CD spectroscopy using an Aviv 62AD DS CD spectrophotometer (Lakefield, NJ). For CD analysis, peptides were dissolved in deionized water, PBS or a mixture of TFE:H_2O, (50:50 v/v), and concentrations were standardized at 40 μM for each peptide by UV-Vis spectroscopy. The CD spectra for the peptides (40 μM) were collected in a 1 mL cuvette (1 cm path length). The data was collected using a 1 nm bandwidth and 1 min step size for wavelengths from 190 to 280 nm at 25°C. The raw data obtained was then converted to molar ellipticity ($[\Theta] = \Theta/cl$, where Θ is the relative ellipticity (mdeg), c is the peptide concentration (M), and l is the path length (mm)), was blank corrected, and plotted as a function of molar ellipticity [Θ] versus wavelength (nm).

2.7.5. CELL LINES AND CELL CULTURE

The human NK cells, cell line NK92-MI (American Type Culture Collection, ATCC), were cultured in MEME, (Sigma Aldrich). The cell culture media was alpha modified with sodium bicarbonate and without ribonucleosides and deoxyribonucleosides, purchased from Sigma Aldrich. Media was supplemented with 2 mM L-glutamine (Lonza, Walkersville, MD, USA); 0.2 mM myo-inositol, 0.1 mM 2-mercaptoethanol (99%), and 0.02 mM folic acid (≥97%) (Sigma Aldrich) and 1% (v/v) penicillin/streptomycin (Sigma Aldrich). Heat-inactivated fetal bovine serum and horse serum (Sigma Aldrich) were added to a final concentration of 12.5% in total

volume. Cell cultures were maintained at 2-3x10^5 viable cells/mL at 37°C in 5% CO_2 humidified air.

2.7.6. FLOW CYTOMETRY

For detection of cell surface expression levels of NKp30, the NK92-MI cells were washed with FACS buffer (PBS, 1% FBS), suspended in APC-labeled human NKp30 mAb (2 μg/mL in FACS, clone 210845 from R&D Systems), and incubated at room temperature for 30 minutes in the dark. Cells were then washed and analyzed by flow cytometry on a MACSQuant® analyzer (MiltenyilBiotec).

To determine direct binding of B7H6 and the synthetic peptides, **7**-**12**, NK92-MI cells were washed with FACS buffer and suspended with either soluble B7H6 (1 μM in PBS) labeled with AlexaFluor 488 Microscale Protein labeling Kit (Life Technologies), or the FITC-labeled peptides (0.1 - 10 μM in PBS) for 30 min (R.T., dark), washed and analyzed by flow cytometry.

To determine the optimal amount of B7H6 for direct binding studies, NK92-MI cells were washed with FACS buffer and suspended with either soluble B7H6 (20 μl, 1 μM in PBS) or soluble B7H6 (50 μl, 1 μM in PBS), both labeled with AlexaFluor 488 Microscale Protein labeling Kit (Life Technologies), for 30 min (R.T., dark), washed and analyzed by flow cytometry.

For competitive displacement studies, NK92-MI cells were initially suspended with either AlexaFluor 488-labeled soluble B7H6 (1 μM in PBS) or the FITC-labeled peptides, **7**-**12** (10 μM in PBS) for 30 min (R.T., dark). NK cells were washed with FACS buffer, centrifuged and suspended with the APC-labeled human NKp30 mAb (2 μg/mL in FACS) for another 30 minutes (R.T., dark). Cells were then washed with FACS buffer and analyzed by flow cytometry.

For competitive blocking studies, NK92-MI cells were initially treated with the APC-labeled human NKp30 mAb (2 μg/mL in FACS) for 30 min (R.T., dark). NK cells were washed

with FACS buffer, centrifuged and suspended with either AlexaFluor 488-labeled soluble B7H6 (1 μM in PBS) or the FITC-labeled peptides, **7-12** (10 μM in PBS) for an additional 30 min (R.T., dark). Cells were finally washed with FACS buffer and analyzed by flow cytometry.

For peptide blocking studies, NK92-MI cells were initially treated with soluble B7H6 (1 μM in PBS) for 30 min (R.T.). NK cells were washed with FACS buffer, centrifuged and suspended with the FITC-labeled peptides, **7-12** (10 μM in PBS) for an additional 30 min (R.T., dark). Cells were finally washed with FACS buffer and analyzed by flow cytometry.

2.7.7. ENZYME-LINKED IMMUNOSORBENT ASSAY

To assess the ability of the synthesized peptides to elicit immunostimulatory activity; the NK92-MI cells were incubated in 96 well plates at $5x10^4$ viable cells/well, and left untreated with growing media, or treated with B7H6 (0.5 μM) or the peptides, **1-6** and **13-16** (10 μM) at 37°C in 5% CO_2 humidified air. The cell culture was incubated for 24 h. and the supernatants were recovered for the detection of the inflammatory cytokines IFN-γ or TNF-α by ELISA kits following vendor instructions (ThermoScientific Inc.).

2.7.8. STATISTICAL ANALYSIS

Cytokine data were analyzed by using the unpaired two-tailed *t* test. GraphPad Prism 4 provided the software for the statistical analysis.

2.7.9. CELL VIABILITY

To evaluate the NK cells' viability following treatment with the synthetic peptides, **1-6**, or B7H6, the NK92-MI cells were incubated for 24 h in a 96 well plate, at $5x10^4$ viable cells/well.

NK cells were left untreated, and treated with soluble B7H6 (0.5 μM) or the peptides, **1**-**6** (10 μM) at 37°C in 5% CO_2 humidified air. Cells were then collected and washed with FACS buffer, centrifuged, and suspended in Guava Nexin Reagent® (100 μL/tube, from EMD Millipore). Following incubation (20 min) at room temperature in the dark, the NK cells were analyzed for early and late apoptotic events by flow cytometry following the vendor instructions.

REFERENCES

1. Vivier, E.; Tomaselo, E.; Baratin, M.; Walzer, T.; Ugolini, S. *Nat. Immunol*. **2008**, 9, 503-510.

2. Waldhauer, I.; Steinle, A. *Oncogene*. **2008**, 27, 5932-5943.

3. Kaplan, D.H.; Shankaran. V.; Dighe. A.S.; Stockert. E.; Aguet. M.; Old. L.J. *Proc. Natl. Acad. Sci*. **1998**, 95, 7556-7561.

4. Shankaran. V.; Ikeda. H.; Bruce. A.T.; White. J.M.; Swanson. P.E.; Old. L.J. *Nature*. **2001**, 410, 1107-1111.

5. Kim, S.; Iizuka, K.; Aguila, H.L.; Weissman,I.L.; Yokoyama, W.M. *Proc. Natl. Acad. Sci*. **2000**, 97, 2731-2736.

6. Villegas. F.R.; Coca, S.; Villarrubia, V.G.; Jimenez, R.; Chillon, M.J.; Jareno, J.; Zuil, M.; Callol, L. *Lung Cancer*. **2002**, 35, 23-28.

7. Ljunggren, H.G.; Malmberg, K.J. *Nat. Rev. Immunol*. **2007**, 7, 329-339.

8. Langers, I.; Renoux, V.M.; Thiry, M.; Delvenne, P.; Jacobs, N. *Biologics*. **2012**, 6, 73-82.

9. Cheng, M.; Chen, Y.; Xiao, W.; Sun, R.; Tian, Z. *Cell Mol. Immunol*. **2013**, 10, 230-252.

10. Rezvani, K.; Rouce, R.H. *Front Immunol.* **2015**, 6, 578.

11. Dunn, G.P.; Ikeda, H.; Bruce, A.T.; Koebel, C.; Uppaluri, R.; Bui, J.; Chan, R.; Diamond, M.; White, J.M.; Sheehan, K.C.; Schreiber, R.D. *Immunol. Res*. **2005**, 32, 231-245.

12. Cheng, M.; Zhang, J.; Jiang, W.; Chen, Y.; Tian, Z. *Front Med*. **2012**, 6, 56-66.

13. Klingemann, H.; Boissel, L. *Horm. Metab. Res*. **2008**, 40, 122-125.

14. Eguizabal, C.; Zenarruzabeitia, O.; Monge, J.; Santos, S.; Vesga, M.A.; Maruri, N.; Arrieta, A.; Riñón, M.; Tamayo-Orbegozo, E.; Amo, L.; Larrucea, S.; Borrego, F. *Front Immunol*. **2014**, 5, 1-10.

15. Farag, S.S.; Fehniger, T.A.; Becknell, B.; Blaser, B.W.; Caligiuri, M.A. *Expert Opin. Biol. Ther*. **2003**, 3, 237-250.

16. Srivastava, S.; Lundqvist, A.; Childs, R.W. *Cytotherapy*. **2008**, 10, 775-783.

17. Vivier, E.; Raulet, D.H.; Moretta,A.; Caligiuri, A.; Zitvogel, L.; Lanier, L.L.; Yokoyama, W.M.; Ugolini, S. *Science*. **2011**, 331, 44-49.

18. Koch, J.; Steinle, A.; Watzl, C.; Mandelboim, O. *Trends Immunol*. **2013**, 34, 182-191.

19. Pende, D.; Parolini, S.; Pessino, A.; Sivori, S.; Augugliaro, R.; Morelli, L.; Marcenaro, E.; Accame, L.; Malaspina, A.; Biassoni, R.; Bottino, C.; Moretta, L.; Moretta, A. *J. Exp. Med*. **1999**, 190, 1505-1516.

20. Li, Y.; Wang, Q.; Mariuzza, A. *J. Exp. Med*. **2011**, 208, 703-714.

21. Brandt, C.S.; Baratin, M.; Yi, E.C.; Kennedy, J.; Gao, Z.; Fox, B.; Haldeman, B.; Ostrander, C.D.; Kaifu, T.; Chabannon, C.; Moretta, A.; West, R.; Xu, W.F.; Vivier, E.; Levin, S.D. *J. Exp. Med*. **2009**, 206, 1495-1503.

22. Fiegler, N.; Textor, S.; Arnold, A.; Rolle, A.; Oehme, I.; Breuhahn, K.; Moldenhauer, G.; Witzens-Harig, M.; Cerwenka, A. *Blood*. **2013**, 122, 684-693.

23. Kaifu, T.; Escaliere, B.; Gastinel, L.N.; Vivier, E.; Baratin, M. *Cell. Mol. Life Sci*. **2011**, 68, 3531-3539.

24. Cantoni, C.; Bottino, C.; Vitale, M.; Pessino, A.; Augugliaro, R.; Malaspina, A.; Parolini, S.; Moretta, L.; Moretta, A.; Biassoni, R. *J. Exp. Med*. **1999**, 189, 787-796.

25. Pessino, A.; Sivori, S.; Bottino, C.; Malaspina, A.; Morelli, L.; Moretta, L.; Biassoni, R., Moretta, A. *J. Exp. Med*. **1998**, 188, 953-960.

26. Garcỉa-Martỉn, F.; Quintanar-Audelo, M.; Garcỉa-Ramos, Y.; Cruz, L.J.; Gravel, C.; Furic, R.; Côté, S.; Tulla-Puche, J.; Albericio, F. *J. Comb. Chem.* **2006**, 8, 213-220.

27. Hood, C.A.; Fuentes, G.; Patel, H.; Page, K.; Menakuru, M.; Park, J.H. *J. Pept. Sci*. **2008**, 14, 97-101.

28. Kelly, S.M.; Price, N.C. *Curr. Protein Pept. Sci*. **2000**, 1, 349-384.

29. Joseph, S.C.; Blackman, B.A.; Kelly, M.L.; Phillips, M.; Beaury, M.W.; Martinez, I.; Parronchi, C.J.; Bitsaktsis, C.; Blake, A.D.; Sabatino, D. *J. Pept. Sci*. **2014**, 20, 736-745.

30. See, D.; Mason, S.; Roshan, R. *Immunol. Invest*. **2002**, 2, 137-153.

31. Demo, S.D.; Masuda, E.; Rossi, A.B.; Throndset, B.T.; Gerard, A.L.; Chan, E.H.; Armstrong, R.J.; Fox, B.P.; Lorens, J.B.; Payan, D.G.; Scheller, R.H.; Fisher, J.M. *Cytometry* **1999**, 36, 340–348.

32. Harris, T.J.; Drake, C.G. *J. Immunother. Cancer*. **2013**, 1, 12.

33. Kantoff, P.W.; Higano, C.S.; Shore, N.D.; Berger, E.R.; Small, E.J.; Penson, D.F.; Redfern, C.H.; Ferrari, A.C.; Dreicer, R.; Sims, R.B.; Xu,Y.; Frohlich, M. W.; Schelhammer, P.F. *N. Engl. J. Med*. **2010**, 363, 411-422.

34. Germain, C.; Campigna, E.; Salhi, I.; Morisseau, S.; Navarro-Teulon, I.; Mach, J.P.; Pelegrin, A.; Robert, B. *Protein Eng. Des. Sel*. **2008**, 21, 665-672.

35. Nishimura, Y.; Tomita, Y.; Yuno, A.; Yoshitake, Y.; Shinohara, M. *Cancer Sci*. **2015**, 106, 505-511.

36. Verma, S.; Miles, D.; Gianni, L.; Krop, I.E.; Welslau, M.; Baselga, J.; Pegram, M.; Oh, D.Y.; Diera, V.; Guardino, E.; Fang, L.; Lu, M.W.; Olsen, S.; Blackwell, K. *N. Engl. J. Med*. **2012**, 367, 1783-1791.

37. Rosenberg, S.A.; Yang, J.C.; Restifo, N.P. Nat. Med. **2004**, 10, 909-915.

38. Kim, J.W.; Gulley J.L. *Expert Opin. Biol. Ther*. **2012**, 12, 463-478.

39. Multhhoff, G.; Pfister, K.; Gehrmann, M.; Hantschel, M.; Gross, C.; Hafner, M. *Cell Stress Chaperones*. **2001**, 6, 337-344.

40. Specht, H.M.; Ahrens, N.; Blankenstein, C.; Duell, T.; Fietkau, R.; Gaipl, U.S.; Günther C.; Gunther, S.; Habl, G.; Hautmann, H.; Hautman, M.; Huber, R.M.; Molls, M.; Offner, R.; Rödel, C.; Rödel, F.; Schütz, M.; Combs, S.E.; Multhoff, G. *Frontiers Immunol*. **2015**, 6, 1-9.

41. Thakur, A.K.; Kishore, R. *Biopolymers*. **2006**, 81, 440-449.

42. de Alba, E.; Jiménez, M.A.; Rico, M.; Nieto, J.L. *Fold Des*. **1996**, 1, 133-44.

43. Roccatano, D.; Colombo, G.; Fioroni, M.; Mark, A.E. *Proc. Natl. Acad. Sci*. **2002**, 99, 12179-12184.

44. Salinas, R.K.; Shida, C.S.; Pertinhez, T.A.; Spisni, A.; Nakaie, C.R.; Paiva, A.C.; Schreier, S. *Biopolymers*. **2002**, 65, 21-31.

45. Reiersen, H.; Rees, A.R. *Protein Eng*. **2000**, 13, 739-744.

46. Joyce, M.G.; Tran, P.; Zhuravleva, M. A.; Jaw, J.; Colonna, M.; Sun, P.D. *Proc. Natl. Acad. Sci*. **2011**, 108, 6223-6228.

47. Wlodkowic, D.; Telford, W.; Skommer, J.; Darzynkiewicz, Z. *Methods Cell Biol*. **2011**, 103, 55-98.

48. Kuipers, B.J.H.; Gruppen, H. J. *Agric. Food Chem*. **2007**, 55, 5445-5451.

CHAPTER 3: PEP42, A CANCER-TARGETING PEPTIDE THAT RECOGNIZES CELL SURFACE GRP78 ON THE SURFACE OF CANCER CELLS

3.1. ABSTRACT

The need for selective cancer targeting ligands, that can selectively and efficiently target cancer cells, has led to more efficient delivery of drug payloads while reducing harmful side effects. In an effort to identify novel therapeutic leads, a series of cyclic peptides generated by phage-display bio-panning led to the isolation of peptidic ligands which targeted and penetrated human melanoma Me6652/4 tumor cells. The peptidic ligand was identified as a 13-mer cyclic peptide, namely Pep42, which selectively binds and internalizes into Me6652/4 cells. Interestingly, Pep42 was found to bind selectively to the oncoprotein receptor, GRP78, a chaperone protein and key modulator of the UPR mechanism. GRP78 is also known to be overexpressed and cell surface localized in tumor cells. In this study, Pep42, its FITC-labeled derivatives and a series of poly(ethylene glycol)-linked Pep42 sequences with reactive *N*-succinimidyl carbamate linkages have been developed by solid phase peptide synthesis. Pep42 and its FITC-labeled derivatives have been tested for their capabilities to bind to the HepG2 human hepatocellular carcinoma cells. Flow cytometry revealed comparable binding of the synthetic peptides relative to the anti-GRP78 primary antibody at equal concentrations (100 nM). A blocking assay in between the human anti-NKp30 mAb or Pep42, and the specific N-20 GRP78 peptide blocker showed similar blocking capabilities of either the primary antibody or Pep42, suggesting binding specificity to GRP78. In a cell death assay, Pep42 was found to be non-toxic. Moreover, the reactive *N*-succinimidyl carbamate derived peptides were envisioned to behave as reactive probes for their incorporation within bioactive proteins such as B7H6. Therefore, Pep42 may prove to be a promising cancer targeting peptide for the development of immunostimulatory peptide-protein conjugates.

3.2. INTRODUCTION

The unfolded protein response (UPR) is an adaptive mechanism responsible for maintaining the endoplasmic reticulum (ER) homeostasis.[1] The ER a cellular organelle primarily responsible for protein synthesis, folding and maturation. The 78 kilodalton glucose regulated protein 78, GRP78, (also known as the immunoglobulin heavy chain binding protein BiP), is a chaperone and a member of the heat shock family of proteins, that plays a key role in protein folding and regulation of the UPR mechanism in the ER.[2] Moreover, GRP78 regulates intracellular signaling pathways associated with development of the embryo, aging, Ca^{2+} homeostasis, and the insulin/IGF-1 signaling pathway.[3] When in homeostatic conditions of the ER, GRP78 binds to the three transmembrane sensors of ER stress. These include the activating transcription factor 6 (ATF6) α and β isoforms, the protein kinase RNA-like ER kinase (PERK), and the inositol-requiring enzyme 1α (IRE1α), and IRE1β, thus inhibiting its activity.[4] Under stress conditions of the ER, GRP78 is released from the transmembrane stress sensors leading to its activation and initiation of the UPR mechanism. The UPR mechanism results in reduced protein translation, degradation of misfolded proteins, an increased protein folding capacity and increased efficiency of quality control mechanisms associated with the ER; including the upregulation of GRP78.[1,5] Under chronic ER stress conditions, the UPR is capable of triggering cell death by apoptosis.[6,7]

The cancer microenvironment is characterized by conditions such as altered glucose metabolism, altered blood flow, and hypoxia; all conditions that induce ER stress.[8] Under these conditions, ER stress signaling pathways play an important role in tumor progression and survival [8] Tumor transformation promotes GRP78 overexpression and cell surface translocation, where GRP78 plays a pivotal role as an oncoprotein receptor modulating cell proliferation, conferring

apoptosis resistance and chemoresistance. Thus, GRP78 maintains inherent pro-survival characteristics that aid in tumor progression and metastatic spread (**Figure 3.1**).[9-13] Moreover, GRP78 has been found to be cell surface expressed and localized on cancer cells, but not on normal tissues, making it a valuable biomarker for the development of cancer-targeting strategies.[13-16] Finally, cell surface expression of GRP78 has enabled selective tumor targeting, as demonstrated by the use of antibodies and short peptidic ligands, potentially minimizing off-tumor side effects and increasing delivery efficiency.[17-19]

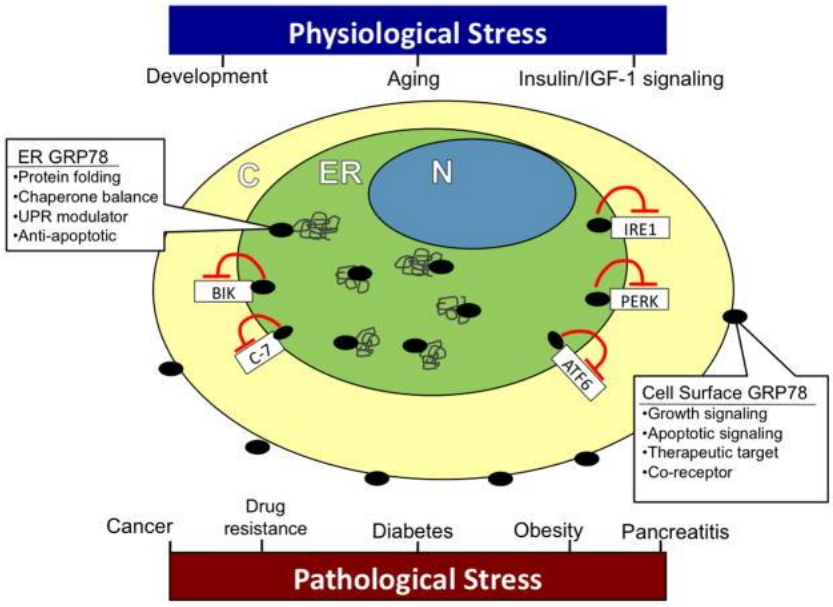

Figure 3.1. Role of GRP78 under physiological and pathological stress. Figure adapted from *Curr Opin Cell Biol*, **2011**, *23*, 150-156.[3]

In an effort to identify peptidic ligands for drug delivery that could target cell surface GRP78 on cancer cells with high specificity, Janda and co-workers reported the phage display bio-panning peptide library selection of Pep42.[14] Importantly, Pep42, a 13-mer cyclic peptide of amino acid sequence $\overline{\text{CTVALPGGYVRVC}}$, bound selectively to the highly metastatic human melanoma cell line Me6652/4, but poorly to the low metastatic cell line Me6652/56 that exhibits

normal GRP78 function and expression.[14,20] Interestingly, internalization of a mutated Pep42 cyclic sequence, Mut42, in which the *C*-terminal Val12 was substituted for Lys, for fluorescein isothiocyanate (FITC) labeling, revealed that the cyclic constraint was required for cell uptake and internalization. Alternatively, the linear sequence, Lin42, failed to internalize within cells (**Figure 3.2**).[14] Moreover, a photoaffinity assay of the photoliable peptide ligand Mut42-Bpa-biotin, followed by SDS-PAGE and western blot analyses, identified GRP78 as the cell surface receptor for Pep42.[14] Finally, pre-incubation of the Me6652/4 cell line with anti-GRP78 monoclonal antibody inhibited binding and subsequent internalization of Mut42. Taken together, these results demonstrates that Pep42 selectively binds to cell surface GRP78 and internalizes through receptor mediated endocytosis.[14]

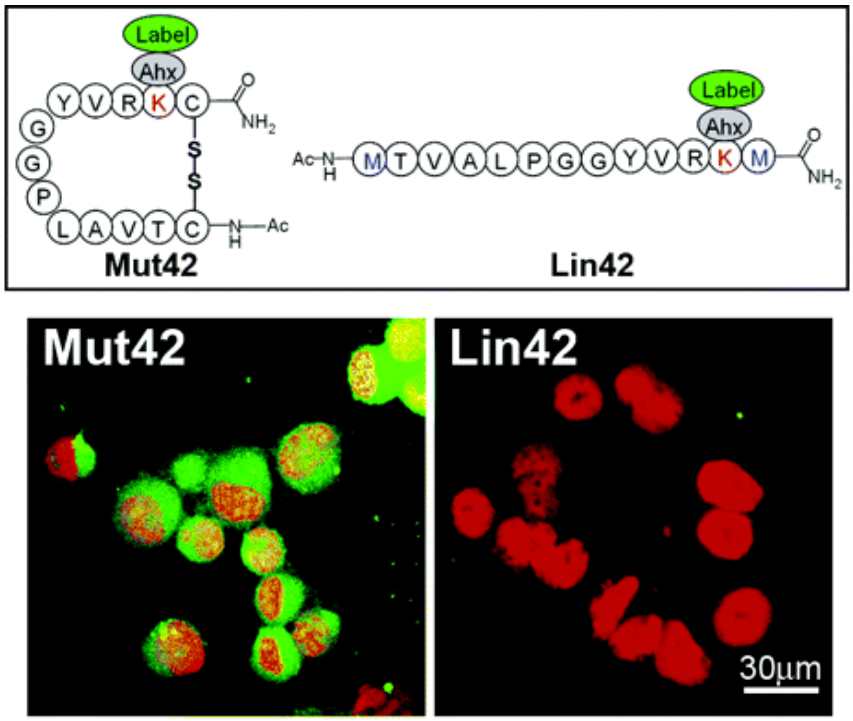

Figure 3.2. Role of Pep42 structure on Me6652/4 cell internalization. Figure adapted from *Biochemistry*, **2006**, *45*, 9434-9444.[14]

In a more recent study, Joseph and co-workers, evaluated the internalization capabilities of Pep42 when coupled to varying lengths (3-12) of poly(arginine) sequences, known to possess ionic binding and cell membrane translocation capabilities.[21-23] Flow cytometry studies on the cell surface GRP78 overexpressing cell line HepG2 revealed comparable binding affinity and selectivity of the FITC-labeled Pep42 sequence compared to the Alexa Fluor 488-labeled N-20 anti-GRP78 primary antibody.[24] Interestingly, the FITC-labeled Pep42-(poly)arginine peptides showed increased fluorescence signaling activity that was dependent on the length of the poly(arginine) sequences (0, 3, 6, 9, 12). These results indicate the cell translocation capabilities of Pep42 is contingent on the lengths of the polyarginine sequences, with the lengthier polyarginines (6-12) providing greater cell uptake when compared to the shorter polyarginine sequences (0-3). Moreover, FITC signaling decreased when the HepG2 cells were pre-incubated with the N-20 GRP78 specific peptide blocker then followed by peptide treatment, suggesting antibody blocking of GRP78 and inhibition of GRP78-dependent uptake of the FITC-labeled poly(arginine) derived Pep42 sequences (**Figure 3.3**).[24] Laser scanning confocal microscopy studies confirmed the selective binding and internalization of the FITC-Pep42-(poly)arginine sequences within HepG2 cells, which was also blocked when the cells were pretreated with the N-20 GRP78 peptide blocker.[24]

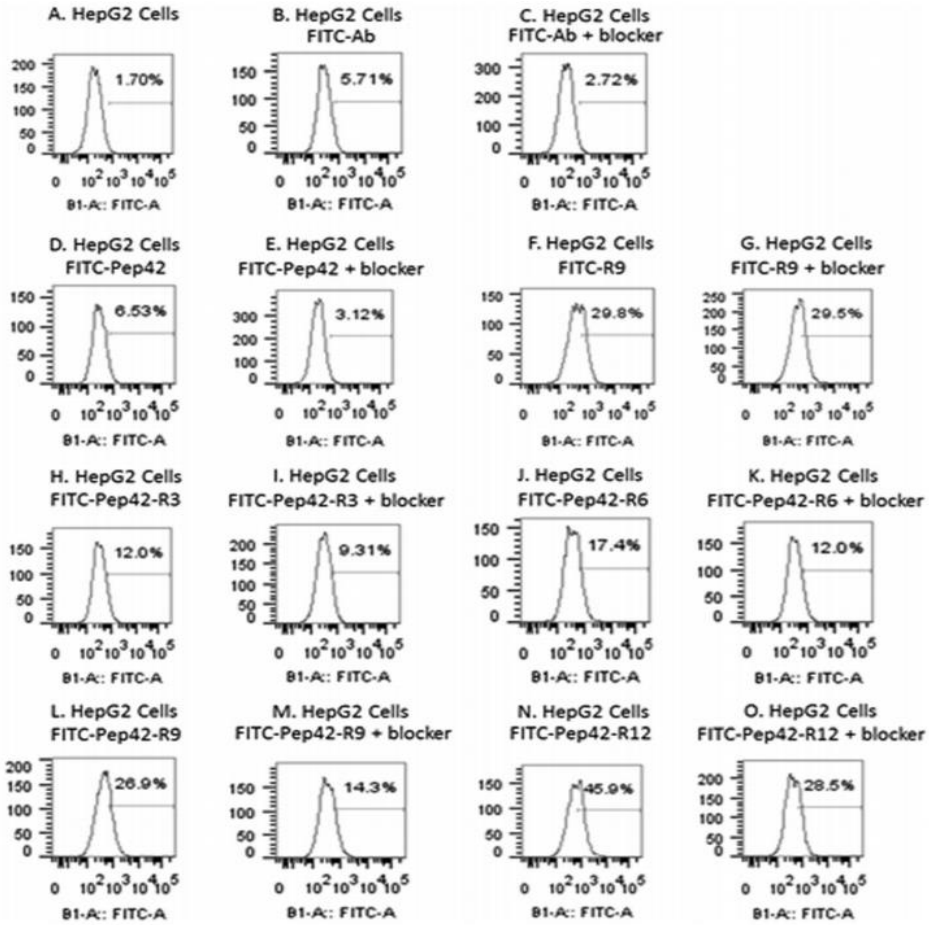

Figure 3.3. Fluorescence signaling activity of FITC-Pep42-(poly)arginine sequences on human hepatocellular carcinoma cell line HepG2. Figure adapted from *J. Pept. Sci.*, **2014**, *20*, 736-745.[24]

Highlighting the previous work conducted by Joseph and co-workers, in this chapter we report the synthesis, characterization and biological evaluation of Pep42, and its FITC-labeled derivative, on the human hepatocellular carcinoma cell line HepG2. Moreover, we also report the activation of Pep42 with a reactive *N*-succinimidyl carbamate linkage, which was envisioned to facilitate conjugation with bio-active proteins, including B7H6. These studies will set the stage for the development of GRP78-targeting immunostimultaory peptide-protein conjugates (Chapter 4).

3.3. PROJECT OBJECTIVES

The main research objectives of this chapter are related to the synthesis, characterization, and biological evaluation of Pep42 and its FITC-labeled sequences. Moreover, a description detailing the synthesis and characterization of poly(ethylene glycol) PEG-derived Pep42 is also reported in this chapter. The incorporation of a *C*-terminal Lys is used for activation via *N*-succinimidyl carbamate (NSC) chemistry. The latter is expected to be useful for the site-selective conjugation of Pep42 with bio-active proteins, such as B7H6, for the development of peptide-protein conjugates that may be applied in cancer immunotherapy applications. The peptides were developed by the Fmoc SPPS method for the rapid production of the Pep42 derived sequences. The incorporation of FITC was used for labeling Pep42 for biological studies in HepG2 cells, whereas PEG-linked Pep42 with the *C*-terminal NSCs were synthesized for follow-up bioconjugation studies. Following peptide synthesis, ESI-LCMS was used to analyze, purify and confirm the identities of the peptides. The binding affinity, specificity, and internalization capabilities of the FITC derived Pep42 were determined in HepG2 cells which were found to overexpress GRP78 at the cell surface according to flow cytometry. Therefore, Pep42 exhibits the effective capabilities to target HepG2 cells that display cell surface GRP78. These findings are important for the development of cell surface recognition studies that can lead to the identification of targeting and activating ligands for tumor immunotherapy applications (Chapter 4). Moreover, the toxicity of these synthetic peptides to HepG2 cells was assessed by evaluating apoptosis using a Trypan blue cell exclusion staining technique. Pep42 was found to be non-toxic to the HepG2 cells, underscoring its potential benign utility as a targeting or delivery vector in tumors cells that express cell surface GRP78.

3.4. RESULTS

3.4.1. SOLID PHASE PEPTIDE SYNTHESIS

The synthesis of the Pep42 peptide sequence CTVALPGGYVRVC-$CONH_2$, **17**, was accomplished by conventional Fmoc-based solid phase peptide synthesis on a Rink amide linker hydrophilic PEG-based resin (NovaPEG, 0.52mmol/g).[24] In our synthetic approach, HCTU was selected as coupling reagent with NMM acting as base and DMF as solvent resulting good coupling efficiencies in 20 min.[26] Fmoc deblocking was accomplished with piperidine and the *N*-terminus was elongated with 6-aminohexanoic acid, (Ahx) resulting in the Ahx-Pep42 sequence which was further labeled with FITC to yield peptide **2** for its use in biological studies (**Figure 3.4**). Peptides, **17** and **18**, were further purified by semi-preparative RP HPLC and isolated in purities ≥93%, and pure yields of 14% and 24% respectively. The identities of the synthetic peptides **17** and **18** were confirmed by mass spectrometry which validated sequence composition based on mass/charge ratios (**Table 3.1**).

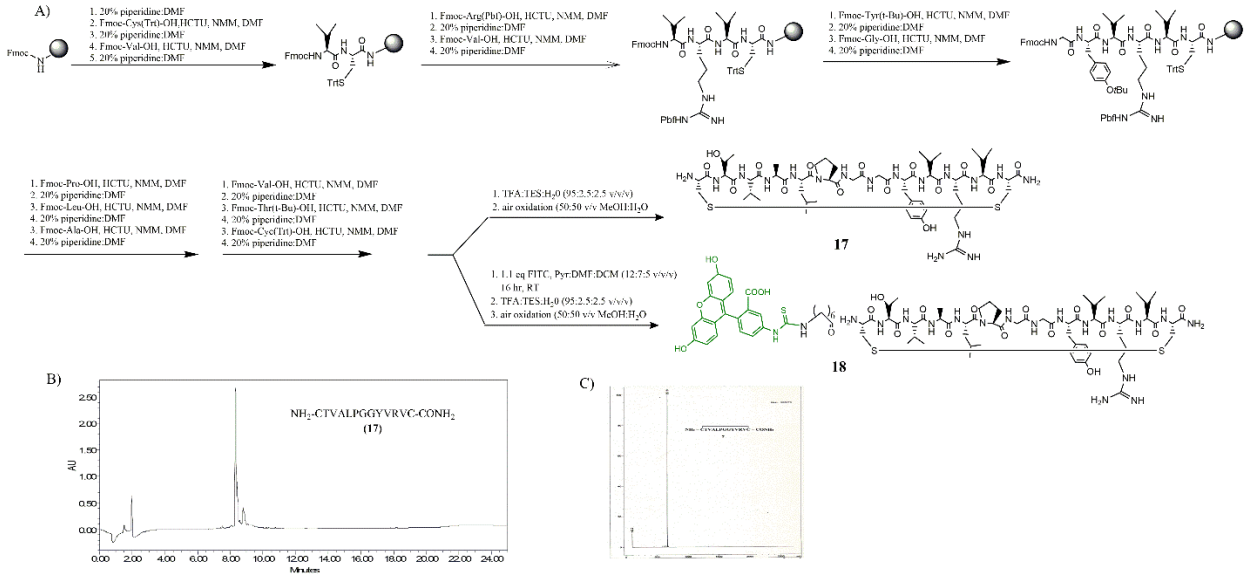

Figure 3.4. Representative solid phase peptide synthesis and LCMS characterization for peptides **17** and **18**. (A) Fmoc-solid-phase peptide synthesis and FITC labeling for peptides **17** and **18**, respectively. (B) RP-HPLC for CTVALPGGYVRVC-$CONH_2$, **17** and (C) MS for CTVALPGGYVRVC-$CONH_2$, **17**.

Table 3.1. Characterization of the synthetic peptides **17** and **18**.

Peptide	Sequence	Crude Purity (%)[a]	Purified Purity (%)[b]	Pure Yield (%)[c]	MW (g/mol)[d]	Z[e]	RT (min)[f]	RT (min)[g]
17	NH_2-CTVALPGGYVRVC-$CONH_2$	93	99(98)	14	667.9 (667.8)	2	11.2	9.40
18	FITC-$(CH_2)_5$-CTVALPGGYVRVC-$CONH_2$	95	95(95)	24	451.9 (452.1)	4	8.70	11.4

[a]Crude purities by RP-HPLC at 214 nm using 2-82% MeCN/H_2O with 0.1% TFA over 18 min.
[b]Purified purities by RP-HPLC at 214 nm using 2-82% MeCN(MeOH)/H_2O with 0.1% TFA(FA) over 18 min.
[c]Pure yields based on the resin loading.
[d]Observed mass (expected mass) as $[M + H]^+/Z$ detected by LCMS in positive mode.
[e]Charged state of the peptides as detected by LCMS in positive mode.
[f]Retention times using 2-82% MeOH/H2O (0.1% FA) over 18 min.
[g]Retention times using 2-82% MeCN/H2O (0.1% TFA) over 18 min.

The synthesis of the *C*-terminal PEG-based Pep42 sequences were also accomplished by conventional Fmoc-based solid phase peptide synthesis on the NovaPEG resin (0.47mmol/g).[24,26] Peptides **19-21** were further labeled with FITC to obtain peptides **22-24** for their use in biological studies (**Figure 3.5**). Peptides were recovered in crude yields (16-41%) and purities (35-82%) according to RP HPLC. The identities of the synthetic peptides were confirmed by mass spectrometry which validated sequence composition based on mass/charge ratios (**Table 3.2)**.

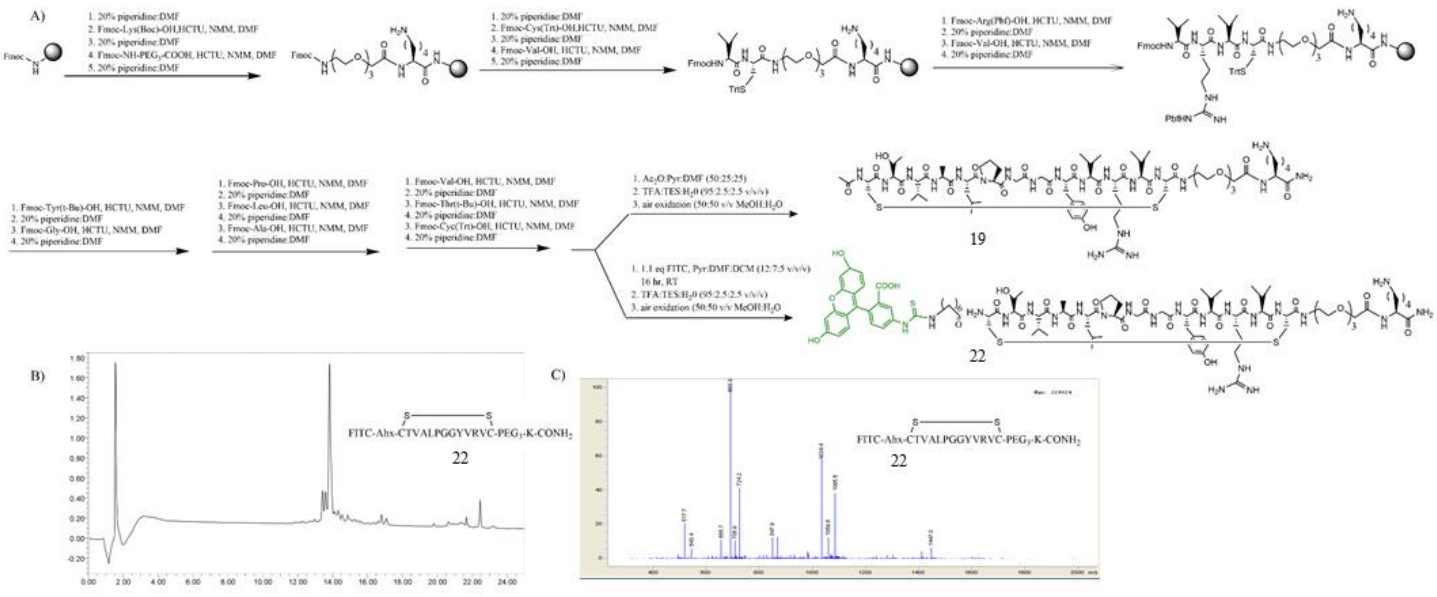

Figure 3.5. Representative solid phase peptide synthesis and LCMS characterization for peptides **19** and **22**. (A) Fmoc-solid-phase peptide synthesis and FITC labeling for peptides **19** and **22**, respectively. (B) RP HPLC analyses for FITC-Ahx-CTVALPGGYVRVC-PEG_3-K-$CONH_2$, **22** and (C) ESI-MS analyses for FITC-Ahx-CTVALPGGYVRVC-PEG_3-K-$CONH_2$, **22**.

Table 3.2. Characterization of the synthetic peptides **19-24**.

Peptide	Sequence	Crude Purity (%)[a]	Crude Yield (%)[b]	MW (g/mol)[c]	Z[d]	RT (min)[e]	RT (min)[g,h]
19	CH_3-CO-NH-$(CH_2)_5$-CTVALPGGYVRVC-PEG_3-K-$CONH_2$	67	21	912.5 (910.9)	2	12.2	7.21
				609.0 (607.6)	3		
20	CH_3-CO-NH-$(CH_2)_5$-CTVALPGGYVRVC-PEG_6-K-$CONH_2$	82	33	1013.6 (1012.5)	2	12.5	7.29
21	CH_3-CO-NH-$(CH_2)_5$-CTVALPGGYVRVC-PEG_{12}-K-$CONH_2$	72	41	1217.2 (1216.1)	2	12.8	7.47
				811.8 (811.1)	3		
22	FITC-NH_2-$(CH_2)_5$-CTVALPGGYVRVC-PEG_3-K-$CONH_2$	81	16	1085.4 (1085.5)	2	15.7[f]	6.75[h]
				724.3 (723.3)	3		
23	FITC- NH-$(CH_2)_5$-CTVALPGGYVRVC-PEG_6-K-$CONH_2$	35	19	1187.2 (1186.0)	2	14.3	8.62
				791.8 (790.6)	3		
24	FITC- NH-$(CH_2)_5$-CTVALPGGYVRVC-PEG_{12}-K-$CONH_2$	45	28	1390.7 (1391.1)	2	14.4	8.70
				928.6 (927.7)	3		
				696.0 (696.0)	4		

[a]Crude purities by RP-HPLC at 220 nm using 2-80% MeOH/H_2O with 0.1% FA over 18 min.
[b]Crude yields based on the resin loading..
[c]Observed mass (expected mass) as $[M + H]^+/Z$ detected by LCMS in positive mode.
[d]Charged state of the peptides as detected by LCMS in positive mode.
[e]Retention times using 2-80% MeOH/H2O (0.1% FA) over 18 min.
[f]Retention times using 20-80% MeOH/H2O (0.1% FA) over 18 min.
[g]Retention times using 2-80% MeCN/H2O (0.1% FA) over 18 min.
[h]Retention times using 20-80% MeCN/H2O (0.1% FA) over 18 min.

3.4.2 SOLUTION-PHASE SYNTHESIS OF THE NSC DERIVED PEPTIDES

The crude FITC labeled synthetic peptides, **22-24**, were further activated at the ε-amino group of the *C*-terminal Lys residue using described NSC chemistry for activating and ligating peptides onto proteins.[32] In our synthetic approach, crude peptides **22-24** were reacted with excess disuccinimidyl carbonate (DSC) and trimethylamine (TEA) in anhydrous DMF for 1 h at room temperature. Under these reaction conditions, the formation of the *C*-terminal NSC-derived peptides, **25-27**, were closely monitored by LC-MS (**Figure 3.6**). The analyses confirmed good conversions (30-75%) and stability of the NSC-activated peptides as little decomposition was observed following work-up and purification of the peptides. The characterization data for the peptides indicated good crude yield recoveries (13-28%) and purities (24-31%) followed by RP

HPLC purifications. Moreover, the identities of the peptides, **25-27**, were confirmed as their mass:charge ratios using ESI MS (**Table 3.3**).

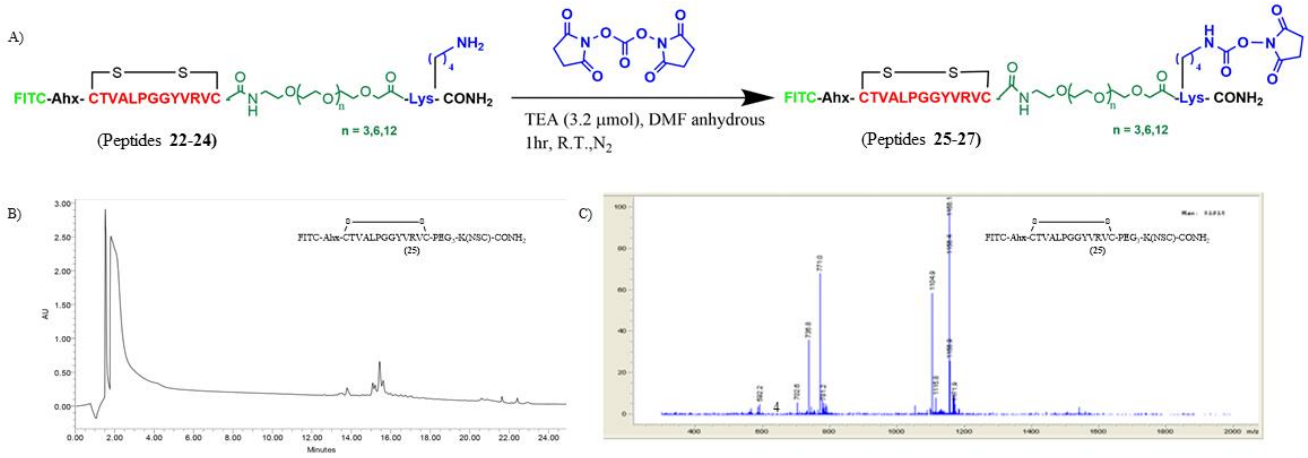

Figure 3.6. Schematic representation of the formation of the NSC peptides **25-27** and LCMS characterization of peptide **25**. (A) General schematic of the DSC reaction with the FITC-labeled Pep42 derived peptides. (B) RP-HPLC analyses of FITC-Ahx-CTVALPGGYVRVC-PEG_3-K(NSC)-$CONH_2$, **25**. (C) ESI-MS analyses of FITC-Ahx-CTVALPGGYVRVC-PEG_3-K(NSC)-$CONH_2$, **25**.

Table 3.3. Characterization of the NSC derived peptides **25-27**.

Peptide	Sequence	Conversion (%)	Crude Purity (%)[a]	Crude Yield (%)[b]	MW (g/mol)[c]	Z[d]	RT (min)[e]	RT (min)[f,g]
25	FITC-NH_2-$(CH_2)_5$-CTVALPGGYVRVC-PEG_3-K(NSC)-$CONH_2$	60	24	13	1156.1 (1155.0)	2	15.4	9.363[g]
					771.0 (770.0)	3		
26	FITC- NH-$(CH_2)_5$-CTVALPGGYVRVC-PEG_6-K(NSC)-$CONH_2$	29	25	14	1257.6 (1256.5)	2	15.9	13.5
					838.7 (837.7)	3		
27	FITC- NH-$(CH_2)_5$-CTVALPGGYVRVC-PEG_{12}-K(NSC)-$CONH_2$	75	29	28	1461.6 (1461.9)	2	16.0	13.4

[a]Crude purities by RP-HPLC at 220 nm using 2-80% MeOH/H_2O with 0.1% FA over 18 min.
[b]Crude yields based on the resin loading..
[c]Observed mass (expected mass) as $[M + H]^+/Z$ detected by LCMS in positive mode.
[d]Charged state of the peptides as detected by LCMS in positive mode.
[e]Retention times using 2-80% MeOH/H2O (0.1% FA) over 18 min.
[f]Retention times using 2-80% MeCN/H2O (0.1% FA) over 18 min.
[g]Retention times using 20-80% MeCN/H2O (0.1% FA) over 18 min.

3.4.3. DIRECT BINDING STUDIES OF FITC-Pep42 ON THE HepG2 CELLS.

In order to evaluate the ability of the FITC-labeled Pep42, **18**, to bind to the cell surface of human hepatocellular carcinoma cells, HepG2 cells were incubated for 30 minutes with either AlexaFluor 488-labeled N-20 anti-GRP78 mAb (100 nM) or peptide **18** (100 nM) in PBS. Their binding capabilities were compared by flow cytometry (**Figure 3.7**). Flow cytometry revealed comparable HepG2 cell binding (5.71-6.53%) between the anti-GRP78 mAb and the FITC-Pep42 peptide, **18**. Moreover, the peptide was found to display selective binding on the HepG2 cells, as seen with a decreased signal (3.12%) when HepG2 cells were pre-incubated with the corresponding N-20 GRP78 peptide blocker (10 mg/ml) (**Figure 3.7**).

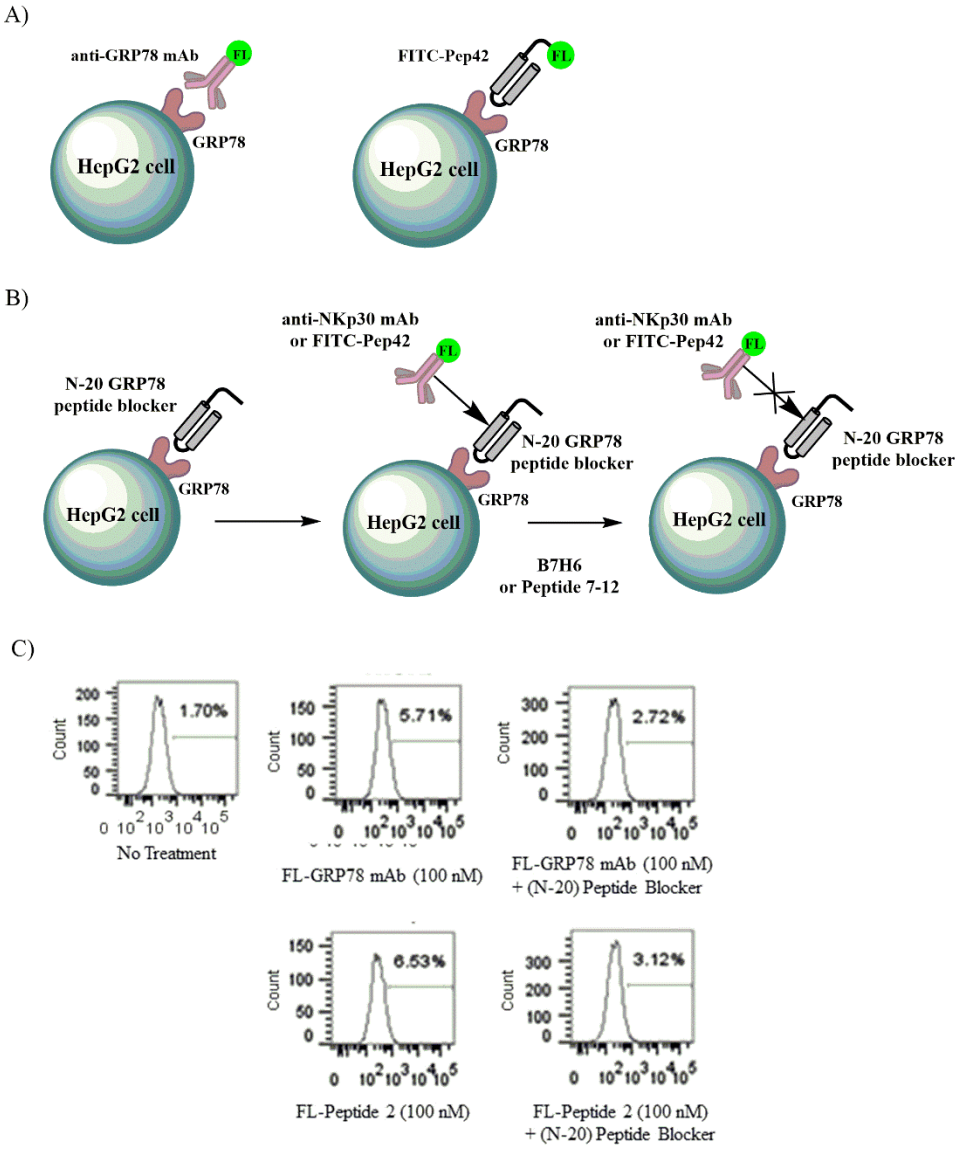

Figure 3.7. Binding studies on the HepG2 cells. (A) Figurative representation of the HepG2 cells' binding to either the AlexaFluor 488-labeled N-20 anti-GRP78 mAb or the FITC-labeled peptide **18**. (B) Figurative representation of the HepG2 cells' pretreated with N-20 GRP78 peptide blocker followed by treatment with either the AlexaFluor 488-labeled N-20 anti-GRP78 mAb or the FITC-labeled peptide **18**. (C) Flow cytometry analyses of the HepG2 cells' binding to the AlexaFluor 488-labeled N-20 anti-GRP78 mAb (100 nM) or the FITC-labeled peptide **18** (100 nM), with or without N-20 GRP78 peptide blocker (10 mg/ml).

3.4.4. HEPG2 CELLS' VIABILITY.

In order to test the cytotoxicity of the synthetic Pep42, a Trypan blue cell staining assay was conducted with the HepG2 cells treated with Pep42. Cell viability assays quantified the number of dead cells, 5-10%, following peptide treatment at a concentration of 0.15 mM (**Figure 3.8**). Therefore, Pep42 was found to be non-toxic to the HepG2 cells, underscoring its potential utility as a safe, tumor targeting delivery vector.

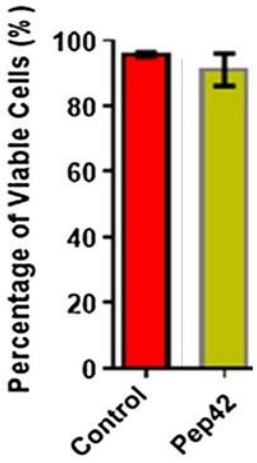

Figure 3.8. HepG2 cells' viability assessed by Trypan blue staining assay. The HepG2 cells were incubated with either no treatment (control) or the synthetic peptide, **17**, (0.15 mM) for 48 h at 37 °C. The cells were then treated with enzyme-free dissociation buffer for 3 min at 37 °C, re-suspended in PBS, and stained with Trypan blue 0.4 % stain (100 μl). Cell viability was counted using a countess automated cell counter. Statistical significance was determined by analysis of variance ($p<0.05$).

3.5. DISCUSSION

Synthesis of the cyclic hydrophobic peptide Pep42, **17**, its FITC-labeled derivative, **18**, and the PEG-derived sequences, **19-24**, were accomplished using the hydrophilic NovaPEG resin. This resin was chosen due to its high swelling capabilities in H_2O, DMF, DCM and TFA, that results in improved coupling efficiencies, better isolated peptide purities and yields during solid phase peptide synthesis (SPPS). This resin has been used in the synthesis of challenging, hydrophobic peptide sequences and has improved synthesis yields and peptide crude purities by reducing peptide aggregation on solid phase. The higher swelling capabilities of the PEG-based resins function to enhance the surface area for reaction on solid phase. Therefore, these resins have been found to outperform the classical Merrifield-based polystyrene resins and are in regular use in Fmoc-based solid phase peptide synthesis.[27] The Fmoc-SPPS protocol followed for peptide synthesis has been previously described in Chapter 2, and was developed according to standard procedures for the synthesis of Pep42 **17**, and FITC-labeled Pep42, **18**, and the PEG-derived sequences, **19-24**, (**Figures 3.4** and **3.5**).[24,25] The efficiency of the peptide synthesis procedure was analyzed by RP-HPLC and revealed sufficient peptide crude purities (93-95%) and isolated yields (14-24%) for further biological investigations. Key to the efficient synthesis of Pep42 is the quantitative conversion of the linear, free thiol, to the cyclic, disulfide-linked, Pep42 sequence. In our method, air oxidation in a combination of H_2O:MeOH, resulted in slow but complete conversion of linear to cyclic Pep42. Alternatively, air oxidation in the presence of denaturants including GnHCl, may be employed to enhance the rate of the disulfide bond forming reaction but with the requirement of additional desalting and refolding steps.[28] The Pep42 sequence identities were validated by ESI-MS, and confirmed the molecular weights of the peptides as selected mass:charge ratios (**Table 3.1**).

Synthesis of the PEG-derived Pep42 sequences, **19-21**, and their FITC-labeled derivatives, **22-24**, was also accomplished by standard Fmoc-SPPS on the NovaPEG resin as described above. The PEG linkers (3, 6, 12) were found to be amenable to standard Fmoc-SPPS procedures and incorporated as their Fmoc-NH-PEG_3-propionic acid for the synthesis of peptides **19-21**, and the FITC-labeled peptides, **22-24** (**Figure 3.5**).[24,26] Peptide synthesis was analyzed by RP-HPLC and revealed good crude purities (35-82%) and yields (16-41%), presumably due to the effect of the PEG-linker, which has been shown to reduce aggregation and poor coupling efficiencies of lengthy, hydrophobic sequences during the course of Fmoc-SPPS.[25] Peptide sequence identities (**19-24**) were validated by ESI-MS, that confirmed the molecular weights of the peptides as selected mass:charge ratios (**Table 3.2**).

The FITC-labeled Pep42 peptides **22-24** were then converted to their active NSC derivatives **25-27** following a literature described activation procedure.[32] In our synthetic method, the crude peptides **22-24** with reactive *C*-terminal Lys were activated with an excess of DSC and TEA in anhydrous DMF, under N_2 conditions, to afford the NSC activated peptides, **25-27** (**Figure 3.6**). The ε-amino group of Lys was expected to be selectively activated by these reaction conditions due to its enhanced nucleophilcity in comparison to the remaining residues within the sequence. However, side reactions have been reported, due to the generation of reactive isocyanates that can be minimized by the addition of substoichiometric amounts of TEA. [32] Unstable isocyanates may react with other, potentially nucleophilic groups such as alcohols, thiols and phenols that may contribute to lower selectivity and the formation of side-products. Stable cyclic urea products may also be anticipated by the addition of multiple Lys residues within the peptide sequence. In our case, reaction conditions were adopted to minimize unwanted side reactions and to favor the formation of the desired NSC-activated peptides. Following activation,

the reaction was quenched with a 1% TFA/H_2O. The formation of the NSC-derived peptides, **25-27**, was confirmed by ESI-MS and RP-HPLC. Further RP-HPLC analyses confirmed the generation of a more hydrophobic NSC derivative shown by the more retained peaks in two solvent systems MeOH/H_2O and MeCN/H_2O. ESI-MS analyses of the NSC-derived peptides confirmed activation at the expected ε amino group of the Lys residue in the peptide sequence, and showed a stable NSC derivative in solution, even after 48 h of the activation reaction. Further ESI-MS analyses were used to calculate the percent conversions, indicating efficient production of the NSC-derived peptides using the reported conditions (30-75%) (**Table 3.3.**). The NSC-derived Pep42 sequences may therefore be applied to the ligation with B7H6, for the generation of bifunctional peptide-protein conjugates that can target GRP78 presenting tumor cells and effect NK-dependent immunostimulatory activity towards their eradication. A brief description of this on-going and future work is presented briefly in Chapter 4.

The HepG2 hepatoblastoma cell line is known to express GRP78 at the cell surface. Previous studies have determined that GRP78 knockdown in HepG2 cells results in notable cell death, indicating that the HepG2 cells are addicted to GRP78.[29,30] Flow cytometry assays were used to confirm the cell surface expression levels of GRP78 on the HepG2 cells with the Alexa Fluor 488-labeled N20- anti-GRP78 primary antibody.[24] The FITC-Pep42 displayed comparable binding to the HepG2 cells as the anti-GRP78 antibody. Moreover, the binding of both the GRP78 primary antibody (100 nM) and the FITC-Pep42 to the HepG2 cells were found to be blocked comparably when the HepG2 cells were pretreated in the presence of the N-20 GRP78 blocking peptide. These results confirm the HepG2 cell surface binding specificities of Pep42 for the GRP78 receptor (**Figure 3.7**). Also of note, Pep42 was found to penetrate poorly in HepG2 cells, limiting its function to cell surface binding activity. Cell uptake efficiency may be enhanced by the

incorporation of the poly(arginine) sequences that are known to function as cell penetrating peptides.[24] Thus, Pep42 remains an efficient GRP78 cell surface binding ligand and its internalization capabilities may be further enhanced by the incorporation of polyarginine sequences.

The toxicity of Pep42 on the hepatocellular cancer cell line HepG2 was analyzed by a Trypan blue cell staining assay.[31] The cell death assay exhibited low cell death (**Figure 3.5**) after treatment with Pep42 (0.15 mM). Taken together, all the findings highlight the potential use of Pep42 as a cancer targeting peptide for the detection and treatment of GRP78-harboring tumors.

3.6. CONCLUSIONS

In this chapter, the synthesis, characterization and biological evaluation of the GRP78 targeting peptide Pep42 on the HepG2 cell line has been studied. The selection of Pep42 as a cancer targeting cyclic peptide was first revealed by Janda and co-workers as a highly selective ligand for the GRP78 surface receptor on melanoma cells through phage display bio-panning.[14] With the use of a polar, poly(ethylene glycol)-based resin (NovaPEG), Pep42 and its FITC-labeled derivatives were successfully synthesized in good yields (14-24%) and purities (>95%) following RP-HPLC and ESI-MS analyses and separation. Flow cytometry revealed comparable binding abilities of FITC-Pep42 to GRP78 when compared to the Alexa Fluor 488-labeled N20-anti-GRP78 primary antibody. The GRP78 binding interactions were abolished when the HepG2 cells were pretreated with a N20-GRP78 peptide blocker, indicating GRP78 binding specificity for the Pep42 sequence on the HepG2 cells. Moreover, a *C*-terminal activation procedure using NSC chemistry has been developed for the Pep42 sequence. This method not only resulted in the effective activation of peptides but may also be applied for the ligation of peptides onto bio-active

proteins, including B7H6. The latter is a focal point of our on-going studies (Chapter 4) aimed at the development of new GRP78-targeting ligands for cancer immunotherapy applications.

3.7. MATERIALS AND METHODS

3.7.1 MATERIALS

Amino acids for the synthesis of all peptides, Fmoc-Arg(Pbf), Fmoc-Cys(Trt), Fmoc-Leu, Fmoc-Pro, Fmoc-Val, Fmoc-Gly, Fmoc-Tyr(t-Bu), Fmoc-Thr(t-Bu), Fmoc-Ala, and Fmoc-εAhx, were purchased from Novabiochem (San Diego, CA, USA), and Fmoc-NH-PEG_3-Propionic Acid from aapptec (Lousville, KY). Peptide syntheses were conducted on a Rink Amide ChemMatrix (0.52 mmol/g) (Novabiochem, San Diego CA, USA). 2-(6-chloro-1H-benzotriazole-1-yl)-1,1,3,3-tetramethylaminium hexafluorophosphate, HCTU, was purchased from Advanced ChemTech (Louisville, KY, USA). Fluorescein isothiocyanate, FITC, was purchased from Advanced ChemTech (Louisville, KY) as a mixture of isomers and used in the dark to fluorescently label all peptides. Trifluoroacetic acid, TFA, (Biograde) was purchased from VWR (Radnor, PA, USA); *N*-*N*-dimethylformamide, DMF, was purchased from J.T. Baker (St. Lousville, KY). Acetonitrile, MeCN, and methyl alcohol, MeOH, dichloromethane, DCM, piperidine, *N*-methylmorpholine, triethylsilane (98+%), TES, were all purchased from Aldrich (Milwaukee, WI). Diethyl ether (99%, ACS), Et_2O, used to precipitate peptides was purchased from Sigma Aldrich (St. Louis, MO, USA). All chemicals were used directly as received.

3.7.2. PEPTIDE SYNTHESIS

All peptides were synthesized by stepwise manual solid phase peptide synthesis using Fmoc-chemistry. Fmoc-amino acids (300 mol%, 0.16 mmol) were coupled on a Rink amide linker

poly(ethylene glycol) solid support (0.52 mmol/g, 0.05 mmols) for 20 minutes using [HCTU (300 mol%, 0.16 mmol), NMM (600 mol%, 0.31 mmol) in DMF (4 mL). A 20% piperidine in DMF solution (4 mL) was used for Fmoc deprotection (10 min). Amino acid couplings and Fmoc deprotections were repeated until the desired sequences were completed. Peptide cleavage and deprotection from the solid support was accomplished using a mixture of TFA:TES:H_2O, (95:2.5:2.5 v/v/v, 2 ml) for 4 h. Peptide samples were concentrated under nitrogen to a viscous oil, precipitated with cold Et_2O, and centrifuged to a white pellet. The supernatant was decanted and the peptide pellets were dissolved in MeOH/H_2O for LCMS analyses. For FITC labeling the resin containing peptide was swollen in DMF for 1 h. A slurry of FITC (1.1 equiv., 0.057 mmol) in pyridine/DMF/DCM (12:7:5 v/v) was prepared and added to the reaction vessel for overnight reaction on an overhead shaker. After FITC-labeling was completed, the resin was washed with DMF (3 x 3 mL), MeOH (3 x 3 mL), and DCM (3 x 3 mL). Sample analyses were performed on a Waters Alliance Separation Module 2695 and detected with a Waters 2998 photodiode array (PDA) detector at 214 nm, using a linear binary gradient (2-80% MeCN/H_2O, 0.1% TFA, over 18 min). Characterization was conducted on an Agilent 1100 series ESI-LCMS with single quadrupole mass analyzer and LC conditions which used a linear binary gradient (2-80% MeCN/H_2O, 0.1% TFA, over 18 min) in positive mode. Analytical RP-HPLC was performed using a Zorbax RX-C18 (4.6 x 250 mm, 5 μm particle size) or Waters 2695 Symmetry® C18 column (3.9 x 150 mm, 5μm particle size), using the conditions previously described. Samples collected after purification were lyophilized to a white solid and re-dissolved in water to confirm purity and identity by LCMS analyses.

3.7.3. SYNTHESIS OF THE NSC DERIVED PEPTIDES

DSC (65 μmol, 16.6 mg) was dissolved in anhydrous DMF at room temperature, under N_2 conditions. The crude FITC derived peptides **22-24** (6.5 μmol) were dissolved in dry DMF and trimethylamine (3.2 μmol, 0.45 ml) was then added to the peptide solution. Peptide solutions were combined with the DSC/DMF mixture and reacted. The reaction mixture was stirred at room temperature for 1 h and quenched with 20 mL of TFA in water (1% volume/volume). Peptides were analyzed by RP-HPLC using a Waters 2695 Symmetry® C18 column (3.9 x 150 mm, 5 μm particle size) with a linear binary gradient, 20-80% MeCN/H_2O, 0.1% FA, over 18 min at 25°C, with a 1 mL/min flow rate and detection at 220 nm. Peptide purities and identities were confirmed by LCMS as described above.

3.7.4. CELL LINES AND CELL CULTURE

The human hepatocellular carcinoma cells, cell line HepG2 (American Type Culture Collection, ATCC), were cultured in EMEM, (Sigma Aldrich) supplemented with 10% heat-inactivated fetal bovine serum (Sigma Aldrich). Cell cultures were maintained at 75% confluency at 37°C in 5% CO_2 humidified air.

3.7.4. FLOW CYTOMETRY

For detection of cell surface expression levels of GRP78 and binding of FITC-Pep42, the HepG2 cells were plated in 12-well plates with DMEM, at a 50,000 cell/well density, for 48 h at 37 °C. HepG2 cells were further washed with PBS and dissociated with dissociation buffer (Life Technologies Corporation, Grand Island, NY). Cells were then re-suspended in FACS buffer (PBS, 1% FBS), and labeled with either anti-GRP78 (N-20) mAb-AlexaFluor 488 (100 nM) or

FITC-Pep42 (100 nM), and incubated at room temperature for 30 minutes in the dark. Cells were then washed and analyzed by flow cytometry on a MACSQuant® analyzer (MiltenyilBiotec). For peptide blocking studies, HepG2 cells were initially treated with GRP78 N-20 blocking peptide (10 mg/ml) for 30 min (R.T.) followed by incubation with either anti-GRP78 (N-20) mAb-AlexaFluor 488 (100 nM) or FITC-Pep42 (100 nM) for an additional 30 min (R.T., dark). Cells were finally washed with FACS buffer and analyzed by flow cytometry.

3.7.5. CELL VIABILITY

A Trypan blue cell viability assay was used to evaluate the survival of HepG2 cells following treatment with Pep42. HepG2 cells were incubated in 24-well plates, for 24 h, in serum-free basal media and then incubated for another 48 h in the presence of Pep42 (0.15 mM) at 37 °C. Following treatment cells were treated with enzyme-free dissociation buffer, to detach them from the plates, for 3 min at 37 °C. Cells were further centrifuged and re-suspended in PBS and stained with Trypan blue 0.4% stain solution (100 μl). Cell viability was determined by Trypan blue exclusion using a countess cell counter. Data was collected in replicate measurements ($n \geq 3$), analyzed in GraphPad Prism 5.9, and statistically analyzed for variance ($p < 0.05$).

REFERENCES

49. Walter, P.; Ron, D. *Science.* **2011**, *334*, 1081-1086.

50. Ni, M.; Lee, A.S. *FEBS Lett*. **2007**, *581*, 3641-3651.

51. Pfaffenbach, K.T.; Lee, A.S. *Curr. Opin. Cell Biol*. **2011**, *23*, 150-156.

52. Rutkowski, D.T.; Kaufman, R.J. *Trends Cell Biol*. **2006**, *14*, 20-28.

53. Hetz, C.; Chevet, E.; Harding, H.P. *Nature Rev. Drug Disc*. **2013**, *12*, 703-718.

54. Tabas, I.; Ron, D. *Nature Cell Biol*. **2011**, *13*, 184-190.

55. Woehlbier, U.; Hetz, C. *Trends Biochem. Sci*. **2011**, *36*, 329-337.

56. Moenner, M.; Pluquet, O.; Bouchecareilh, M.; Chevet, E. *Cancer Res*. **2007**, *67*, 10631-10634.

57. Reddy, R.K.; Mao, C.; Baumeister, P.; Austin, R.C.; Kaufman, R.J.; Lee, A.S. *J. Biol. Chem.* **2003**, *278*, 20915-20924.

58. Fernandez, P.M.; Tabbara, S.O.; Jacobs, L.K.; Manning, F.C.; Tsangaris, T.N.; Schwartz, A.M.; Kennedy, K.A.; Patierno, S.R. *Breast Cancer Res. Treat.* **2000**, *59*, 15-26.

59. Li, J.; Lee, A.S.; *Curr. Mol. Med*. **2006**, *6*, 45-54.

60. Zhang, Y.; Liu, R.; Ni, M.; Gill, P.; Lee, A.S. *J. Biol. Chem*. **2010**, *285*, 15065-15075.

61. Arap, M.A.; Lahdenranta, J.; Mintz, P.J.; Hajitou, A.; Sarkis, A.S.; Arap, W.; Pasqualini, R. *Cancer Cell*. **2004**, *6*, 275-284.

62. Kim, Y.; Lillo, A.M.; Steiniger, S.C.; Liu, Y.; Ballatore, C.; Anichini, A.; Mortarini, R.; Kaufmann, G.F.; Zhou, B.; Felding-Habermann, B.; Janda, K.D. *Biochemistry*. **2006**, *45*, 9434-9444.

63. Liu, Y.; Steiniger, S.C.; Kim, Y.; Kaufmann, G.F.; Felding-Habermann, B.; Janda, K.D. *Mol. Pharm*. **2007**, *4*, 435-447.

64. Yoneda, Y.; Steiniger, S.C.; Capkoca, K.; Mee, J.M.; Liu, Y.; Kaufmann, G.F.; Janda, K.D. *Bioorg. Med. Chem. Lett*. **2008**, *18*, 1632-1636.

65. Landon, L.A.; Deutscher, S.L. *J. Cell. Biochem*. **2003**, 90, 509-517.

66. Mandelin, J.; Cardó-Vila, M.; Driessen, W.H.; Mathew, P.; Navone, N.M.; Lin, S.H.; Logothetis, C.J.; Rietz, A.C.; Dobroff, A.S.; Proneth, B.; Sidman, R.L.; Pasqualini, R.; Arap, W.; *Proc. Natl. Acad. Sci. U S A.* **2015**, *112*, 3776-3781.

67. Kapoor, S.; Martin, M.; Schultz, M. *J. Nuc. Med.* **2014**, *55*, 443.

68. Anichini, A.; Mortarini, R.; Fossati, G.; Parmiani, G. *Int. J. Cancer*. **1986**, 38, 505-511.

69. Schmidt, N.; Mishra, A.; Lai, G.H.; Wong, G.C.L. *FEBS Lett.* **2010**, *584*, 1806-1813.

70. Alhakamy, N.A.; Dhar, P.; Berkland, C.J. *Mol. Pharm*. **2016**, *13*, 1047-1057.

71. Nakase, I.; Takeuchi, T.; Futaki, S. *Methods Mol. Biol*. **2015**, *1324*, 387-396.

72. Joseph, S.C.; Blackman, B.A.; Kelly, M.L.; Phillips, M.; Beaury, M.W.; Martinez, I.; Parronchi, C.J.; Bitsaktsis, C.; Blake, A.D.; Sabatino, D. *J. Pept. Sci*. **2014**, 20, 736-745.

73. Garcỉa-Martỉn, F.; Quintanar-Audelo, M.; Garcỉa-Ramos, Y.; Cruz, L.J.; Gravel, C.; Furic, R.; Côté, S.; Tulla-Puche, J.; Albericio, F. J. *Comb. Chem*. **2006**, 8, 213-220.

74. Hood, C.A.; Fuentes, G.; Patel, H.; Page, K.; Menakuru, M.; Park, J.H. *J. Pept. Sci*. **2008**, 14, 97-101.

75. Acosta, G.A.; del Fresno, M.; Paradis-Bas, M.; Rigau-DeLlobet, M.; Côté, S.; Royo, M.; Albericio, F. *J. Pept. Sci*. **2009**, *15*, 629-633.

76. Trivedi, M.V.; Laurence, J.S.; Siahaan, T.J. *Curr. Protein Pept. Sci.* **2009**, *10*, 614–625.

77. Maina, A.; Blackman, B.A.; Parronchi, C.J.; Morozko, E.; Bender, M.E.; Blake, A.D.; Sabatino, D. *Bioorg. Med. Chem. Lett*. **2013**, *23*, 5270-5274.

78. Patel, M.R.; Kozuch, S.D.; Cultrara, C.N.; Yadav, R.; Huang, S.; Samuni, U.; Koren, J.; Chiosis, G.; Sabatino, D. *Nano Lett.*, 2016, *16*, 6099–6108.

79. Lee, G.J. Histochemistry. **1989**, *91*, 357-359.

Mhidia, R.; Vallin, A.; Ollivier, N.; Blanpain, A.; Shi, G.; Christiano, R.; Johannes, L.; Melnyk, O. *Bioconjug. Chem.* **2010,** *21*, 219-228.

CHAPTER 4: CONTRIBUTIONS TO KNOWLEDGE AND FUTURE WORK

4.1. CONCLUSIONS AND CONTRIBUTIONS TO KNOWLEDGE ACCOMPLISHED IN THIS THESIS

4.1.1. THE DISCOVERY OF B7H6-DERIVED IMMUNOSTIMULATORY PEPTIDES OF LYMPHOCYTIC NK92-MI CELLS

The design, synthesis, and characterization of a novel class of NK cell-dependent immunostimulatory peptides (IPs) derived from the binding site interface of B7H6 and NKp30 have been described in Chapter 2.[14] A structure–activity relationship study revealed that the synthetic peptides disclosed in this study exhibited secondary structures that varied on the solvent system. The peptides encompassing the FG loop of B7H6 displayed the putative turn conformation in a TFE:H_2O mixture that was expected to contribute to NKp30 receptor binding and activation of NK cells' immunostimulatory activities. Flow cytometry analyses confirmed binding of the FITC-labeled B7H6 derived peptides to the NK cells at 10 μM concentrations. Moreover, competitive binding experiments revealed partial displacement upon treatment with the anti-NKp30 mAb suggesting NKp30 binding specificities for the B7H6 derived peptides. In order to determine the immunostimulatory capabilities of the peptides with the NK cells, an ELISA demonstrated that the short pentapeptide, TVPLN, and the peptide derived form the secondary structure of B7H6, TSMGFGVTPLK, notably stimulated the secretion of TNF-α but not IFN-γ. Moreover, these peptides posed no observable cytotoxicity (apoptosis) to the NK92-MI cells. In spite of these desirable properties, none of the synthetic peptides were found to outperform the native, B7H6 ligand. Therefore, these studies have effectively produced a new class of B7H6-derived immunostimulatory ligands for their potential applications in tumor immunotherapy.

4.1.2. PEP42, A CANCER-TARGETING PEPTIDE THAT RECOGNIZES CELL SURFACE GRP78 ON CANCER CELLS

The synthesis, characterization and biological evaluation of the GRP78 targeting peptide Pep42 on the HepG2 cell line has been studied in Chapter 3.[15] The selection of Pep42 as a cancer targeting cyclic peptide was first revealed by Janda and co-workers as a highly selective ligand for the GRP78 surface receptor on melanoma cancer cells through phage display bio-panning.[16-18] With the use of a polar, PEG-based resin (NovaPEG), Pep42 and its FITC-labeled derivatives were successfully synthesized in good yields (14-24%) and purities (>95%) following RP-HPLC and ESI-MS. Moreover, Fmoc-SPPS was also used for the generation of *C*-terminal containing Pep42-PEG peptides. These peptides contained a reactive Lys residue which was coupled to DSC to yield the NSC-activated peptides. These peptides are considered to be useful substrates for bio-conjugation studies, including in the ligation of peptides with bio-active proteins.[19] In this study, the generation of NSC-derived Pep42 sequences was developed for their ligation with native B7H6. Flow cytometry analyses revealed FITC-Pep42 having comparable binding capabilities to GRP78 when compared to the specific Alexa Fluor 488-labeled N20-anti-GRP78 primary antibody. The GRP78 binding interactions were abolished when the HepG2 cells were pretreated with a N20-GRP78 peptide blocker, indicating GRP78 binding specificity for the Pep42 sequence on the HepG2 cells. Taken altogether, this study opens an opportunity for the development of GRP78-targeting ligands for cancer immunotherapy applications.

4.2. FUTURE WORK

4.2.1. RATIONAL DESIGN FOR THE DEVELOPMENT OF CANCER-TARGETING IMMUNOSTIMULATORY PEPTIDE-PROTEIN CONJUGATES

The evolution of synthetic biology has led to the development of protein biologics such as the monoclonal antibodies (mAb), small antibody fragments (Fab or Fc regions) and the antibody-drug conjugates (ADC) that are widely used in cancer immunotherapy applications.[1] Recently, B7H6 has been identified as a tumor associated ligand and activator for the NKp30 receptor, found on the surface of activated and resting NK cells.[2] NKp30 is responsible for NK cell immunosurveillance and the secretion of pro-inflammatory cytokines, such as IFN-γ and TNF-α.[20,21] Thus, tumors that present the cell surface B7H6 antigen are effectively recognized by activated NK cells which triggers immunstimulatory activities that leads to the destruction of the targeted tumor cells. However, low levels B7H6 or the absence of cell surface B7H6 has been found in the more malignant, resilient tumors that have evolved NK-dependent resistance.[22] In these cases, metalloproteases function to shed B7H6 from the cancer cell surface, promoting tumor escape from NK-dependent immunosurveillance and the rise of tumor spread and malignancy. GRP78 is a chaperone protein overexpressed and cell surface localized on a wide range of tumors, where it promotes tumor initiation, progression and metastatic spread.[22] Therefore, GRP78 has been validated as a clinically relevant biomarker for the development of cancer-targeting ligands. Towards this end, the short, 13-mer cyclic peptide, Pep42, has been selected through phage display bio-panning as a specific GRP78 ligand.[16] Therefore, we propose the rational design and development of a novel class of cancer-targeting immunostimulatory peptide-protein (CTIPP) conjugates, containing the GRP78 targeting sequence Pep42 and B7H6 for NK cell binding and activation (**Figure 4.1**). Furthermore, an aminohexanoic acid linker will be introduced at the *N*-

terminus of the Pep42 sequences for FITC-labeling by Fmoc-solid phase peptide synthesis. A series of PEG-derived Pep42 sequences will be introduced as spacers, while a *C*-terminal Lys residue will allow for the chemical ligation of the Pep42 derived sequences and B7H6 using the well-established NSC chemistry.[19] In this case, the activated NSC-peptides are anticipated to ligate with any of the 10 Lys residues on B7H6 to form stable, irreversible urea linkages.

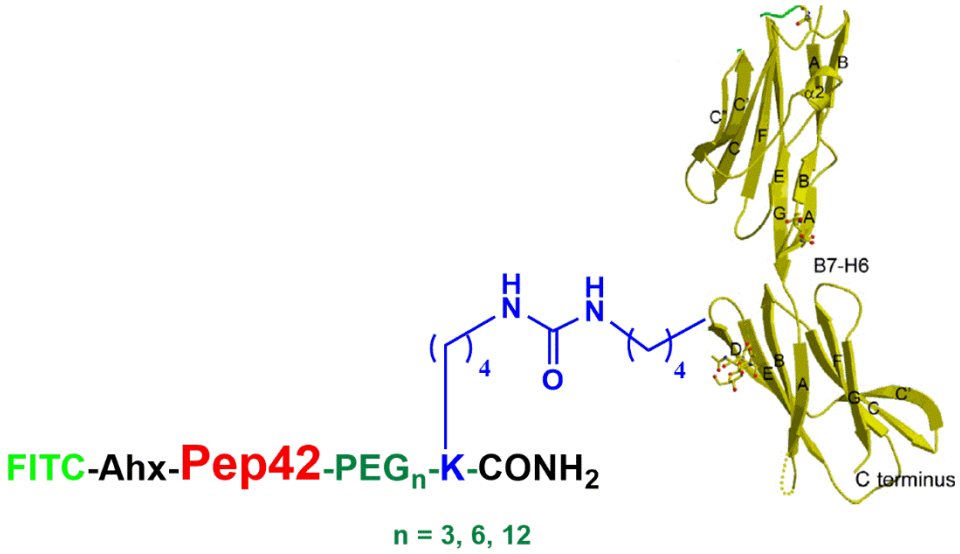

Figure 4.1. Schematic representation of the CTIPP, with varying lengths of PEG units.

4.2.2 PEPTIDE-PROTEIN CONJUGATION

Our proposed approach for the formation of the conjugated B7H6-Pep42 sequence is also based on literature precedence.[19] We anticipate ligation of Pep42 onto B7H6 **(Figure 4.2)** to be achieved in similar fashion, by reacting B7H6 in PBS at pH 7.4 with the FITC-labeled Pep42-PEG-derived sequences that have been activated to the NSC at the *C*-terminus. The anticipated formation of the peptide-protein conjugate will be analyzed by a combination of RP-HPLC, 10% Bis-Tris PAGE, and ESI-MS in order to confirm the extent and location of conjugation for the Pep42 sequences onto the B7H6 protein.

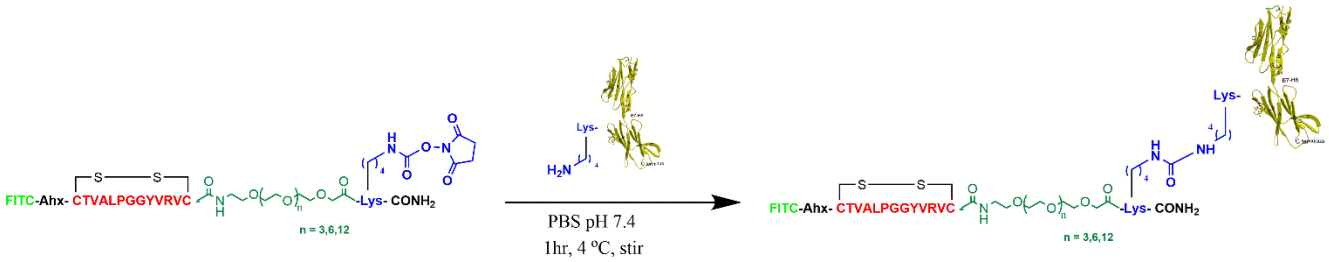

Figure 4.2. Schematic representation of the B7H6-Pep42 conjugation reaction.

4.2.3. BIOLOGY OF THE CTIPP BIOCONJUGATES

4.2.3.1. BINDING CAPABILITIES OF THE CITPP CONJUGATES ON THE NK92-MI AND THE HEPG2 CELLS.

The binding capabilities of the FITC-labeled CTIPP conjugates to the HepG2 and NK92-MI cells will be initially determined by flow cytometry. Moreover, this study will also reveal the binding specificities of the CTIPP conjugates with the GRP78 and NKp30 receptors. The binding capabilities of the CTIPP conjugates will be compared to the soluble natural ligand, B7H6-Fc and the anti-NKp30 APC labeled mAb on the cell surface of the NK92-MI cells. The binding capabilities of the CTIPP conjugates will also be compared to that of the AlexaFluor 488-labeled N-20 anti-GRP78 mAb on the cell surface of the HepG2 cell line. These binding experiments will be initially performed independently and then in combination, in order to test the receptor binding specificities of the CTIPP conjugates when treated with and without the mAbs for GRP78 and NKp30. Taken together, these binding experiments will provide key insights into the binding occupancy and receptor binding specificities of the CTIPP conjugates for the GRP78 and NKp30 receptors located on the surfaces of the HepG2 and the NK92-MI cells.

4.2.3.2. IMMUNOSTIMULATORY ACTIVITIES OF THE NK92-MI CELLS.

The sustained capabilities of the CTIPP conjugates to elicit NK-dependent immunostimulatory activities will be assessed by measuring the secreted amounts of the inflammatory cytokines TNF-α, IFN-γ and IL-6, and will be compared to that of the soluble natural ligand B7H6-Fc by a standard ELISA.[24]

4.2.3.3. NK92-MI AND HEPG2 CELLS' VIABILITY.

A Guava-Nexin® Reagent (EMD Millipore), designed to assess early and late-stage apoptosis by flow cytometry, will be used to evaluate the cytotoxicity of the CTIPP conjugates on the HepG2 and NK92-MI cells.[25] Either the NK92-MI cells or the HepG2 cells will be incubated with the CTIPP conjugates in a concentration dependent manner and evaluated for the presence of apoptotic events by flow cytometry analyses.

4.2.3.4. CTIPP DEPENDENT NK92-MI CELL MIGRATION AND CYTOTOXICITY

Co-culture assays of the effector (NK92-MI) and target (HepG2) cells with and without the CTIPP conjugates will provide important information on the NK92-MI cell migration, immunistimulatory and cytotoxicities onto the HepG2 cells.[26] NK92-MI cell migration will be measured within transwell migration chambers, confocal fluorescence microscopy will provide images indicating the cell-in-cell structures, and the D275/propidium iodide dyes will provide information on cytotoxicity by counter-staining dead *vs*. live cells.

4.2.3.5. *IN-VIVO* BIOLOGICAL ACTIVITY

The *in vivo* studies of the CTIPP conjugates will be conducted in mice xenograft models transplanted with the HepG2 cells and the NK92-MI cells in order to analyze the influence of the

bioconjugates on tumor size and systematic immunological events. Mice toxicity, pharmacokinetic and tissue distribution properties will also be evaluated by adopting methods described in the literature.[27]

4.2.4. DESIGN, SYNTHESIS, CHARACTERIZATON AND BIOLOGICAL EVALUATION OF AN NKP30 DERIVED CANCER TARGETING PEPTIDES.

4.2.4.1. RATIONAL DESIGN

In an effort to develop a new class of CTPs, we propose the rational design of a library of short peptide sequences derived from the binding interface of B7H6:NKp30. The CTPs will combine amino acid residues present in the primary sequences and secondary structures of the NKp30 receptor binding domains. The crystal structure analysis of the NKp30-B7H6 binding interface revealed a receptor-ligand stoichiometry of 1:1, encompassing twelve NKp30 amino acid residues bound to eleven B7H6 residues.[2] The NKp30 receptor, a type I transmembrane protein, binds to B7H6 through the front and back β-sheets of its C-like domain.[2] The amino acids located in the pocket of NKp30, and responsible for direct contact with B7H6, comprise residues from strands C and F, particularly the aminoacids in loops BC (residues 50-54, IGSVT), and FG (111-114, EVLG), along with helix α2 (residues 80-86, LASSRFL) respectively. In particular, residues Gly51 and Val 53 engage in the only two hydrogen bond interactions, and Glu111 forms the only salt bridge, while residues Ile50, Gly51, Ser52, Val53, Leu80, Ser82, Phe85, Leu86, Glu111, Leu113, Gly114 complement binding via Van der Waals contacts (**Figure 4.2**).[2]

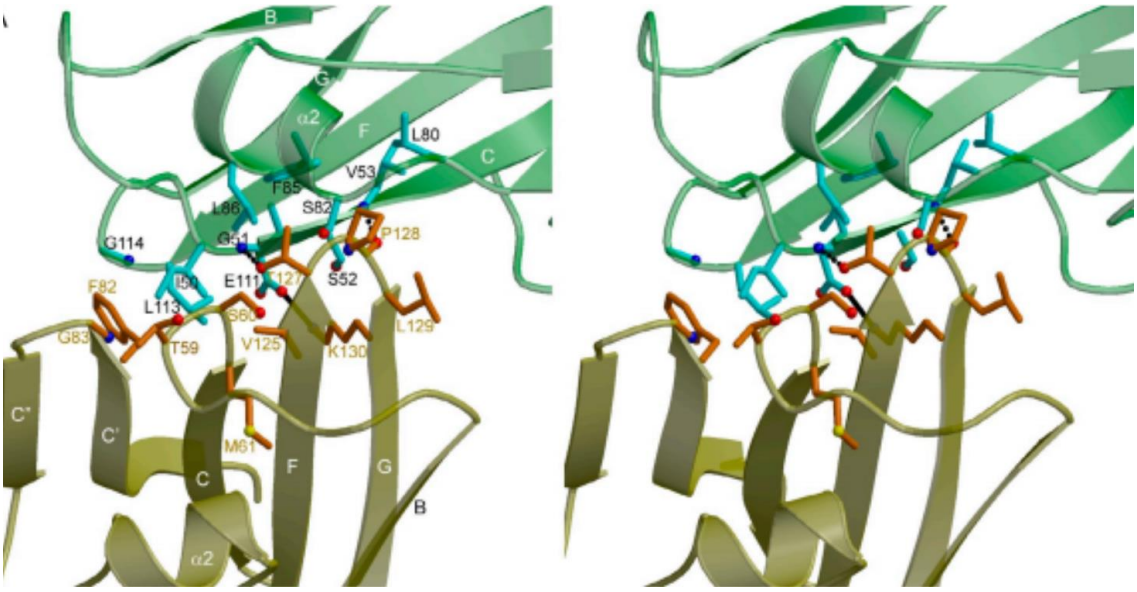

Figure 4.3. The NKp30:B7H6 interface. Stereo view of the NKp30-B7H6 interface. The side chains interacting residues are shown in ball-and-stick representation, with carbon atoms in cyan (NKp30) or orange (B7H6), nitrogen atoms in blue and oxygen atoms in red. Hydrogen bonds are drawn as dotted black lines. A salt bridge linking residues NKp30 Glu111 and B7H6 Lys130 is shown as a solid black line. Figure adapted from *J. Exp. Med.* **2011**, *208*, 703-714.[(2)]

Based on the described interaction in between the NKp30:B7H6,[(2)] the primary amino acid residues participating in binding, as well as the residues that were found to be adjacent to the binding hotspots and that promote secondary structure stability were selected as the lead amino acid residues for making a small library of peptides designed as B7H6-targeting peptides (**Table 4.1**). As such, B7H6-targeting peptides may encompass a new class of CTPs, useful for the selective detection and treatment of tumors that express the B7H6 antigen on the cell surface.

Table 4.1. Sequence and structures of NKp30 derived peptides.

FITC-$(CH_2)_5$-FLH-$CONH_2$	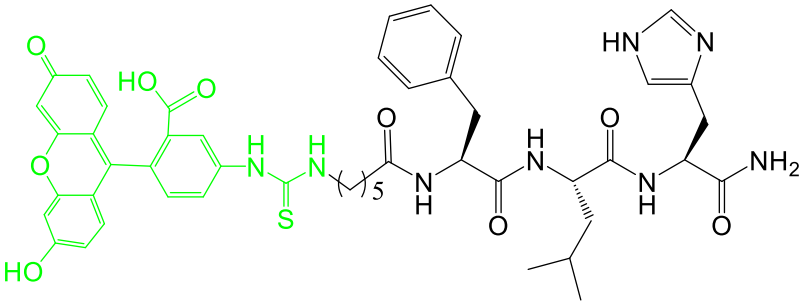
FITC-$(CH_2)_5$-LASSRFLH-$CONH_2$	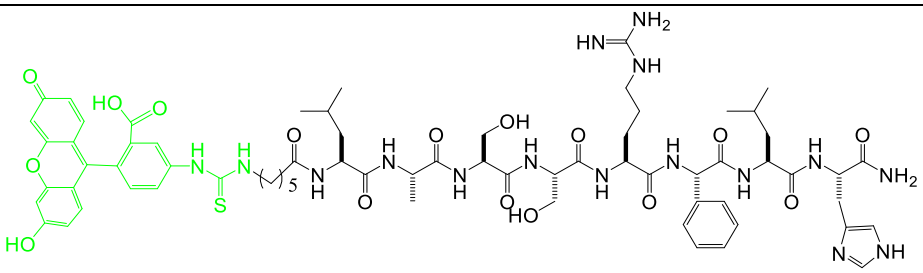
FITC-$(CH_2)_5$-IGSV-$CONH_2$	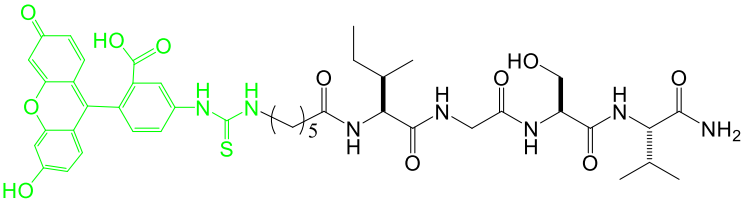
FITC-$(CH_2)_5$-IGSVTW-$CONH_2$	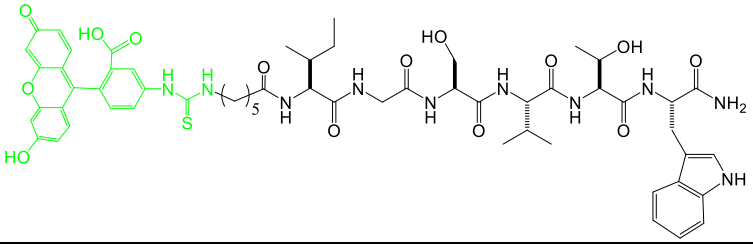
FITC-$(CH_2)_5$-RVEVL-$CONH_2$	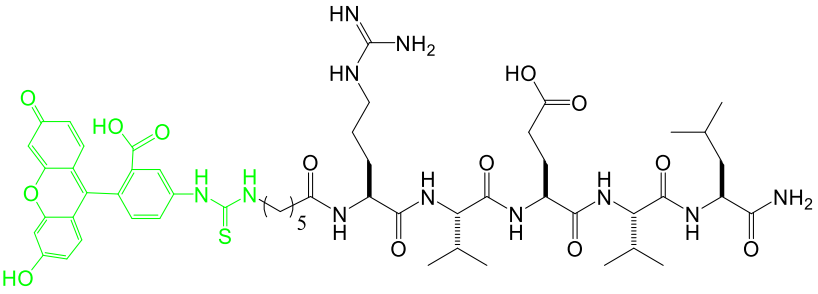
FITC-$(CH_2)_5$-VCRVEVL-$CONH_2$	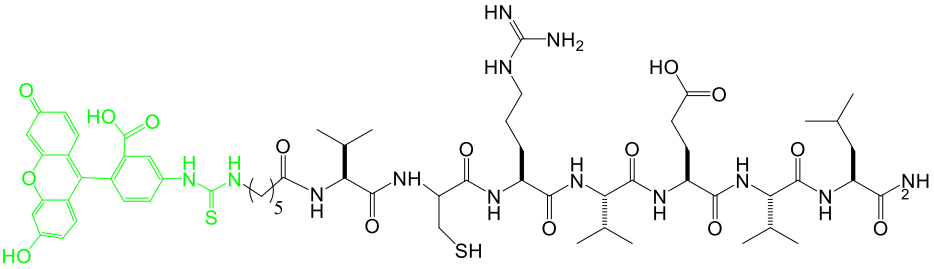

FITC-$(CH_2)_5$-ECRVEVLG-$CONH_2$	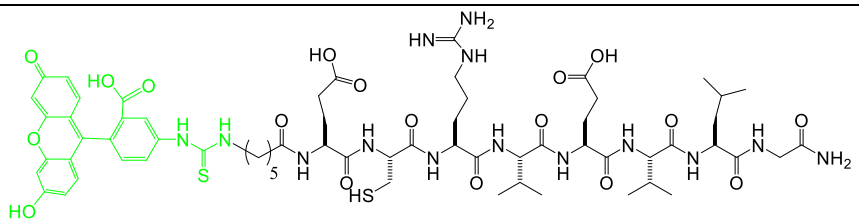
FITC-$(CH_2)_5$-RVEGRVEVLG-$CONH_2$	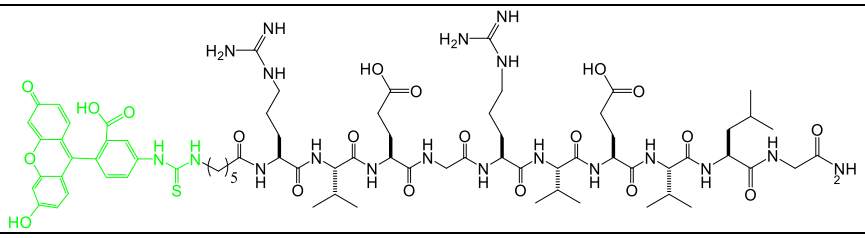
FITC-$(CH_2)_5$-IGSVEVLG-$CONH_2$	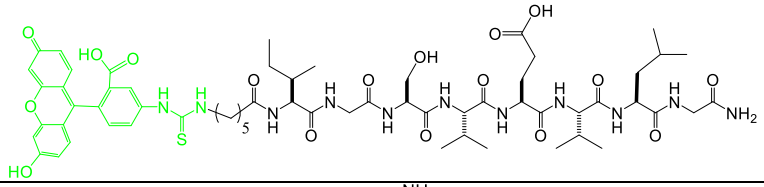
FITC-$(CH_2)_5$-LASSRFLAIGSVEVLG-$CONH_2$	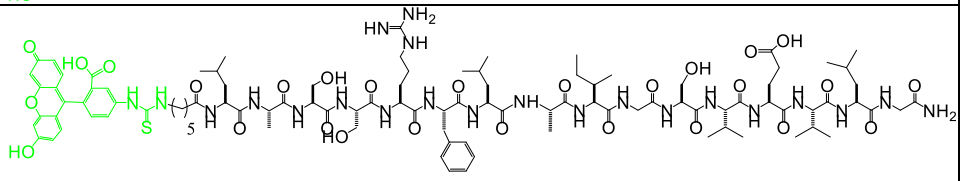

4.2.4.2. SYNTHESIS AND CHARACTERIZATION OF THE NKP30 DERIVED SYNTHETIC PEPTIDES

With the assistance of Francesca Romeo, BSc, and Andreich Darwich, undergraduate student at Seton Hall University, conventional Fmoc-SPPS was employed for the synthesis of NKp30-derived CTPs. Peptides were cleaved and deprotected from the solid support following synthesis, analyzed and purified by LCMS prior to biological studies. Peptides were recovered in isolated yields (1.5-13%) and purities (60-99%) according to RP HPLC. The identities of the synthetic peptides **28-35** were confirmed by mass spectrometry which validated sequence composition based on mass/charge ratios (**Table 4.2)**.

Table 4.2. Characterization of the NKp30 derived synthetic peptides **28-35**.

Entry	Sequence	Crude purity (%)[a]	Isolated yield (%)[b]	Purified purity (%)[e]	MW (g/mol)[c]	Z[d]	RT (min)[e]	RT (min)[f]
28	FITC-NH-$(CH_2)_5$-FLH-$CONH_2$	98	3.4	98	459.2 (916.7)	2	12.0	5.38
29	FITC-NH-$(CH_2)_5$-IGSV-$CONH_2$	96	12	96	876.3 (875.6)	1	14.0	7.56
30	FITC-NH-$(CH_2)_5$-RVEVL-$CONH_2$	97	13	97	558.8 (1115.7)	2	11.8	4.04
31	FITC-NH-$(CH_2)_5$-IGSVTW-$CONH_2$	77	6.9	60	1163.3 (1162.9) 388.8 (388.6)	1 3	16.0	8.67
32	FITC-NH-$(CH_2)_5$-ECRVEVLG-$CONH_2$	66	2.0	98	703.3 (1405.2)	2	11.4	5.57
33	FITC-NH-$(CH_2)_5$-LASSRFLH-$CONH_2$	52	1.5	96	716.3 (716.1) 477.9 (477.4)	2 3	10.3	5.59
34	FITC-NH-$(CH_2)_5$-IGSVEVLG-$CONH_2$	68	7.1	76	637.7 (1274.1)	2	16.5	8.41
35	FITC-NH-$(CH_2)_5$-RVEGRVEVLG-$CONH_2$	80	7.2	99	539.0 (1614.5)	3	9.74	5.54

[a]Crude purities by RP-HPLC at 220 nm using 20-80% MeOH/H_2O with 0.1% FA over 18 min.
[b]Isolated yields based on the resin loading.
[c]Observed mass (expected mass) as [M + H]+/Z detected by LCMS in positive mode.
[d]Charged state of the peptides as detected by LCMS in positive mode.
[e]Retention times using 20-80% MeOH/H_2O (0.1% FA) over 18 min.
[f]Retention times using 20-80% MeCN/H_2O (0.1% FA) over 18 min.

4.2.4.3. BIOLOGICAL STUDIES

Administration of the FITC-labeled NKp30 derived peptides to the HeLa cells, known to express cell surface B7H6 will be conducted to determine the extent of B7H6 binding on the HeLa cells. Their binding capabilities on the cell surface of the HeLa cells will be compared with and without commercially available anti-B7H6 PE labeled mAb in a concentration dependent manner. Their binding specificities will be tested with the fluorescently labeled NKp30, where inhibition on the binding of the peptides will confirm specificity to the cell surface antigen B7H6. The cytotoxicity of the CTPs on the HeLa cells will be evaluated by flow cytometry by measuring early and late apoptotic events with the Guava-Nexin® Reagent (EMD Millipore).

4.3. REFERENCES

1. Scott, A.M.; Wolchok, J.D.; Old, L.J. *Nature* **2012**, *12*, 278-287.

2. Li, Y.; Wang, Q.; Mariuzza, A. *J. Exp. Med.* **2011**, *208*, 703-714.

3. Brandt, C.S.; Baratin, M.; Yi, E.C.; Kennedy, J.; Gao, Z.; Fox, B.; Haldeman, B.; Ostrander, C.D.; Kaifu, T.; Chabannon, C.; Moretta, A.; West, R.; Xu, W.F.; Vivier, E.; Levin, S.D. *J. Exp. Med.* **2009**, *206*, 1495-1503.

4. Coin, I.; Beyermann, M.; Bienert, M. Solid-phase peptide synthesis: from standard procedures to the synthesis of difficult sequences. *Nat. Protoc.* **2007**, *2*, 3247-3256.

5. Garcia-Martin, F.; Quintanar-Audelo, M.; Garcia-Ramos, Y.; Cruz, L.J.; Gravel, C.; Furic, R.; Cote, S.; Tulla-Puche, J.; Albericio, F. ChemMatrix, a poly(ethylene glycol)-based support for the solid-phase synthesis of complex peptides. *J. Comb. Chem.* **2006**, *8*, 213-220.

6. Zhang, L.H.; Zhang, X. Role of GRP78 in physiology and cancer. *J. Cell. Biochem.* **2010**, *110*, 1299-1305.

7. Vives, E.; Schmidt, J.; Pelegrin, A. Cell-penetrating and cell-targeting peptides in drug delivery. *Biochim. Biophys. Acta* **2008**, *1786*, 126–138.

8. Aina, O.H.; Liu, R.; Sutcliffe, J.L.; Marik, J.; Pan, C.X, Lam, K.S. From combinatorial chemistry to cancer-targeting peptides. *Mol. Pharm*. **2007**, *4*, 631-651.

9. Arap, M.A. Phage display technology-applications and innovations. *Gen. Mol. Biol.* **2005**, *1*, 1-9.

10. Kersemans, V.; Cornelissen, B. Targeting the Tumor: Cell Penetrating Peptides for Molecular Imaging and Radiotherapy. *Pharmaceuticals* **2010**, *3*, 600-620.

11. Dharap, S.S.; Wang, Y.; Chandna, P.; Khandare, J.J.; Qiu, B.; Gunaseelan, S.; Sinko, P.J.; Stein, S.; Farmanfarmaian, A.; Minko, T. Tumor-specific targeting of an anticancer drug delivery system by LHRH peptide. *Proc. Natl. Acad. Sci. USA* **2005**, *102*, 12962-12967.

12. Shukla, R.S.; Qin, B.; Cheng, K. Peptides used in the delivery of small non-coding RNA. *Mol. Pharm*. **2014**, *11*, 3395-408.

13. Soudy, R.; Chen, C.; Kaur, K. Novel peptide-doxorubucin conjugates for targeting breast cancer cells including the multidrug resistant cells. *J. Med. Chem.* **2013**, *56*, 7564-7573.

14. Phillips, M.; Romeo, F.; Bitsaktsis, C.; Sabatino, D. *Biopolymers: Peptide Sci*. **2016**, 106, 658-672.

15. Joseph, S.C.; Blackman, B.A.; Kelly, M.L.; Phillips, M.; Beaury, M.W.; Martinez, I.; Parronchi, C.J.; Bitsaktsis, C.; Blake, A.D.; Sabatino, D. *J. Pept. Sci*. **2014**, 20, 736-745.

16. Kim, Y.; Lillo, A.M.; Steiniger, S.C.; Liu, Y.; Ballatore, C.; Anichini, A.; Mortarini, R.; Kaufmann, G.F.; Zhou, B.; Felding-Habermann, B.; Janda, K.D. *Biochemistry*. **2006**, *45*, 9434-9444.

17. Liu, Y.; Steiniger, S.C.; Kim, Y.; Kaufmann, G.F.; Felding-Habermann, B.; Janda, K.D. *Mol. Pharm*. **2007**, *4*, 435-447.

18. Yoneda, Y.; Steiniger, S.C.; Capkoca, K.; Mee, J.M.; Liu, Y.; Kaufmann, G.F.; Janda, K.D. *Bioorg. Med. Chem. Lett*. **2008**, *18*, 1632-1636.

19. Mhidia, R.; Vallin, A.; Ollivier, N.; Blanpain, A.; Shi, G.; Christiano, R.; Johannes, L.; Melnyk, O. *Bioconjug. Chem.* **2010,** *21*, 219-228.

20. Cantoni, C.; Bottino, C.; Vitale, M.; Pessino, A.; Augugliaro, R.; Malaspina, A.; Parolini, S.; Moretta, L.; Moretta, A.; Biassoni, R. *J. Exp. Med*. **1999**, 189, 787-796.

21. Pessino, A.; Sivori, S.; Bottino, C.; Malaspina, A.; Morelli, L.; Moretta, L.; Biassoni, R., Moretta, A. *J. Exp. Med*. **1998**, 188, 953-960.

22. Schlecker, E.; Fiegler, N.; Arnold, A.; Altevogt, P.; Rose-John, S.; Moldenhauer, G.; Sucker, A.; Paschen, A.; von Strandmann, E.P.; Textor, S.; Cerwenka, A. *Cancer Res*., **2014**, *74*, 3429-3440.

23. Wang, M.; Wey, S.; Zhang, Y.; Ye, R.; Lee, A.S. *ARS*, **2009**, *11*, 2309-2316.

24. See, D.; Mason, S.; Roshan, R. *Immunol. Invest*. **2002**, 2, 137-153.

25. Demo, S.D.; Masuda, E.; Rossi, A.B.; Throndset, B.T.; Gerard, A.L.; Chan, E.H.; Armstrong, R.J.; Fox, B.P.; Lorens, J.B.; Payan, D.G.; Scheller, R.H.; Fisher, J.M. *Cytometry* **1999**, 36, 340–348.

26. Justus, C.R.; Leffler, N.; Ruiz-Echevarria, M.; Yang, L.V. *J. Vis. Exp*. **2014**, 88, 51046.

27. Puaux, A.L.; Ong, L.C.; Jin, Y.; Teh, I.; Hong, M.; Chow, P.K.H.; Golay, X.; Abastado, J.P. *Int. J. Mol. Ima.* **2011**, doi:10.1155/2011/321538.

4.4. PUBLICATIONS AND CONFERENCE PRESENTATIONS

- **Publications**

1. Phillips, M; Romero, F; Bitsaktsis, C; Sabatino, D. **B7H6 Derived Peptides Trigger TNF-α Dependent Immunostimulatory Activity of Lymphocytic NK92-MI Cells**, *Biopolymers.* **2016,** 106, 658-672.

2. Joseph, S.C.; Blackman, B.A.; Kelly, M.L.; Phillips, M.; Beaury, M.W.; Martinez, I.; Parronchi, C.J.; Bitsaktsis, C.; Blake, A.D.; Sabatino, D. **Synthesis, characterization, and biological activity of poly(arginine)-derived cancer-targeting peptides in HepG2 liver cancer cells**. *J. Pept. Sci.* **2014**, 20, 736-745.

- **Conference Proceedings**

1. M. Phillips, C. Bitsaktsis, and D. Sabatino. B7H6: A Bio-Marker for the Development of Cancer-Targeted Immunotherapy Applications. *Proceedings of the 24th American Peptide Symposium, American Peptide Society,* **2015.** http://dx.doi.org/10.17952/24APS.2015.117

- **Book chapter in press**

1. M. PHILLIPS, N.K. RANA, E. CARRION, G. LUISI AND D. SABATINO. Peptide Biomarkers and Assay Development, Peptide-based Drug Discovery: Challenges and New Therapeutics, *The Royal Society of Chemistry,* **2017**. (*In press*)

- **Poster presentations**

1. Mariana Phillips, Constantine Bitsaktsis, David Sabatino*,"**B7H6 Derived Peptides Trigger TNF-α Dependent Immunostimulatory Activity within Lymphocytic NK92-MI Cells**", NYAS, Emerging Approaches in Cancer Immunotherapy, Feb 2016.

2. Mariana Phillips, Constantine Bitsaktsis**,** David Sabatino*,"**B7H6: A Bio-Marker for the Development of Cancer-Targeted Immunotherapy Applications**", APS 21st National meeting, Orlando, Fl, June 2015.

3. Mariana Phillips, Constantine Bitsaktsis**,** David Sabatino*,"**B7H6: A Novel Ligand in Cancer-Based Immunotherapy Approaches**", NYAS, Chemical Biology Year-End Symposium, April 2015.

4. Mariana Phillips, Constantine Bitsaktsis**,** David Sabatino*,"**B7H6: A Novel Approach in Cancer-Targeted Immunotherapy**", NYAS, Emerging Approaches in Cancer Immunotherapy, Feb 2015.

5. Mariana Phillips, David Sabatino*,"**Poly(Arginine) Derived Cancer Targeting Peptides and their GRP78 Targeting Activity in HepG2 Hepatoblastoma Cells**", ACS 247th National meeting, San Francisco, Aug 2014.

Mariana Phillips, Stesha C. Joseph, Lathamol Kurian, Anthony Maina, Brittany A Blackman, Megan Kelly, Hemantbhai Patel, Erik Carrion, Ivonne Martinez, Emily Borland, Francesca Romano, Christopher Parronchi, Allan D. Blake, Constantine Bitsaktsis, Sergiu M. Gorun and David Sabatino*,"Synthesis, Characterization and Biological Activity of Cancer-Targeting Peptides", NYAS, Chemical Biology Year-End Symposium, April 2014.

APPENDIX

TABLE OF CONTENTS

Peptide **1**: NH_2-$(CH_2)_5$-FG-$CONH_2$

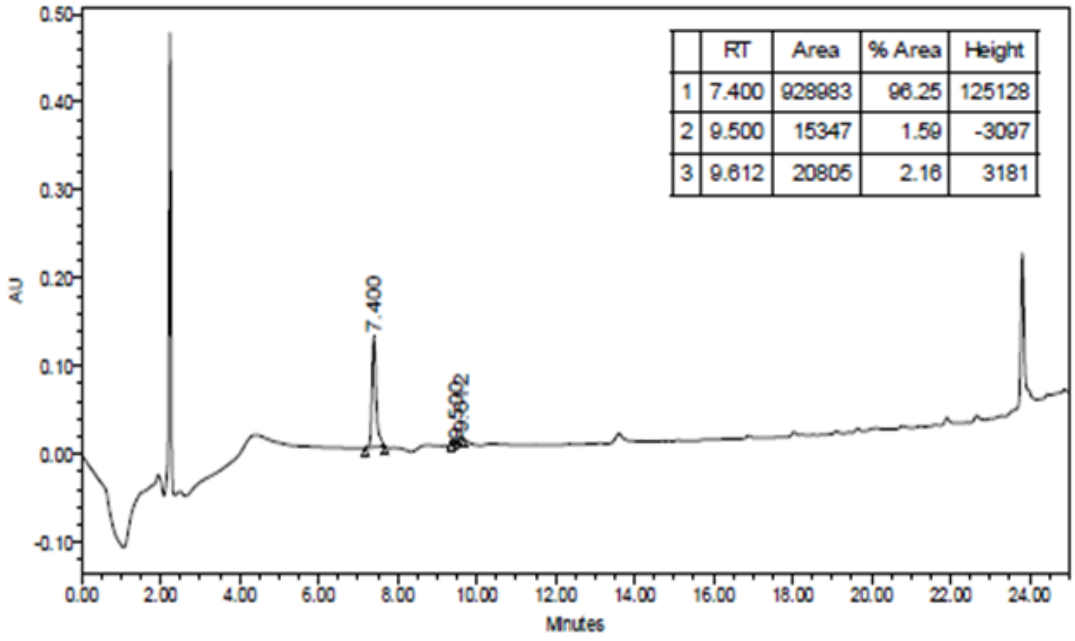

Figure A1. RP-HPLC analysis of pure peptide **1**, using a linear gradient 2-60% MeCN/H_2O (0.1% TFA) over 20 min using a Waters 2695 Symmetry® C18 column (3.9 x 150 mm, 5µm particle size) set at a temperature of 25 °C at a flow rate of 1 mL/min with detection at 220 nm.

Peptide **1**: NH_2-$(CH_2)_5$-FG-$CONH_2$

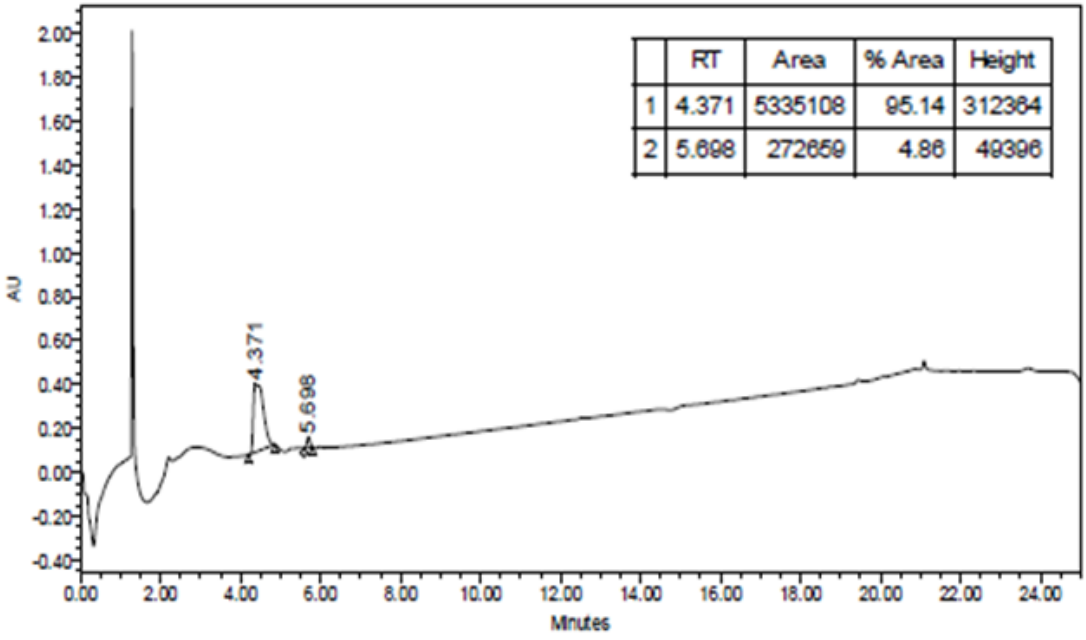

Figure A2. RP-HPLC analysis of pure peptide **1**, using a linear gradient 2-82% MeOH/H_2O (0.1% FA) over 18 min using a Waters 2695 Symmetry® C18 column (3.9 x 150 mm, 5µm particle size) set at a temperature of 25 °C at a flow rate of 1 mL/min with detection at 220 nm.

Peptide **1**: NH_2-$(CH_2)_5$-FG-$CONH_2$

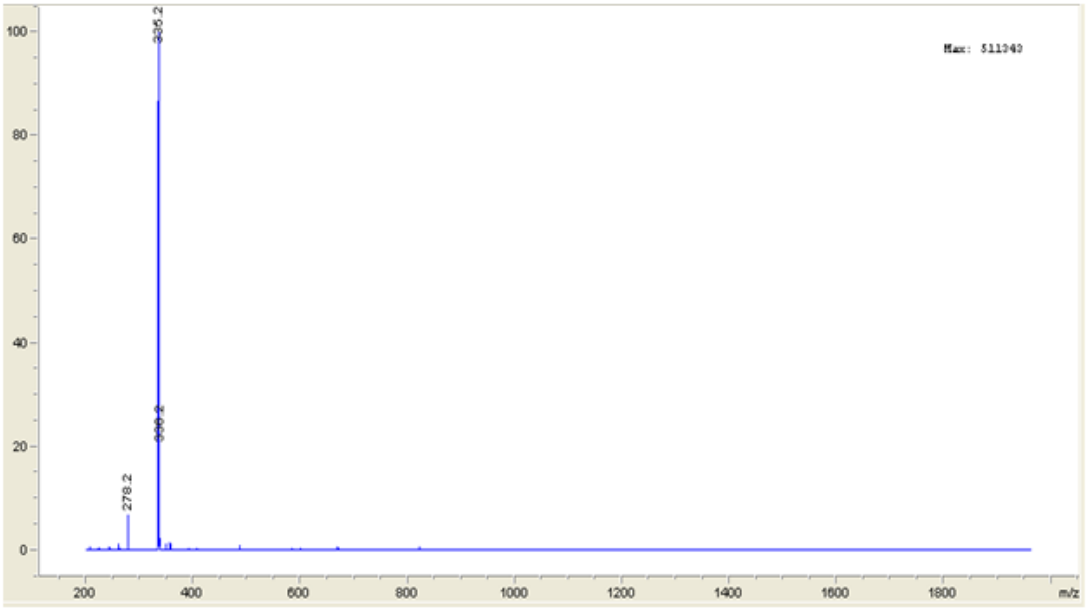

Figure A3. ESI-LCMS analysis of pure peptide **1**, using MS in positive mode and LC linear gradient 2-82% MeOH/H_2O (0.1% FA) over 18 min using a Waters 2695 Symmetry® C18 column (3.9 x 150 mm, 5µm particle size) set at a temperature of 25 °C at a flow rate of 1 mL/min with detection at 220 nm.

Peptide **2**: NH_2-$(CH_2)_5$-TSMG-$CONH_2$

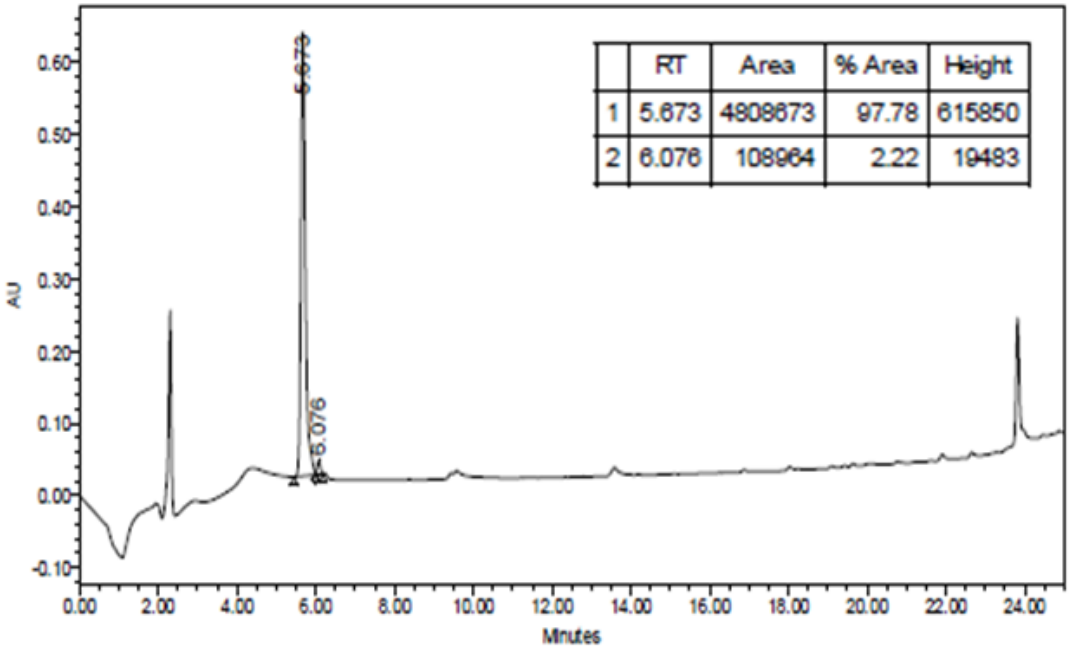

Figure A4. RP-HPLC analysis of pure peptide **2**, using a linear gradient 2-60% MeCN/H_2O (0.1% TFA) over 20 min using a Waters 2695 Symmetry® C18 column (3.9 x 150 mm, 5µm particle size) set at a temperature of 25 °C at a flow rate of 1 mL/min with detection at 220 nm.

Peptide **2**: NH_2-$(CH_2)_5$-TSMG-$CONH_2$

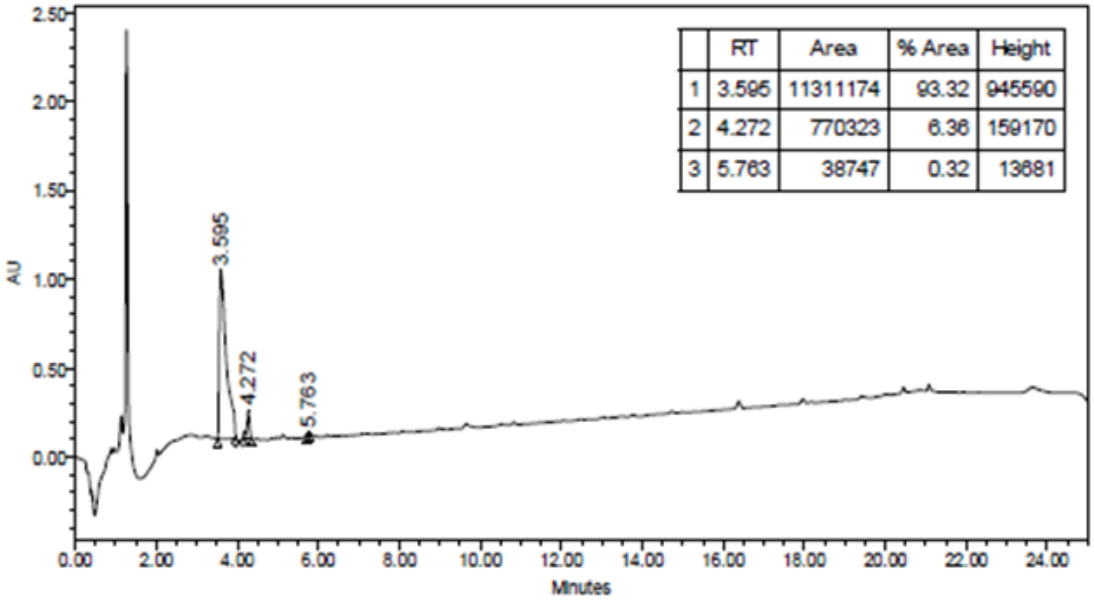

Figure A5. RP-HPLC analysis of pure peptide **2**, using a linear gradient 2-82% MeOH/H_2O (0.1% FA) over 18 min using a Waters 2695 Symmetry® C18 column (3.9 x 150 mm, 5µm particle size) set at a temperature of 25 °C at a flow rate of 1 mL/min with detection at 220 nm.

Peptide **2**: NH_2-$(CH_2)_5$-TSMG-$CONH_2$

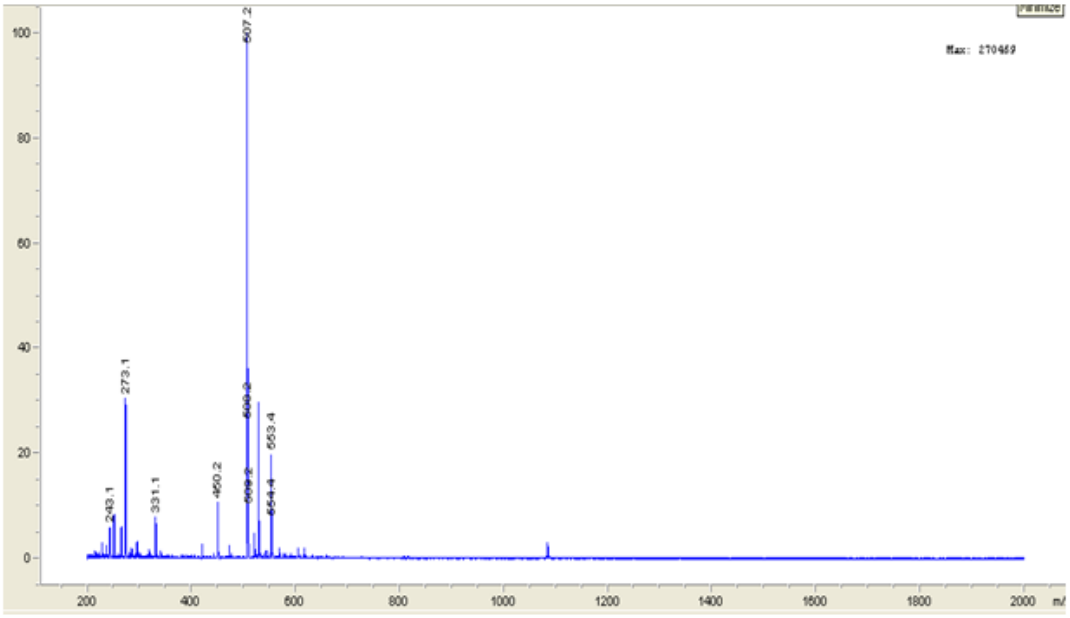

Figure A6. ESI-LCMS analysis of purified peptide **2**, using ESI MS in positive mode and LC linear gradient 2-82% MeOH/H_2O (0.1% FA) over 18 min using a Waters 2695 Symmetry® C18 column (3.9 x 150 mm, 5µm particle size) set at a temperature of 25 °C at a flow rate of 1 mL/min with detection at 220 nm.

Peptide **3**: NH_2-$(CH_2)_5$-VTPLK-$CONH_2$

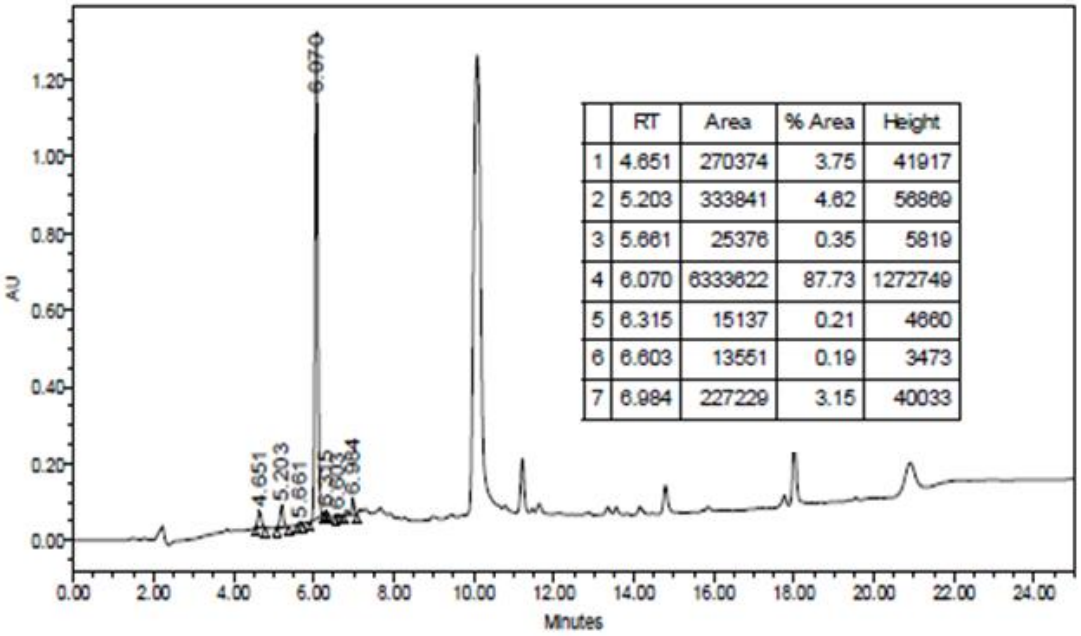

	RT	Area	% Area	Height
1	4.651	270374	3.75	41917
2	5.203	333841	4.62	56869
3	5.661	25376	0.35	5819
4	6.070	6333622	87.73	1272749
5	6.315	15137	0.21	4660
6	6.603	13551	0.19	3473
7	6.984	227229	3.15	40033

Figure A7. RP-HPLC analysis of crude peptide **3**, using a linear gradient 2-82% MeCN/H_2O (0.1% TFA) over 18 min using a Waters 2695 Symmetry® C18 column (3.9 x 150 mm, 5µm particle size) set at a temperature of 25 °C at a flow rate of 1 mL/min with detection at 220 nm.

Peptide **3**: NH_2-$(CH_2)_5$-VTPLK-$CONH_2$

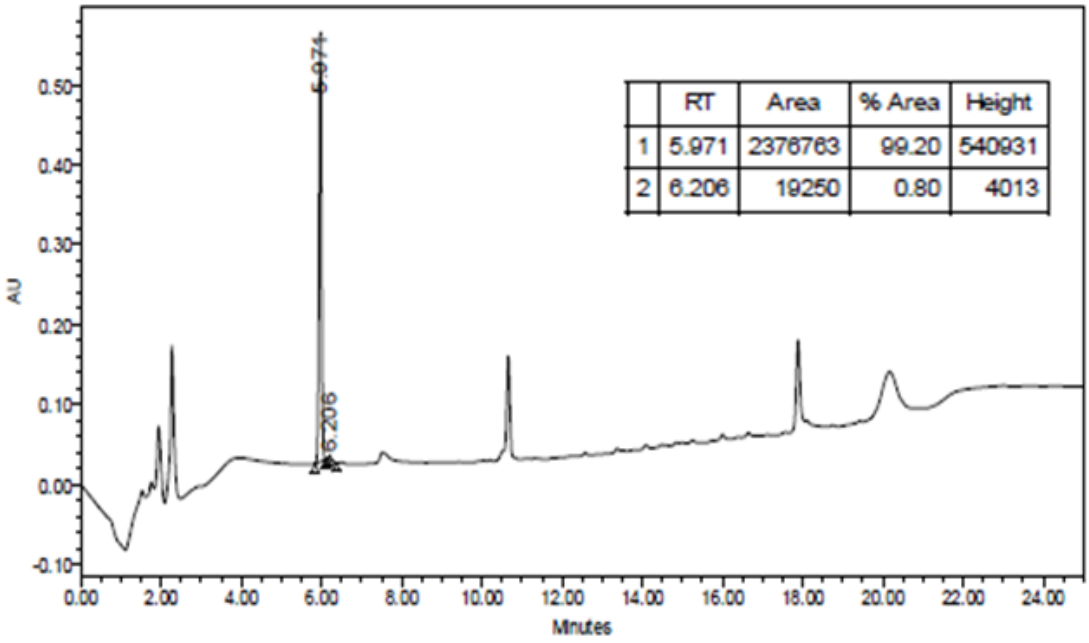

	RT	Area	% Area	Height
1	5.971	2376763	99.20	540931
2	6.206	19250	0.80	4013

Figure A8. RP-HPLC analysis of pure peptide **3**, using a linear gradient 2-82% MeCN/H_2O (0.1% TFA) over 18 min using a Waters 2695 Symmetry® C18 column (3.9 x 150 mm, 5µm particle size) set at a temperature of 25 °C at a flow rate of 1 mL/min with detection at 220 nm.

Peptide **3**: NH_2-$(CH_2)_5$-VTPLK-$CONH_2$

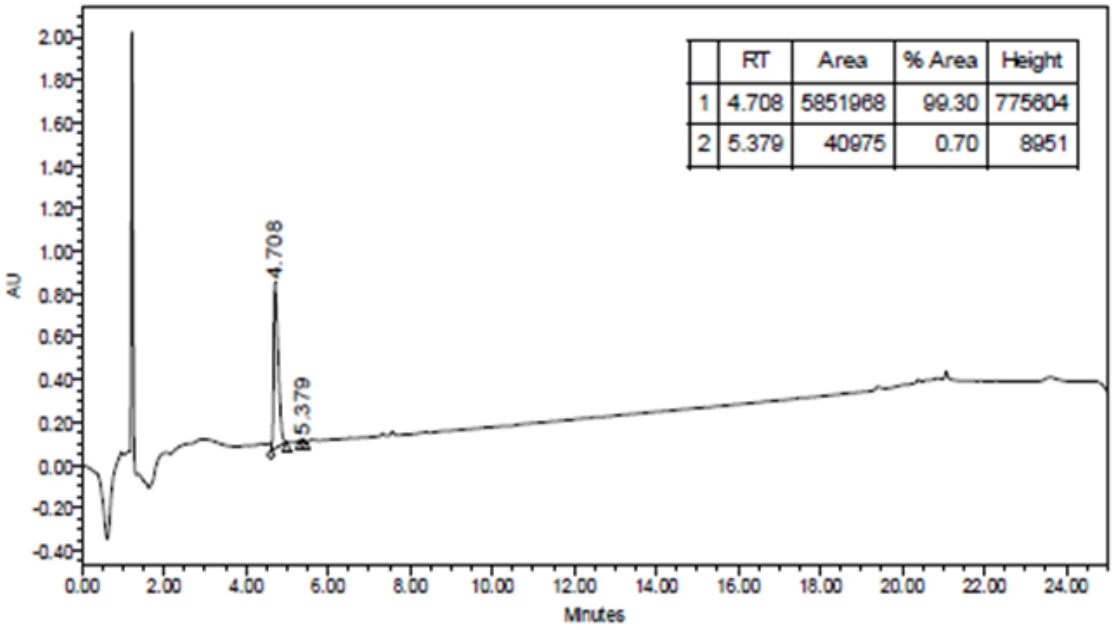

Figure A9. RP-HPLC analysis of pure peptide **3**, using a linear gradient 2-82% MeOH/H_2O (0.1% FA) over 18 min using a Waters 2695 Symmetry® C18 column (3.9 x 150 mm, 5µm particle size) set at a temperature of 25 °C at a flow rate of 1 mL/min with detection at 220 nm.

Peptide **3**: NH_2-$(CH_2)_5$-VTPLK-$CONH_2$

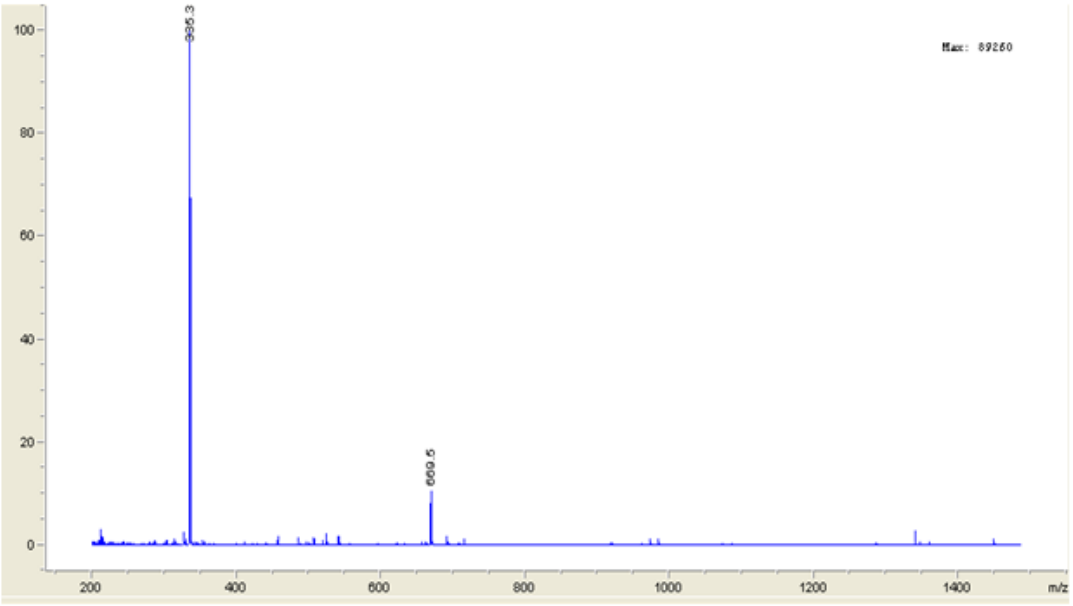

Figure A10. ESI-LCMS analysis of purified peptide **3**, using ESI MS in positive mode and LC linear gradient 2-82% MeOH/H_2O (0.1% FA) over 18 min using a Waters 2695 Symmetry® C18 column (3.9 x 150 mm, 5µm particle size) set at a temperature of 25 °C at a flow rate of 1 mL/min with detection at 220 nm.

Peptide **4**: NH_2-$(CH_2)_5$-FGTSMGVTPLK-$CONH_2$

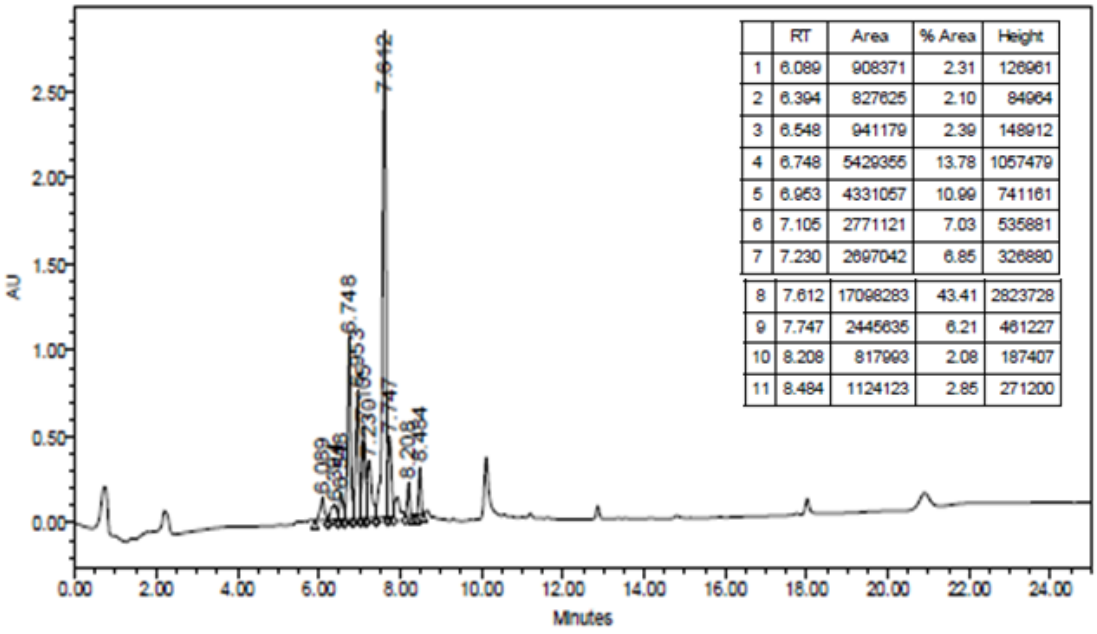

	RT	Area	% Area	Height
1	6.089	908371	2.31	126961
2	6.394	827625	2.10	84964
3	6.548	941179	2.39	148912
4	6.748	5429355	13.78	1057479
5	6.953	4331057	10.99	741161
6	7.105	2771121	7.03	535881
7	7.230	2697042	6.85	326880
8	7.612	17098283	43.41	2823728
9	7.747	2445635	6.21	461227
10	8.208	817993	2.08	187407
11	8.484	1124123	2.85	271200

Figure A11. RP-HPLC analysis of crude peptide **4**, using a linear gradient 2-82% MeCN/H_2O (0.1% TFA) over 18 min using a Waters 2695 Symmetry® C18 column (3.9 x 150 mm, 5µm particle size) set at a temperature of 25 °C at a flow rate of 1 mL/min with detection at 220 nm.

Peptide **4**: NH_2-$(CH_2)_5$-FGTSMGVTPLK-$CONH_2$

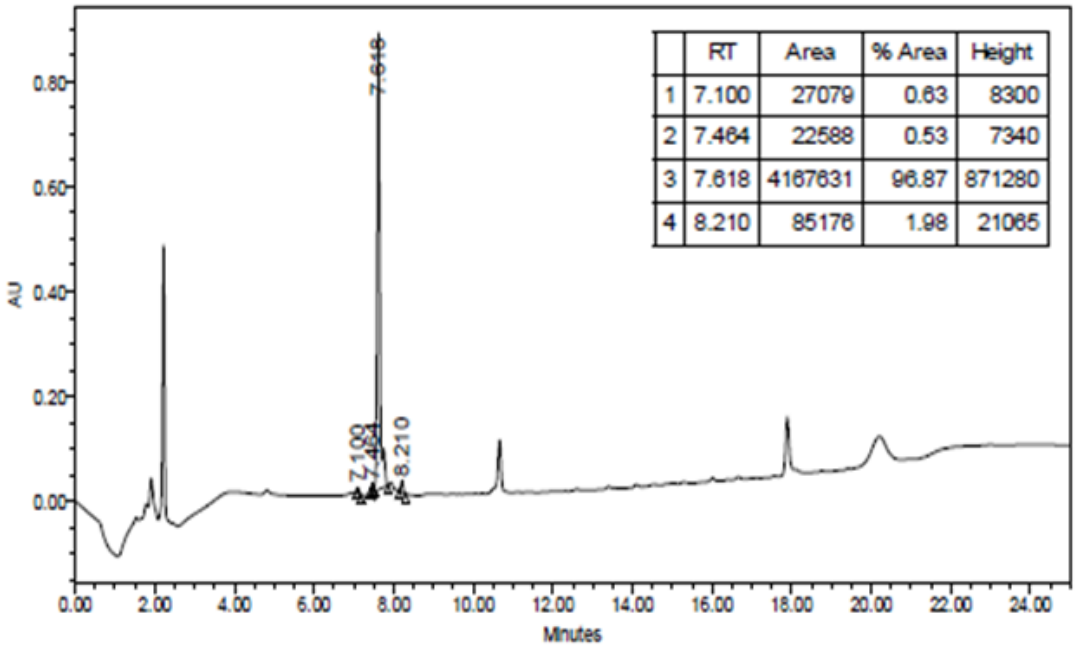

	RT	Area	% Area	Height
1	7.100	27079	0.63	8300
2	7.464	22588	0.53	7340
3	7.618	4167631	96.87	871280
4	8.210	85176	1.98	21065

Figure A12. RP-HPLC analysis of pure peptide **4**, using a linear gradient 2-82% MeCN/H_2O
(0.1% TFA) over 18 min using a Waters 2695 Symmetry® C18 column (3.9 x 150 mm, 5µm particle size) set at a temperature of 25 °C at a flow rate of 1 mL/min with detection at 220 nm.

Peptide **4**: NH_2-$(CH_2)_5$-FGTSMGVTPLK-$CONH_2$

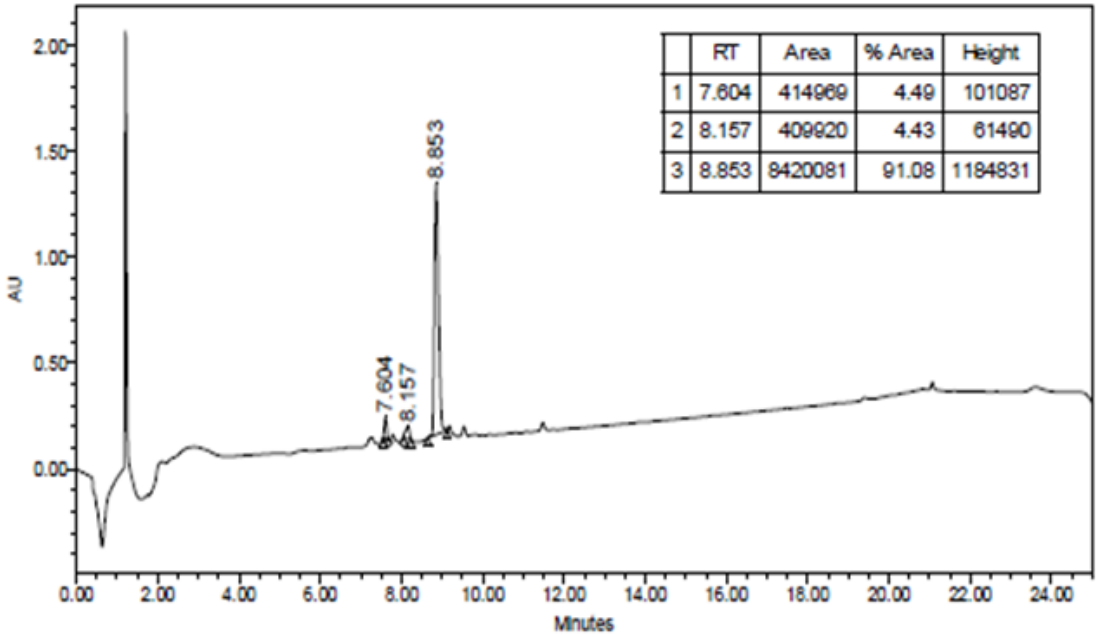

Figure A13. RP-HPLC analysis of pure peptide **4**, using a linear gradient 2-82% MeOH/H_2O (0.1% FA) over 18 min using a Waters 2695 Symmetry® C18 column (3.9 x 150 mm, 5µm particle size) set at a temperature of 25 °C at a flow rate of 1 mL/min with detection at 220 nm.

Peptide **4**: NH_2-$(CH_2)_5$-FGTSMGVTPLK-$CONH_2$

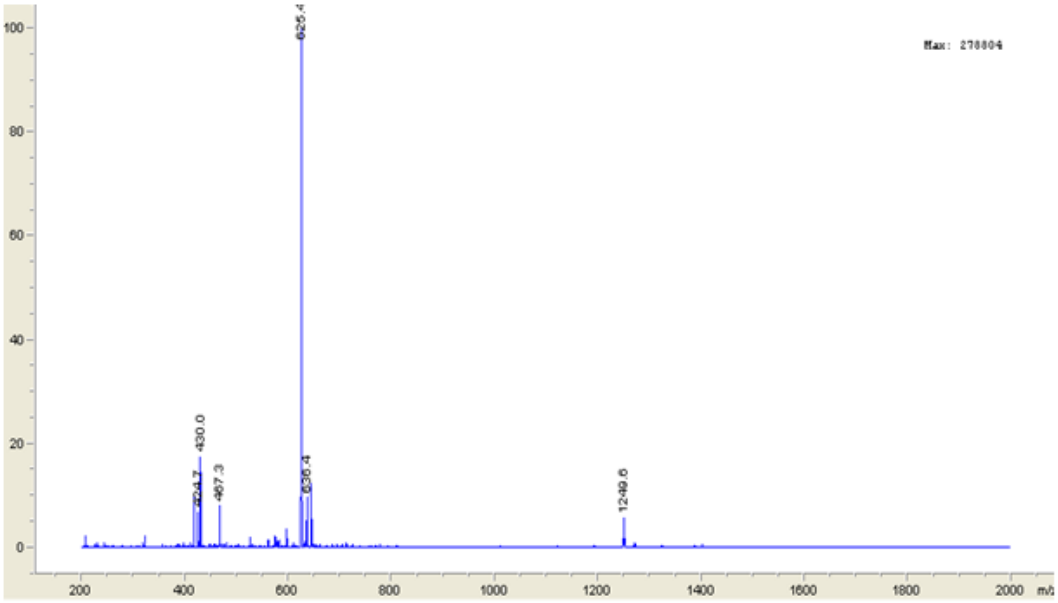

Figure A14. ESI-LCMS analysis of pure peptide **4**, using ESI MS in positive mode and LC linear gradient 2-82% MeOH/H_2O (0.1% FA) over 18 min using a Waters 2695 Symmetry® C18 column (3.9 x 150 mm, 5µm particle size) set at a temperature of 25 °C at a flow rate of 1 mL/min with detection at 220 nm.

Peptide **5**: NH_2-$(CH_2)_5$-TSMGFGVTPLK-$CONH_2$

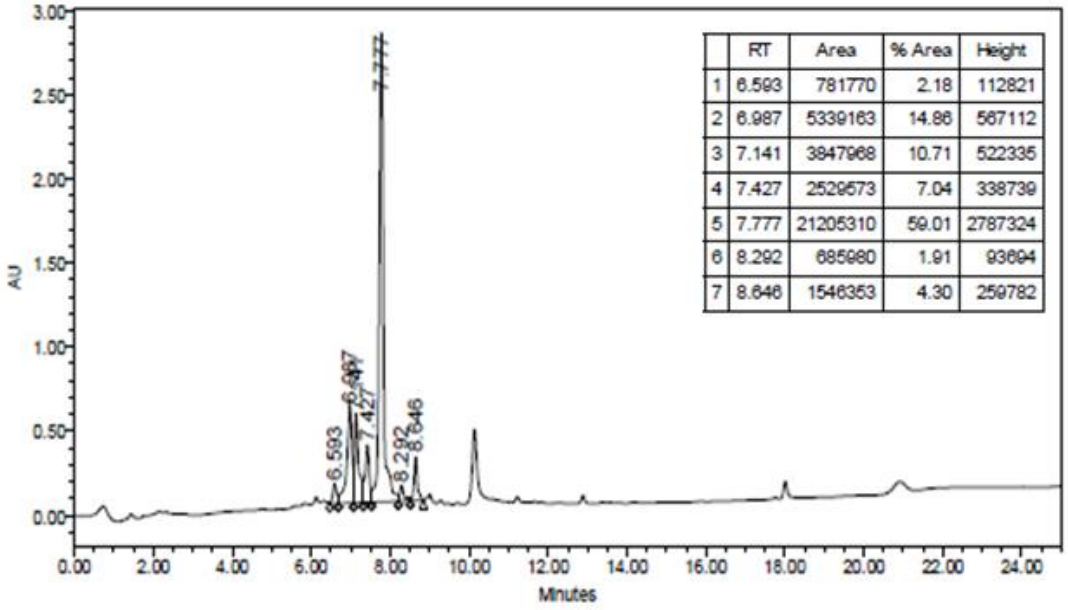

	RT	Area	% Area	Height
1	6.593	781770	2.18	112821
2	6.987	5339163	14.86	567112
3	7.141	3847968	10.71	522335
4	7.427	2529573	7.04	338739
5	7.777	21205310	59.01	2787324
6	8.292	685980	1.91	93694
7	8.646	1546353	4.30	259782

Figure A15. RP-HPLC analysis of crude peptide **5**, using a linear gradient 2-82% MeCN/H_2O (0.1% TFA) over 18 min using a Waters 2695 Symmetry® C18 column (3.9 x 150 mm, 5µm particle size) set at a temperature of 25 °C at a flow rate of 1 mL/min with detection at 220 nm.

Peptide **5**: NH_2-$(CH_2)_5$-TSMGFGVTPLK-$CONH_2$

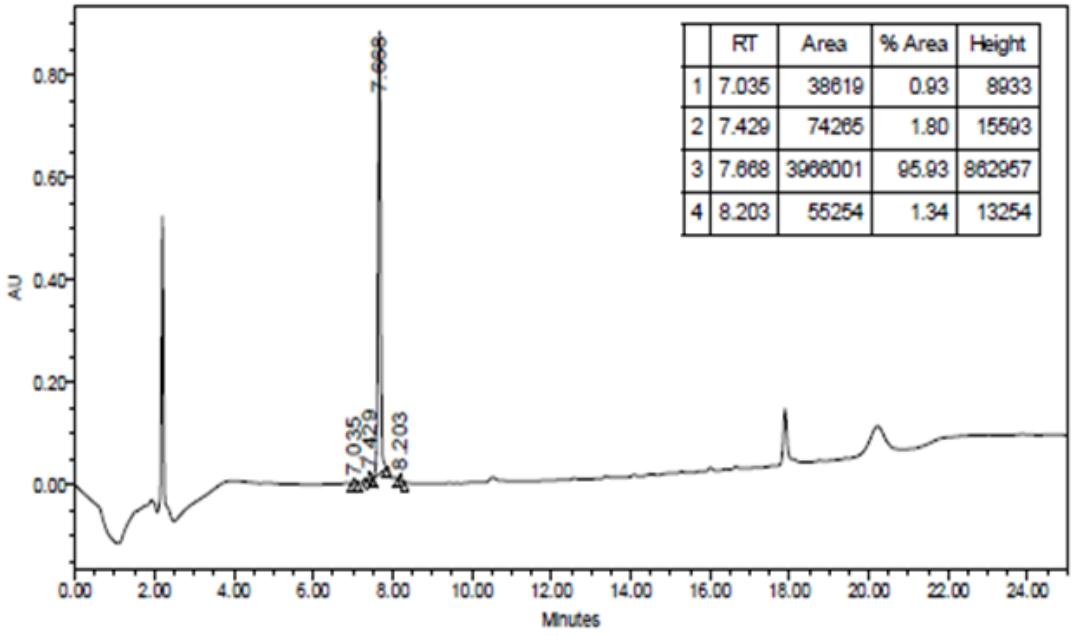

Figure A16. RP-HPLC analysis of pure peptide **5**, using a linear gradient 2-82% MeCN/H_2O (0.1% TFA) over 18 min using a Waters 2695 Symmetry® C18 column (3.9 x 150 mm, 5µm particle size) set at a temperature of 25 °C at a flow rate of 1 mL/min with detection at 220 nm.

Peptide **5**: NH_2-$(CH_2)_5$-TSMGFGVTPLK-$CONH_2$

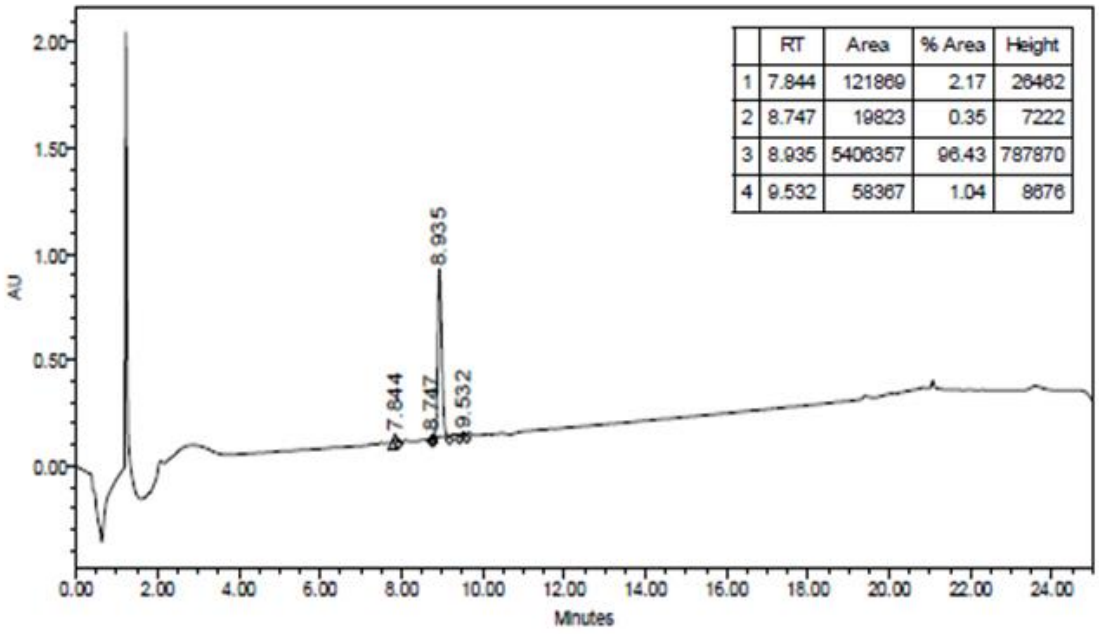

Figure A17. RP-HPLC analysis of pure peptide **5**, using a linear gradient 2-82% MeOH/H_2O (0.1% FA) over 18 min using a Waters 2695 Symmetry® C18 column (3.9 x 150 mm, 5µm particle size) set at a temperature of 25 °C at a flow rate of 1 mL/min with detection at 220 nm.

Peptide **5**: NH_2-$(CH_2)_5$-TSMGFGVTPLK-$CONH_2$

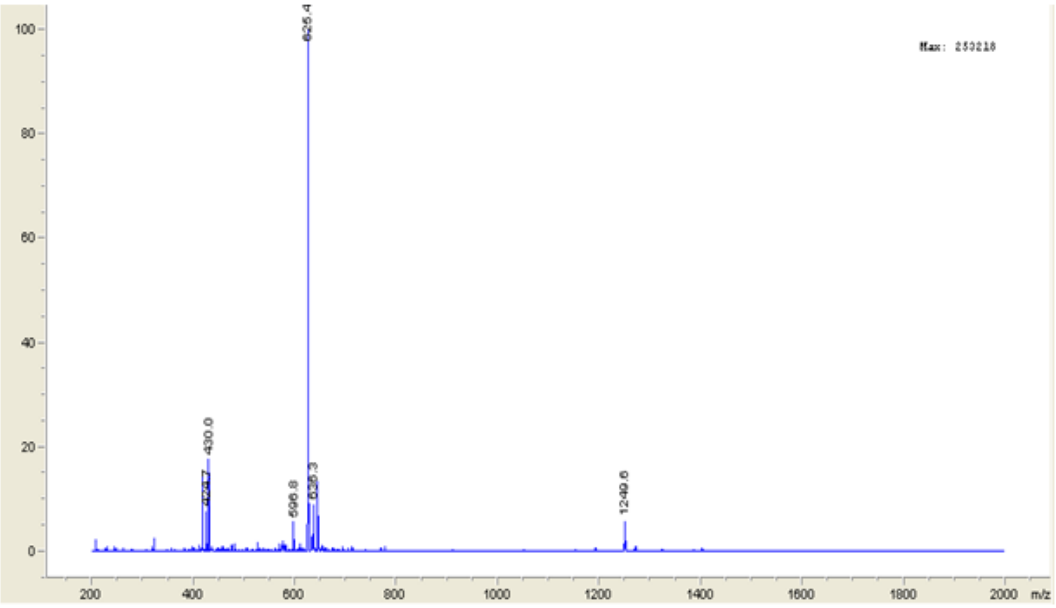

Figure A18. ESI-LCMS analysis of pure peptide **5**, using ESI MS in positive mode and LC linear gradient 2-82% MeOH/H_2O (0.1% FA) over 18 min using a Waters 2695 Symmetry® C18 column (3.9 x 150 mm, 5µm particle size) set at a temperature of 25 °C at a flow rate of 1 mL/min with detection at 220 nm.

Peptide **6**: NH_2-$(CH_2)_5$-TVPLN-$CONH_2$

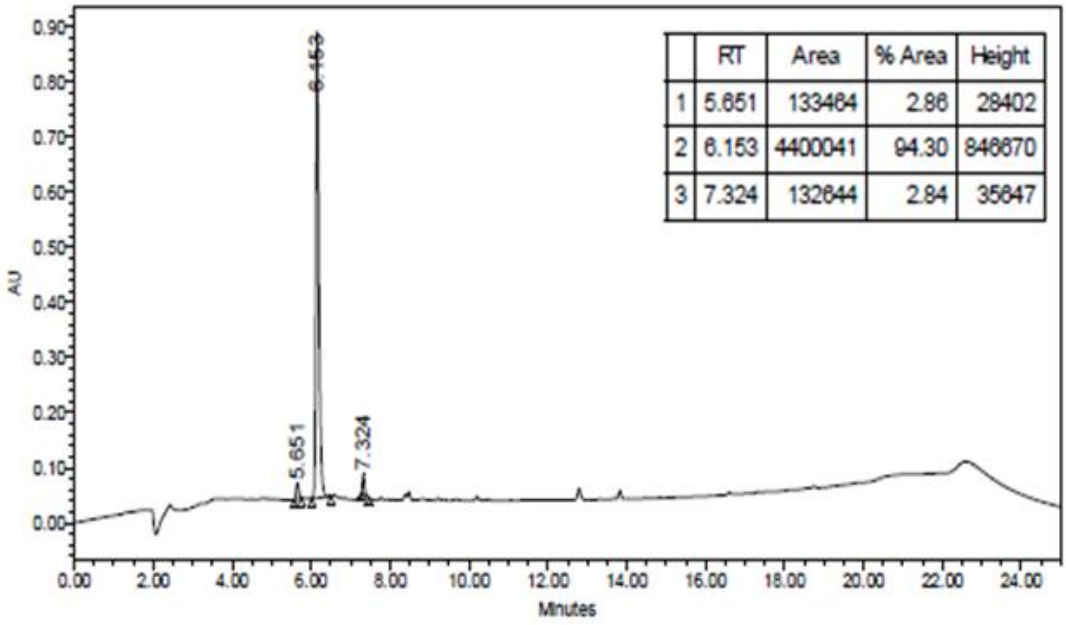

Figure A19. RP-HPLC analysis of pure peptide **6**, using a linear gradient 2-82% MeCN/H_2O (0.1% TFA) over 18 min using a Waters 2695 Symmetry® C18 column (3.9 x 150 mm, 5µm particle size) set at a temperature of 25 °C at a flow rate of 1 mL/min with detection at 220 nm.

Peptide **6**: NH_2-$(CH_2)_5$-TVPLN-$CONH_2$

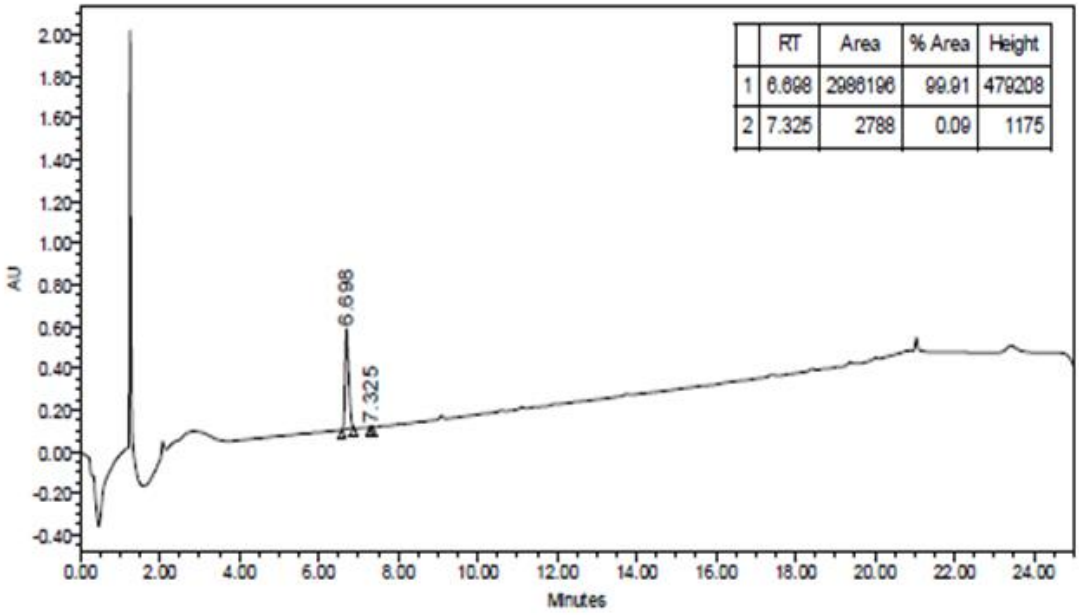

Figure A20. RP-HPLC analysis of pure peptide **6**, using a linear gradient 2-82% MeOH/H_2O (0.1% FA) over 18 min using a Waters 2695 Symmetry® C18 column (3.9 x 150 mm, 5µm particle size) set at a temperature of 25 °C at a flow rate of 1 mL/min with detection at 220 nm.

Peptide **6**: NH_2-$(CH_2)_5$-TVPLN-$CONH_2$

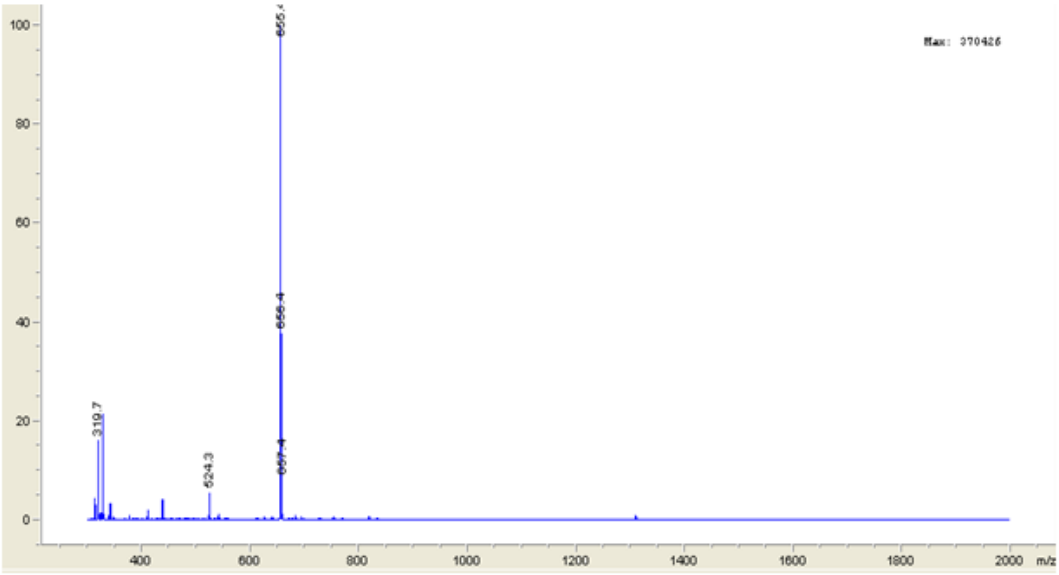

Figure A21. ESI-LCMS analysis of purified peptide **6**, using ESI MS in positive mode and LC linear gradient 2-82% MeOH/H_2O (0.1% FA) over 18 min using a Waters 2695 Symmetry® C18 column (3.9 x 150 mm, 5µm particle size) set at a temperature of 25 °C at a flow rate of 1 mL/min with detection at 220 nm.

Peptide **7**: FITC-NH-$(CH_2)_5$-FG-$CONH_2$

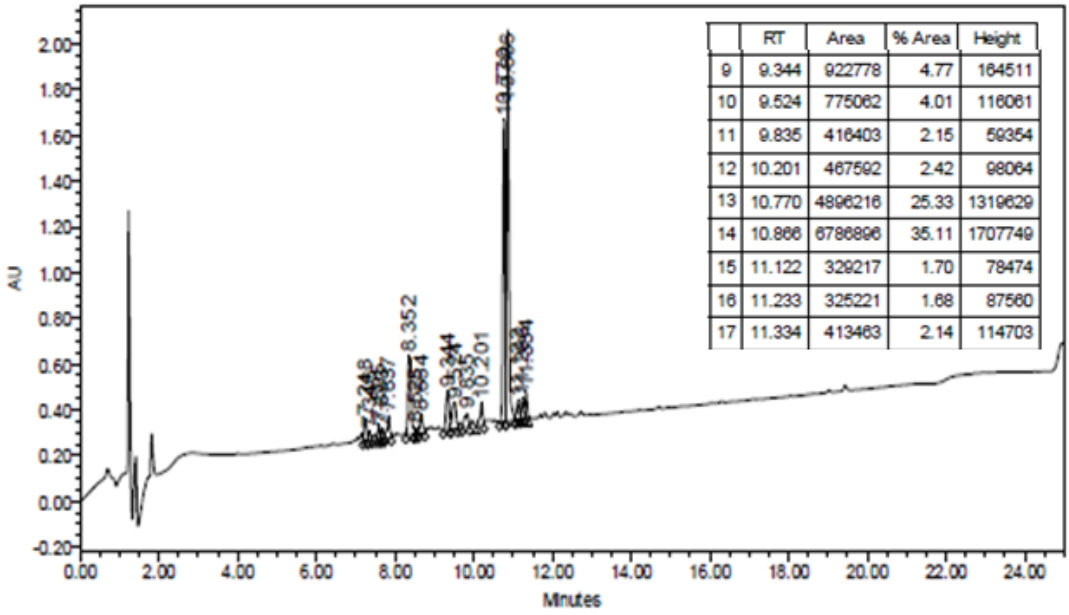

	RT	Area	% Area	Height
9	9.344	922778	4.77	164511
10	9.524	775062	4.01	116061
11	9.835	416403	2.15	59354
12	10.201	467592	2.42	98064
13	10.770	4896216	25.33	1319629
14	10.866	6786896	35.11	1707749
15	11.122	329217	1.70	78474
16	11.233	325221	1.68	87560
17	11.334	413463	2.14	114703

Figure A22. RP-HPLC analysis of crude FITC labeled peptide **7**, using a linear gradient 2-82% MeCN/H_2O (0.1% FA) over 18 min using a Waters 2695 Symmetry® C18 column (3.9 x 150 mm, 5µm particle size) set at a temperature of 25 °C at a flow rate of 1 mL/min with detection at 220 nm.

Peptide **7**: FITC-NH-$(CH_2)_5$-FG-$CONH_2$

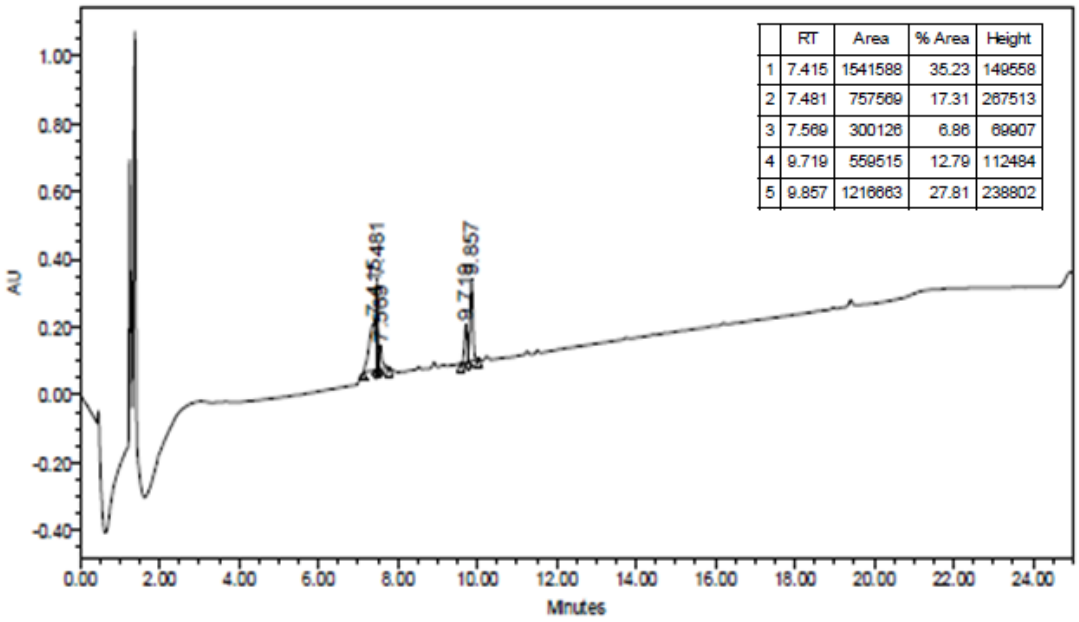

	RT	Area	% Area	Height
1	7.415	1541588	35.23	149558
2	7.481	757569	17.31	267513
3	7.569	300126	6.86	69907
4	9.719	559515	12.79	112484
5	9.857	1216663	27.81	238802

Figure A23. RP-HPLC analysis of pure FITC labeled peptide 7, using a linear gradient 2-82% MeCN/H_2O (0.1% FA) over 18 min using a Waters 2695 Symmetry® C18 column (3.9 x 150 mm, 5µm particle size) set at a temperature of 25 °C at a flow rate of 1 mL/min with detection at 220 nm.

Peptide **7**: FITC-NH_2-$(CH_2)_5$-FG-$CONH_2$

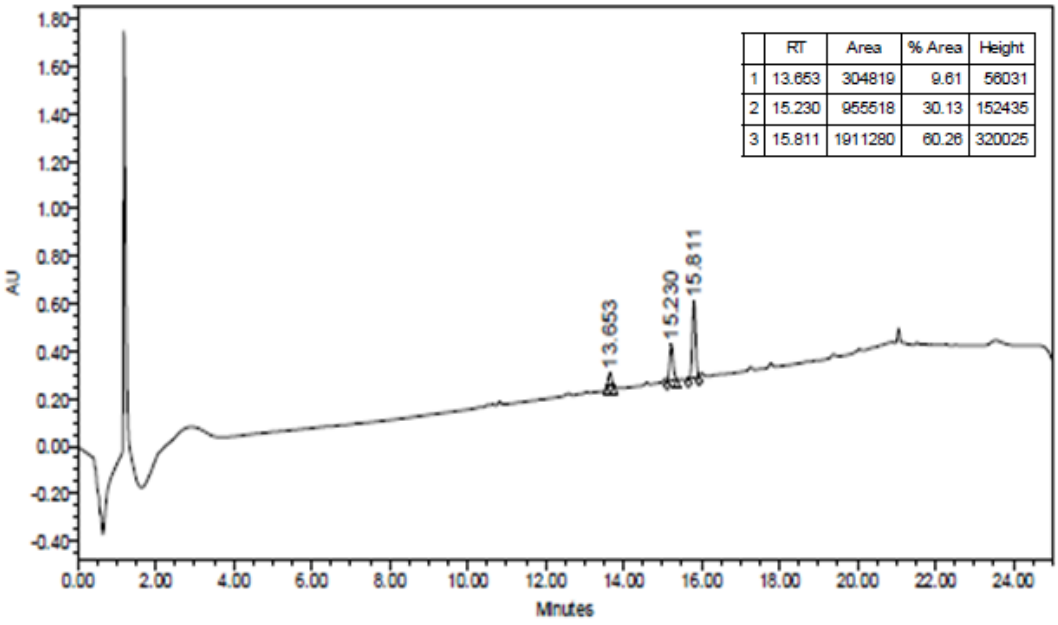

Figure A24. RP-HPLC analysis of pure peptide 7, using a linear gradient 2-82% MeOH/H_2O (0.1% FA) over 18 min using a Waters 2695 Symmetry® C18 column (3.9 x 150 mm, 5µm particle size) set at a temperature of 25 °C at a flow rate of 1 mL/min with detection at 220 nm.

Peptide **7**: FITC-NH_2-$(CH_2)_5$-FG-$CONH_2$

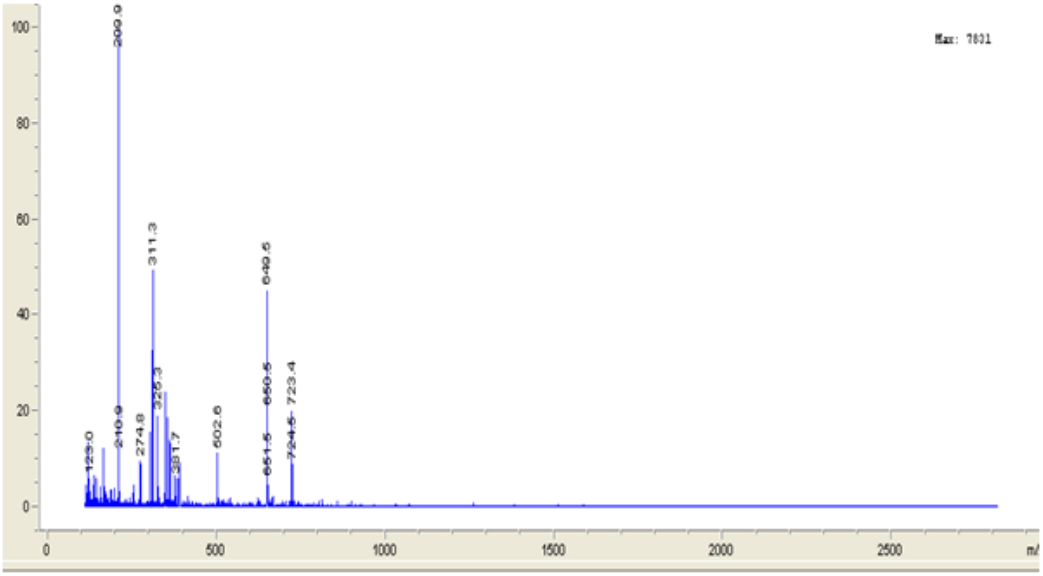

Figure A25. ESI-LCMS analysis of pure peptide 7, using ESI MS in positive mode and LC linear gradient 2-82% MeOH/H_2O (0.1% FA) over 18 min using a Waters 2695 Symmetry® C18 column (3.9 x 150 mm, 5µm particle size) set at a temperature of 25 °C at a flow rate of 1 mL/min with detection at 220 nm.

Peptide **8**: FITC-NH-$(CH_2)_5$-TSMG-$CONH_2$

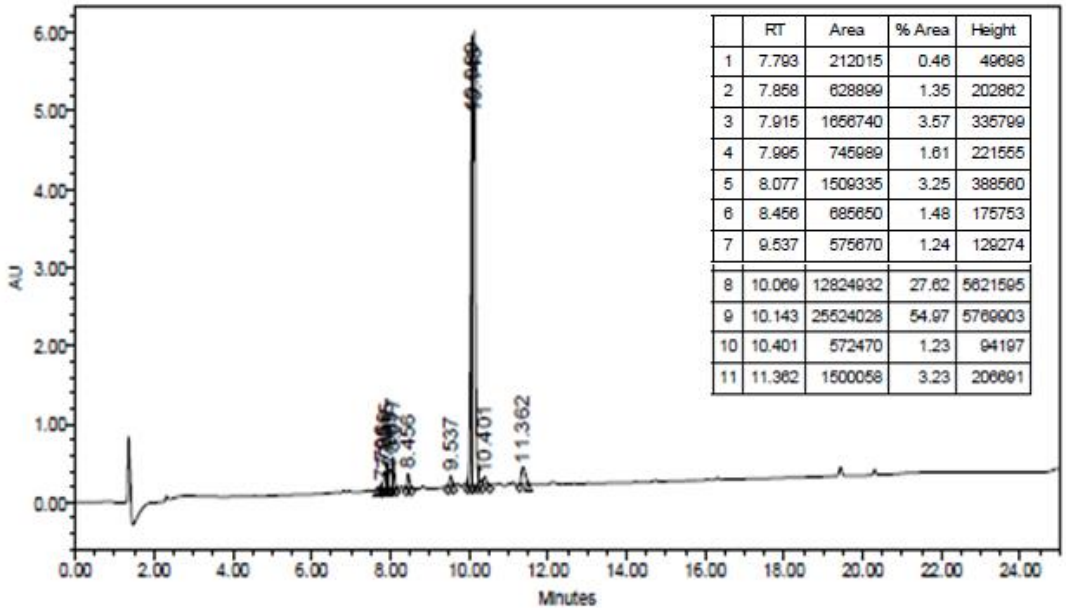

	RT	Area	% Area	Height
1	7.793	212015	0.46	49698
2	7.858	628899	1.35	202862
3	7.915	1656740	3.57	335799
4	7.995	745989	1.61	221555
5	8.077	1509335	3.25	388560
6	8.456	685650	1.48	175753
7	9.537	575670	1.24	129274
8	10.069	12824932	27.62	5621595
9	10.143	25524028	54.97	5769903
10	10.401	572470	1.23	94197
11	11.362	1500058	3.23	206691

Figure A26. RP-HPLC analysis of crude FITC labeled peptide **8**, using a linear gradient 2-82% MeCN/H_2O (0.1% FA) over 18 min using a Waters 2695 Symmetry® C18 column (3.9 x 150 mm, 5µm particle size) set at a temperature of 25 °C at a flow rate of 1 mL/min with detection at 220 nm.

Peptide **8**: FITC-NH-$(CH_2)_5$-TSMG-$CONH_2$

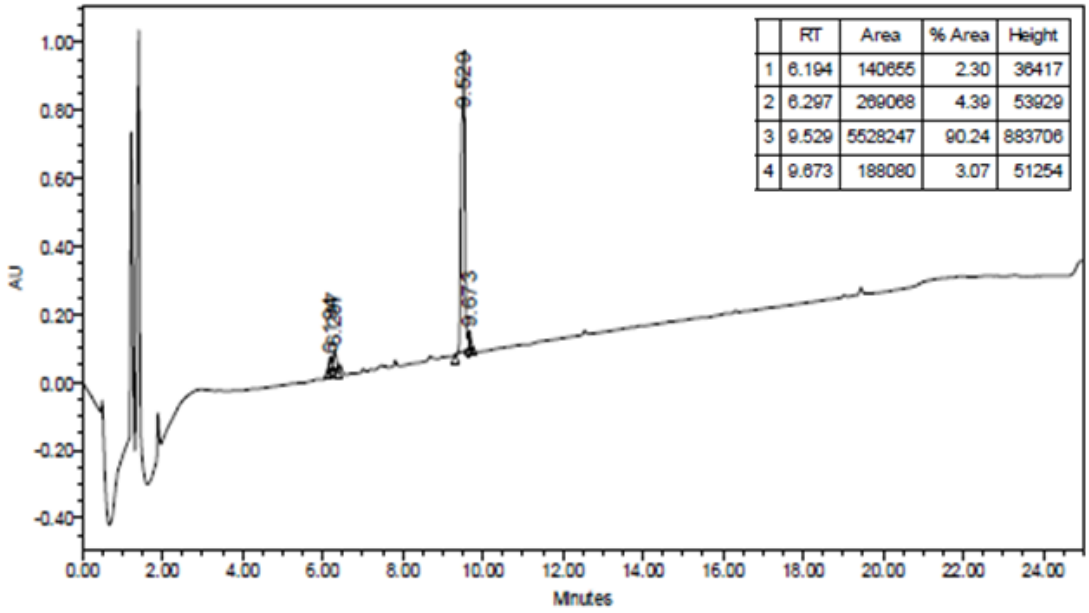

Figure A27. RP-HPLC analysis of pure FITC labeled peptide **8**, using a linear gradient 2-82% MeCN/H_2O (0.1% FA) over 18 min using a Waters 2695 Symmetry® C18 column (3.9 x 150 mm, 5µm particle size) set at a temperature of 25 °C at a flow rate of 1 mL/min with detection at 220 nm.

Peptide **8**: FITC-NH_2-$(CH_2)_5$-TSMG-$CONH_2$

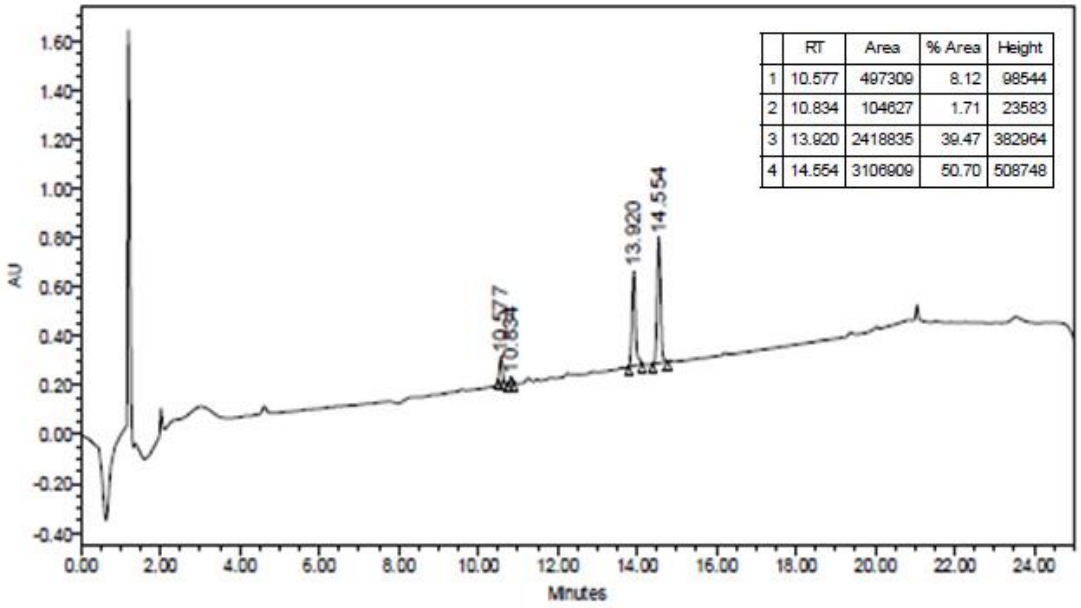

Figure A28. RP-HPLC analysis of pure FITC labeled peptide **8**, using a linear gradient 2-82% MeOH/H_2O (0.1% FA) over 18 min using a Waters 2695 Symmetry® C18 column (3.9 x 150 mm, 5µm particle size) set at a temperature of 25 °C at a flow rate of 1 mL/min with detection at 220 nm.

Peptide **8**: FITC-NH_2-$(CH_2)_5$-TSMG-$CONH_2$

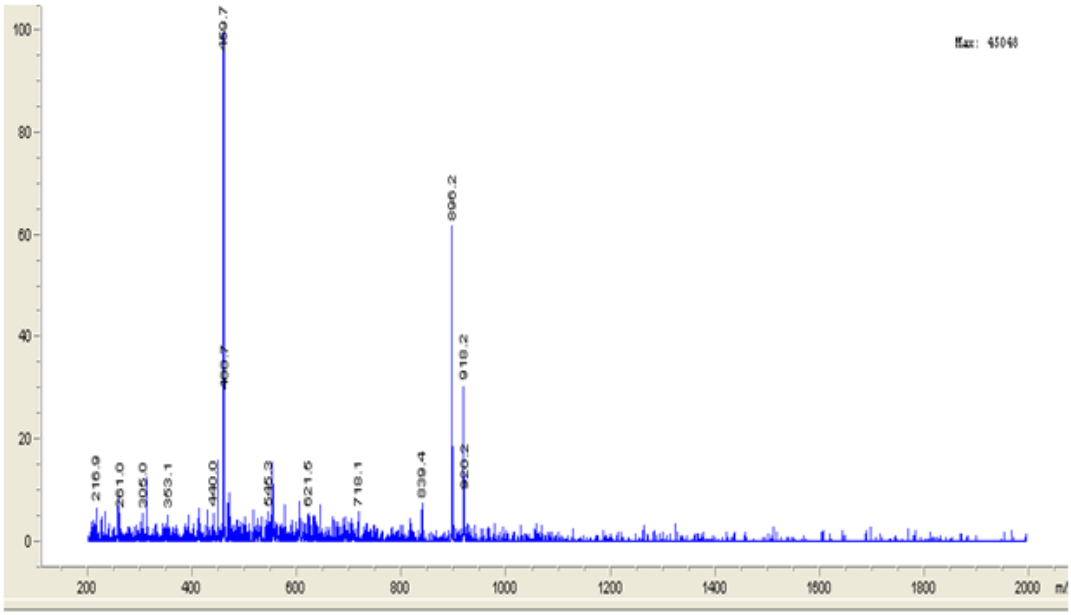

Figure A29. ESI-LCMS analysis of pure FITC labeled peptide **8**, using ESI MS in positive mode and LC linear gradient 2-82% MeOH/H_2O (0.1% FA) over 18 min using a Waters 2695 Symmetry® C18 column (3.9 x 150 mm, 5µm particle size) set at a temperature of 25 °C at a flow rate of 1 mL/min with detection at 220 nm.

Peptide **9**: FITC-NH-$(CH_2)_5$-VTPLK-$CONH_2$

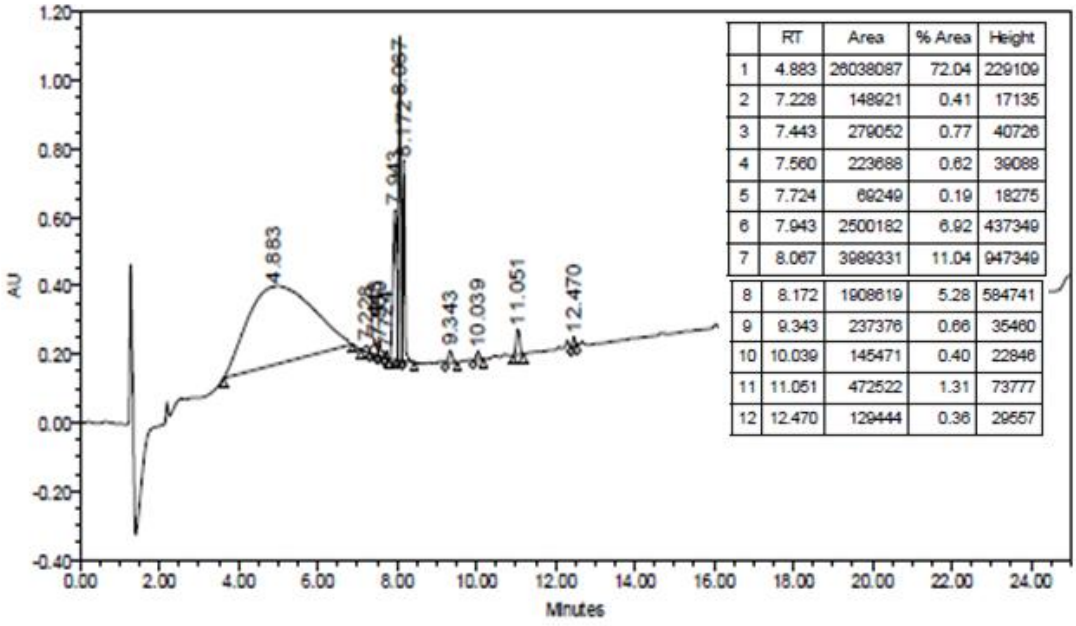

	RT	Area	% Area	Height
1	4.883	26038087	72.04	229109
2	7.228	148921	0.41	17135
3	7.443	279052	0.77	40726
4	7.560	223688	0.62	39088
5	7.724	69249	0.19	18275
6	7.943	2500182	6.92	437349
7	8.067	3989331	11.04	947349
8	8.172	1908619	5.28	584741
9	9.343	237376	0.66	35460
10	10.039	145471	0.40	22846
11	11.051	472522	1.31	73777
12	12.470	129444	0.36	29557

Figure A30. RP-HPLC analysis of crude FITC labeled peptide **9**, using a linear gradient 2-82% MeCN/H_2O (0.1% FA) over 18 min using a Waters 2695 Symmetry® C18 column (3.9 x 150 mm, 5µm particle size) set at a temperature of 25 °C at a flow rate of 1 mL/min with detection at 220 nm.

Peptide **9**: FITC-NH-$(CH_2)_5$-VTPLK-$CONH_2$

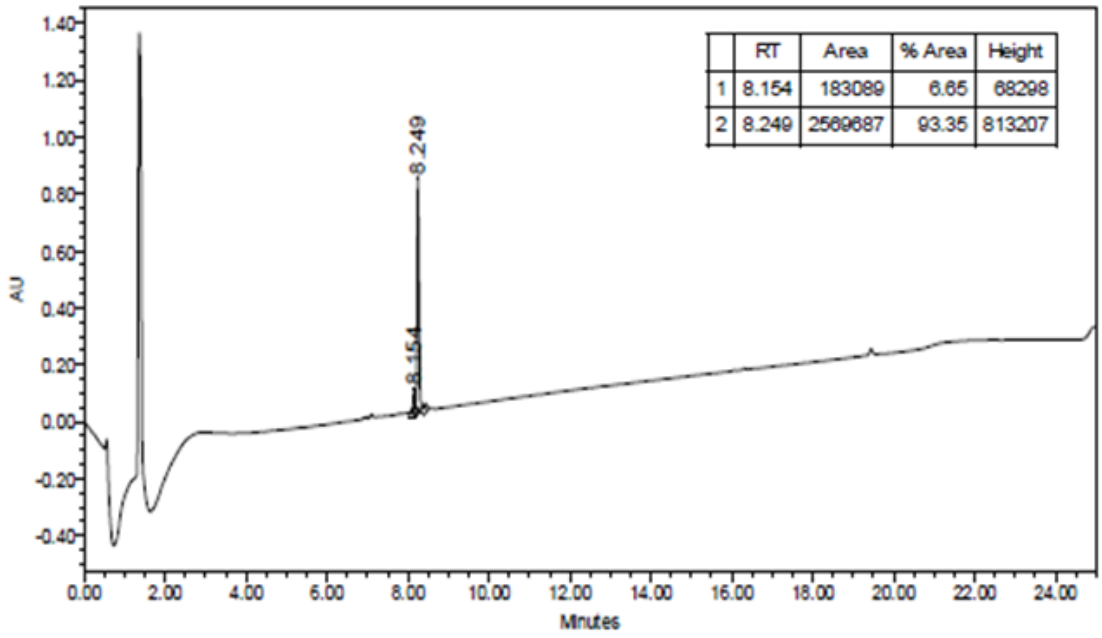

Figure A31. RP-HPLC analysis of pure FITC labeled peptide **9**, using a linear gradient 2-82% MeCN/H_2O (0.1% FA) over 18 min using a Waters 2695 Symmetry® C18 column (3.9 x 150 mm, 5µm particle size) set at a temperature of 25 °C at a flow rate of 1 mL/min with detection at 220 nm.

Peptide **9**: FITC-NH_2-$(CH_2)_5$-VTPLK-$CONH_2$

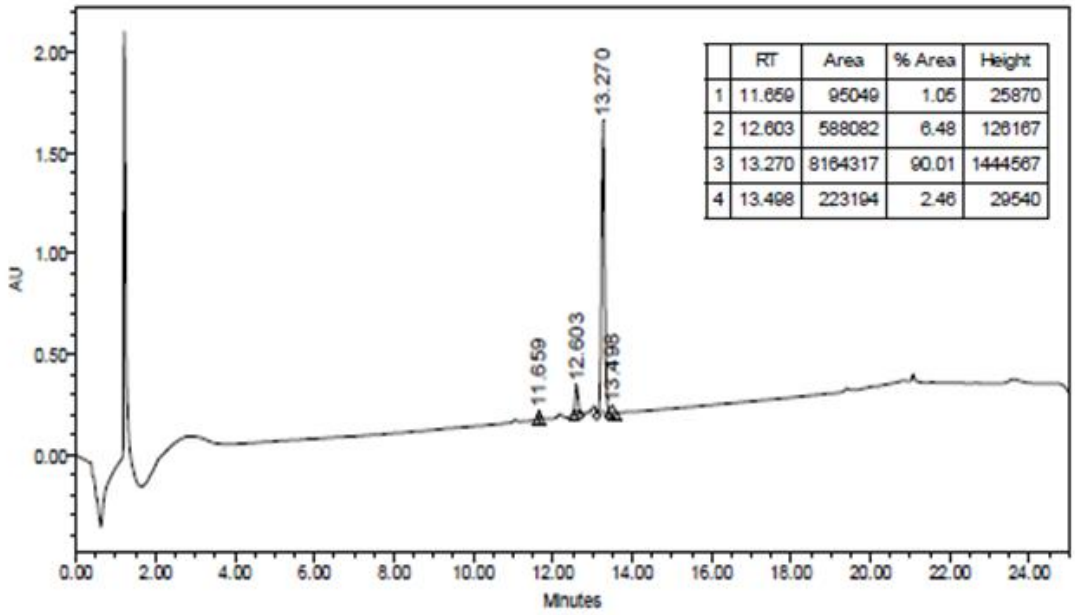

Figure A32. RP-HPLC analysis of pure FITC labeled peptide **9**, using a linear gradient 2-82% MeOH/H_2O (0.1% FA) over 18 min using a Waters 2695 Symmetry® C18 column (3.9 x 150 mm, 5µm particle size) set at a temperature of 25 °C at a flow rate of 1 mL/min with detection at 220 nm.

Peptide **9**: FITC-NH_2-$(CH_2)_5$-VTPLK-$CONH_2$

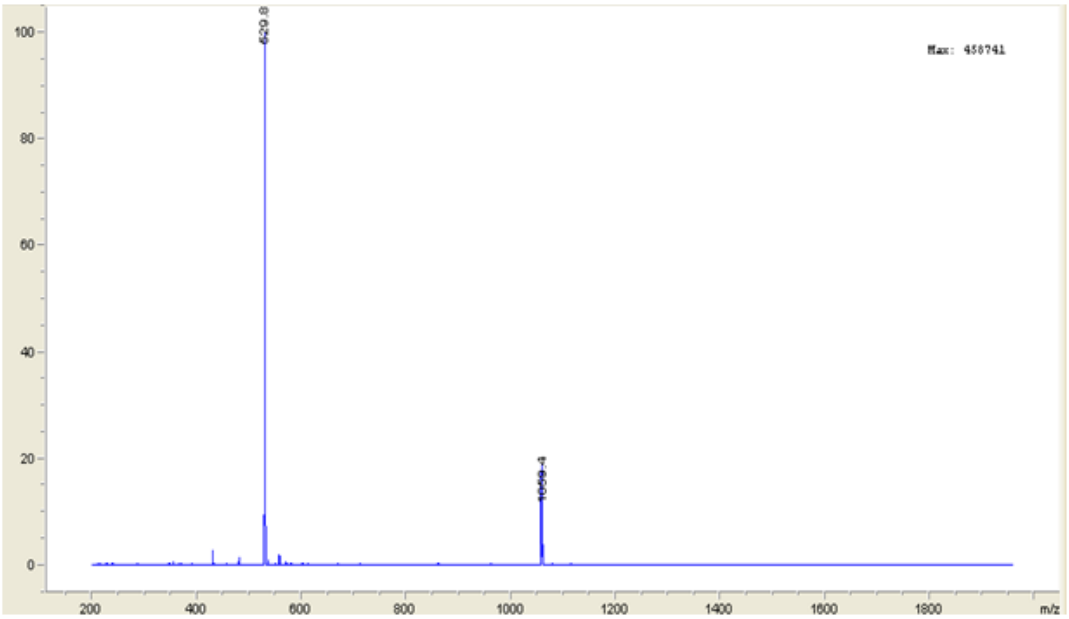

Figure A33. ESI-LCMS analysis of pure FITC labeled peptide **9**, using ESI MS in positive mode and LC linear gradient 2-82% MeOH/H_2O (0.1% FA) over 18 min using a Waters 2695 Symmetry® C18 column (3.9 x 150 mm, 5µm particle size) set at a temperature of 25 °C at a flow rate of 1 mL/min with detection at 220 nm.

Peptide **10**: FITC-NH-$(CH_2)_5$-FGTSMGVTPLK-$CONH_2$

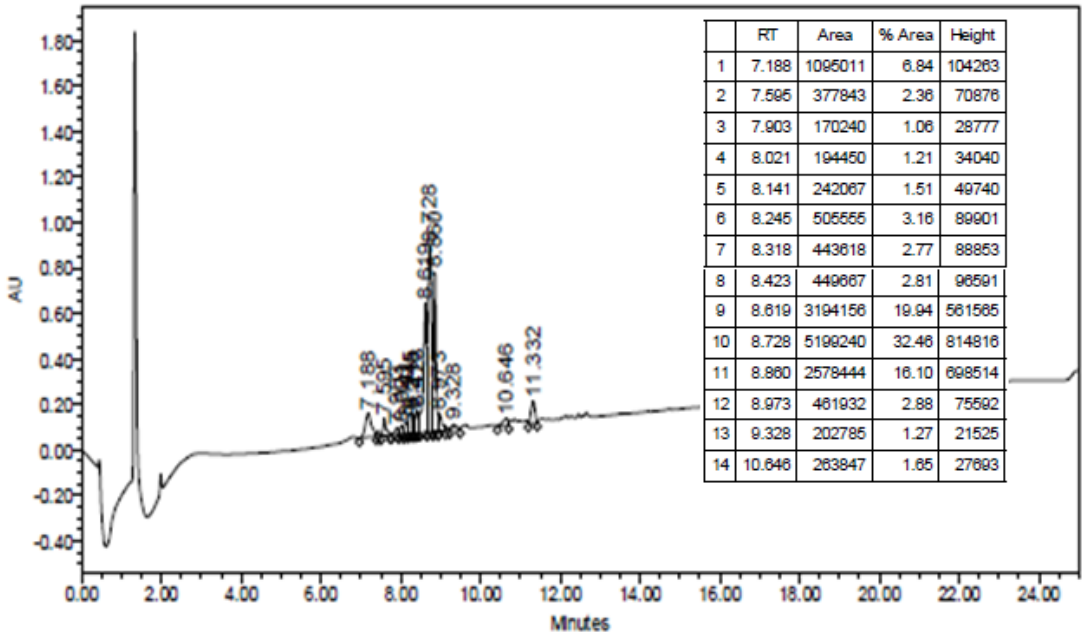

	RT	Area	% Area	Height
1	7.188	1095011	6.84	104263
2	7.595	377843	2.36	70876
3	7.903	170240	1.06	28777
4	8.021	194450	1.21	34040
5	8.141	242067	1.51	49740
6	8.245	505555	3.16	89901
7	8.318	443618	2.77	88853
8	8.423	449667	2.81	96591
9	8.619	3194156	19.94	561565
10	8.728	5199240	32.46	814816
11	8.860	2578444	16.10	698514
12	8.973	461932	2.88	75592
13	9.328	202785	1.27	21525
14	10.646	263847	1.65	27693

Figure A34. RP-HPLC analysis of crude FITC labeled peptide **10**, using a linear gradient 2-82% MeCN/H_2O (0.1% FA) over 18 min using a Waters 2695 Symmetry® C18 column (3.9 x 150 mm, 5µm particle size) set at a temperature of 25 °C at a flow rate of 1 mL/min with detection at 220 nm.

Peptide **10**: FITC-NH-$(CH_2)_5$-FGTSMGVTPLK-$CONH_2$

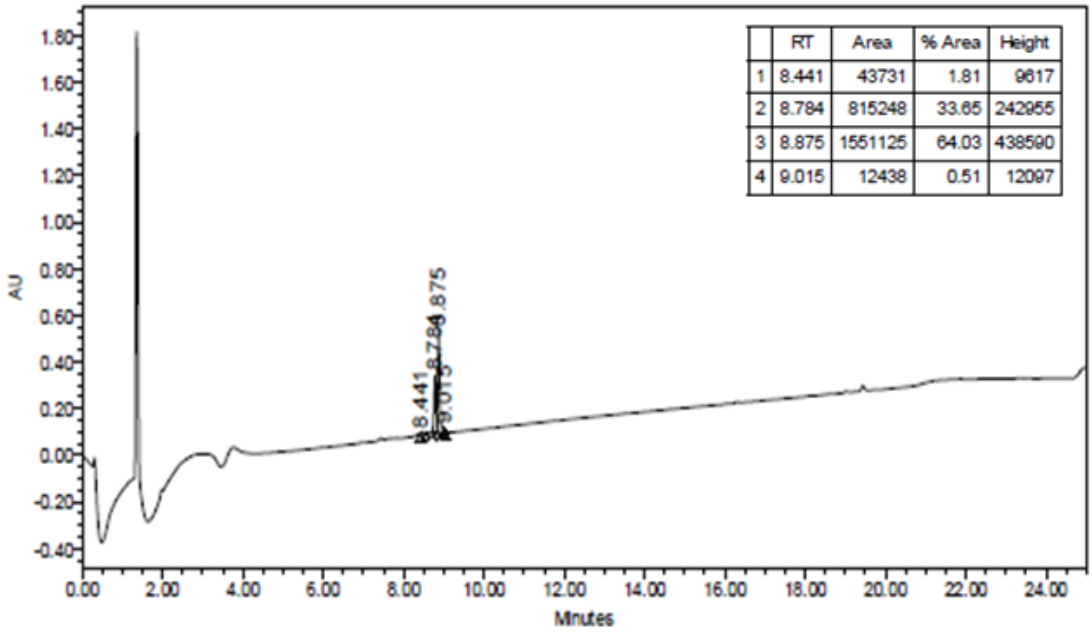

Figure A35. RP-HPLC analysis of pure FITC labeled peptide **10**, using a linear gradient 2-82% MeCN/H_2O (0.1% FA) over 18 min using a Waters 2695 Symmetry® C18 column (3.9 x 150 mm, 5µm particle size) set at a temperature of 25 °C at a flow rate of 1 mL/min with detection at 220 nm.

Peptide **10**: FITC-NH_2-$(CH_2)_5$-FGTSMGVTPLK-$CONH_2$

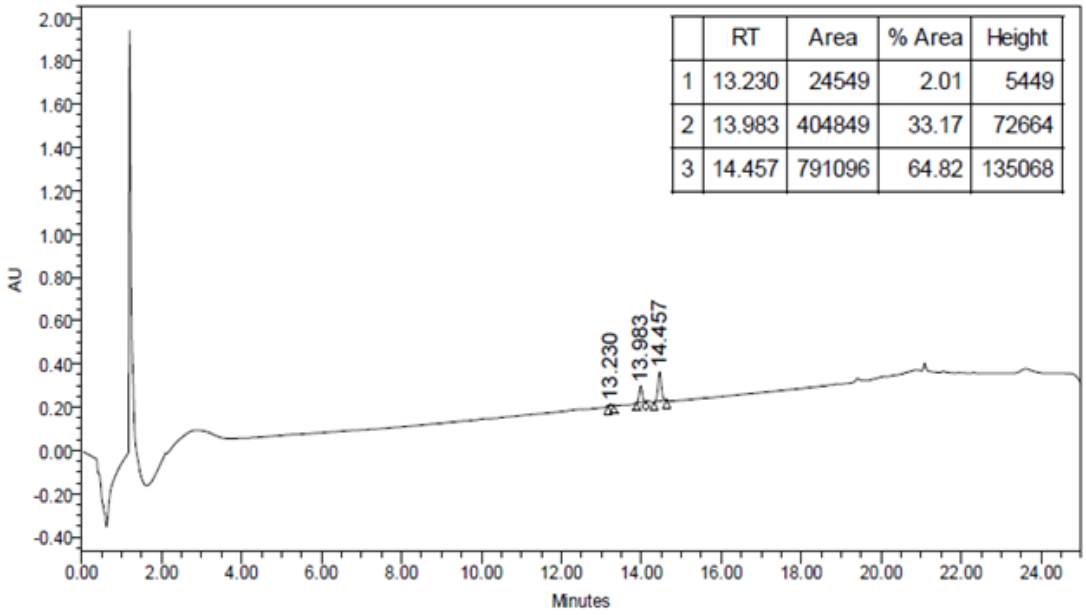

Figure A36. RP-HPLC analysis of pure FITC labeled peptide **10**, using a linear gradient 2-82% MeOH/H_2O (0.1% FA) over 18 min using a Waters 2695 Symmetry® C18 column (3.9 x 150 mm, 5µm particle size) set at a temperature of 25 °C at a flow rate of 1 mL/min with detection at 220 nm.

Peptide **10**: FITC-NH_2-$(CH_2)_5$-FGTSMGVTPLK-$CONH_2$

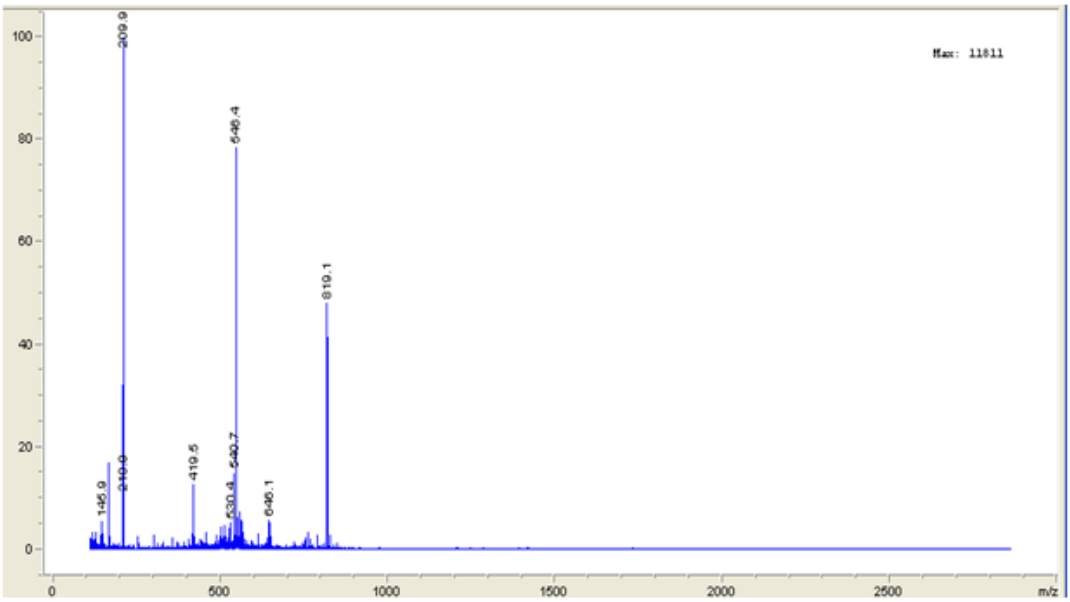

Figure A37. ESI-LCMS analysis of pure FITC labeled peptide **10**, using ESI MS in positive mode and LC linear gradient 2-82% MeOH/H_2O (0.1% FA) over 18 min using a Waters 2695 Symmetry® C18 column (3.9 x 150 mm, 5µm particle size) set at a temperature of 25 °C at a flow rate of 1 mL/min with detection at 220 nm.

Peptide **11**: FITC-NH-$(CH_2)_5$-TSMGFGVTPLK-$CONH_2$

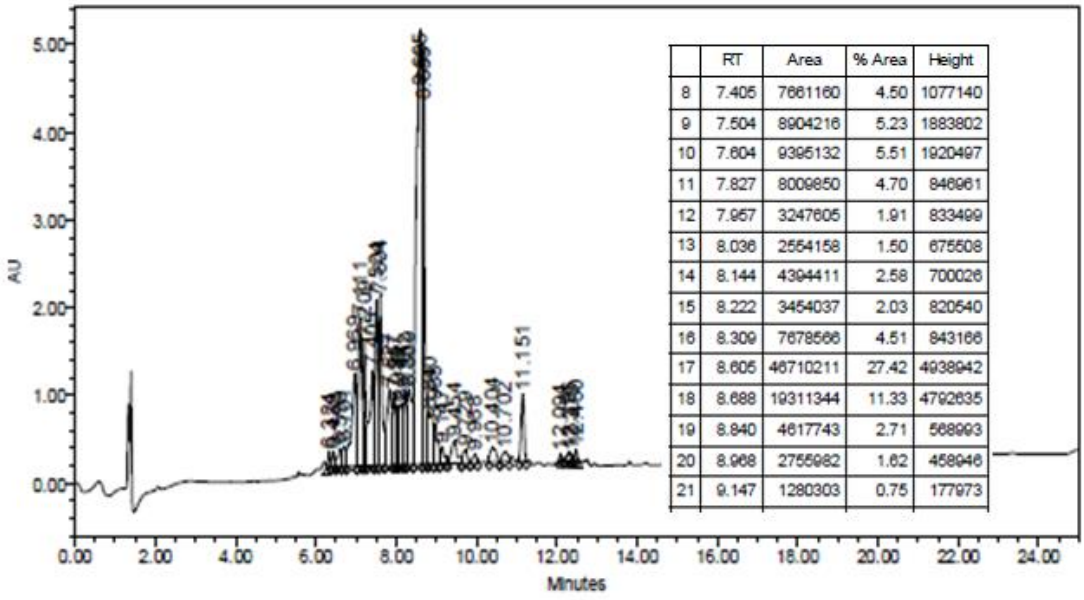

	RT	Area	% Area	Height
8	7.405	7661160	4.50	1077140
9	7.504	8904216	5.23	1883802
10	7.604	9395132	5.51	1920497
11	7.827	8009850	4.70	846961
12	7.957	3247605	1.91	833499
13	8.036	2554158	1.50	675508
14	8.144	4394411	2.58	700026
15	8.222	3454037	2.03	820540
16	8.309	7678566	4.51	843166
17	8.605	46710211	27.42	4938942
18	8.688	19311344	11.33	4792635
19	8.840	4617743	2.71	568993
20	8.968	2755982	1.62	458946
21	9.147	1280303	0.75	177973

Figure A38. RP-HPLC analysis of crude FITC labeled peptide **11**, using a linear gradient 2-82% MeCN/H_2O (0.1% FA) over 18 min using a Waters 2695 Symmetry® C18 column (3.9 x 150 mm, 5µm particle size) set at a temperature of 25 °C at a flow rate of 1 mL/min with detection at 220 nm.

Peptide **11**: FITC-NH-$(CH_2)_5$-TSMGFGVTPLK-$CONH_2$

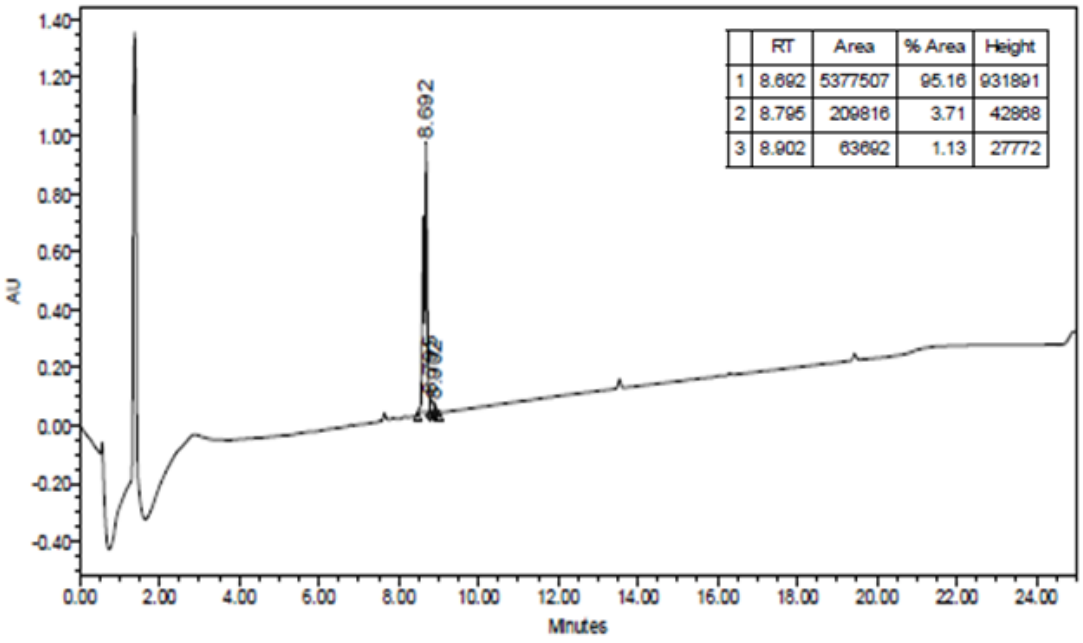

Figure A39. RP-HPLC analysis of pure FITC labeled peptide **11**, using a linear gradient 2-82% MeCN/H_2O (0.1% FA) over 18 min using a Waters 2695 Symmetry® C18 column (3.9 x 150 mm, 5µm particle size) set at a temperature of 25 °C at a flow rate of 1 mL/min with detection at 220 nm.

Peptide **11**: FITC-NH_2-$(CH_2)_5$-TSMGFGVTPLK-$CONH_2$

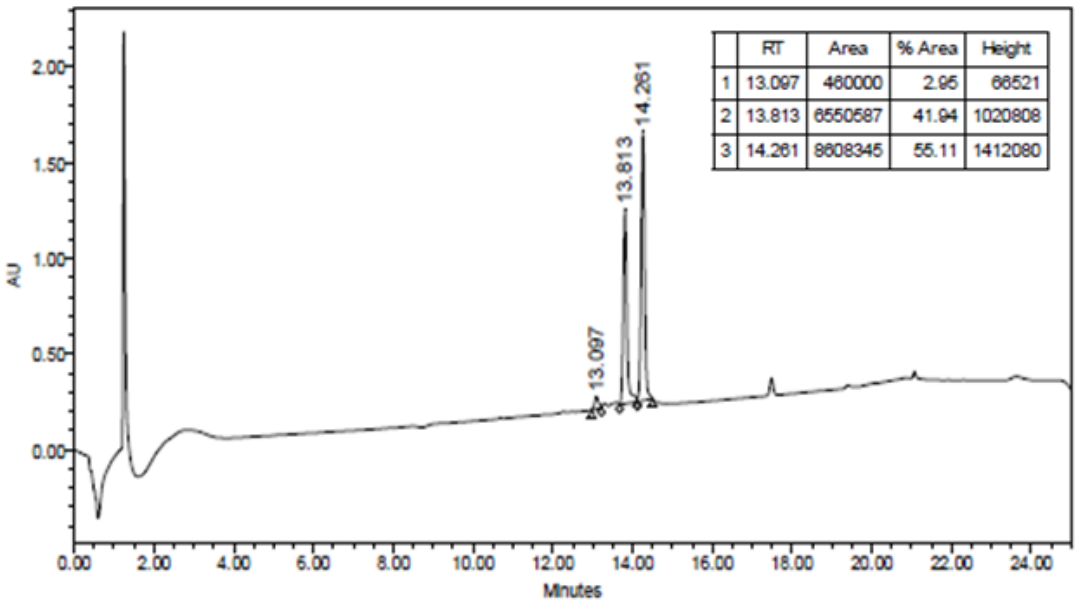

Figure A40. RP-HPLC analysis of FITC labeled pure peptide **11**, using a linear gradient 2-82% MeOH/H_2O (0.1% FA) over 18 min using a Waters 2695 Symmetry® C18 column (3.9 x 150 mm, 5µm particle size) set at a temperature of 25 °C at a flow rate of 1 mL/min with detection at 220 nm.

Peptide **11**: FITC-NH_2-$(CH_2)_5$-TSMGFGVTPLK-$CONH_2$

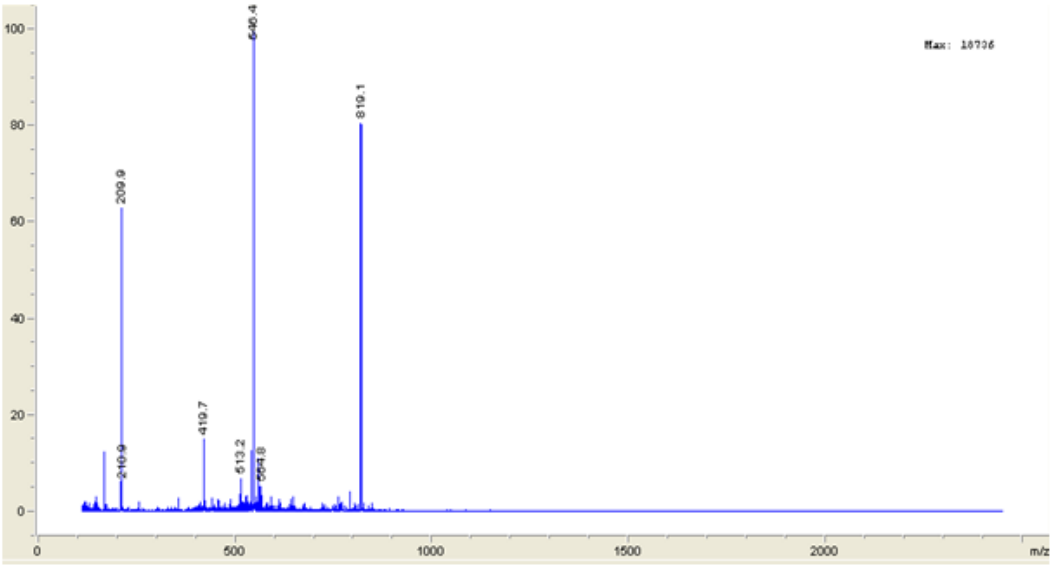

Figure A41. ESI-LCMS analysis of pure FITC labeled peptide **11**, using ESI MS in positive mode and LC linear gradient 2-82% MeOH/H_2O (0.1% FA) over 18 min using a Waters 2695 Symmetry® C18 column (3.9 x 150 mm, 5µm particle size) set at a temperature of 25 °C at a flow rate of 1 mL/min with detection at 220 nm.

Peptide **12**: FITC-NH-$(CH_2)_5$-TVPLN-$CONH_2$

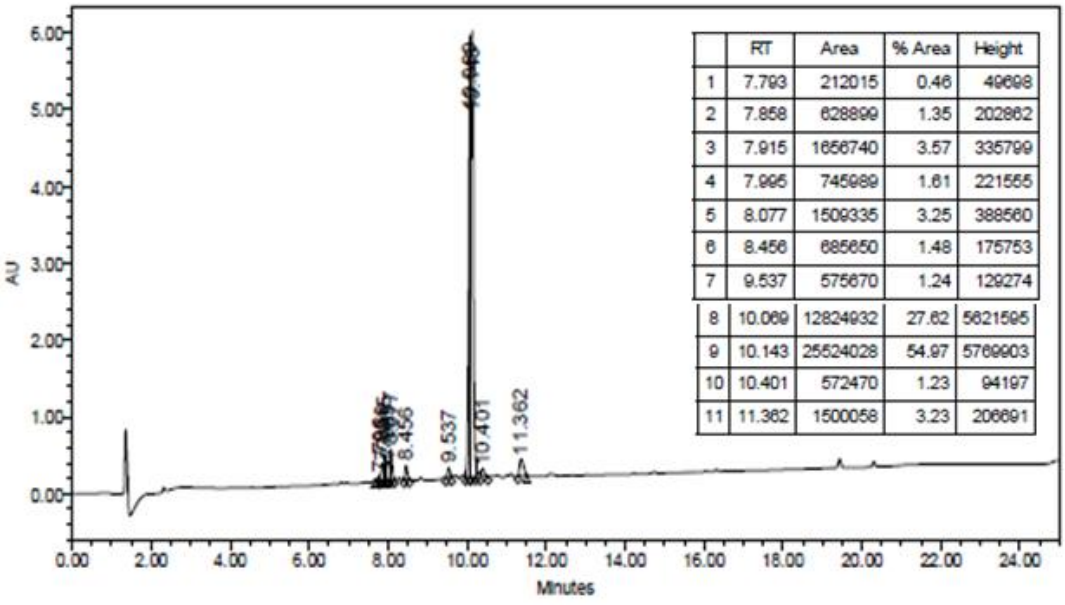

	RT	Area	% Area	Height
1	7.793	212015	0.46	49698
2	7.858	628899	1.35	202862
3	7.915	1656740	3.57	335799
4	7.996	745989	1.61	221555
5	8.077	1509335	3.25	388560
6	8.456	685650	1.48	175753
7	9.537	575670	1.24	129274
8	10.069	12824932	27.62	5621595
9	10.143	25524028	54.97	5769903
10	10.401	572470	1.23	94197
11	11.362	1500058	3.23	206691

Figure A42. RP-HPLC analysis of crude FITC labeled peptide **12**, using a linear gradient 2-82% MeCN/H_2O (0.1% FA) over 18 min using a Waters 2695 Symmetry® C18 column (3.9 x 150 mm, 5µm particle size) set at a temperature of 25 °C at a flow rate of 1 mL/min with detection at 220 nm.

Peptide **12**: FITC-NH-$(CH_2)_5$-TVPLN-$CONH_2$

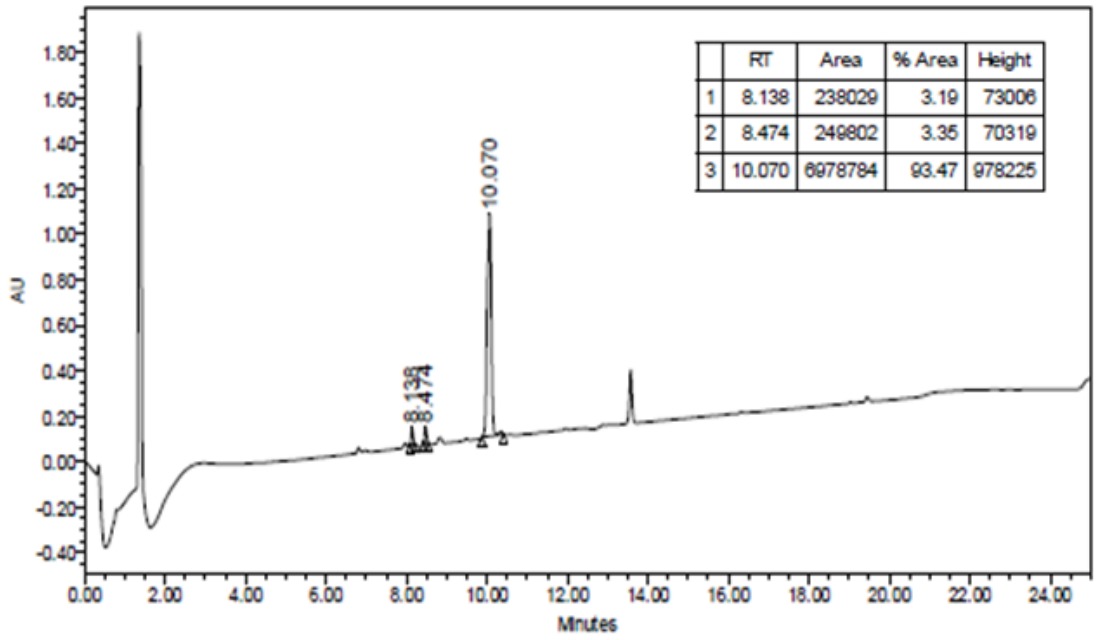

Figure A43. RP-HPLC analysis of pure FITC labeled peptide **12**, using a linear gradient 2-82% MeCN/H_2O (0.1% FA) over 18 min using a Waters 2695 Symmetry® C18 column (3.9 x 150 mm, 5µm particle size) set at a temperature of 25 °C at a flow rate of 1 mL/min with detection at 220 nm.

Peptide **12**: FITC-NH_2-$(CH_2)_5$-TVPLN-$CONH_2$

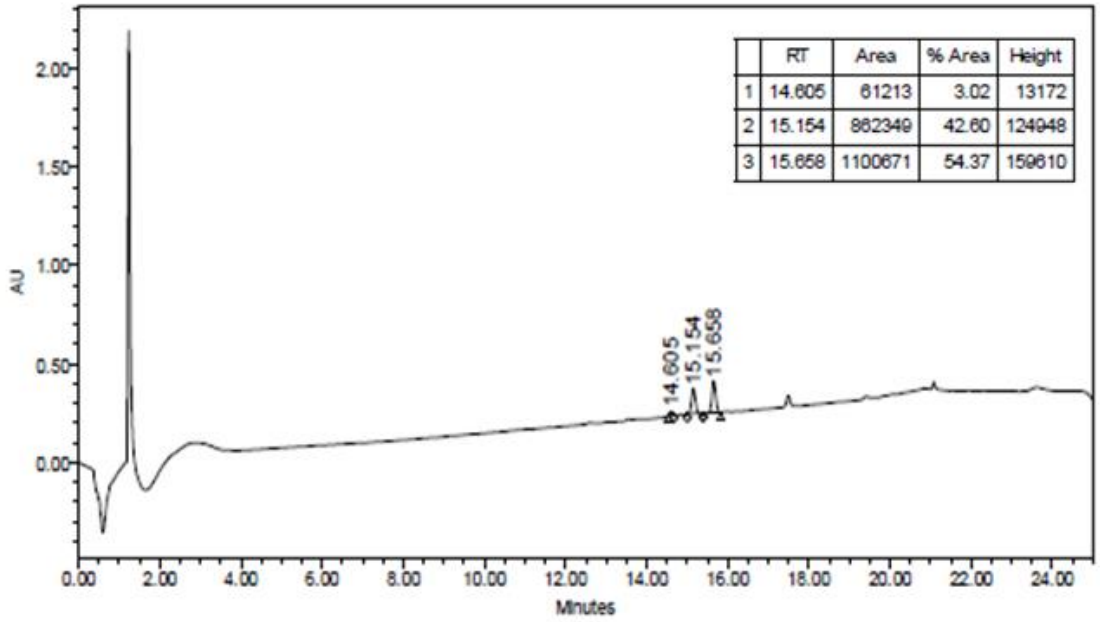

Figure A44. RP-HPLC analysis of pure FITC labeled peptide **12**, using a linear gradient 2-82% MeOH/H_2O (0.1% FA) over 18 min using a Waters 2695 Symmetry® C18 column (3.9 x 150 mm, 5µm particle size) set at a temperature of 25 °C at a flow rate of 1 mL/min with detection at 220 nm.

Peptide **12**: FITC-NH_2-$(CH_2)_5$-TVPLN-$CONH_2$

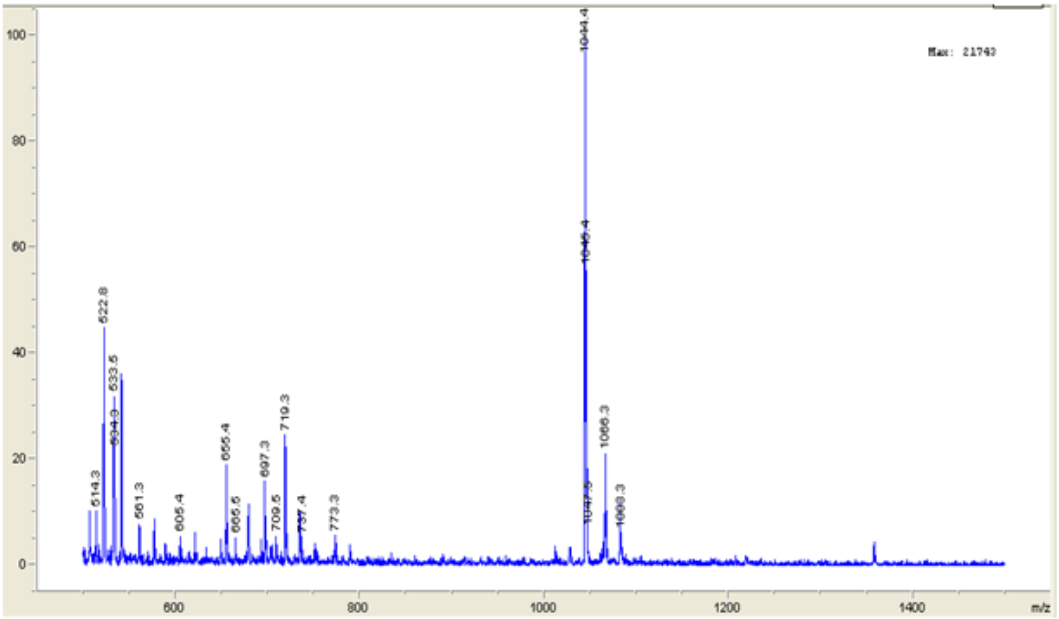

Figure A45. ESI-LCMS analysis of pure FITC labeled peptide **12**, using ESI MS in positive mode and LC linear gradient 2-82% MeOH/H_2O (0.1% FA) over 18 min using a Waters 2695 Symmetry® C18 column (3.9 x 150 mm, 5µm particle size) set at a temperature of 25 °C at a flow rate of 1 mL/min with detection at 220 nm.

Peptide **13**: NH_2-$(CH_2)_5$-NLPVT-$CONH_2$

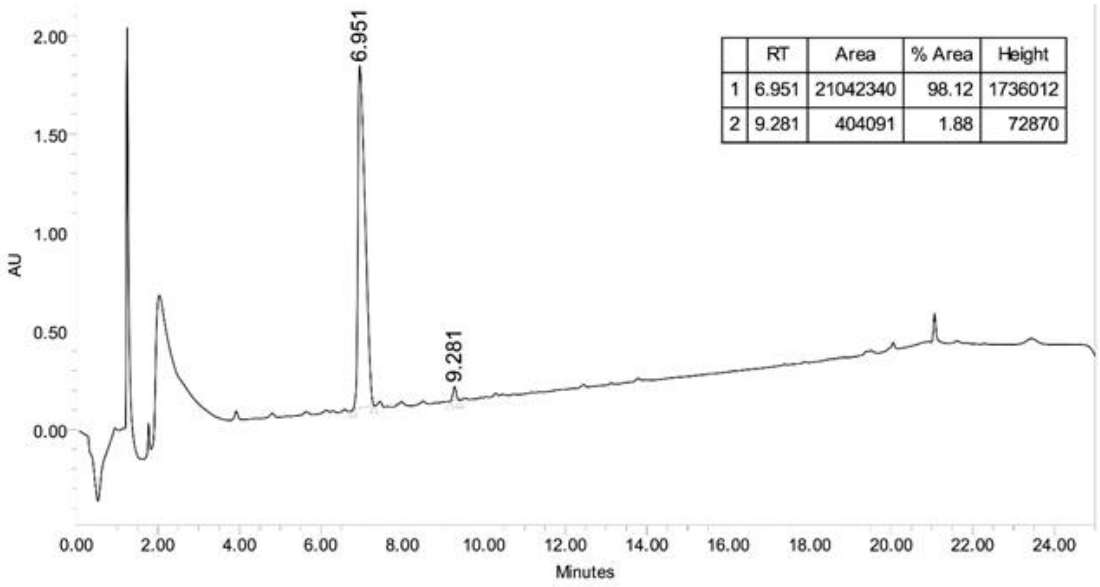

	RT	Area	% Area	Height
1	6.951	21042340	98.12	1736012
2	9.281	404091	1.88	72870

Figure A46. RP-HPLC analysis of pure peptide **13**, using a linear gradient 2-82% MeOH/H_2O (0.1% TFA) over 18 min using a Waters 2695 Symmetry® C18 column (3.9 x 150 mm, 5µm particle size) set at a temperature of 25 °C at a flow rate of 1 mL/min with detection at 220 nm.

Peptide **13**: NH_2-$(CH_2)_5$-NLPVT-$CONH_2$

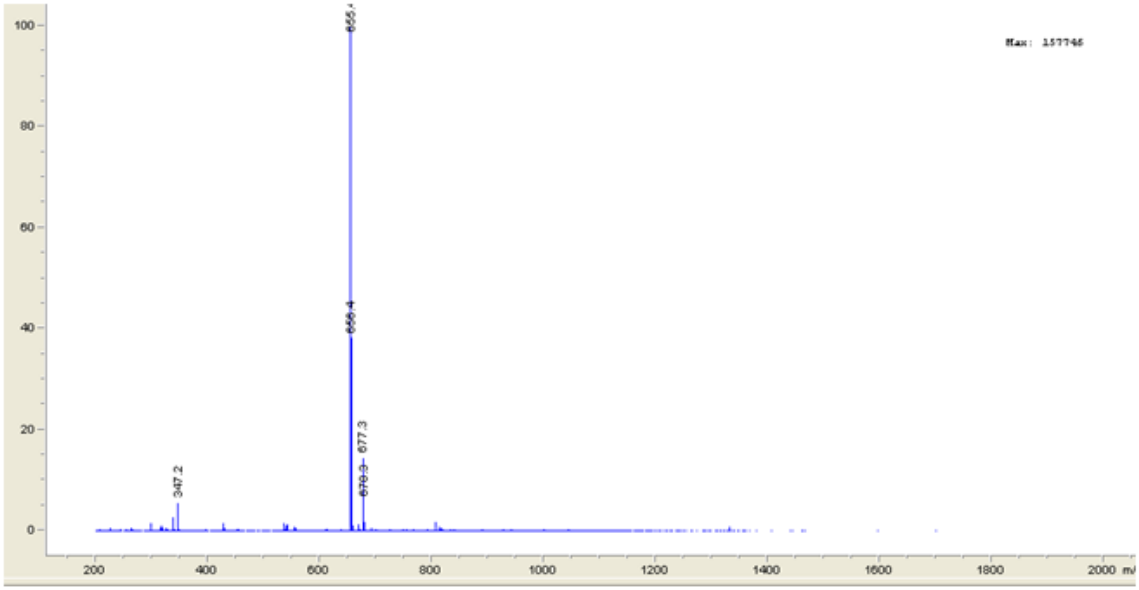

Figure A47. ESI-LCMS analysis of pure peptide **13**, using MS in positive mode and LC linear gradient 2-82% MeOH/H_2O (0.1% FA) over 18 min using a Waters 2695 Symmetry® C18 column (3.9 x 150 mm, 5µm particle size) set at a temperature of 25 °C at a flow rate of 1 mL/min with detection at 220 nm.

Peptide **14**: NH_2-$(CH_2)_5$-VLNTP-$CONH_2$

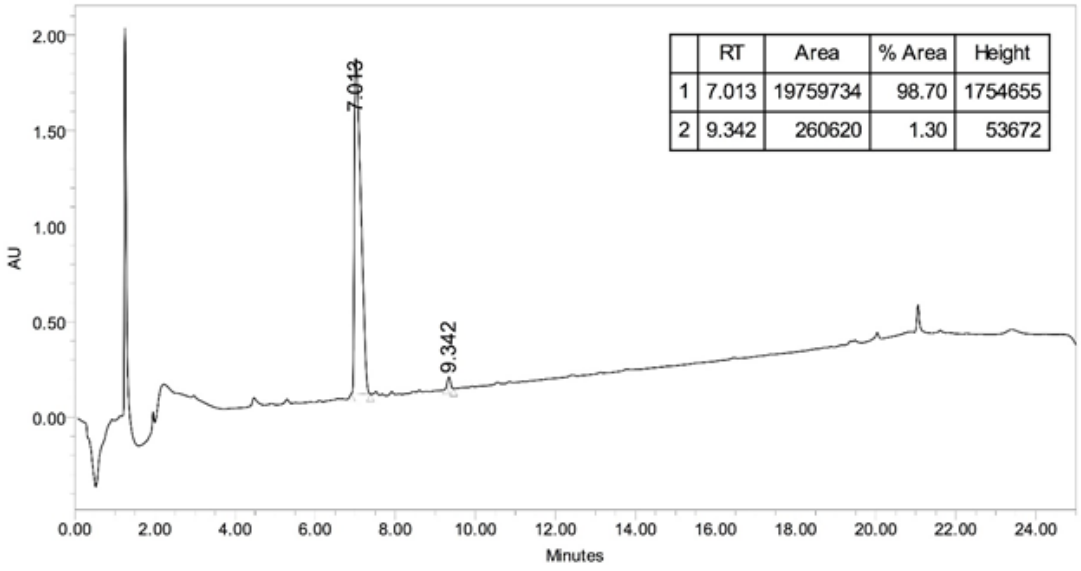

	RT	Area	% Area	Height
1	7.013	19759734	98.70	1754655
2	9.342	260620	1.30	53672

Figure A48. RP-HPLC analysis of pure peptide **14**, using a linear gradient 2-82% MeOH/H_2O (0.1% TFA) over 18 min using a Waters 2695 Symmetry® C18 column (3.9 x 150 mm, 5µm particle size) set at a temperature of 25 °C at a flow rate of 1 mL/min with detection at 220 nm.

Peptide **14**: NH_2-$(CH_2)_5$-VLNTP-$CONH_2$

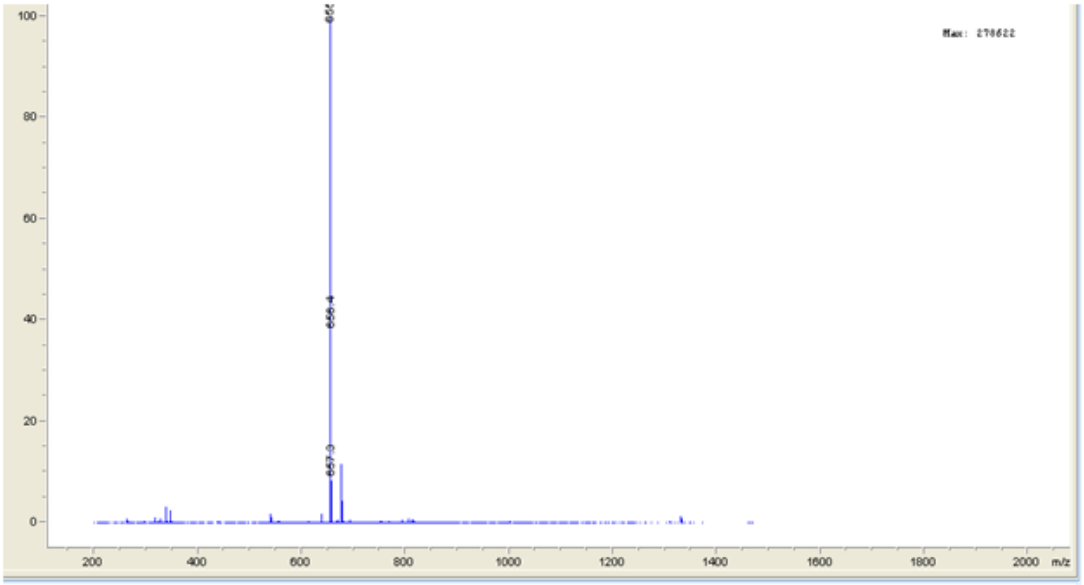

Figure A49. ESI-LCMS analysis of purified peptide **14**, using ESI MS in positive mode and LC linear gradient 2-82% MeOH/H_2O (0.1% FA) over 18 min using a Waters 2695 Symmetry® C18 column (3.9 x 150 mm, 5µm particle size) set at a temperature of 25 °C at a flow rate of 1 mL/min with detection at 220 nm.

Peptide **15**: NH_2-$(CH_2)_5$-GAMGT-$CONH_2$

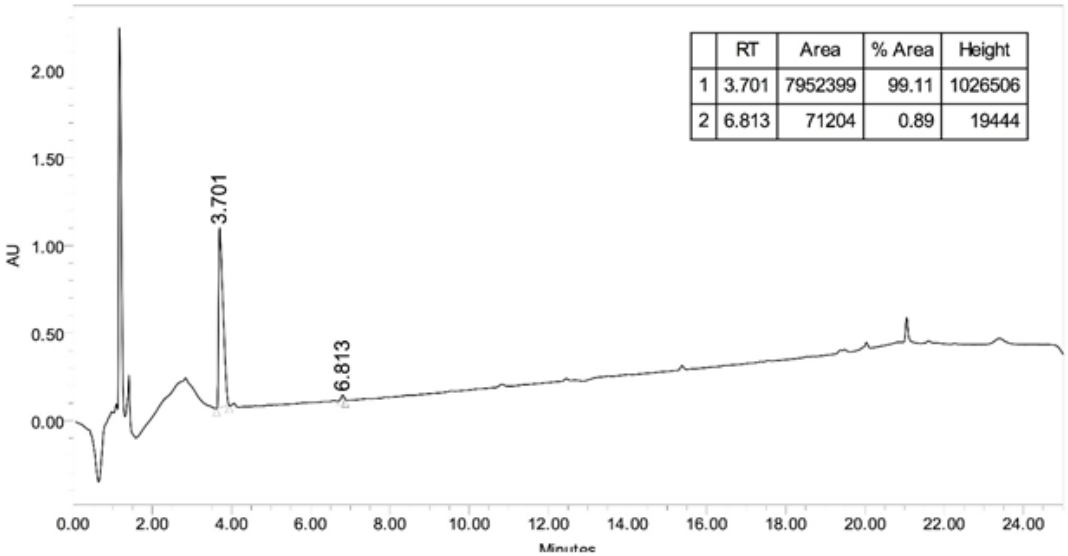

Figure A50. RP-HPLC analysis of pure peptide **15**, using a linear gradient 2-82% MeOH/H_2O (0.1% TFA) over 18 min using a Waters 2695 Symmetry® C18 column (3.9 x 150 mm, 5µm particle size) set at a temperature of 25 °C at a flow rate of 1 mL/min with detection at 220 nm.

Peptide **15**: NH_2-$(CH_2)_5$-GAMGT-$CONH_2$

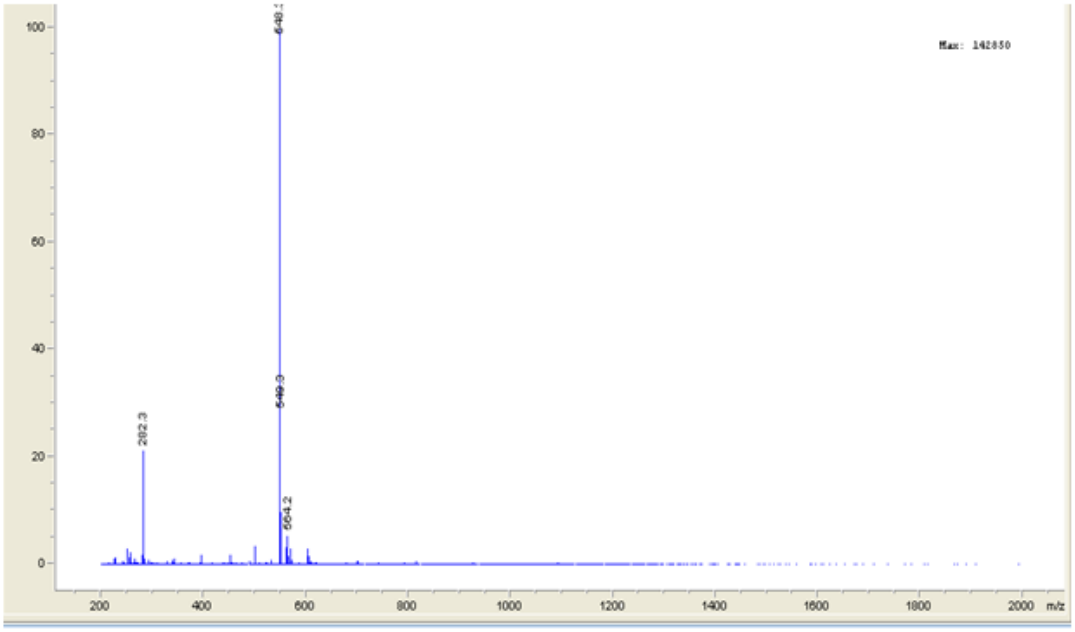

Figure A51. ESI-LCMS analysis of purified peptide **15**, using ESI MS in positive mode and LC linear gradient 2-82% MeOH/H_2O (0.1% FA) over 18 min using a Waters 2695 Symmetry® C18 column (3.9 x 150 mm, 5µm particle size) set at a temperature of 25 °C at a flow rate of 1 mL/min with detection at 220 nm.

Peptide **16**: NH_2-$(CH_2)_5$-FAPGI-$CONH_2$

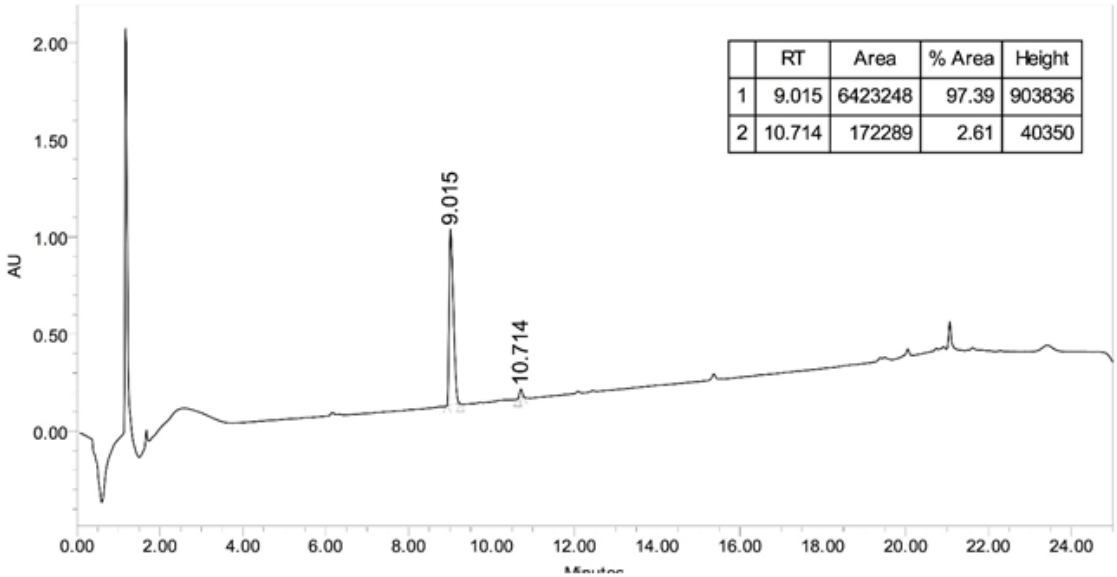

	RT	Area	% Area	Height
1	9.015	6423248	97.39	903836
2	10.714	172289	2.61	40350

Figure A52. RP-HPLC analysis of pure peptide **16**, using a linear gradient 2-82% MeOH/H_2O (0.1% TFA) over 18 min using a Waters 2695 Symmetry® C18 column (3.9 x 150 mm, 5µm particle size) set at a temperature of 25 °C at a flow rate of 1 mL/min with detection at 220 nm.

Peptide **16**: NH_2-$(CH_2)_5$-FAPGI-$CONH_2$

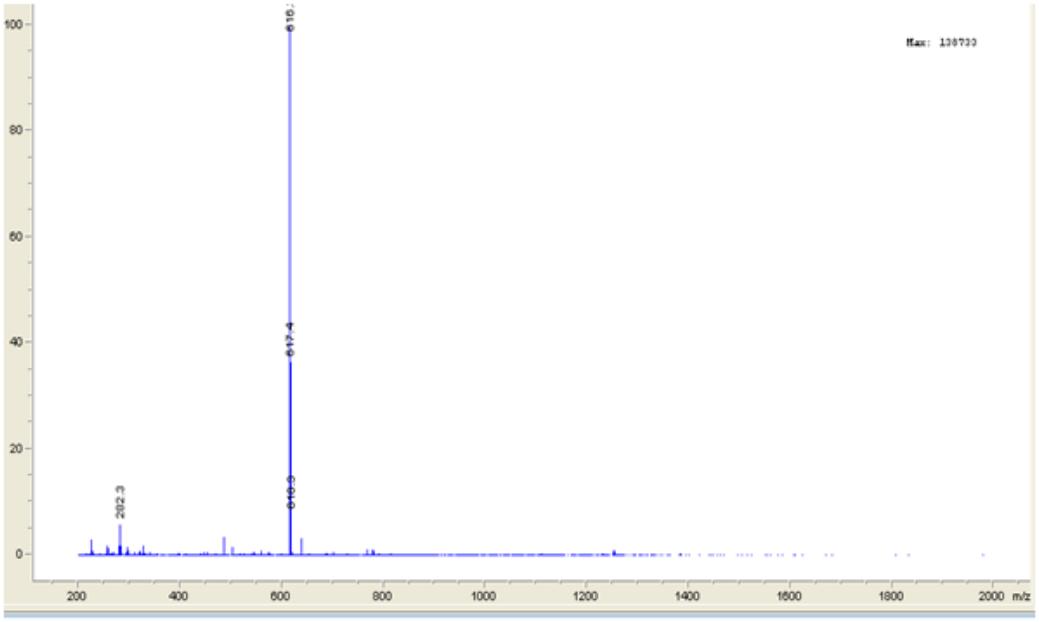

Figure A53. ESI-LCMS analysis of pure peptide **16**, using ESI MS in positive mode and LC linear gradient 2-82% MeOH/H_2O (0.1% FA) over 18 min using a Waters 2695 Symmetry® C18 column (3.9 x 150 mm, 5µm particle size) set at a temperature of 25 °C at a flow rate of 1 mL/min with detection at 220 nm.

A)

Peptide		Sequence
13	Reversed	NH_2-$(CH_2)_5$-NLPVT-$CONH_2$
14	Scrambled	NH_2-$(CH_2)_5$-VLNTP-$CONH_2$
15	Negative	NH_2-$(CH_2)_5$-GAMGT-$CONH_2$
16	Negative	NH_2-$(CH_2)_5$-FAPGI-$CONH_2$

B)

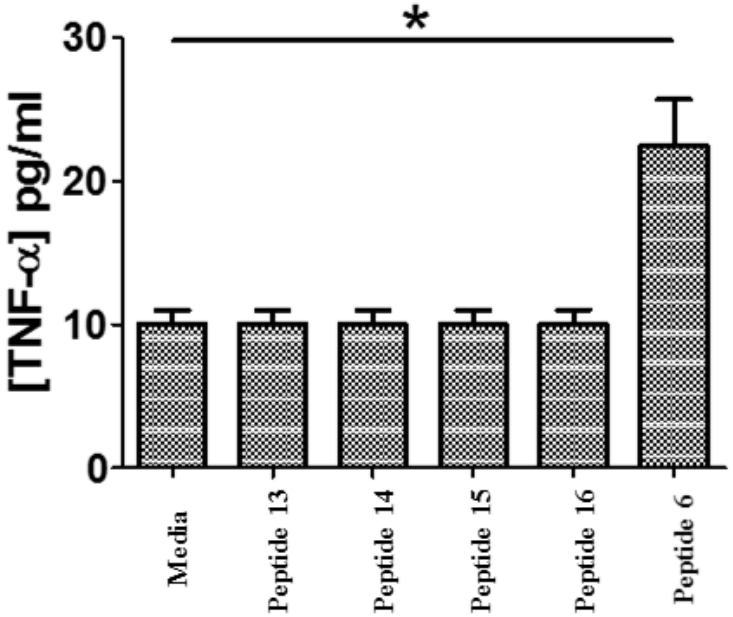

Figure A54. Immunostimulatory activities of negative control peptides **13**-**16**, and peptide **6** on the NK92-MI cells. (A) Table describing the negative control sequences, where sequence **13** and **14** are modifications of peptide **6**, and **15** and **16** are random sequences. (B) TNF-α detection following treatment with peptides, **6**, **13**-**16** (10 μM), on the NK92-MI cells (*****p< 0.1). This data is the average of three independent experiments.

Peptide **19**: Ac-$(CH_2)_5$-CTVALPGGYVRVC-PEG_3-K-$CONH_2$

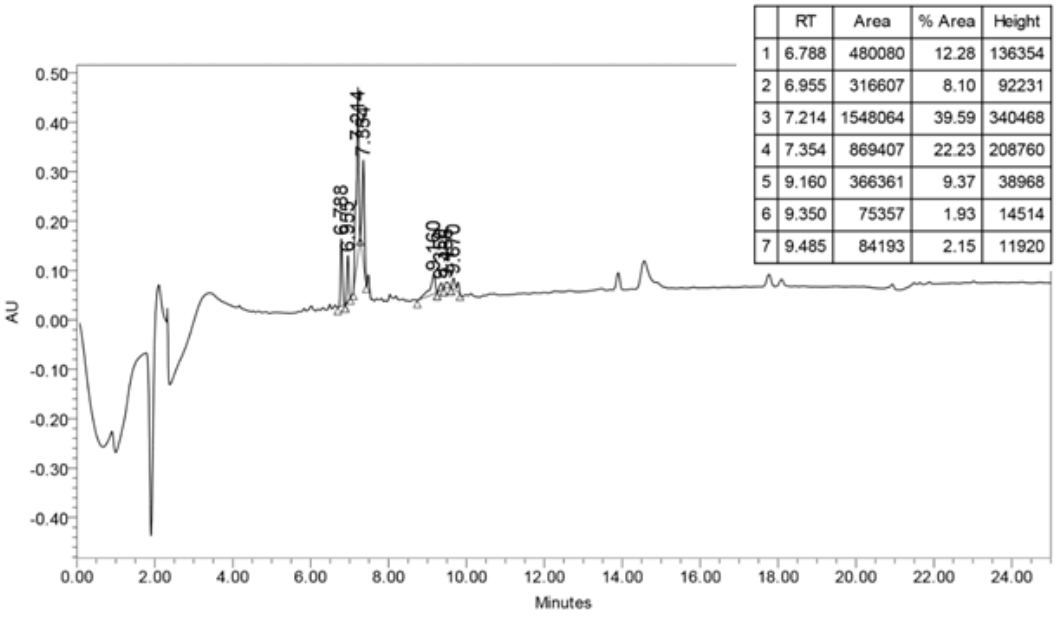

	RT	Area	% Area	Height
1	6.788	480080	12.28	136354
2	6.955	316607	8.10	92231
3	7.214	1548064	39.59	340468
4	7.354	869407	22.23	208760
5	9.160	366361	9.37	38968
6	9.350	75357	1.93	14514
7	9.485	84193	2.15	11920

FIGURE A55. RP-HPLC analysis of crude peptide **19**, using a linear gradient 2-80% MeCN/H_2O (0.1% FA) over 18 min using a Waters 2695 Symmetry® C18 column (3.9 x 150 mm, 5µm particle size) set at a temperature of 25 °C at a flow rate of 1 mL/min with detection at 220 nm.

Peptide **19**: Ac- $(CH_2)_5$-CTVALPGGYVRVC-PEG_3-K-$CONH_2$

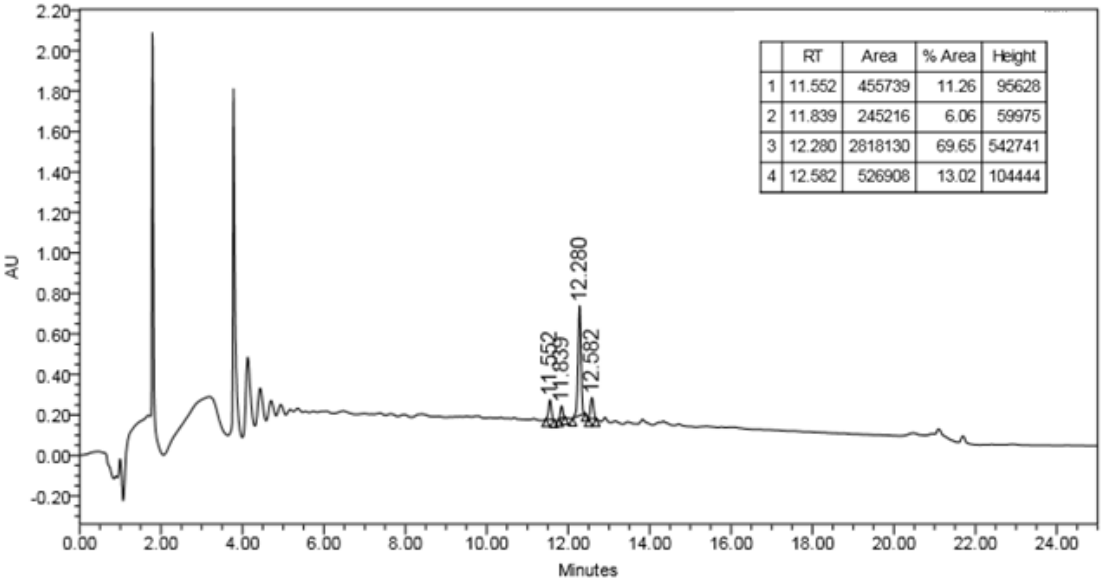

FIGURE A56. RP-HPLC analysis of crude peptide **19**, using a linear gradient 2-80% MeOH/H_2O (0.1% FA) over 18 min using a Waters 2695 Symmetry® C18 column (3.9 x 150 mm, 5µm particle size) set at a temperature of 25 °C at a flow rate of 1 mL/min with detection at 220 nm.

Peptide **19**: Ac-$(CH_2)_5$-CTVALPGGYVRVC-PEG_3-K-$CONH_2$

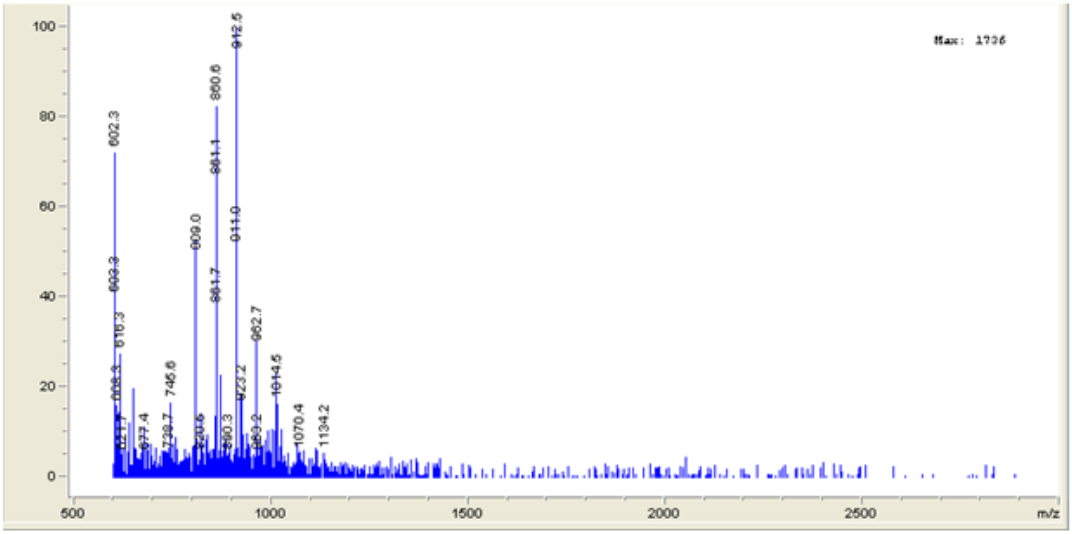

FIGURE A57. ESI-LCMS analysis of crude peptide **19**, using ESI MS in positive mode and LC linear gradient 2-80% MeOH/H_2O (0.1% FA) over 18 min using a Waters 2695 Symmetry® C18 column (3.9 x 150 mm, 5µm particle size) set at a temperature of 25 °C at a flow rate of 1 mL/min with detection at 220 nm.

Peptide **20**: Ac-$(CH_2)_5$-CTVALPGGYVRVC-PEG_6-K-$CONH_2$

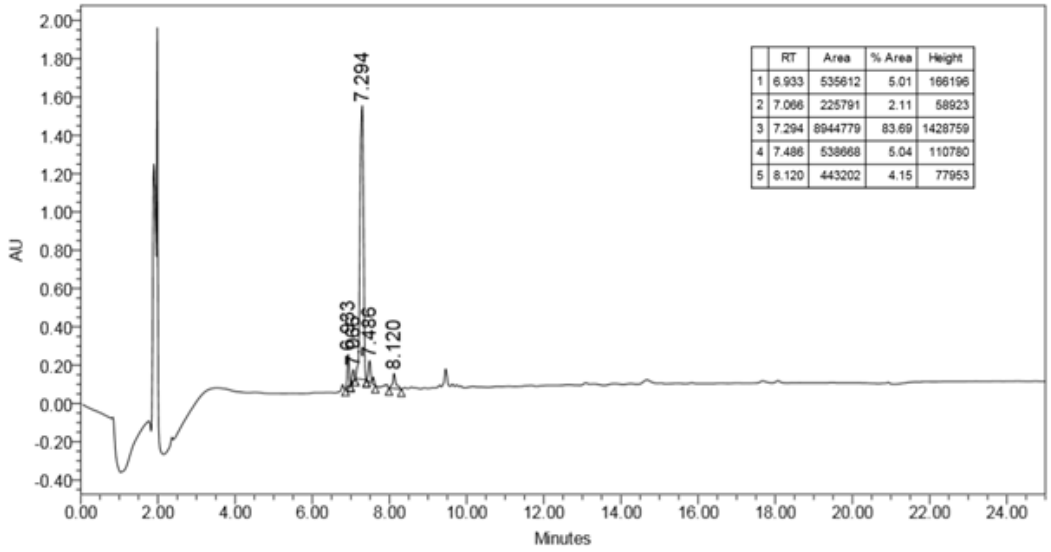

FIGURE A58. RP-HPLC analysis of crude peptide **20** using a linear gradient 2-80% MeCN/H_2O (0.1% FA) over 18 min using a Waters 2695 Symmetry® C18 column (3.9 x 150 mm, 5µm particle size) set at a temperature of 25 °C at a flow rate of 1 mL/min with detection at 220 nm.

Peptide **20**: Ac-$(CH_2)_5$-CTVALPGGYVRVC-PEG_6-K-$CONH_2$

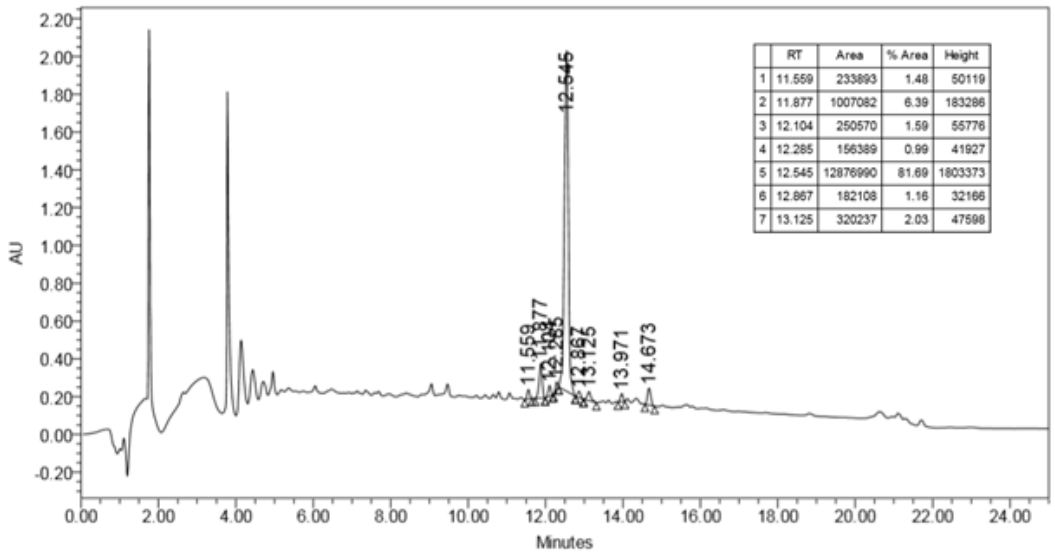

	RT	Area	% Area	Height
1	11.559	233893	1.48	50119
2	11.877	1007082	6.39	183286
3	12.104	250570	1.59	55776
4	12.285	156389	0.99	41927
5	12.545	12876990	81.69	1803373
6	12.867	182108	1.16	32166
7	13.125	320237	2.03	47598

FIGURE A59. RP-HPLC analysis of crude peptide **20**, using a linear gradient 2-80% MeOH/H_2O (0.1% FA) over 18 min using a Waters 2695 Symmetry® C18 column (3.9 x 150 mm, 5µm particle size) set at a temperature of 25 °C at a flow rate of 1 mL/min with detection at 220 nm.

Peptide **20**: Ac-$(CH_2)_5$-CTVALPGGYVRVC-PEG_6-K-$CONH_2$

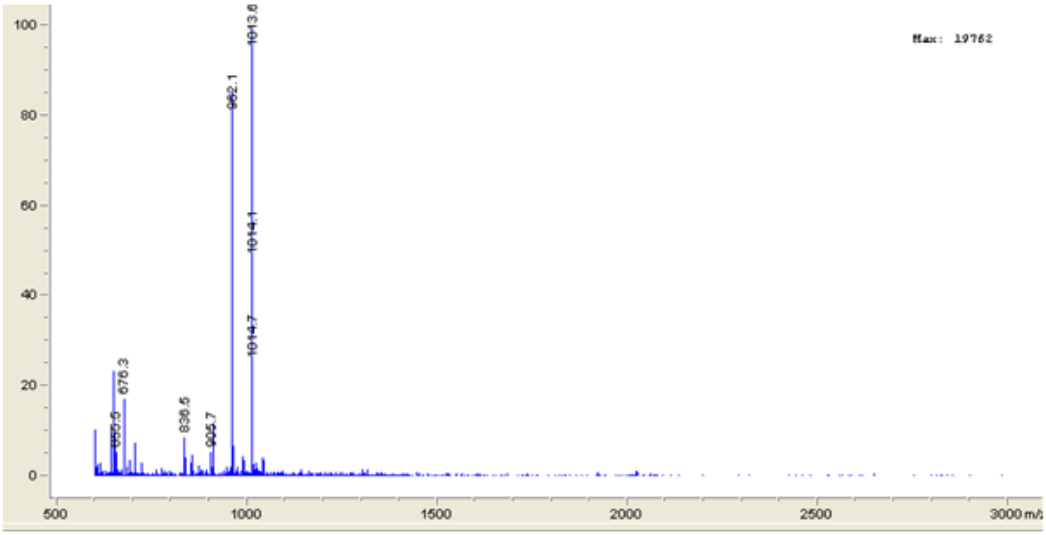

FIGURE A60. ESI-LCMS analysis of crude peptide **20**, using ESI MS in positive mode and LC linear gradient 2-80% MeOH/H_2O (0.1% FA) over 18 min using a Waters 2695 Symmetry® C18 column (3.9 x 150 mm, 5µm particle size) set at a temperature of 25 °C at a flow rate of 1 mL/min with detection at 220 nm.

Peptide **21**: Ac-$(CH_2)_5$-CTVALPGGYVRVC-PEG_{12}-K-$CONH_2$

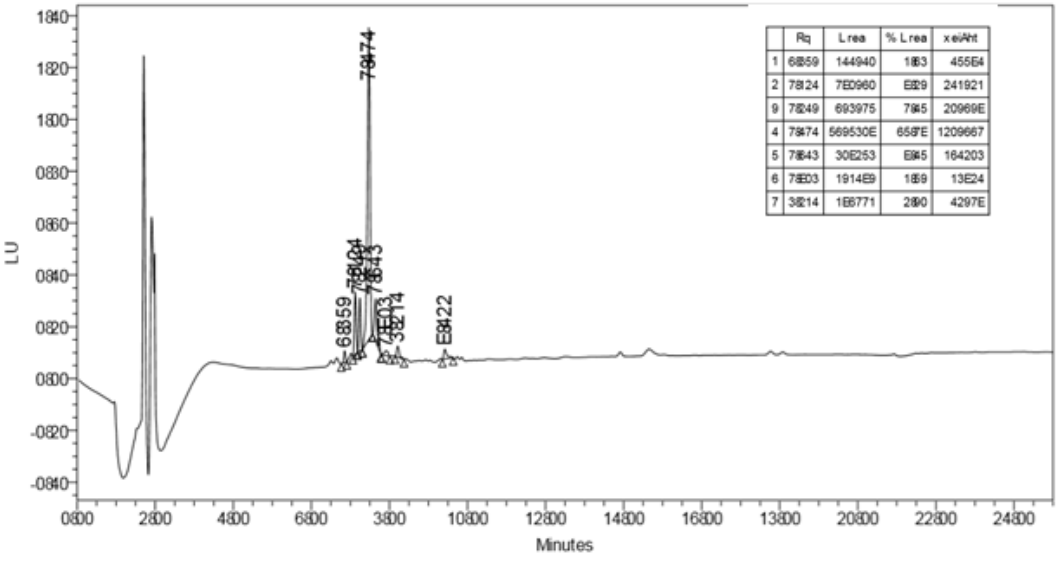

FIGURE A61. RP-HPLC analysis of crude peptide **21** using a linear gradient 2-80% MeCN/H_2O (0.1% FA) over 18 min using a Waters 2695 Symmetry® C18 column (3.9 x 150 mm, 5µm particle size) set at a temperature of 25 °C at a flow rate of 1 mL/min with detection at 220 nm.

Peptide **21**: Ac-$(CH_2)_5$-CTVALPGGYVRVC-PEG_{12}-K-$CONH_2$

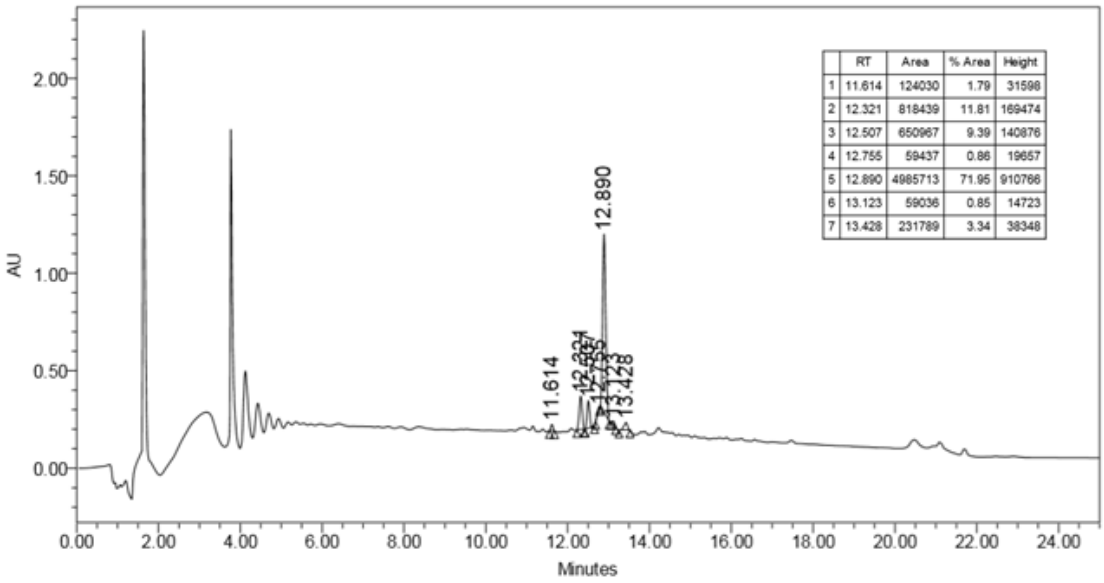

FIGURE A62. RP-HPLC analysis of crude peptide **21**, using a linear gradient 2-80% MeOH/H_2O (0.1% FA) over 18 min using a Waters 2695 Symmetry® C18 column (3.9 x 150 mm, 5µm particle size) set at a temperature of 25 °C at a flow rate of 1 mL/min with detection at 220 nm.

Peptide **21**: Ac-$(CH_2)_5$-CTVALPGGYVRVC-PEG_{12}-K-$CONH_2$

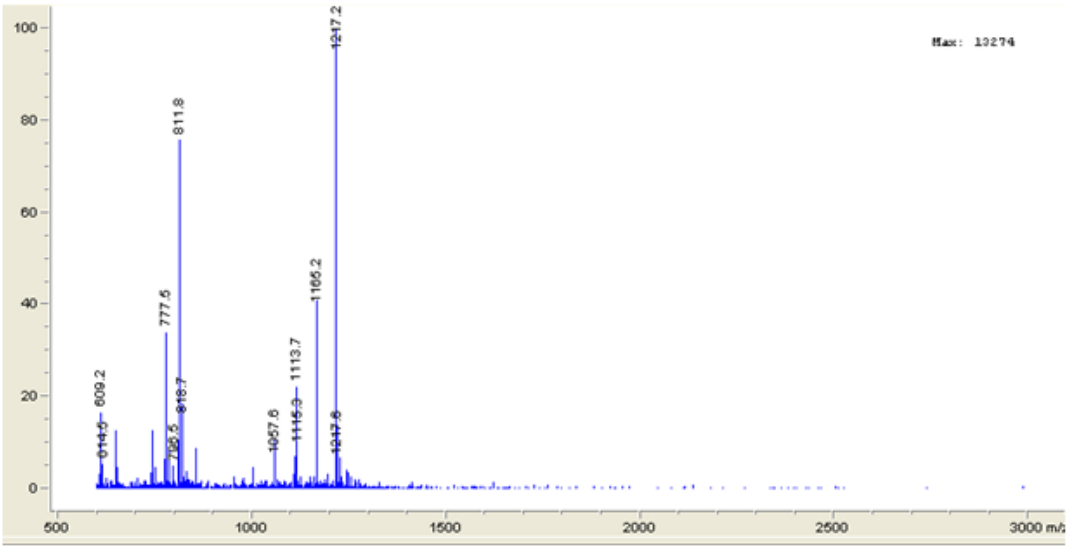

FIGURE A63. ESI-LCMS analysis of crude peptide **21**, using ESI MS in positive mode and LC linear gradient 2-80% MeOH/H_2O (0.1% FA) over 18 min using a Waters 2695 Symmetry® C18 column (3.9 x 150 mm, 5µm particle size) set at a temperature of 25 °C at a flow rate of 1 mL/min with detection at 220 nm.

Peptide **22**: FITC-$(CH_2)_5$-CTVALPGGYVRVC-PEG_3-K-$CONH_2$

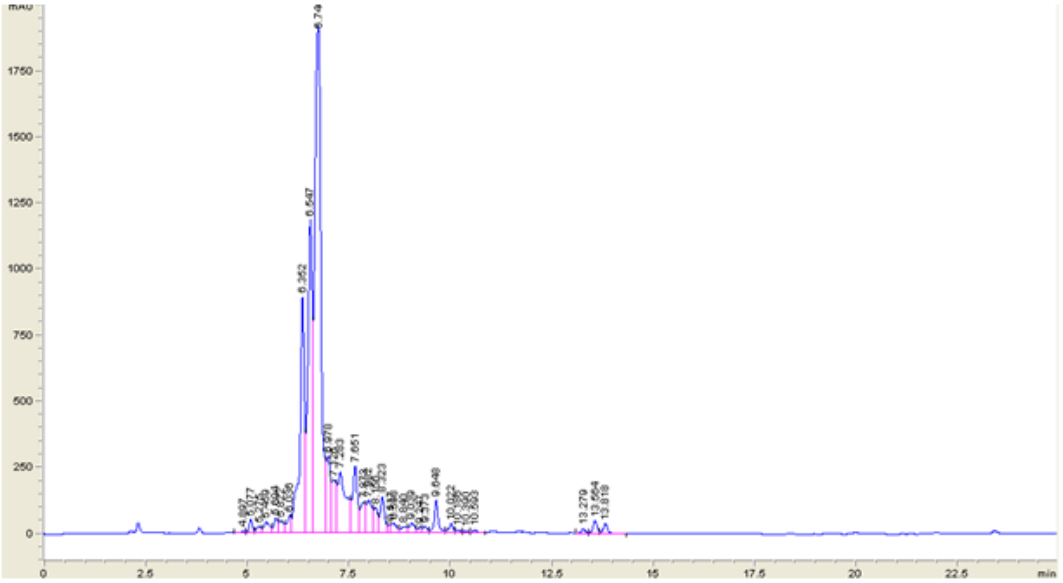

FIGURE A64. RP-HPLC analysis of crude peptide **22** using a linear gradient 20-80% MeCN/H_2O (0.1% FA) over 18 min using a Waters 2695 Symmetry® C18 column (3.9 x 150 mm, 5µm particle size) set at a temperature of 25 °C at a flow rate of 1 mL/min with detection at 220 nm.

Peptide **22**: FITC-$(CH_2)_5$-CTVALPGGYVRVC-PEG_3-K-$CONH_2$

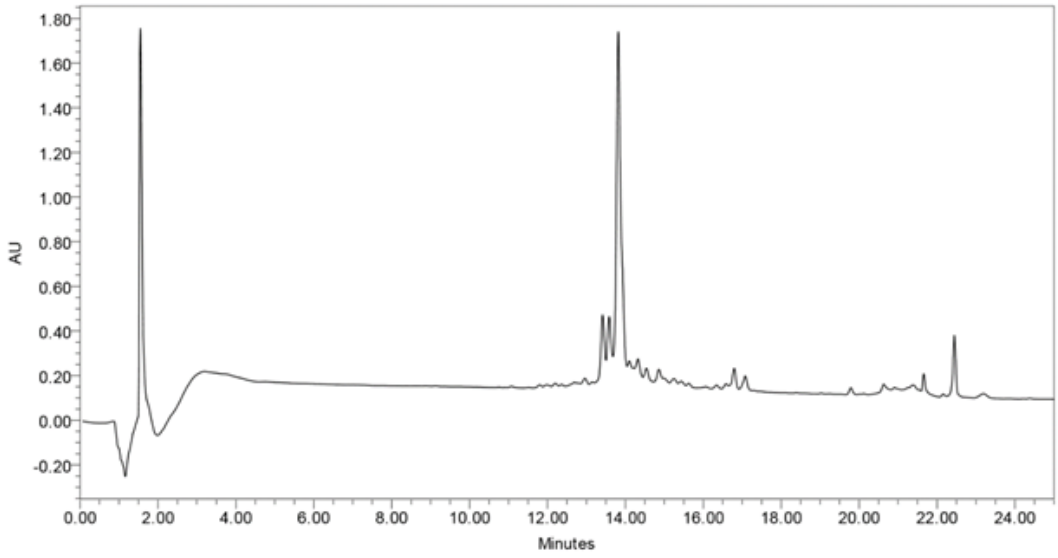

FIGURE A65. RP-HPLC analysis of crude peptide **22**, using a linear gradient 2-80% MeOH/H_2O (0.1% FA) over 18 min using a Waters 2695 Symmetry® C18 column (3.9 x 150 mm, 5µm particle size) set at a temperature of 25 °C at a flow rate of 1 mL/min with detection at 220 nm.

Peptide **22**: FITC-$(CH_2)_5$-CTVALPGGYVRVC-PEG_3-K-$CONH_2$

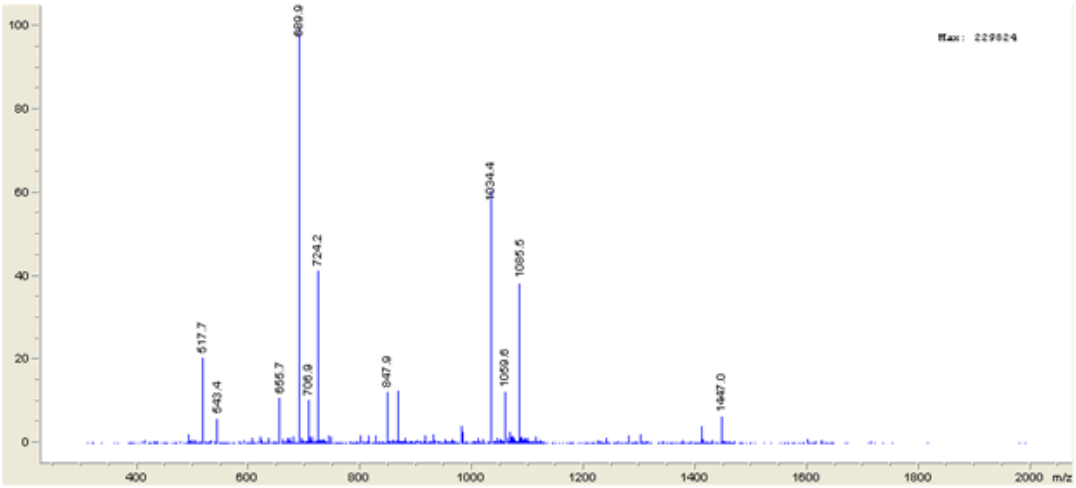

FIGURE A66. ESI-LCMS analysis of crude peptide **22**, using ESI MS in positive mode and LC linear gradient 2-80% MeOH/H_2O (0.1% FA) over 18 min using a Waters 2695 Symmetry® C18 column (3.9 x 150 mm, 5µm particle size) set at a temperature of 25 °C at a flow rate of 1 mL/min with detection at 220 nm.

Peptide **23**: FITC-$(CH_2)_5$-CTVALPGGYVRVC-PEG_6-K-$CONH_2$

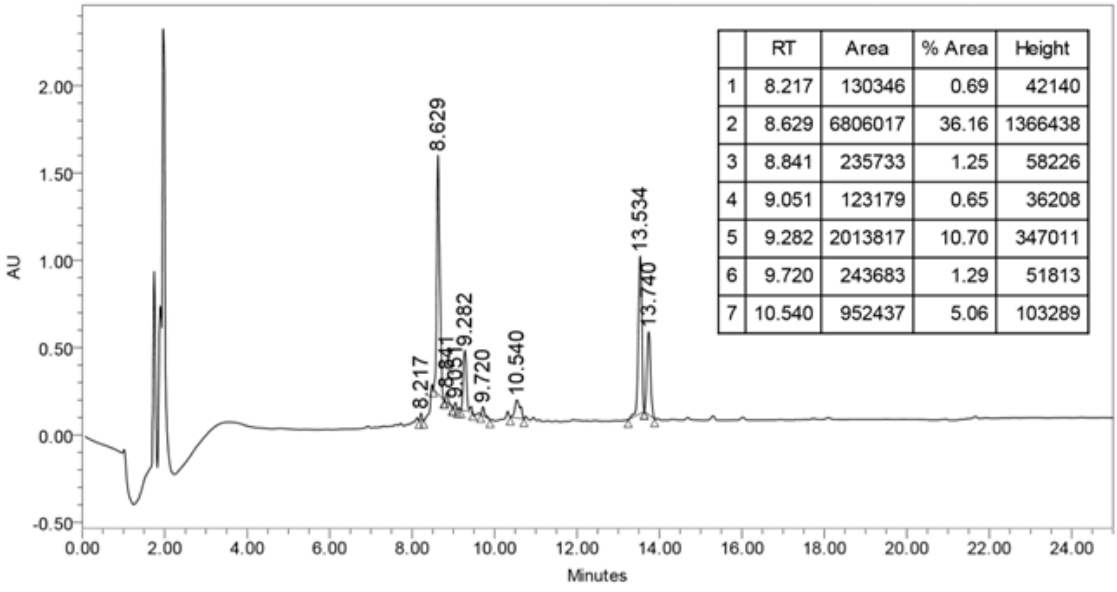

FIGURE A67. RP-HPLC analysis of crude peptide **23** using a linear gradient 2-80% MeCN/H_2O (0.1% FA) over 18 min using a Waters 2695 Symmetry® C18 column (3.9 x 150 mm, 5µm particle size) set at a temperature of 25 °C at a flow rate of 1 mL/min with detection at 220 nm.

Peptide **23**: FITC-$(CH_2)_5$-CTVALPGGYVRVC-PEG_6-K-$CONH_2$

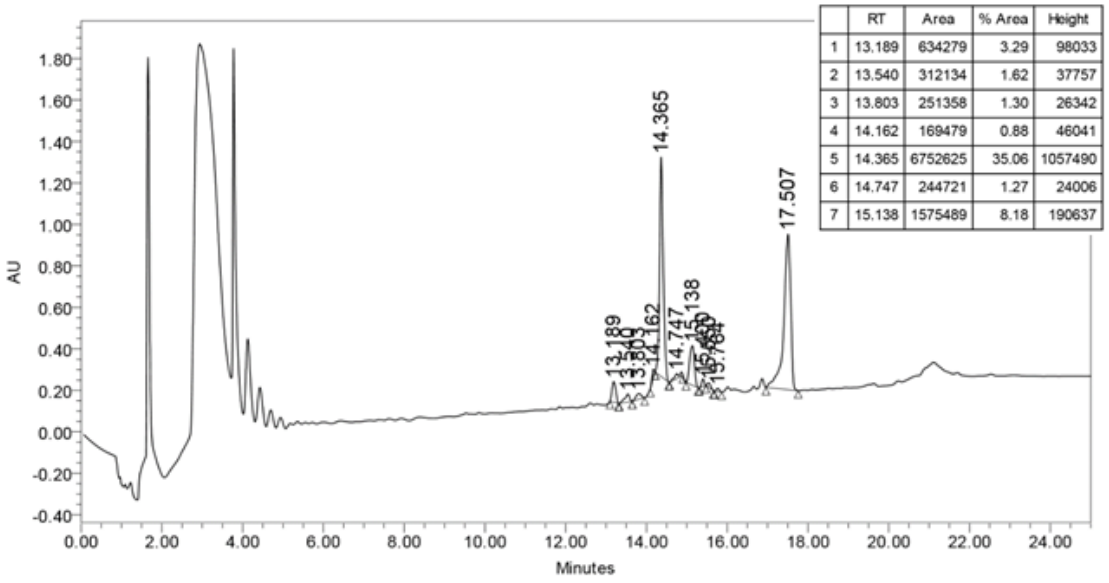

	RT	Area	% Area	Height
1	13.189	634279	3.29	98033
2	13.540	312134	1.62	37757
3	13.803	251358	1.30	26342
4	14.162	169479	0.88	46041
5	14.365	6752625	35.06	1057490
6	14.747	244721	1.27	24006
7	15.138	1575489	8.18	190637

FIGURE A68. RP-HPLC analysis of crude peptide **23**, using a linear gradient 2-80% MeOH/H_2O (0.1% FA) over 18 min using a Waters 2695 Symmetry® C18 column (3.9 x 150 mm, 5µm particle size) set at a temperature of 25 °C at a flow rate of 1 mL/min with detection at 220 nm.

Peptide **23**: FITC-$(CH_2)_5$-CTVALPGGYVRVC-PEG_6-K-$CONH_2$

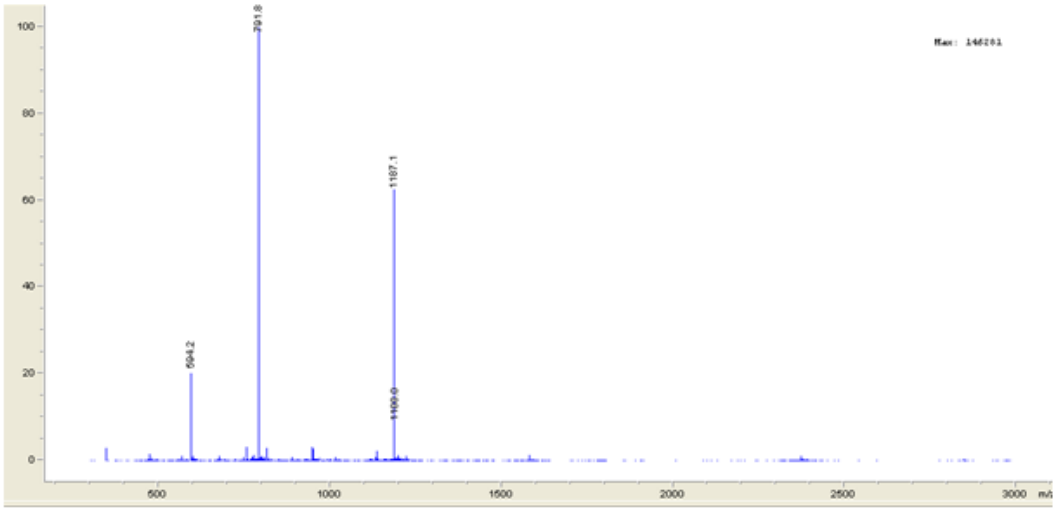

FIGURE A69. ESI-LCMS analysis of crude peptide **23**, using ESI MS in positive mode and LC linear gradient 2-80% MeOH/H_2O (0.1% FA) over 18 min using a Waters 2695 Symmetry® C18 column (3.9 x 150 mm, 5µm particle size) set at a temperature of 25 °C at a flow rate of 1 mL/min with detection at 220 nm.

Peptide **24**: FITC-$(CH_2)_5$-CTVALPGGYVRVC-PEG_{12}-K-$CONH_2$

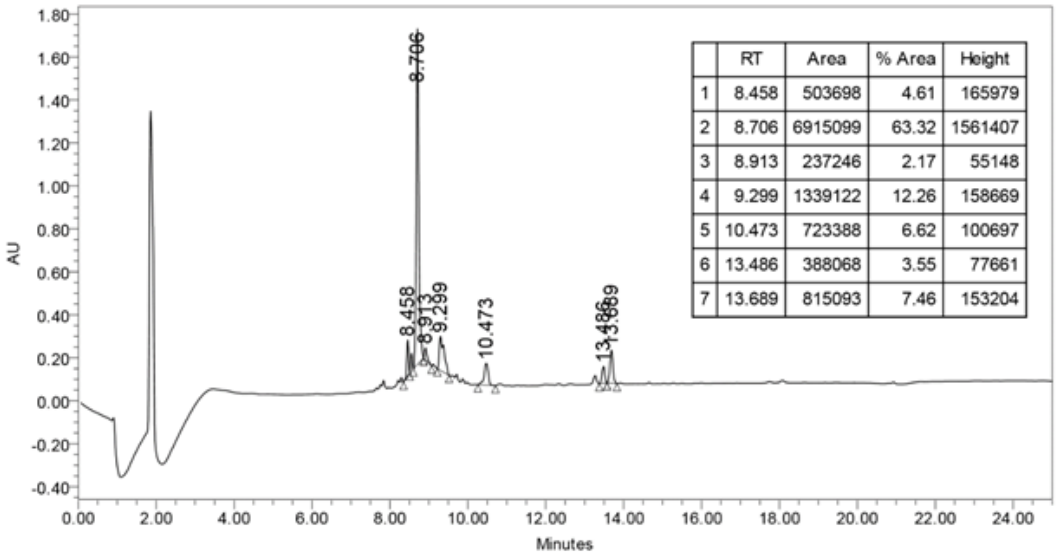

	RT	Area	% Area	Height
1	8.458	503698	4.61	165979
2	8.706	6915099	63.32	1561407
3	8.913	237246	2.17	55148
4	9.299	1339122	12.26	158669
5	10.473	723388	6.62	100697
6	13.486	388068	3.55	77661
7	13.689	815093	7.46	153204

FIGURE A70. RP-HPLC analysis of crude peptide **24** using a linear gradient 2-80% MeCN/H_2O (0.1% FA) over 18 min using a Waters 2695 Symmetry® C18 column (3.9 x 150 mm, 5µm particle size) set at a temperature of 25 °C at a flow rate of 1 mL/min with detection at 220 nm.

Peptide **24**: FITC-$(CH_2)_5$-CTVALPGGYVRVC-PEG_{12}-K-$CONH_2$

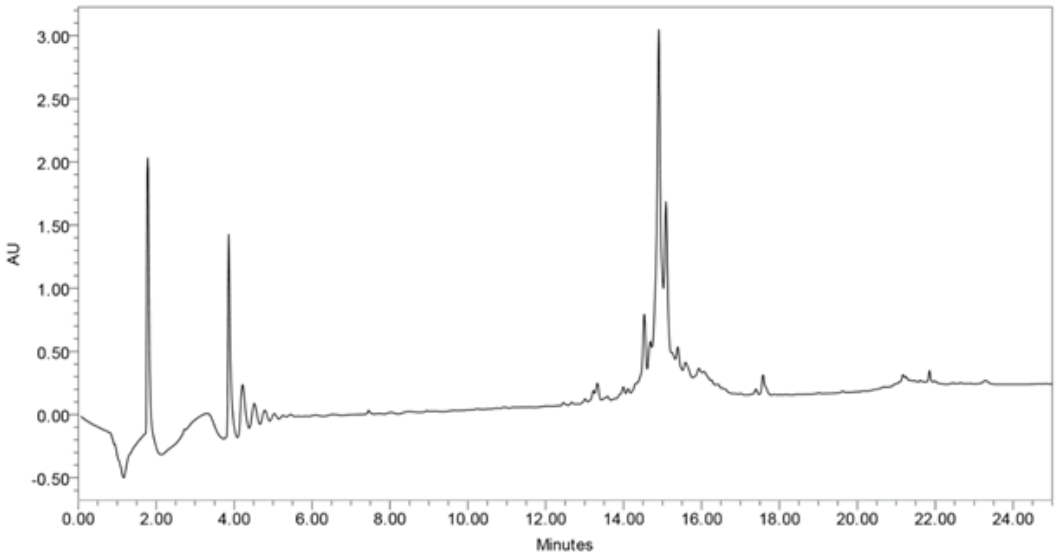

FIGURE A71. RP-HPLC analysis of crude peptide **24**, using a linear gradient 2-80% MeOH/H_2O (0.1% FA) over 18 min using a Waters 2695 Symmetry® C18 column (3.9 x 150 mm, 5µm particle size) set at a temperature of 25 °C at a flow rate of 1 mL/min with detection at 220 nm.

Peptide **24**: FITC-$(CH_2)_5$-CTVALPGGYVRVC-PEG_{12}-K-$CONH_2$

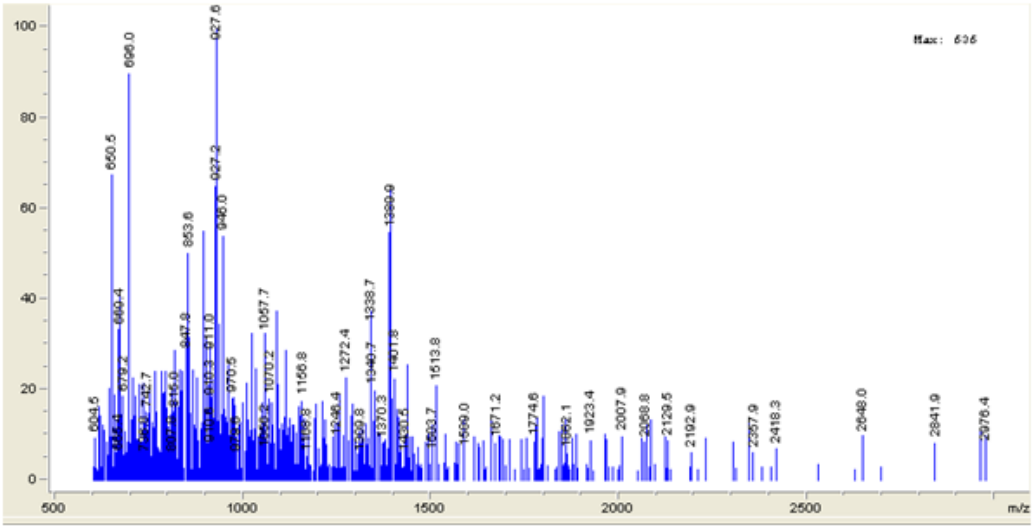

FIGURE A72. ESI-LCMS analysis of crude peptide **24**, using ESI MS in positive mode and LC linear gradient 2-80% MeOH/H_2O (0.1% FA) over 18 min using a Waters 2695 Symmetry® C18 column (3.9 x 150 mm, 5µm particle size) set at a temperature of 25 °C at a flow rate of 1 mL/min with detection at 220 nm.

Peptide **25**: FITC-$(CH_2)_5$-CTVALPGGYVRVC-PEG_3-K(NSC)-$CONH_2$

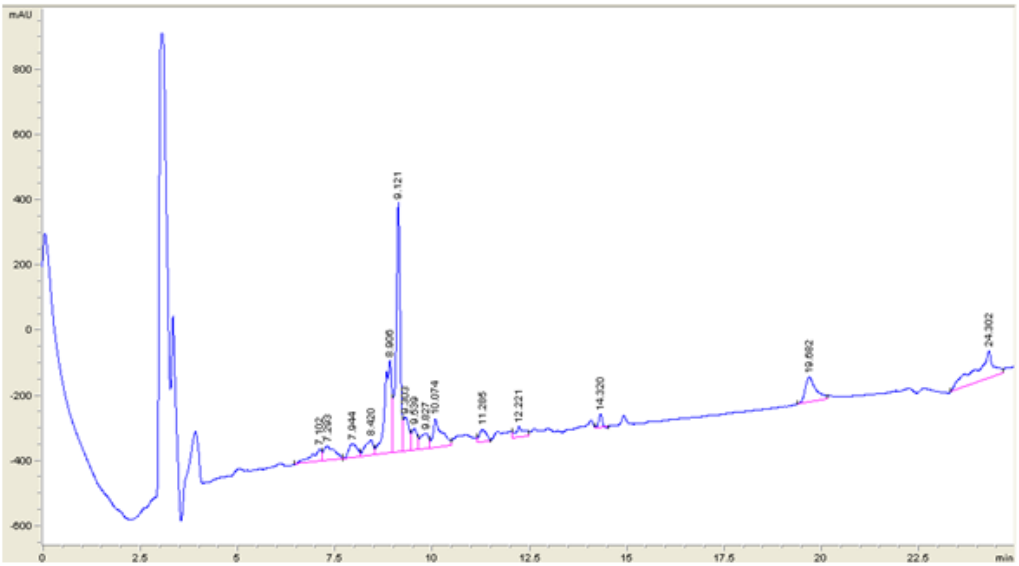

FIGURE A73. RP-HPLC analysis of crude peptide **25** using a linear gradient 20-80% MeCN/H_2O (0.1% FA) over 18 min using a Waters 2695 Symmetry® C18 column (3.9 x 150 mm, 5µm particle size) set at a temperature of 25 °C at a flow rate of 1 mL/min with detection at 220 nm.

Peptide **25**: FITC-$(CH_2)_5$-CTVALPGGYVRVC-PEG_3-K(NSC)-$CONH_2$

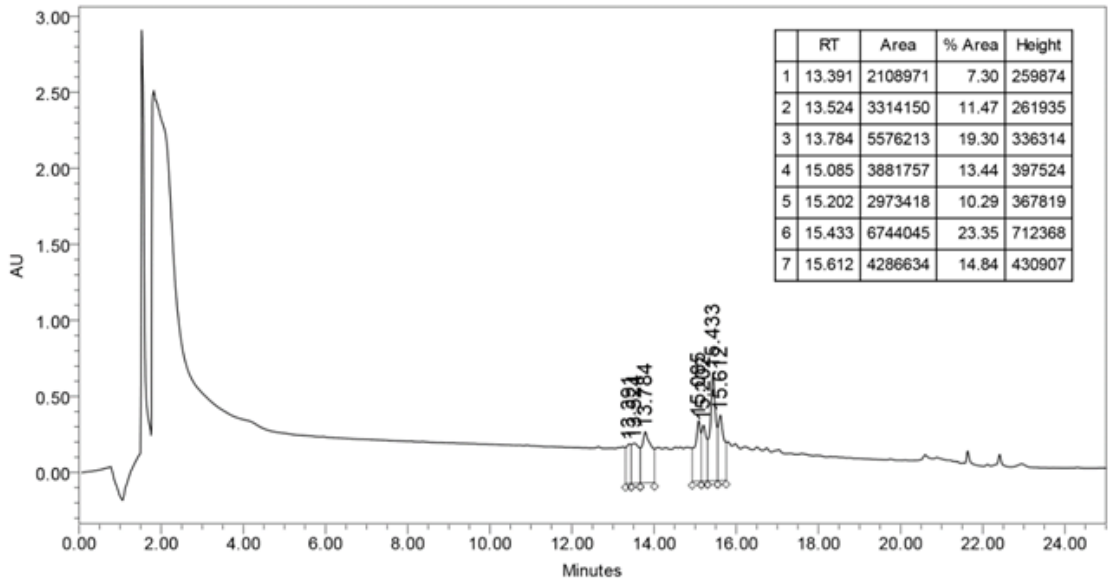

	RT	Area	% Area	Height
1	13.391	2108971	7.30	259874
2	13.524	3314150	11.47	261935
3	13.784	5576213	19.30	336314
4	15.085	3881757	13.44	397524
5	15.202	2973418	10.29	367819
6	15.433	6744045	23.35	712368
7	15.612	4286634	14.84	430907

FIGURE A74. RP-HPLC analysis of crude peptide **25**, using a linear gradient 2-80% MeOH/H_2O (0.1% FA) over 18 min using a Waters 2695 Symmetry® C18 column (3.9 x 150 mm, 5µm particle size) set at a temperature of 25 °C at a flow rate of 1 mL/min with detection at 220 nm.

Peptide **25**: FITC-$(CH_2)_5$-CTVALPGGYVRVC-PEG_3-K(NSC)-$CONH_2$

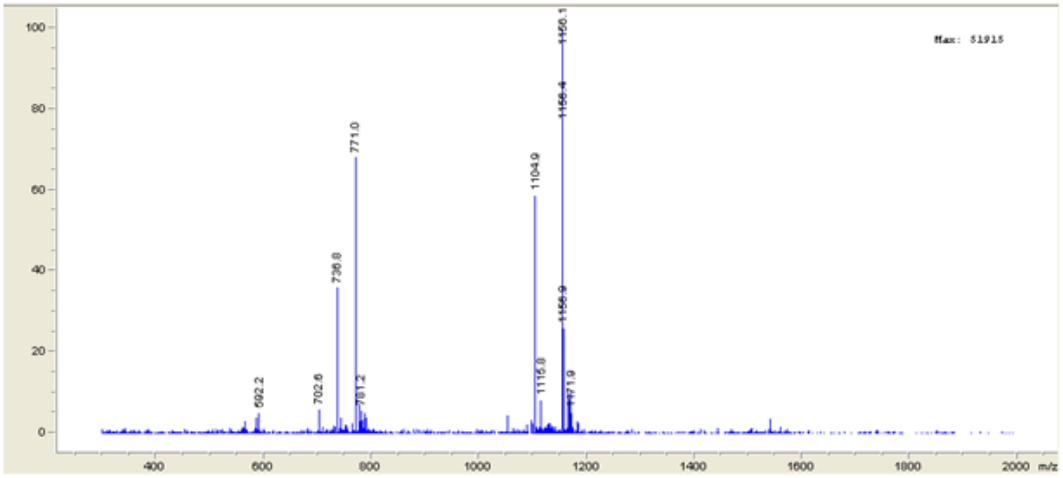

FIGURE A75. ESI-LCMS analysis of crude peptide **25**, using ESI MS in positive mode and LC linear gradient 2-80% MeOH/H_2O (0.1% FA) over 18 min using a Waters 2695 Symmetry® C18 column (3.9 x 150 mm, 5µm particle size) set at a temperature of 25 °C at a flow rate of 1 mL/min with detection at 220 nm.

Peptide **26**: FITC-$(CH_2)_5$-CTVALPGGYVRVC-PEG_6-K(NSC)-$CONH_2$

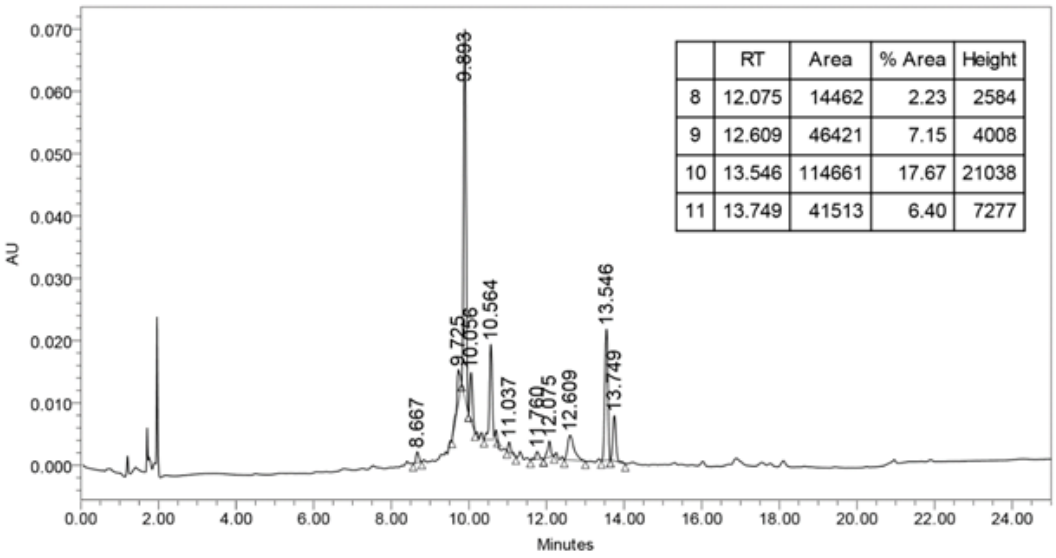

	RT	Area	% Area	Height
8	12.075	14462	2.23	2584
9	12.609	46421	7.15	4008
10	13.546	114661	17.67	21038
11	13.749	41513	6.40	7277

FIGURE A76. RP-HPLC analysis of crude peptide **26** using a linear gradient 2-80% MeCN/H_2O (0.1% FA) over 18 min using a Waters 2695 Symmetry® C18 column (3.9 x 150 mm, 5µm particle size) set at a temperature of 25 °C at a flow rate of 1 mL/min with detection at 280 nm.

Peptide **26**: FITC-$(CH_2)_5$-CTVALPGGYVRVC-PEG_6-K(NSC)-$CONH_2$

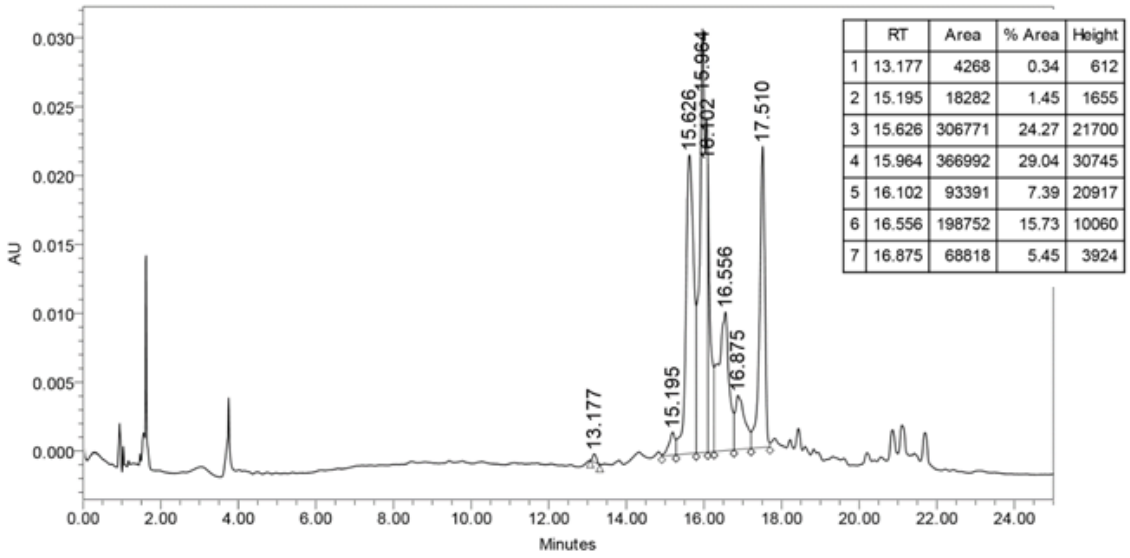

	RT	Area	% Area	Height
1	13.177	4268	0.34	612
2	15.195	18282	1.45	1655
3	15.626	306771	24.27	21700
4	15.964	366992	29.04	30745
5	16.102	93391	7.39	20917
6	16.556	198752	15.73	10060
7	16.875	68818	5.45	3924

FIGURE A77. RP-HPLC analysis of crude peptide **26**, using a linear gradient 2-80% MeOH/H_2O (0.1% FA) over 18 min using a Waters 2695 Symmetry® C18 column (3.9 x 150 mm, 5µm particle size) set at a temperature of 25 °C at a flow rate of 1 mL/min with detection at 280 nm.

Peptide **26**: FITC-$(CH_2)_5$-CTVALPGGYVRVC-PEG_6-K(NSC)-$CONH_2$

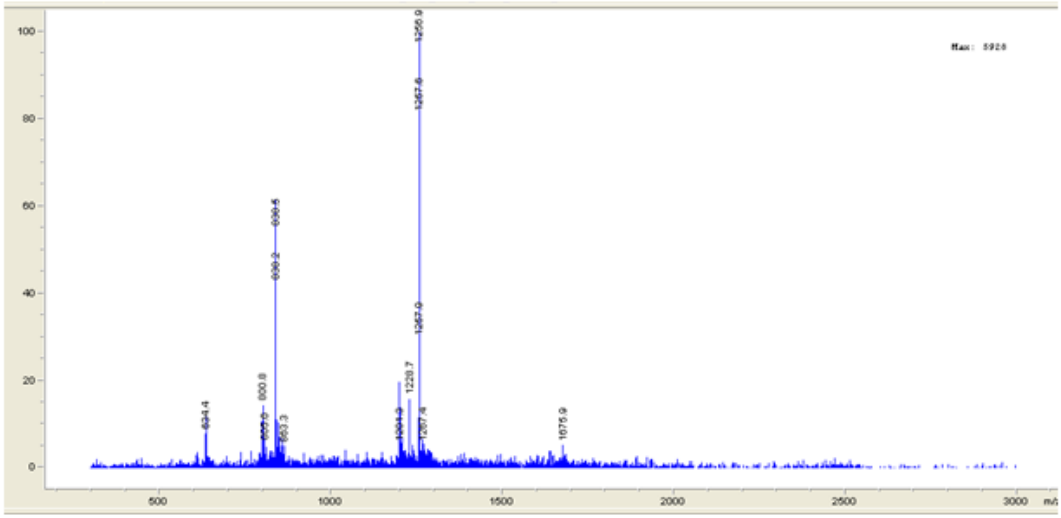

FIGURE A78. ESI-LCMS analysis of crude peptide **26**, using ESI MS in positive mode and LC linear gradient 2-80% MeOH/H_2O (0.1% FA) over 18 min using a Waters 2695 Symmetry® C18 column (3.9 x 150 mm, 5µm particle size) set at a temperature of 25 °C at a flow rate of 1 mL/min with detection at 220 nm.

Peptide **27**: FITC-$(CH_2)_5$-CTVALPGGYVRVC-PEG_{12}-K(NSC)-$CONH_2$

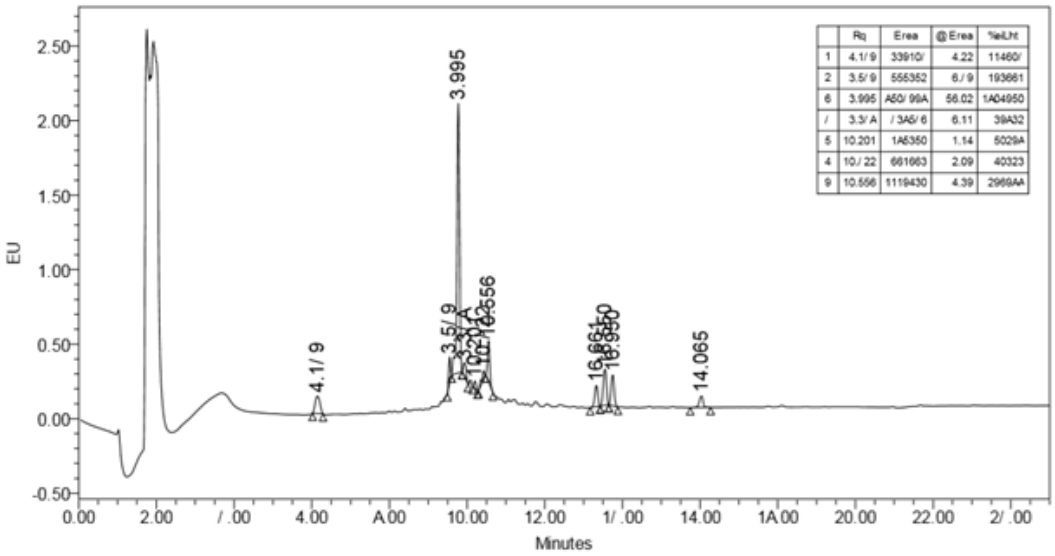

	Rq	Erea	@Erea	%eLht
1	4.1/ 9	33910/	4.22	11460/
2	3.5/ 9	555352	6./ 9	193661
6	3.995	A50/ 99A	56.02	1A04950
/	3.3/ A	/ 3A6/ 6	6.11	39A32
5	10.201	1A6350	1.14	5029A
4	10./ 22	661663	2.09	40323
9	10.556	1119430	4.39	2969AA

FIGURE A79. RP-HPLC analysis of crude peptide **27** using a linear gradient 2-80% MeCN/H_2O (0.1% FA) over 18 min using a Waters 2695 Symmetry® C18 column (3.9 x 150 mm, 5µm particle size) set at a temperature of 25 °C at a flow rate of 1 mL/min with detection at 220 nm.

Peptide **27**: FITC-$(CH_2)_5$-CTVALPGGYVRVC-PEG_{12}-K(NSC)-$CONH_2$

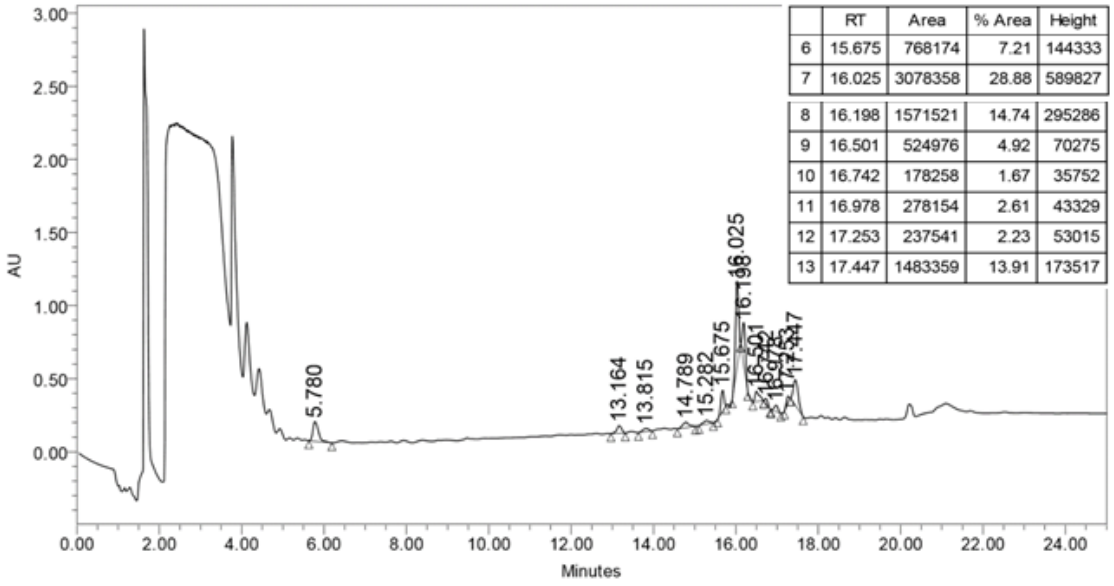

	RT	Area	% Area	Height
6	15.675	768174	7.21	144333
7	16.025	3078358	28.88	589827
8	16.198	1571521	14.74	295286
9	16.501	524976	4.92	70275
10	16.742	178258	1.67	35752
11	16.978	278154	2.61	43329
12	17.253	237541	2.23	53015
13	17.447	1483359	13.91	173517

FIGURE A80. RP-HPLC analysis of crude peptide **27**, using a linear gradient 2-80% MeOH/H_2O (0.1% FA) over 18 min using a Waters 2695 Symmetry® C18 column (3.9 x 150 mm, 5µm particle size) set at a temperature of 25 °C at a flow rate of 1 mL/min with detection at 220 nm.

Peptide **27**: FITC-$(CH_2)_5$-CTVALPGGYVRVC-PEG_{12}-K(NSC)-$CONH_2$

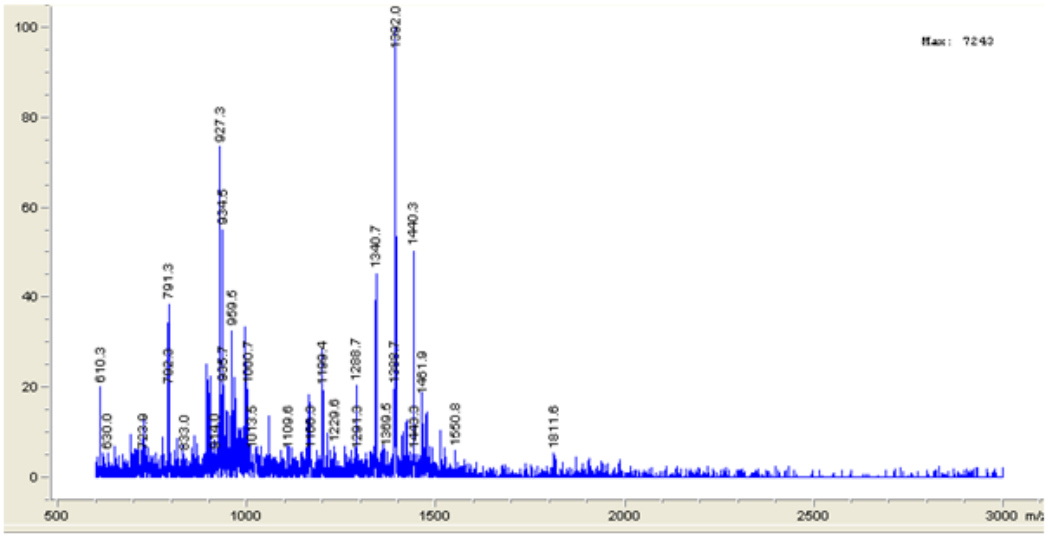

FIGURE A81. ESI-LCMS analysis of crude peptide **27**, using ESI MS in positive mode and LC linear gradient 2-80% MeOH/H_2O (0.1% FA) over 18 min using a Waters 2695 Symmetry® C18 column (3.9 x 150 mm, 5µm particle size) set at a temperature of 25 °C at a flow rate of 1 mL/min with detection at 220 nm.